MULTISCALE SPECTRAL-DOMAIN PARAMETERIZATION FOR HISTORY MATCHING IN STRUCTURED AND UNSTRUCTURED GRID GEOMETRIES

A Dissertation

by

ERIC WHITTET BHARK

Submitted to the Office of Graduate Studies of
Texas A&M University
in partial fulfillment of the requirements for the degree of

DOCTOR OF PHILOSOPHY

August 2011

Major Subject: Petroleum Engineering

Multiscale Spectral-Domain Parameterization for History Matching in Structured and Unstructured Grid Geometries

MULTISCALE SPECTRAL-DOMAIN PARAMETERIZATION FOR HISTORY MATCHING IN STRUCTURED AND UNSTRUCTURED GRID GEOMETRIES

A Dissertation

by

ERIC WHITTET BHARK

Submitted to the Office of Graduate Studies of
Texas A&M University
in partial fulfillment of the requirements for the degree of

DOCTOR OF PHILOSOPHY

Approved by:

Co-Chairs of Committee,	Akhil Datta-Gupta
	Behnam Jafarpour
Committee Members,	Yalchin Efendiev
	Ding Zhu
Head of Department,	Stephen Holditch

August 2011

Major Subject: Petroleum Engineering

ABSTRACT

Multiscale Spectral-Domain Parameterization for History Matching in Structured and Unstructured Grid Geometries. (August 2011)

Eric Whittet Bhark, B.S., Boston College; M.S., New Mexico Institute of Mining and Technology

Co-Chairs of Advisory Committee: Dr. Akhil Datta-Gupta
Dr. Behnam Jafarpour

Reservoir model calibration to production data, also known as history matching, is an essential tool for the prediction of fluid displacement patterns and related decisions concerning reservoir management and field development. The history matching of high resolution geologic models is, however, known to define an ill-posed inverse problem such that the solution of geologic heterogeneity is always non-unique and potentially unstable. A common approach to improving ill-posedness is to parameterize the estimable geologic model components, imposing a type of regularization that exploits geologic continuity by explicitly or implicitly grouping similar properties while retaining at least the minimum heterogeneity resolution required to reproduce the data. This dissertation develops novel methods of model parameterization within the class of techniques based on a linear transformation.

Three principal research contributions are made in this dissertation. First is the development of an adaptive multiscale history matching formulation in the frequency domain using the discrete cosine parameterization. Geologic model calibration is performed by its sequential refinement to a spatial scale sufficient to match the data. The approach enables improvement in solution non-uniqueness and stability, and further balances model and data resolution as determined by a parameter identifiability metric. Second, a model-independent parameterization based on grid connectivity information is developed as a generalization of the cosine parameterization for applicability to generic

grid geometries. The parameterization relates the spatial reservoir parameters to the modal shapes or harmonics of the grid on which they are defined, merging with a Fourier analysis in special cases (i.e., for rectangular grid cells of constant dimensions), and enabling a multiscale calibration of the reservoir model in the spectral domain. Third, a model-dependent parameterization is developed to combine grid connectivity with prior geologic information within a spectral domain representation. The resulting parameterization is capable of reducing geologic models while imposing prior heterogeneity on the calibrated model using the adaptive multiscale workflow.

In addition to methodological developments of the parameterization methods, an important consideration in this dissertation is their applicability to field scale reservoir models with varying levels of prior geologic complexity on par with current industry standards.

TABLE OF CONTENTS

Page

Page

LIST OF FIGURES

FIGURE Page

FIGURE Page

FIGURE Page

FIGURE Page

FIGURE Page

FIGURE Page

FIGURE Page

LIST OF TABLES

1. INTRODUCTION: RESERVOIR MODEL PARAMETERIZATION FOR HISTORY MATCHING

1.1 Introduction to the Problem

Reservoir model calibration to dynamic data, also known as history matching, is an essential tool for the prediction of fluid displacement patterns and related decision options concerning reservoir management and field development. A primary component of history matching is the characterization of subsurface heterogeneity that dominates the spatial and temporal variability in displacement behavior according to the existing well pattern and schedule. To account for the disparity in resolution of various types of dynamic measurements available, from seismic down to the core, data integration algorithms must follow suit in their ability to identify and update reservoir heterogeneity over a wide range of spatial scales in a manner consistent with and adaptive to data resolution.

The characterization of reservoir heterogeneity typically begins with the conceptual geologic model and the identification of regional attributes such as facies or depositional sequences, domain boundaries and boundary conditions, and faults or other sources of regional hydraulic (dis)continuity. Finer-scale patterns of heterogeneity within regional features may then be populated and updated when appropriate. Accordingly, research and field application together have emphasized the establishment of reservoir engineering workflows that systematically reconcile the geologic model, from the regional to grid-cell scale, with multi-resolution static and dynamic data. Related approaches to both manual and assisted history matching typically apply a structured approach and employ a series of data integration algorithms that are each suited to the scale of the estimated features and the type and resolution of the available data (Landa and Horne, 1997; Williams et al., 1998; Caers, 2003; Yin et al., 2010; Cheng et al.,

---

This dissertation follows the style of Journal of Petroleum Science and Engineering.

2008). Approaches following this parsimonious rationale integrate data such as 3D/4D seismic, formation testing of pressure, pressure transient analysis and production phase cuts in a step-wise sequence, beginning at the global scale and often with the most simple description, followed by an attempt to update finer-scale details only when supported by the data or by related reservoir management decisions.

Such structured approaches to data integration, whether following a top-down or bottom-up philosophy, typically use a method of spatial parameter characterization to capture relevant geologic features, at the spatial scale(s) of interest, with the ultimate goal of reducing the estimable parameter set. It is well understood that the calibration of high-resolution geologic models poses an underdetermined inverse problem with the number of updated reservoir properties defined at individual grid cells considerably larger than the number of measured data. In this scenario the updated geologic model, or solution to the inverse problem, is always non-unique. Multiple solutions consistent with geologic data and interpretation may reproduce the observed flow data but fail to predict future performance correctly (Gavalas et al., 1976; Carrera and Neuman, 1986a, 1986b; Yeh, 1986; Tikhonov and Arsenin, 1977; Tarantola, 2005; Moore and Doherty, 2005; Oliver et al., 2008). Therefore, either the explicit or implicit re-definition of spatial properties into parameter groups provides a means for regularization by which the inverse problem becomes more tractable (McLaughlin and Townley, 1996; Reynolds et al., 1996; Doherty, 2003; Carrera et al., 2005). Both approaches to re-parameterization, reviewed below, stabilize the solution by imposing one or more assumptions related to the underlying geologic model (Carrera and Neuman, 1986a, 1986b; Tikhonov and Arsenin, 1977; Vasco et al., 1999; Tarantola, 2005; Tonkin and Doherty, 2009; Oliver and Chen, 2011) and fundamentally exploit the inherent spatial continuity in geologic features, strategically grouping like properties while at the same time retaining the heterogeneity required to match the data and honor prior information at the appropriate scale (Carrera and Neuman, 1986c; Carrera et al., 2005; Yoon et al., 2001; Jafarpour and McLaughlin, 2009; Kim et al., 2010).

1.2 The History Matching Problem

Before posing the solution to the history matching problem as a re-parameterized geologic model in **Subsection 1.3**, in this subsection (**1.2**) a formal description of the general history matching problem is first presented. The estimation of geologic model parameters from field measurements that are related to the states (i.e., pressure, saturation) of the reservoir system defines an inverse problem because it is the opposite, forward problem that relates known geologic parameters to the unknown or predicted reservoir states. In the most general description, history matching problems contain three primary components: definition of (1) the forward model, (2) the objective function and (3) a scheme for minimization of the objective function by calibrating the estimable parameters.

The forward model is constructed as the system of physical laws that govern the flow and transport processes modeled and are used to predict the responses of the reservoir system given a set of reservoir parameters. These fundamental laws describing the dynamics of the reservoir system include a fluid mass conservation equation(s), Darcy's flow equation, and equations of state that generally relate pressure, temperature and saturation to fluid transport and rock properties. In application, and for the purposes of the research presented in this dissertation, the forward model involves numerical simulation which may or may not be computationally expensive depending on the type of flow and transport processes characterized and their level of spatial and temporal characterization. Because all aspects of subsurface reservoir description are uncertain, the predictive capacity of the forward model is limited by the accuracy of the reservoir model parameters, which must be calibrated to all known static and dynamic measurements. In this research we focus on the calibration of static geologic heterogeneity, i.e., porosity and permeability, which are only partially known due to limited accessibility (e.g., locally at wells) and cost constraints associated with data acquisition (e.g., reservoir scale seismic measurements).

The objective function in history matching defines a measure of the difference between the observed dynamic data and the corresponding predicted or numerically simulated responses. In this research these measurements consist of reservoir pressure and fluid saturations measured at wells. It is through minimization of the objective function that the estimable parameters are calibrated to the dynamic data. Because the reservoir states, and therefore the objective function terms, are typically nonlinearly related to the reservoir parameters, the process of minimization is iterative. Presented now are the forward model (**Subsection 1.2.1**) and the numerical approach to the solution of the history matching problem by iterative minimization of the objective function with a nonlinear optimization technique (**Subsection 1.2.2**).

1.2.1 Forward Model

The multiphase petroleum reservoir flow models applied in this dissertation, denoted as **g**[**m**] and where **m** represents the set of calibrated geologic parameters, can be described in the most general form by the black oil model under the assumption that fluid displacement is dominated by viscous forces. In the following formulation compressibility and gravity are considered and capillarity neglected, although the methods presented are in general independent of the choice of physical mechanisms. The phases are referred to as water (*w*), oil (*o*) and gas (*g*). Simultaneous flow of the three phases is governed by the following equations (e.g., Datta-Gupta and King, 2007)

$$\phi \frac{\partial}{\partial t}\left(\frac{S_j}{B_j}\right) + \nabla \cdot \left(\frac{\vec{v}_j}{B_j}\right) = q_j^s, \quad j = w, o \tag{1.1}$$

$$\phi \frac{\partial}{\partial t}\left(\frac{S_g}{B_g} + \frac{S_o R_{so}}{B_o}\right) + \nabla \cdot \left(\frac{\vec{v}_o R_{so}}{B_o} + \frac{\vec{v}_g}{B_g}\right) = q_g^s \tag{1.2}$$

where the phase velocity is

$$v_j = -\frac{k(x)k_{rj}(S_j)}{\mu_j}\left(\nabla p_j + \rho_j g \nabla z\right), \quad j = w, o, g \,. \tag{1.3}$$

The following variables are defined: B_j is the formation volume factor for phase j, S_j is the saturation of phase j, R_{so} is the solution gas oil ratio, p_j is the j phase pressure, q_j^s is the source term of phase j, μ_j is the viscosity of phase j, ρ_j is the density of phase j, g is acceleration due to gravity, z is depth below a datum, $k(x)$ is the heterogeneous absolute permeability field where x denotes a generic spatial location, and k_{rj} is the phase-saturation dependent relative permeability. It is useful to recognize that the model in Eqs. (1.1) and (1.2) are general and reduce to two-phase immiscible flow by ignoring the gas phase. Further simplification to two-phase incompressible and immiscible flow is achieved by $B_j = 1$ and $\partial\left(S_j / B_j\right)/\partial t = 0$. The specific forms of the model applied are defined in the relevant application sections.

1.2.2 Inverse Modeling

In the most simple form, the inverse problem is posed as the nonlinear discrete problem

$$\begin{aligned} &\text{Find } \mathbf{m} \text{ such that} \\ &\mathbf{g}[\mathbf{m}] = \mathbf{d} \end{aligned} \tag{1.4}$$

where, for the purpose of this dissertation, **g** nonlinearly relates the m-length column vector of parameters **m**, per Eqs. (1.1) and (1.2), to the n-length column vector of the model responses or dynamic observation data **d**. For a suite of plausible reasons including measurement errors, modeling errors and incorrect definition of the geologic system and fluids models, Eq. (1.4) typically has no solution and is in practice solved by minimizing an objective function, $f(\mathbf{m})$, that defines a measure of deviation of the modeled responses from those observed. In this dissertation, the solution to the parameter estimation (model calibration) problem is therefore posed as an unconstrained optimization problem, i.e.,

$$\text{Find } \mathbf{m} \text{ such that } \min_{\mathbf{m}} f(\mathbf{m}) \tag{1.5}$$

where the parameters **m** comprise a real vector with at least one component and f is a smooth function. Although the global minimum $\tilde{\mathbf{m}}$ is sought such that $f(\tilde{\mathbf{m}}) \leq f(\mathbf{m})$ for all **m**, because of the large parameter dimension combined with the unknown shape of the objective function surface, a local minimum that provides adequate minimization of f is sought in practice.

In this dissertation the solution to Eq. (1.5) assumes a deterministic form in which a single (uncertain) prior geologic model is updated to achieve the history match. The deterministic formulation of this inverse problem is presented next in **Subsection 1.2.2.1**, and the numerical approach to parameter estimation is then described in **Subsection 1.2.2.1.1** using a robust quasi-Newton method. Although not applied, it is recognized that the approaches of parameter estimation in this dissertation could also be applied in a probabilistic framework. For completeness, an overview of this general approach is presented in **Subsection 1.2.2.2**.

1.2.2.1 Deterministic Inversion

To find a local minimum upon traversal of the objective function surface beginning from a prior parameter location (corresponding to a prior geologic model), the deterministic inversion uses Taylor's theorem to define the criteria upon which solution convergence is achieved. To establish nomenclature for the coming discussion, Taylor's theorem is expressed here as

$$f(\mathbf{m}+\mathbf{p}) = f(\mathbf{m}) + \mathbf{p}^{\mathrm{T}}\nabla f(\mathbf{m}) + \frac{1}{2}\mathbf{p}^{\mathrm{T}}\nabla^2 f(\mathbf{m}+t\mathbf{p})\mathbf{p} \tag{1.6}$$

for $t \in (0,1)$ and where **p** is a parameter update vector. A local minimum is deemed reached for the parameter set $\hat{\mathbf{m}}$ when two *sufficient* conditions are met. The first-order

condition requires that $\nabla f(\hat{\mathbf{m}}) = 0$, or that there is no descent direction at the solution. The second-order optimality condition is that $\nabla^2 f(\hat{\mathbf{m}})$, if it exists, is positive definite. This condition guarantees that the curvature about $\hat{\mathbf{m}}$ is positive, confirming that no local descent direction exists.

Primarily as a result of the nonlinearity of **g**, the parameters are solved for iteratively using, in this dissertation, a line search strategy. Beginning from the prior parameter set $\mathbf{m}_0$, a direction $\mathbf{p}_k$ is chosen, where k denotes the current iteration, and a search is completed along this direction until an objective function value of satisfactory reduction is achieved. The details of the search algorithm and requirements connoted by the term 'satisfactory' are discussed next in **Subsection 1.2.2.1.1**. This amounts to solving the one dimensional minimization problem for the step length α, i.e.,

$$\min_{\alpha>0} f(\mathbf{m}_k + \alpha \mathbf{p}_k). \tag{1.7}$$

A large variety of algorithms in some form complete the iterative line search using different search directions, and all are valid so long as the direction is one of descent, where $\mathbf{p}^{\mathrm{T}} \nabla \mathbf{f}_k$ is the rate of change in f along the direction **p** at $\mathbf{m}_k$. A commonly applied direction, because it considers the curvature of the objective function, is the Newton direction. Returning to the second-order Taylor series and using k to indicate the iteration, Eq. (1.6) is re-written as

$$f(\mathbf{m}_k + \mathbf{p}) \approx f_k + \mathbf{p}^{\mathrm{T}} \nabla \mathbf{f}_k + \frac{1}{2} \mathbf{p}^{\mathrm{T}} \mathbf{H}_k \mathbf{p} \tag{1.8}$$

where **H** is the discrete Hessian, which replaces $\nabla^2 \mathbf{f}_k$ in Eq. (1.6) under the assumption that $\nabla^2 \mathbf{f}_k$ is sufficiently smooth. The true objective function is now approximated by a quadratic model, and the Newton direction can be obtained by finding **p** that minimizes

Eq. (1.8), or by setting the derivative of Eq. (1.8) to zero and solving for **p**. From this, the Newton direction is

$$\mathbf{p}_k = -\mathbf{H}^{-1}\nabla\mathbf{f}_k \,. \tag{1.9}$$

The Hessian must be positive definite if **p** is a descent direction and can be used in a line search. The method of ensuring this condition is discussed below. Notice that a step length of unity is implicit in the application of Eq. (1.9) in Eq. (1.7).

In addition to the requirement that a positive definite Hessian always exists for a useful descent direction, the Hessian is often impractical to compute at each iteration, always so in high-resolution geologic model calibration. For this reason, in this dissertation a quasi-Newton approach is used to determine the descent direction that approximates Newton's method. The difference is that the actual Hessian, $\mathbf{H}_k$, is approximated at each iteration (by $\mathbf{B}_k$) using the information provided by the change in gradient between iterations that is related to the curvature of *f* along the search direction. Relevant details of this algorithm are now presented.

1.2.2.1.1 Numerical Approach to Deterministic Parameter Estimation: BFGS Quasi-Newton Method Inversion

In this dissertation, the BFGS quasi-Newton algorithm is applied to minimize the data misfit objective function, thereby improving estimation of the model parameters as explained. In all research applications the routines used are based on the MATLAB® optimization toolbox. There are several approaches to the implementation of BFGS, and rather than presenting the optimization (for model calibration) as a black-box algorithm, this subsection elucidates some key points of the implementation that are used throughout this dissertation. The following discussions summarize Nocedal and Wright (2006), Oliver et al. (2008) and the MATLAB Optimization Toolbox User's Guide (2010).

The Hessian approximation, which is at the heart of quasi-Newton methods, can be fundamentally understood by returning to Taylor's theorem. If *f* is twice continuously differentiable (hence the smoothness condition of Eq. [1.8]), then by Taylor's theorem the perturbed gradient can be expressed as

$$\nabla f(\mathbf{m}+\mathbf{p}) = \nabla f(\mathbf{m}) + \int_0^1 \nabla^2 f(\mathbf{m}+t\mathbf{p})\mathbf{p}\, dt \,. \tag{1.10}$$

By the addition and subtraction of the term $\nabla^2 f(\mathbf{m})\mathbf{p}$ to the right hand side of Eq. (1.10), and further by assuming that the resultant integral $\int_0^1 \left[\nabla^2 f(\mathbf{m}+t\mathbf{p}) - \nabla^2 f(\mathbf{m})\right]\mathbf{p}dt$ is negligible as $o(\|\mathbf{p}\|)$, then when $\mathbf{m} = \mathbf{m}_k$ and $\mathbf{p} = \mathbf{m}_{k+1} - \mathbf{m}_k$, Eq. (1.10) can be expressed as

$$\nabla \mathbf{f}_{k+1} = \nabla \mathbf{f}_k + \nabla^2 \mathbf{f}_k (\mathbf{m}_{k+1} - \mathbf{m}_k). \tag{1.11}$$

Near the local minimum at $\hat{\mathbf{m}}$ the curvature approximation begins to dominate in Eq. (1.11) as the gradient is close to zero, and what is known as the secant equation is then achieved, i.e.,

$$\mathbf{B}_{k+1}\mathbf{s}_k = \mathbf{y}_k \tag{1.12}$$

where $\mathbf{s}_k = \mathbf{m}_{k+1} - \mathbf{m}_k$, $\mathbf{y}_k = \nabla \mathbf{f}_{k+1} - \nabla \mathbf{f}_k$, and $\mathbf{B}_{k+1}$ is the approximated Hessian. The subscript k+1 is given to indicate that the update of **B** at each iteration is forced to satisfy the secant equation as a constraint, although it is alone inadequate for exact computation of the update.

In order to achieve a unique update of the Hessian approximation, the additional constraints of (1) symmetry, (2) a low-rank difference between $\mathbf{B}_k$ and $\mathbf{B}_{k+1}$ and (3) positive definiteness of $\mathbf{B}_{k+1}$ are required. The method by which this final condition is

honored in relation to Eq. (1.12) is described in more detail below as it largely influences the line search algorithm. In total, minimization of the problem

$$\min_{\mathbf{B}} \left\| \mathbf{B} - \mathbf{B}_k \right\| \quad \text{subject to } \mathbf{B} = \mathbf{B}^{\mathrm{T}},\ \mathbf{B}\mathbf{s}_k = \mathbf{y}_k \tag{1.13}$$

with use of the Frobenius norm yields a unique solution to **B**. The solution can be rearranged for the update formula

$$\mathbf{B}_{k+1} = \mathbf{B}_k - \frac{\mathbf{B}_k s_k s_k^{\mathrm{T}} \mathbf{B}_k}{s_k^{\mathrm{T}} \mathbf{B}_k s_k} + \frac{y_k y_k^{\mathrm{T}}}{y_k^{\mathrm{T}} s_k} \,. \tag{1.14}$$

This solution approach is valid for a broad class of quasi-Newton methods. For the BFGS algorithm specifically, the optimization in Eq. (1.13) is posed in terms of the inverse Hessian, with equivalent constraints, such that the parameter update vector in Eq. (1.9) can be computed directly.

In terms of implementation, from Eq. (1.14) it is clear that at each accepted (k+1) iteration of the minimization, both the new parameter vector and the objective function gradient are required at the new parameter location to compute $\mathbf{B}_{k+1}$ (note that these metrics are provided within our history matching algorithms via methods described later in the relevant sections of this dissertation). However, the update must be constrained to be positive definite so that the resultant direction of search (Eq. [1.9]) is in a descent direction. If **B** is initialized to be positive definite at the start of the optimization, then this constraint is guaranteed at all steps k if $\mathbf{s}_k^{\mathrm{T}} \mathbf{y}_k > 0$. The proof of this statement is shown by pre-multiplying Eq. (1.12) by $\mathbf{s}_k^{\mathrm{T}}$, where $\mathbf{B}_{k+1}$ is positive definite if the inner product $\mathbf{s}_k^{\mathrm{T}} \mathbf{B}_{k+1} \mathbf{s}_k > 0$. In our implementation, $\mathbf{B}_{k=0}$ is defined as the $m \times m$ identity matrix. When the objective function surface is not convex, which is typically the case in practice, then $\mathbf{s}_k^{\mathrm{T}} \mathbf{y}_k$ can be negative. In this case, the step length α (Eq. [1.7]) must be

constrained to ensure its positivity. This is a primary objective of the BFGS approach. In order to describe how this is achieved, a few details of the line search algorithm and implementation must first be explained.

First, at the outset of any given iteration, a step length of unity is selected, and the objective function and gradient are computed at the new location. The parameter update is accepted if two conditions are met, collectively known as the Wolfe conditions. The first requires that a sufficient decrease in the objective function is attained and is determined by the inequality

$$f\left(\mathbf{m}_k + \alpha_k \mathbf{p}_k\right) \leq f\left(\mathbf{m}_k\right) + c_1 \alpha \nabla \mathbf{f}_k^{\mathrm{T}} \mathbf{p}_k \,, \tag{1.15}$$

where $c_1 \in (0,1)$. More specifically, Eq. (1.15) implies that the decrease from point $\mathbf{m}_k$ is proportional to the directional derivative, $\nabla \mathbf{f}_k^{\mathrm{T}} \mathbf{p}_k$, by α_k and must in fact lie below the linear function $f\left(\mathbf{m}_k\right) + \nabla \mathbf{f}_k^{\mathrm{T}} \mathbf{p}_k$ throughout parameter space. In application, c_1 is typically chosen to be << 1 to effectively ensure this condition. The second line search condition enforces a parameter update of sufficient distance from the starting point, which Eq. (1.15) does not consider, and is enforced by the inequality

$$\nabla f\left(\mathbf{m}_k + \alpha_k \mathbf{p}_k\right)^{\mathrm{T}} \mathbf{p}_k \geq c_2 \nabla \mathbf{f}_k^{\mathrm{T}} \mathbf{p}_k \,, \tag{1.16}$$

where $c_1 \in (c_1,1)$. Simply stated, the slope of the objective function surface at the trial location $\mathbf{m}_k + \alpha \mathbf{p}_k$, which is the left hand side of the equation, must be greater than or equal to c_2 times the slope of the surface at $\mathbf{m}_k$. Generally speaking, this condition is useful to determine if the step size should be increased if the slope at the trial location becomes more negative, or decreased if becoming slightly to strongly positive, thus very roughly approximating the convex surface near a local minima.

Returning now to the trial step or parameter update at the outset of a given iteration, if the Wolfe conditions (which are discussed further below) are not met, then a rather complex series of decisions are made based on comparison of both the objective function and gradient at the new and previous locations to determine the length of the next trial step, which can be backwards or (less commonly) forwards. A general description of the multiple conditional scenarios are described in the above-referenced MATLAB® documentation, in which it is also stated that the coefficients in Eqs. (1.15) and (1.16) are determined in part empirically from algorithmic development using many test cases.

If the local region of the objective function surface is sufficiently convex, then the parameter update vector is immediately accepted following only one or two trials of the line search, the step length is re-set to unity, and a new search direction is computed for procession to iteration k+1. If non-convex then a cubic polynomial interpolation is performed, which requires computation of the gradient at at least three trial locations, to locate an acceptable minimum at which $\mathbf{s}_k^{\mathrm{T}}\mathbf{y}_k > 0$, with k indicating the current iteration. This amounts to the location of a sufficiently small gradient term along the polynomial. If the line search update $\mathbf{m}_{k+1} = \mathbf{m}_k + \alpha_k \mathbf{p}_k$ is rearranged for equality with $\mathbf{s}_k = \mathbf{m}_{k+1} - \mathbf{m}_k$, then

$$\mathbf{s}_k^{\mathrm{T}}\mathbf{y}_k = \alpha_k\left(\nabla\mathbf{f}_{k+1}^{\mathrm{T}}\mathbf{p} - \nabla\mathbf{f}_k^{\mathrm{T}}\mathbf{p}\right). \tag{1.17}$$

The gradient term at the (previously selected) kth location, $\nabla\mathbf{f}_k^{\mathrm{T}}\mathbf{p}$, is always negative; therefore, $\nabla\mathbf{f}_{k+1}^{\mathrm{T}}\mathbf{p}$ must simply be small enough to ensure that the right hand side of Eq. (1.17) is positive. It can also be shown that this condition is in fact guaranteed to hold if the Wolfe conditions as stated above are imposed on the line search.

Finally, as $\mathbf{m}_k$ approaches a local minimum and the quadratic model become more suitable for characterization of the objective function surface, the acceptance rate of the update increases and the value of α_k approaches unity as $\nabla\mathbf{f}_k^{\mathrm{T}}\mathbf{p}$ becomes more accurate.

1.2.2.2 Probabilistic Inversion

The approaches to parameter estimation presented in this dissertation could also be applied in a probabilistic framework (Ulrych et al., 2001; Tarantola, 2005) which is widely used for uncertainty quantification. The Bayesian approach to stochastic inversion seeks to characterize the posterior probability density function (*pdf*) of the unknown parameters by combining observed data (described through a likelihood function) with a prior *pdf* for model parameters (Tarantola, 2005). The analogy to the deterministic approach seeks a single solution (e.g., the maximum of the posterior) and is limited to simple assumptions for the likelihood and prior (e.g., Gaussian or Laplacian *pdfs*) such that a single mode exists. It also requires that the non-linear forward problem can be iteratively linearized and assumes that the prior and likelihood equally contribute to the posterior. A more practical alternative is the ensemble methods where the prior and posterior *pdf*s are approximated with a finite number of samples (particles). The main ensemble techniques in subsurface modeling are those that either condition each prior sample realization individually on available data (e.g., Sahuquillo et al., 1992; LaVenue et al., 1995; RamaRao et al., 1995; Gomez-Hernandez et al., 1997) or those that simultaneously update an ensemble of prior sample realizations to generate an ensemble of conditional realizations (e.g., Evensen, 1994; Chen and Zhang, 2006; Wen and Chen, 2006; Nowak, 2009). A recent review of these techniques can be found in Hendricks Franssen et al. (2009). The deterministic approach may be viewed as the individual calibration of only one of multiple realizations that together, when combined with a likelihood function based on calibration performance, could be used to quantify predictive uncertainty as in the GLUE methodology (e.g., Freer et al., 1996). Regardless of the conceptual approach to calibration, an effective parameter description such as provided by the methods in this dissertation is expected to improve the solution procedure.

1.3 Parameter Estimation

Having formally defined the type of history matching problem and the means to the solution of **m** in Eq. (1.4) using a deterministic least-squares formulation, in this subsection (**1.3**) the re-parameterization of **m** is presented as a method of regularization by which the history matching problem becomes more tractable. The broad topic of parameterization by linear transformation, which is applied in this research, and its general utility in history matching is introduced in **Subsection 1.3.1**. The application of parameterization following the deterministic approach to inversion is then described in **Subsection 1.3.2**. As stated, a single prior geologic model is considered for a history match, so the intent of this discussion is to describe how the uncertainty in prior information fundamentally determines the manner in which parameterization is applied. Last, the general approach of adaptive multiscale parameter estimation is described in **Subsection 1.3.3** and its suitability for history matching using parameterization by linear transformation is verified through a literature review.

1.3.1 Parameterization by Linear Transformation

Of the many variants of parameterization methods, this dissertation concentrates on the broad class of techniques based on a general linear transformation where the spatial parameters are updated in a coordinate system of lower dimensionality that is more amenable to their independent estimation. Carrera et al. (2005) review approaches to parameterization by linear transformation commonly applied in the petroleum and groundwater literature including zonation [also Jacquard and Jain, 1965; Jahns, 1966; Chavent and Bissell, 1998; Grimstad et al., 2003], pilot points [also de Marsily, 1978; Lavenue and Pickens, 1992; Alcolea et al., 2006] and conditional simulation. They succinctly encapsulate all approaches with the general formulation

$$\mathbf{u} = \mathbf{u}_o + \mathbf{\Phi v} = \mathbf{u}_o + \sum_{i=1}^{m} \phi_i v_i \tag{1.18}$$

where the column vector $\mathbf{u}_o$ corresponds to a prior model assumption with dimension equal to that of the estimable reservoir property field (m), $\mathbf{v}$ is a vector of the model parameters updated and $\mathbf{\Phi}$ is a matrix with columns corresponding to interpolation functions that act on $\mathbf{v}$ to populate all pertinent cells in the spatial property $\mathbf{u}$. The right-most term of Eq. (1.18) simply show that the transformation can be computed as a weighted linear combination of the matrix columns, where the weights are the estimated parameters in the transform domain. Variants of Eq. (1.18) also describe the different approaches to linear transformation introduced in this dissertation; however, the matrix $\mathbf{\Phi}$ is alternatively defined as a linear basis that maps the parameters in $\mathbf{v}$ from the transform domain in which parameter estimation is performed. These specific forms of Eq. (1.18) are presented in the relevant sections below.

In the application of Eq. (1.18) for history matching, there are three primary considerations that require definition: (1) selection of the appropriate basis $\mathbf{\Phi}$, (2) selection of the reduced number of basis elements or columns of $\mathbf{\Phi}$ (relative to the full spatial parameter dimension) that are to be applied for geologic characterization, and (3) selection of the method of transform parameter estimation. Relative to this research, this last point is addressed by use of a deterministic nonlinear optimization and was the topic of **Subsection 1.2**. However, the first two considerations, selection of the parameterization basis and the means of model reduction, comprise the remaining focus of this dissertation and encapsulate all challenges associated with parameterized model calibration. In the remainder of this subsection (**1.3.1**), linear transform bases commonly applied in petroleum reservoir and groundwater model calibration, and the means by which they enable a reduced model description, are reviewed. For this a basis is categorized as one of two types: constructed from prior geologic information and assumptions, or pre-determined and independent of the prior reservoir property model.

1.3.1.1 Model-Dependent Transform Bases

Methods of linear transform dependent on prior model assumptions have commonly utilized the parameter covariance matrix. The Karhunen-Loeve transform (KLT) or principle component analysis (PCA) has been widely used (Gavalas et al., 1976; Karhunen, 1947; Loéve, 1978; Reynolds et al., 1996; Li and Cirpka, 2006; Ma et al., 2008; Jafarpour and McLaughlin, 2009). In this approach the estimable property defined at any grid cell is represented as the linear expansion of the weighted eigenvectors of the property covariance matrix. The eigenvectors form the transform basis and are typically ranked by their corresponding eigenvalues, from largest to smallest, that are related to the variance contribution of each eigenvector to the total parameter variance. The expansion is optimal in the mean-squared-error sense among the linear class of transformations; therefore, the KLT coefficients present the fewest number of parameters that capture the maximum amount of variation for any low-rank approximation. Accordingly, the sorted eigenvectors convey larger to smaller scales of spatial parameter variation. A limitation of this approach is that in realistic problems with high-resolution models, the covariance can be unknown (or uncertain), resulting in misleading basis functions when prior model assumptions are incorrect (Jafarpour and McLaughlin, 2009). Eigendecomposition of the covariance matrix, required for each parameter update, is also prohibitively expensive for high resolution models relative to current computational capability. Last, the preservation of moments beyond second-order (i.e., covariance), as well as complex continuous geologic structures (e.g., channel systems), are not guaranteed in the KL expansion during the parameter updates.

To avoid the expense of eigendecomposition, Li and Cirpka (2006) assume periodicity of a random fluctuation in the property heterogeneity used for model calibration, since the eigenfunctions of its corresponding periodic covariance are known analytically. The corresponding eigenvalues, required for reconstruction of the random function, are then computed from a fast Fourier transform. They also generalize the formulation to non-periodic or unstructured grids by mapping the non-periodic fluctuation to a uniform

periodic grid with identical mean and covariance per cell. Sarma et al. (2008) manage the expense of eigendecomposition and preserve higher-order statistics representative of complex geologic structures by performing the linear expansion in a space of high dimensionality, or feature space, in which nonlinear parameter relationships are approximately linearized for their uncorrelated updating (see also **Section 6**). The transformation to feature space is performed using a kernel function, with the key understanding that application of the kernel function is equivalent to any dot product performed in feature space (Schölkopf and Smola, 2002), which in the context of parameterization is the forward transform or the action of a basis function on the spatial parameter set. A complication with this approach arises for the reverse mapping from feature space, known as the pre-image problem, which poses a nonlinear optimization problem. The selection of an appropriate kernel function is also subjective, for which there are only guidelines, and the correlation of the parameters in feature space cannot be inspected.

1.3.1.2 Model-Independent Transform Bases

The second category of linear transform bases are model-independent (or generic) and therefore rely on a general ability of the basis to efficiently capture and de-correlate the information of any function in a low-rank approximation. Two such approaches that have recently been applied in subsurface heterogeneity parameterization are the discrete cosine transform (DCT) basis (Jafarpour and McLaughlin, 2009) and the discrete wavelet transform (DWT) basis (Lu and Horne, 2000; Guan et al., 2004; Sahni and Horne, 2005; Jafarpour, 2010), both widely used in image compression (Gonzales and Woods, 2002). The DCT, of which there are eight formulations that vary based on the assumption of symmetry at domain boundaries, is a type of discrete Fourier transform that reconstructs a discrete n-length signal as the sum of n cosine harmonics (Britanak et al., 2007). It is the type-II DCT, or DCT-2, that has been applied in the papers cited, a technicality that becomes relevant throughout this dissertation. The DWT represents a type of basis that, generally speaking, acts as lowpass and highpass filters, or summating

and differencing operators, that split the frequency content of a discrete signal into two sets of coefficients that represent its low- and high-frequency components without loss (Vetterli et al., 2010). One of the DWT's main advantages is that the transform coefficients simultaneously depict space-frequency resolution permitting representation of both smooth and discontinuous spatial features at multiple resolutions.

The advantages of both the Fourier and wavelet approach are related to the efficiency in basis construction and application, optimal compression performance, and adaptation to prior model information. The variants of all DCT and DWT bases have analytical descriptions and are computed only once for a given estimation problem. The basis functions (for either transform) are pairwise orthonormal and therefore the basis inverse, required for mapping from the transform to the spatial domain after every parameter update, is simply the transpose. For the DCT, maximal compression power results from its asymptotic convergence to PCA of a first-order stationary Markov process (Ahmed et al., 1974). Approaches to production data assimilation using the DCT also recognize a key strength as the ability to capture larger-scales of geologic continuity and hydraulic property connectivity in the presence of sparse data with a significantly reduced number of parameters (Jafarpour and McLaughlin, 2009). That is, a linear combination of lower-frequency cosine functions naturally enforces field connectivity structure when warranted. For the DWT, optimal compression performance results from its adaptive ability to detect and characterize local and global spatial features at different resolutions. However, space-frequency localization also presents a limitation in the context of prior model assumptions, discussed later in this section.

In history matching applications, the DCT and DWT parameterizations have been used to characterize and calibrate the prior model with a low-rank approximation that captures important multiscale and multiresolution features, respectively, that are sensitive to production data. The key step of parameter reduction results from the truncation of model components in the transform domain that are either shown or assumed to be insensitive to the available data. Accordingly, both approaches can benefit from prior

information when available by varying the level of model compression or parameter reduction, but do not require any knowledge of the prior model for basis construction and therefore are not limited to prior assumptions in the case that they may be incorrect or uncertain.

The strengths of the DCT and DWT are, however, coupled with their limitations. The DCT, or any Fourier domain representation, does not contain spatial information. Updating of a parameter in the transform domain results in a global update of the spatial hydraulic property; therefore, the estimation of a local feature in space is dependent upon the existence of a suitable linear combination of cosine functions which may not exist at a low dimensionality (required for parameterization). Conversely, although the DWT is able to update spatial parameters or features locally, the estimation of finer-scale detail may require additional data types. For example, Lu and Horne (2000) found that low-resolution coefficients were identified by production data, but that additional seismic information at each grid cell was required to simultaneously resolve finer-scale edge information of the coarser scale features. More recently, Jafarpour (2010) used the DWT to reconstruct geologic facies from flow data and concluded that the low resolution of the data may not allow for full exploitation of the space-frequency localization advantage of the wavelets. Regarding practical implementation, both traditional Fourier and wavelet approaches are limited to use on uniform structured grids due to periodic sampling requirements and have not been applied in the literature to irregular corner-point or unstructured grid geometries, although wavelets in general have been applied to irregularly discretized signals (Daubechies et al., 1999).

1.3.2 Consideration of the Prior Model

An understanding of prior model information is imperative before any form of history matching is attempted and, following the previous discussion, the appropriate selection of a geologic model parameterization concurrently requires this understanding. The prior geologic model can be completely unknown or un-informed, but can also be well-

informed at high resolution from the integration of multiple static data sources (e.g., well logs, seismic surveys, etc.). In this research, prior information in the form of spatially continuous geologic features (i.e., porosity, permeability fields) within pre-defined structural boundaries, which are assumed known, are considered as the estimable parameters. To be clear, parameterization is not applied for the adjustment of the stratigraphic or facies structure itself, which falls into the scope of a different intention in history matching (Roggero and Hu, 1998; Hoffman and Caers, 2005; Jafarpour and Khodabakhshi, 2010; Xie et al., 2010). Therefore, the parameter estimation algorithm, regardless of whether a parameterization technique is used, should be adaptive to prior model information, as well as to the associated flow and transport behavior (the details of such criteria are presented in **Section 2**).

In this dissertation, all approaches to parameter estimation are conceptually developed in practical consideration of the prior geologic model, again which may be completely un-informed to well-informed. In the case of an un-informed prior (e.g., a homogenous field), the intent of parameter estimation is to *identify* global features over the complete grid or model domain from the production data alone. In the case of a well-informed prior, the intention is to minimally *update* the existing model at locations and spatial scales warranted by the production data, and to leave unchanged the field at locations either insensitive to or consistent with production data. To provide the flexibility for consideration of either case, the parameterization is applied following the approach of Eq. (1.18) although using the multiplicative formulation

$$\mathbf{u} = \mathbf{u}_0 \cdot \boldsymbol{\Phi}\mathbf{v} \tag{1.19}$$

where the entrywise product $\mathbf{A}\cdot\mathbf{B}$ of matrices $\mathbf{A} = (a_{ij})$ and $\mathbf{B} = (b_{ij})$ is $a_{ij}b_{ij}$, and $\mathbf{u}_o$ is the prior spatial model. Using this formulation, model updating is performed with a multiplier field that is superimposed onto the prior model, at grid cell resolution, with an initial value of unity at each grid cell. The multiplier field is characterized in the transform domain by a reduced set of spectral coefficients $\mathbf{v}$ that represent its scalar

projection onto the transformation basis functions, or columns of **A**. That is, **v** represents the parameters in the transform domain and the product **Φv** defines the multiplier field in the spatial domain. The specific formulations applied are presented in the relevant sections.

In certain cases, however, where the prior model is too dissimilar to the reference (a statement that can only be made using synthetic applications), then a prior multiplier cannot be used to achieve a solution and **Φ** (in Eqs. [1.18] and [1.19]) must be applied as a compression transformation basis. In this case Eq. (1.18) is reformulated as

$$\mathbf{u} = \mathbf{\Phi v} \,. \tag{1.20}$$

As introduced in **Subsection 1.1**, the transformation basis **Φ** is used to characterize and update the prior model with a low-rank approximation that captures the important, typically larger scale, heterogeneity to which the production data are sensitive. Therefore, in Eq. (1.20) **v** represents the scalar projection of the prior model onto basis functions that in some manner characterize the important heterogeneity and permit its updating by the adjustment of **v**. Concurrently, parameter reduction is enabled by the truncation of spatial features in the prior, to which the data are either shown or assumed to be insensitive, by the exclusion of basis functions in **Φ** that represent those features.

1.3.3 Adaptive Multiscale Approaches

Returning to the structured framework in which the history matching problem was posed in **Subsection 1.1**, and in consideration of the prior model (**Subsection 1.3.2**), an appropriate approach to parameterized history matching is that of adaptive multiscale parameter estimation. The motive of this broad class of techniques is to characterize geologic features relevant to the data, at spatial locations and scales of interest, to achieve a balance between parameter and data resolution while (most importantly) reducing the estimable parameter set. This subsection reviews adaptive multiscale approaches applied in the literature to establish the suitability of this approach for

parameterization by linear transformation, and also importantly to place the contributions of this research in context. The applied requirements of this approach for use in reservoir model calibration are both presented and exemplified in **Section 2** during a history matching application.

Adaptive multiscale parameter estimation algorithms, as a rule, rescale the geologic model in the spatial domain during some type of iterative sequence, sequentially coarsening and/or refining global and local regions of the model based on a pre-defined measure. At each step, the ‘multiscale’ component enables adjustment of the spatial scale over which individual parameters are defined, and the ‘adaptive’ component enforces these changes in a manner consistent with data sensitivity to the scaled parameters. These components together improve the parameter set convergence on a cost function surface that increases or decreases in dimension at each step as the set iterates toward a local minimum.

Jahns (1966) performed one of the earliest approaches to adaptive multiscale parameter estimation in recognition of the unfavorable influence of over-parameterization and parameter correlation on iterative descent behavior and non-uniqueness. He proposed the sequential spatial refinement of reservoir parameter groups near wells, suggesting guidelines to select the initial scale of parameterization based on the number of data available, and terminated the refinement when data misfit updates were below a set tolerance. Yoon et al. (2001) also used the approach of uniform global refinement with the further aim of achieving a balance between production data and model resolution. Then, they conditioned the model to match well data at scales finer than the global parameter resolution using a sequential simulation technique based on residuals computed at fine-scale measurement locations.

Subsequent adaptive multiscale methods have been designed to avoid potential over-parameterization by global refinement and apply a suite of schemes to locally update parameter resolution. With the intent of large-scale or global estimation of permeability

structure, Grimstad et al. (2004) sequentially refine the number and location of parameter zones by selecting at each step the combination that minimizes a quadratic misfit or cost function surface. The cost function is efficiently constructed from a linear approximation of the data response to parameters and accounts for the influence of data error on misfit. Such Adaptive Multiscale Estimation (AME) techniques further require strategies for non-uniform grid refinement. The approaches of Chavent and Bissell (1998) and Ben Ameur et al. (2002) use the AME paradigm to avoid over-parameterization at a sequential refinement step by taking advantage of piece-wise continuity in parameter zones. They defer to an indicator metric related to the gradient contribution per parameter, computed as the sum of adjoint-derived data-misfit sensitivities to the immediate-neighbor discontinuity within a refined zone, and retain a selected percentage of the most sensitive parameters. Feng and Mannseth (2009) use a comprehensive adaptive multiscale approach via a predictor-corrector strategy. The predictor step applies AME to develop a coarse and locally refined parameter zonation using a linearization of the model output at each refinement step, similar to Grimstad et al. (2004), and terminate refinement using a sensitivity-based indicator metric. As with the above-mentioned AME methods, the resultant parameter fields may show large contrasts in size and parameter values at juxtaposing zones that are inconsistent with geologic description, and further do not consider a prior model description, i.e., the approaches assume an uninformed prior. These issues are mitigated by the corrector step of Feng and Mannseth (2009). They first downscale the estimable property to a smoothly varying field consistent with the prior model and well data using a conditioning step of Kriging at the gridblock scale, similar to the conditioning step of Yoon et al. (2001). Then, a second step of data-misfit minimization is performed at the gridblock scale, using a low-order description of the parameter field with smoothly varying basis functions related to the prior covariance model, to correct production data misfit degraded from Kriging. Although complex, the predictor-corrector scheme is an improved data-driven multiscale approach that combines adaptive local refinement and a

refinement termination criterion while honoring hard and dynamic data at any scale down to the grid cell.

1.4 Research Objectives and Dissertation Contributions

The motive of this research is to expand upon the current state of the art in parameterization by linear transformation for history matching. In addition to theoretical developments, an emphasis is placed on the development of parameterization methods that are applicable to large reservoir models, on par with current industry standards and computational modeling capabilities, and also varying levels of prior geologic complexity.

There are three primary components of this research. First in **Section 2**, the DCT parameterization is applied in a novel adaptive multiscale history matching workflow in the frequency domain. The algorithm performs sequential model refinement by the addition of DCT basis elements that represent finer-scale spatial details, enabling the successive refinement of heterogeneity up to a spatial scale sufficient to match the observed data. Key contributions are the application of quantitative measures to demonstrate improvement of iterative solution convergence, and the achievement of a balance between model and data resolution. The results establish the validity of the proposed adaptive multiscale algorithm in the frequency or spectral domain, which is employed in some form throughout this dissertation.

In **Section 3**, a new model-independent basis constructed from grid-connectivity information is developed as a generalization of the DCT basis. The term ‘generalized’ refers to the parameterizations generic applicability to any grid structure and domain geometry. The development of the grid-connectivity-based transform (GCT) basis begins from first principles, merging discrete Fourier analysis and spectral graph theory. The basis functions represent the modal shapes or harmonics of the grid, are defined by a modal frequency, and converge to the DCT for certain grid geometries and boundary assumptions; therefore, reservoir model calibration is performed in the spectral domain

and merges with a Fourier analysis in ideal cases. Using an adaptive multiscale workflow, the GCT parameterization is successfully applied for history matching of several synthetic and semi-synthetic reservoir models of varying geometry and geologic complexity, and also of a field case in **Section 4**. An effort is made to highlight the several properties of the GCT basis for which it has a practically efficient construct and application.

As the final research component of this dissertation, **Section 5** presents the development of a more complex, and also to some extent heuristic, model-dependent transformation basis as a special case of the model-independent case (i.e., the GCT). To achieve this, grid connectivity is combined with prior model information within an adjacency metric. The adjacency information is then transformed to the spectral domain for construction of the parameterization basis. The definition of cell adjacency is general for any grid geometry and type of prior model heterogeneity; therefore, the adjacency-based parameterization retains the same flexibility in application as the GCT. The inclusion of prior information into the parameterization can be increased when prior information is well informed, and on the contrary when prior information is un-informed or too uncertain, the adjacency measures that control the influence the prior incorporation can be relaxed to the point that the transform basis reverts to the GCT basis, or to an effectively model-independent parameterization. Several examples of this flexibility are demonstrated, and guidelines are proposed for construction of the parameterization basis for generic geologic heterogeneity. In history matching implementation, the parameterization is shown well suited for application in an adaptive multiscale workflow, and applications are presented that show the strengths as well as limitations of the parameterization.

Section 6 concluded this dissertation with a summary of the key results of the research developments and applications in **Sections 2** though **5**. Recommendations and proposals for further research, extending from the concepts presented in **Section 5**, are also presented.

2. THE DISCRETE COSINE TRANSFORM PARAMETERIZATION: ADAPTIVE MULTISCALE HISTORY MATCHING*

2.1 Summary

History matching problems are typically underdetermined and are at once confronted with the problems of solution non-uniqueness, instability, and the requirement to both reproduce field observations and provide reliable forecasts. We address these challenges with an adaptive multiscale history matching formulation that parameterizes the reservoir properties in the frequency domain. The geologic model updating is carried out by successively increasing the level of detail up to a spatial scale sufficient to match the observed data. Our method begins by constructing a coarse representation of the field using the lowest-frequency components of its discrete cosine parameterization. This substantially reduces the number of unknown parameters to be resolved during history matching, leading to a better posed inverse problem. A gradient-based minimization is then performed to match the production data. Next, the updated model is incrementally refined in the frequency domain and the minimization is repeated until the data misfit is reduced below a pre-specified criterion or until no further improvements are observed. During minimization, components of the gradient insensitive to production information are removed by a truncated singular value decomposition (TSVD), facilitating iterative convergence and providing additional regularization. In this manner a balance is achieved between parameter reduction which is required for stability, and the spatial resolution of heterogeneity required for reproduction of the production history. The low-frequency approximation of the permeability field helps to honor geologic continuity and is particularly suited for resolving the large-scale heterogeneity that has a dominant influence on the field-scale flow regime and production response. Applications of the

---

*Part of this section is reprinted with permission from "An Adaptively Scaled Frequency-Domain Parameterization For History Matching" by Bhark, E., Jafarpour, B., Datta-Gupta, A., 2011. Journal of Petroleum Science and Engineering. 75 (3-4), 289-303. Copyright 2011 by Elsevier.

approach are demonstrated using the SPE10 and PUNQ-S3 models and involve waterflood history matching with water-cut and bottom-hole pressure data. Our results show that the principle geologic features of the reference field are adequately resolved only if we begin at low resolution. As the resolution is iteratively increased, the history match is improved while the TSVD step removes insensitive parameter combinations thereby decreasing the likelihood of convergence to less plausible local minima. Notably, in all our applications an adequate history match is achieved using less than one percent of the original parameter dimension, which leads to increased solution stability and computational savings in history matching large geologic models.

2.2 Introduction

It is understood that the integration of production data into a high-resolution, heterogeneous reservoir model involves an underdetermined and ill-posed inverse problem that can result in non-unique and potentially unstable solutions. In this section, these challenges are at once addressed using a multiscale, frequency-based parameterization of the calibrated heterogeneity in an adaptive history matching workflow in which the scale is refined to a level of spatial detail justified by the data content. Our approach is motivated by the previous development of adaptive approaches to parameterization in solving subsurface inverse problems for petroleum reservoirs and groundwater models. In this context, the fundamental role of parameterization is to describe the geologic model by a reduced number of parameters to remove parameter redundancy while retaining important features of the model.

A review of adaptive multiscale parameter estimation algorithms was presented in **Subsection 1.2.2**. To reiterate the key points of this discussion, the purpose of adaptive refinement steps is to improve the parameter set convergence on a cost function surface that increases in dimension at each refinement step as the set iterates toward a local minimum. Adaptive multiscale approaches, as a rule, rescale the geologic model in the spatial domain, sequentially coarsening and/or refining global and local regions of the

model based on a pre-defined measure. We posit, and aim for in this analysis, that a comprehensive and practical multiscale history matching algorithm should incorporate the following three elements:

(1) The ability to integrate diverse sources of data available for reservoir parameter estimation including dynamic data (e.g., production data), hard data (e.g., well log data) and qualitative geologic interpretation.

(2) The capability to adaptively refine regions of the model based on sensitivity to the aforementioned data.

(3) A termination criterion that achieves the level of regularization at which the estimable parameters cannot be resolved by the data.

In this section (**2**) we introduce a data integration approach that is consistent with varying levels of uncertainty in the prior model by characterization of the reservoir model in the frequency domain via the discrete cosine parameterization. Similar to the above methods, the inverse problem is implicitly regularized by reducing the estimable property field to a coarse or low-frequency approximation, and then is adaptively refined to a scale at which model and data resolution are balanced as indicated by an identifiability metric related to parameter resolution. The compression power of the transform permits a description of the model with a significantly reduced number of parameters without incorporating irresolvable fine-scale detail. This decreases the likelihood of converging to a local minimum related to high-frequency features and also permits additional regularization using efficient singular value decomposition of the parameter sensitivity matrix. The cosine parameterization is further able to enforce continuity, when warranted, in geologic features during model updating without introducing unnatural (e.g., blocky) model descriptions that typically result in spatial multiscale methods. The approach in general is applicable with and without prior models. That is, the method can be applied to estimate unknown global features or to minimally update a reservoir model that is already well-defined from other data sources.

Last, the method is directly amenable to uncertainty analysis when we consider finer levels of detail that cannot be resolved by observations. One way to achieve this goal is to use a null space projection analysis. At the solution, local uncertainty can be superimposed on the larger-scale reservoir model, within a Monte Carlo framework, in order to quantify the local uncertainty around the minimum into which the solution has converged. The entire method can be incorporated in a straightforward workflow using a commercial simulator.

In the following subsections, the history matching workflow is first outlined at a high level and then individual components of the workflow and their implementation are described in detail. The method is demonstrated with a synthetic case where each step of the workflow is presented and its utility highlighted. Following a two dimensional example, we apply the method to the top five layers of the SPE10 reservoir model to demonstrate the effectiveness of the multiscale parameterization approach for solving large-scale ill-posed inverse problems. Finally, we history match the PUNQ-S3 reservoir model to both demonstrate the practicality of the method and compare our results with those from several other papers. We also demonstrate the efficacy of our approach to local uncertainty analysis in a production forecast.

2.3 Methods

This subsection presents the primary steps of the proposed history matching workflow (see the figure on page 31). The method follows a deterministic formulation in which a single prior or conceptual geologic model is constructed using all available data and then updated via history matching as production data become available. In our formulation, the history match consists of minimizing a cost function, presented below in **Subsection 2.3.2**, involving the misfit between measured and simulated data by tuning one or more estimable reservoir parameters, permeability and porosity in our applications. When a standard grid-based spatial description of parameters is used the inverse problem is ill-posed and requires regularization in the form of prior knowledge. Common forms of

prior information typically used include explicitly defined geologic property models generated from geostatistical integration of static data, direct or indirect measurements of the parameters (e.g., hard data at well locations), or spatial constraints based generally on natural geologic continuity, e.g., a smoothness term (Carrera, 1987; Tikhonov and Arsenin, 1977; Yeh, 1986). In the approach we have adopted, a deterministic least-squares formulation penalizing deviation from the dynamic and static (when they exist) data misfit is used (Datta-Gupta and King, 2007; McLaughlin and Townley, 1996; Menke, 1989; Tarantola, 2005). Here, inclusion of prior knowledge for regularization is completed implicitly by providing a coarse description of the reservoir model via parameterization. This approach avoids subjective weighting of a prior model term explicitly defined in the cost function (Doherty, 2003; Feng and Mannseth, 2009; Parker 1994).

It is useful to appreciate an important and powerful property of the discrete cosine transform (DCT) parameterization. Generation of the DCT basis does not require, but can benefit from, prior knowledge about the property field that includes all static and geologic information. Being a generic image compression transform (Gonzales and Woods, 2002), the DCT basis is constructed simply from harmonics of the cosine function (without needing prior knowledge) and is capable of reducing a significant number of spatial parameters while preserving the essential information in a model. Therefore, the prior description may vary from completely uninformed to well-informed and, together with production data, determines the initial level of parameter compression required for model updating. Typically, as more geologic information is available, higher-frequency detail in the estimable property is better resolved (assuming sufficient data resolution) and less DCT compression is required. Independent of the level of parameter compression, the method is amenable to uncertainty analysis of the updated geologic properties at all spatial scales.

The workflow in Fig. 2.1 (1) begins with the definition of the initial geologic model or estimable parameter set. In (2) the parameter set is redefined in the frequency domain

using the DCT and its low-frequency approximation is constructed by the truncation of high-frequency parameters in the transform domain. The level of truncation is related to knowledge and confidence in the prior model and also to sensitivity of the production data to the DCT coefficients. At the current spatial scale or level of detail, the field is next history matched in (3)-(5) using an iterative gradient-based scheme. The transform between the spatial and frequency domains is performed at each iteration to generate simulated observations during the history matching. Also during each iteration, the inversion is stabilized by re-definition of the parameter sensitivity matrix in its compact form (4). When a minimization stopping criterion is achieved in (5), we test in (6) if either data misfit satisfies a tolerance criterion or if the transform parameters are no longer able to be resolved by the production data, the latter step also evaluated against a metric. If the answer to either is yes, the workflow is complete. If the answer to both is no then the next highest harmonic or level of detail is added to the parameter set in the frequency domain and the geologic model is returned to gradient-based minimization. The following subsections now explain each step.

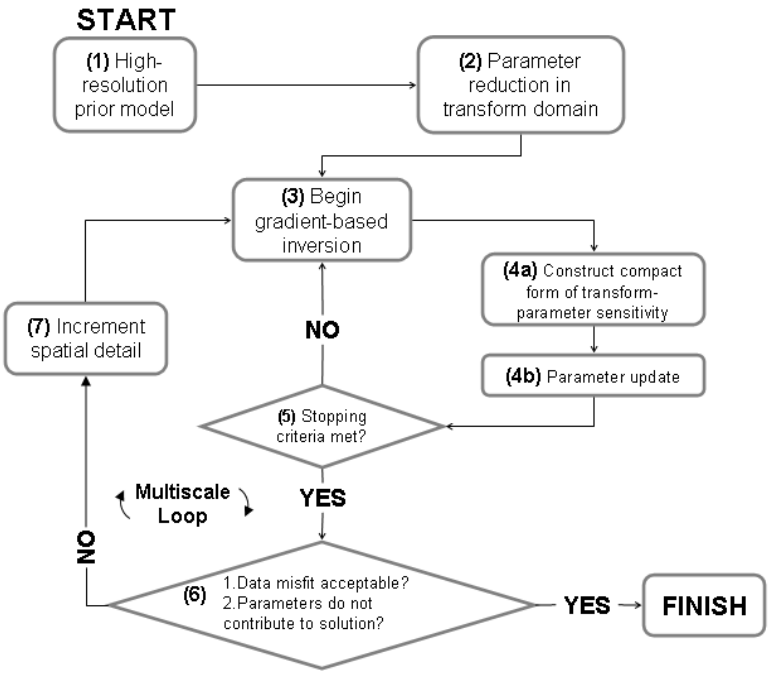

Fig. 2.1. Flowchart of the adaptive multiscale history matching workflow.

2.3.1 Discrete Cosine Parameterization

The DCT is a Fourier-based transform designed for signal decorrelation (Britanak et al., 2007) and commonly used for data compression (Gonzales and Woods, 2002). Jafarpour and McLaughlin (2008) recently introduced the DCT for parameterization of spatially-distributed reservoir properties and have applied it to production data integration. When characterized in the frequency domain using the DCT, high-frequency components of the reservoir properties insensitive to production data can be removed from the estimation problem for a considerably high level of parameter reduction. Thus, the primary strengths of this parameterization reside in its ability to reduce the model size while retaining larger-scale geologic features, along with the benefits associated with frequency domain analysis. This section introduces the DCT with a focus on its suitability for history matching.

Any practical transform-based parameterization method should be computationally fast, maximize information content in the fewest number of transform variables and have uncorrelated variables in the transform domain. Transformation by the theoretical principle components analysis (PCA), i.e., when the theoretical covariance matrix for the model is perfectly known, is optimal in the sense that it yields the lowest root-mean-square error among all K-term linear approximations (Britanak et al., 2007); however, the transform is performed on the parameter covariance matrix which is rarely known in practice and the transformation basis is computationally expensive to construct for large models as well as misleading if prior model assumptions are incorrect (Jafarpour and McLaughlin, 2009). Also, complex geologic features often cannot be adequately described using a two-point correlation function. In pursuit of a generic (predetermined), input-data independent and decorrelating basis for image compression, the DCT basis was initially developed to approximate the PCA basis for a first-order stationary Markov process, representative of an auto-regressive process (Ahmed et al., 1974). Consequently, the analytical form of the DCT basis is independent of the model to be parameterized and is preconstructed off-line, and only once, for a given history-matching

problem. Unlike PCA, it does not require the often uncertain prior assumptions required to construct a parameter covariance matrix.

The DCT basis consists of real cosine functions, so the complexity associated with the imaginary components of the discrete Fourier transform (DFT) is avoided. For a two-dimensional $N_x \times N_y$-gridblock reservoir property field where each gridblock represents a single estimable parameter $u(x,y)$, the two-dimensional DCT $v(r,s)$ has the following form (Gonzales and Woods, 2002):

$$\mathbf{v}(r,s) = \alpha(r)\alpha(s)\sum_{x=0}^{N_x-1}\sum_{y=0}^{N_y-1}\mathbf{u}(x,y)\cos\left[\frac{(2x+1)r\pi}{2N_x}\right]\cos\left[\frac{(2y+1)s\pi}{2N_y}\right] \tag{2.1}$$

for $r = 0, 1, 2, \ldots, N_x\text{-}1$ and where $\alpha(r=0) = \sqrt{\frac{1}{N_x}}$ and $\alpha(r\neq 0) = \sqrt{\frac{2}{N_x}}$, with the same form for N_y and $\alpha(s)$ (note for later presentation that the variable t is used to denote cosine harmonics in the vertical orientation). Just as the one dimensional transform is extended to two dimensions in Eq. (2.1) as the product of cosine functions, the transform is readily extended to three dimensions by including a third cosine term. However, using the separability property of the DCT basis, transformation of a multidimensional signal can be computed as a sequential application of one-dimensional transformations. The full-rank transform is lossless, resulting in an equivalent number of transform variables $v(r,s)$, or DCT coefficients, as the dimension of the original signal. However, a significantly reduced parameterization can be obtained when high frequency detail coefficients are eliminated. The retained DCT coefficients in the parameterization, with a value corresponding to the amplitude of its associated cosine function, are the estimable parameters in the transform domain.

For an N-length signal, direct construction of the basis by Eq. (2.1) requires N^2 operations which, although costly, is acceptable because it is computed only once for a given parameter set. The DCT bases may also be computed with a fast Fourier transform

(FFT) in approximately $N\log_2 N$ operations. When the geologic model is sufficiently large, on the order of tens-of-thousands to millions of gridblocks, that the complete basis exceeds storage capacity, then the separability property of the DCT can be used to perform the transform one dimension at a time for a reduction in memory requirement. However, rather than constructing the complete basis, if only a few of the leading basis functions (from low to high frequency) are required for parameterization, then the analytical solution in Eq. (2.1) can be used to construct only those relevant functions for a considerable reduction of computational complexity.

In this analysis the DCT basis is applied in its matrix form $\mathbf{\Phi}$, where **v** and **u** are defined above and are represented here as vectors. The cosine basis functions correspond to the columns of $\mathbf{\Phi}$ and are orthogonal. That is,

$$\mathbf{v} = \mathbf{\Phi}^{\mathrm{T}}\mathbf{u} = \mathbf{\Phi}^{-1}\mathbf{u} \Leftrightarrow \mathbf{u} = \mathbf{\Phi}\mathbf{v}\,. \tag{2.2}$$

For history matching, parameter reduction is performed by removing from the estimation problem those basis vectors (or columns) of $\mathbf{\Phi}$ that correspond to high-frequency cosine functions to which the production data are, in general, insensitive, resulting in the truncated basis $\tilde{\mathbf{\Phi}}$. Fig. 2.2 shows a two-dimensional representation of the sixty-four DCT basis vectors that would be used to transform an 8 × 8-gridblock reservoir. The basis images are customarily arranged according to their orientation and frequency in a descending order from upper left to lower right in the 2D case (e.g., [Gonzales and Woods, 2002; Jafarpour and McLaughlin, 2009]). The inclusion of only lower-frequency bases $\tilde{\mathbf{\Phi}}$ in Eq. (2.2) results in better preservation of geologic continuity and reduces the dimension of estimable parameters in **v**.

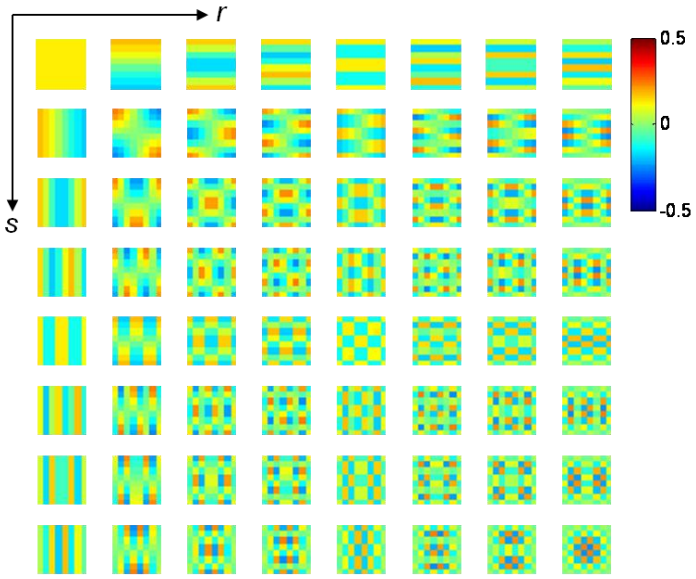

Fig. 2.2. DCT basis images for a 2-D 8 × 8-gridblock model. The bases are arranged according to their spatial orientation (e.g., vertically, horizontally) and from low to high frequency in a descending order from upper left to lower right.

2.3.2 Multiscale Parameter Estimation

The utility of our approach to history matching is in the selective identification of the DCT basis functions required to characterize the geologic model. The first step is to parameterize the initial model by a small set of the lowest-frequency basis vectors in each spatial orientation. This initial level of truncation is determined from knowledge and confidence in the prior model. At the one extreme of a completely uninformed prior it may be reasonable to initially characterize the model by only a single DCT coefficient, corresponding to the constant basis vector (upper-left corner of Fig. 2.2) that would capture the global mean of the field after an inversion. At the other extreme of high confidence in the prior model, truncation of the initial model is performed only to the extent that some measure of dynamic behavior is honored given the corresponding reduction of spatial detail. Both types of approach are demonstrated in this paper.

Once defined, the low-frequency approximation of the initial geologic model is updated by minimization of an objective function $J(\mathrm{v})$ that considers the squared l_2-norm of nonlinear dynamic data misfit as well as static data misfit related to observations at gridblocks, or

$$J(\mathbf{v}) = \left\| \mathbf{C}_d^{-1/2} \left(g(\mathbf{\Phi}_t \mathbf{v}) - \mathbf{d}_{obs} \right) \right\|_2^2 + \mu \left\| \mathbf{C}_m^{-1/2} \left(g(\mathbf{\Phi}_w \mathbf{v}) - \mathbf{d}_{static} \right) \right\|_2^2 \qquad (2.3)$$

where g(**u**) is the nonlinear model relating parameters to observations, $\mathbf{d}_{obs}$ is the dynamic data vector, and $\mathbf{C}_d$ and $\mathbf{C}_m$ are the weight matrices that determine the relative importance of the elements in the observation and model vectors, respectively (note that we have adopted a notation that is consistent with the probabilistic formulation of the problem where these weights correspond to covariance matrices). When multiple data types with different units and magnitudes are considered in Eq. (2.3), for example water production rate and well pressure, the weights along the diagonal of $\mathbf{C}_d$ are set equal to the datum variance of the corresponding observation misfit. The actual variance per datum is unknown in practice and may have multiple sources; therefore, in this analysis we assume that the variance associated with each datum is equal to the total data variance corresponding to the observation type. The matrix $\mathbf{\Phi}_t$ is the truncated DCT basis, $\mathbf{d}_{static}$ is the static data vector corresponding to measurements at individual gridblocks, $\mathbf{\Phi}_w$ contains the rows of the truncated basis $\mathbf{\Phi}_t$ corresponding to those gridblocks, and μ assigns the relative importance to the static misfit term. Note that in our examples a misfit term penalizing deviation from the prior model is not included, for reasons presented in the following section.

When $J(\mathbf{v})$ converges at the current scale and data misfit remains unacceptable, the parameter set is increased by adding those DCT coefficients corresponding to the next highest frequency in each orientation (i.e., x, y and z directions). That is, the next-highest level of spatial detail is added to the parameter set. In a two-dimensional problem, this is equivalent to adding one row and one column of basis functions (as in

Fig. 2.2) to $\mathbf{\Phi}_t$ and $\mathbf{\Phi}_w$ in Eq. (2.3). The introduced coefficients are assigned a small nonzero value to permit continuous differentiation and do not impact data misfit until subsequent iterations when the magnitude of sensitive coefficients increase.

We recognize that the addition of higher frequency basis vectors can be alternatively implemented through a selective procedure, where sensitivity information or solutions from previous iterations are used to guide the basis element selection, and have considered three such approaches. One alternative presumes that a space-frequency relationship exists between the transform parameters, as exists de facto for the variants of the discrete wavelet transform (Strang and Nguyen, 1996), where higher-frequency parameters are recursively related to lower-frequency parameters in a given spatial orientation. Such an approach has been empirically applied for image compression using the DCT (Xiong et al., 1996); however, we did not observe an exploitable spatial relationship in the DCT coefficient spectrum of reservoir parameter fields. A second alternative simply involves a pre-minimization screening procedure in which newly incorporated basis functions are added to the model description only if shown sensitive in relation to data misfit. This approach requires definition of a subjective sensitivity threshold and can be an ambiguous indicator of parameter refinement in the case of sensitivity dependence on solution location. We have observed that exclusion of basis functions using a sensitivity cutoff computed at a single location on a nonconvex response surface may fail to identify important basis functions at later iterates. A third approach to adaptive parameterization takes advantage of the potentially compact or "sparse" model description in the transform domain. Rather than sequentially incorporating spatial detail into the model, all levels of detail or all parameters are evaluated simultaneously using a regularization term that effectively promotes the removal of redundant parameters, as implied by available observations, from the estimation problem (Jafarpour et al., 2010; Li and Jafarpour, 2010). This method is currently being researched.

In consideration of these alternatives, as a robust solution we have added the basis elements uniformly with respect to spatial orientation and used the truncated singular value decomposition (TSVD) to implicitly incorporate more sensitive basis vectors, ensuring a sensitivity matrix of full column rank by removing insensitive parameter combinations. Then, after improvement in the level of spatial detail, $J(\mathbf{v})$ is again reduced in an inversion. We refer to each step of spatial refinement and minimization as a single multiscale loop (Fig. 2.1). The cycle is repeated until data misfit is acceptable or until the parameters can no longer be resolved or identified by the observation data. To appreciate the basis upon which we conceptualize parameter identification the minimization method must first be presented.

2.3.3 Numerical Parameter Estimation

During inversion within a multiscale loop, data misfit in $J(\mathbf{v})$ is iteratively minimized using the gradient-based BFGS quasi-Newton method (Nocedal and Wright, 2006). The gradient with respect to parameters in the physical or spatial domain is constructed using the corresponding parameter sensitivities made available from a commercial reservoir simulator using its built-in adjoint method (Schlumberger, 2009). The gradient is computed with respect to parameters in the DCT domain by the chain rule of differentiation as follows:

$$\begin{aligned} J(\mathbf{v}) &= J_1 + J_2 \\ &= \left(g\left(\mathbf{\Phi}_t \mathbf{v}\right) - \mathbf{d}_{obs}\right)^{\mathrm{T}} \mathbf{C}_d^{-1}\left(g\left(\mathbf{\Phi}_t \mathbf{v}\right) - \mathbf{d}_{obs}\right) + \mu\left(\mathbf{\Phi}_w \mathbf{v} - \mathbf{k}_{static}\right)^{\mathrm{T}} \mathbf{C}_m^{-1}\left(\mathbf{\Phi}_w \mathbf{v} - \mathbf{k}_{static}\right) \end{aligned}$$

$$\begin{aligned} \frac{dJ}{d\mathbf{v}} &= \frac{\partial J_1}{\partial \mathbf{u}}\frac{\partial \mathbf{u}}{\partial \mathbf{v}} + \frac{\partial J_2}{\partial \mathbf{u}}\frac{\partial \mathbf{u}}{\partial \mathbf{v}} = \frac{\partial J_1}{\partial \mathbf{u}}\frac{\partial\left(\mathbf{\Phi}_t \mathbf{v}\right)}{\partial \mathbf{v}} + \frac{\partial J_2}{\partial \mathbf{u}}\frac{\partial\left(\mathbf{\Phi}_w \mathbf{v}\right)}{\partial \mathbf{v}} \\ &= 2\left(g(\mathbf{u}) - \mathbf{d}_{obs}\right)^{\mathrm{T}} \mathbf{C}_d^{-1}\left(\frac{\partial g(\mathbf{u})}{\partial \mathbf{u}}\right)\mathbf{\Phi}_t + 2\mu\left(\mathbf{u}_w - \mathbf{d}_{static}\right)^{\mathrm{T}} \mathbf{C}_m^{-1}\mathbf{\Phi}_w \end{aligned} \quad . \tag{2.4}$$

Because the inversion at a given spatial scale is based on data misfit reduction alone, it is necessary to examine the conditioning and ill-posedness of the inverse problem to assess

solution stability and uniqueness. The solution may in reality converge to a non-optimal local and potentially unstable minimum. Further, when using a gradient-based scheme, insensitive parameter combinations and also correlated parameters should be removed before calculating the gradient direction and parameter update step size. We apply two approaches of implicit regularization to simultaneously address these issues.

First, the DCT-based reduction of the parameter vector length improves ill-posedness and stability by establishing a nearly even- if not overdetermined inverse problem. The low-frequency or lower-order approximation of the model may result in solution bias; however, the tradeoff is that the solution is more likely unique (Aster et al., 2005; Vasco et al., 1997) and that a finer description of the solution may not be justified given the spatially averaged nature of flow observations. Further, the solution is implicitly stabilized by the superposition of low-frequency cosine functions, weighted by the estimable DCT coefficients, as described in the preceding subsection.

Second, insensitive parameter combinations are implicitly removed from the inversion by using the compact form of the sensitivity matrix, constructed from TSVD, prior to its implementation in the gradient in Eq. (2.4). This is performed at each iteration as the sensitivity matrix is updated. If the singular value decomposition (SVD) of the weighted sensitivity matrix is

$$\begin{aligned}\mathbf{C}_d^{-1/2}\mathbf{G} = \mathbf{U}\mathbf{S}\mathbf{V}^T &= \begin{bmatrix}\mathbf{U}_1 & \mathbf{U}_2\end{bmatrix}\begin{bmatrix}\mathbf{S}_1 & \mathbf{0}\\ \mathbf{0} & \mathbf{S}_2\end{bmatrix}\begin{bmatrix}\mathbf{V}_1^T\\ \mathbf{V}_2^T\end{bmatrix} \\ &= \mathbf{U}_1\mathbf{S}_1\mathbf{V}_1^T + \mathbf{U}_2\mathbf{S}_2\mathbf{V}_2^T\end{aligned} \tag{2.5}$$

where $\mathbf{G}$ is the sensitivity matrix, then the compact and more stable (well-conditioned) representation of it is $\mathbf{U}_1\mathbf{S}_1\mathbf{V}_1^T$. A condition number of 100 is specified to distinguish the model and null spaces $\mathbf{V}_1$ and $\mathbf{V}_2$, respectively. Although impractical to perform at each iteration when the parameter dimension is large, the reduced DCT parameterization makes Eq. (2.5) feasible.

2.3.4 Adaptive Parameter Estimation

The adaptive inclusion of higher-frequency DCT coefficients during successive multiscale loops is based on parameter identifiability from the data; there is a level of spatial detail beyond which the coefficients become insensitive and contribute minimally to the solution. Even worse, ad-hoc perturbation of insensitive DCT coefficients can lead to artifact features (e.g. high frequency oscillations) in the solution that may not be geologically plausible. The sensitivity threshold is identified from analysis of the SVD of the weighted parameter sensitivity matrix in Eq. (2.5), per iteration, that describes the linear change in simulated observations with respect to the estimated DCT coefficients. The columns of $\mathbf{V}_1$ define the orthogonal basis for the model space, or resolvable linear parameter combinations, and the columns of $\mathbf{V}_2$ define the orthogonal basis for the null space. The delineation between model and null space is based on a specified condition number (that may differ from that used in the TSVD application described in the preceding subsection). The dominant components of the columns of $\mathbf{V}_1$ indicate the most sensitive parameter combinations per iteration. Accordingly, the ability to locally resolve each individual coefficient can be quantified by an identifiability index, following the nomenclature of Doherty (2008), defined as

$$I_i = \sum_{i=1}^{p} \mathbf{V}_{1,i}^2 \tag{2.6}$$

or the sum of squares of the *i*th component across the standardized basis vectors spanning $\mathbf{V_1}$. The minimum and maximum possible values of I_i are 0.0 and 1.0, respectively. When for parameter *i* the identifiability equals 1.0, then that parameter has a zero projection onto the model null space and is therefore perfectly resolved by the data, and any error associated with the estimate of parameter *i* is from data noise alone (Aster et al., 2005). During minimization, when the index drops below some threshold at a given scale and becomes nearly constant, the inversion is terminated and the parameter solution achieved.

2.3.5 Uncertainty Analysis

The adaptive refinement in spatial details ends when the parameter set loses sensitivity to observation data and the existing parameter set corresponds to a converged (in general local) solution. Levels of detail at finer spatial scales exist in the true (unknown) solution but can only be characterized as uncertainty relative to the observation data available. We propose to add fine scale or high-frequency detail representative of local uncertainty to the global solution. This is accomplished within a Monte Carlo framework and in a manner insensitive to data misfit in order to assess parameter non-uniqueness and ultimately production uncertainty. The analysis is comparable to local perturbations to characterize the 'valley' of the objective function minimum into which the solution has converged.

A review of approximation-based approaches to solution uncertainty evaluation in nonlinear inverse problems is presented in Oliver et al. (2008). Within the comprehensive framework presented, our approach is similar to methods in which a stochastic component of estimation error is added to a smooth model solution that satisfies the data, e.g., Linearization about the Maximum A Posterior model (LMAP). This enables the generation of multiple conditional realizations for evaluation of solution non-uniqueness and production uncertainty. The estimation error is constructed as a linearized approximation using the sensitivity matrix at the solution, or is based on a Taylor expansion in the locality of the global estimate. Our approach similarly utilizes a linear error approximation to assess solution uncertainty. However, we introduce error at a spatial scale finer than the solution and that cannot be resolved by the data, or stated differently, by adding high-frequency parameter variation onto the lower-frequency solution. Conditioning is accomplished without additional data-misfit minimization by adding only the null space component of model error to the solution (Tonkin and Doherty, 2009).

The model null space is defined by linear parameter combinations insensitive to the data and orthogonal to the solution space (Aster et al., 2005), so parameters reintroduced within this subspace do not deteriorate the objective function barring two exceptions that are cited below. At the solution, the weighted sensitivity matrix $\mathbf{C}_d^{-1/2}\mathbf{G}$ is computed where the number of columns in $\mathbf{G}$ reflects the dimension of the lower-frequency solution $\mathbf{r}$ plus the number of high-frequency coefficients being introduced. It is important to understand that the sensitivities are computed at the solution using this expanded parameter set. The newly-introduced DCT coefficients are assigned a zero value, so the expanded solution set is effectively identical to that of the lower-dimensional set. The model and null space are then identified, and local uncertainty is introduced to the solution by adding to it the null space projection of the high-frequency coefficients. In other words, higher-frequency cosine functions are being reintroduced to the geologic model in a manner that is consistent with data misfit and lower-frequency features. If $\mathbf{r}_{hf}$ is the column vector of high-frequency coefficients introduced and $\mathbf{r}_{cf}$ is the update vector expanded to the full parameter dimension, i.e., $\mathbf{r}_{cf} = [\mathbf{0}^{\mathrm{T}}\ \mathbf{r}_{hf}{}^{\mathrm{T}}]^{\mathrm{T}}$ where the zero vector has the solution dimension length($\mathbf{r}$), then the null space projection $\mathbf{r}_{proj}$ is computed as

$$\mathbf{r}_{proj} = \mathbf{V}_2\mathbf{V}_2^T\mathbf{r}_{cf} \tag{2.7}$$

and the final updated solution $\mathbf{r}_{update}$ is

$$\mathbf{r}_{update} = \left[\mathbf{r}^T\ \ \mathbf{0}^T\right]^T + \mathbf{r}_{proj} \tag{2.8}$$

where the zero vector in Eq. (2.8) has dimension length($\mathbf{r}_{hf}$).

The Monte Carlo approach involves the generation of multiple, randomly-populated realizations of $\mathbf{r}_{hf}$ to compute multiple updated models $\mathbf{r}_{update}$. The components (or DCT coefficients) of $\mathbf{r}_{hf}$ are populated by sampling from coefficient distributions, which may or may not be known, and may also honor the correlation between coefficients if known.

The implication that data misfit will not deteriorate by the addition of these parameter combinations sometimes fails in practice when the singular value spectrum decreases gradually and/or when the objective function surface is locally nonlinear at the solution in one or more dimensions. Practical details of this method are presented below for a forecast uncertainty analysis in the PUNQ-S3 case.

2.4 Applications

We demonstrate the application and advantages of the adaptive multiscale approach using two synthetic cases. First, we history match permeability in both a single layer (2D) model and five-layer (3D) model using the SPE10 reservoir to substantiate the approach and chronologically present the methodology in detail. These cases are also intended to show the utility of the method when the prior model is either ill- or well-informed. Next we illustrate the practicality of the approach using the PUNQ-S3 reservoir model which replicates a mature field case where the data are more varied and prior geologic knowledge is better understood. Here we also demonstrate the approach to local uncertainty analysis in a production forecast. The model equations for all cases describe two-phase (oil, water) or three-phase (oil, water, gas) incompressible, immiscible flow with fluid behavior given by the black-oil equations using the ECLIPSE simulator (Schlumberger, 2009).

2.4.1 SPE10 Top Layer

A history match is performed on a two-dimensional, 13,200-gridblock isotropic permeability field under a two-phase blackoil waterflood simulation with 15 injectors and 8 producers. The reference field, based on the SPE10 Model 2 (SPE Comparative Solution Project) top layer, and well pattern are shown in Fig. 2.3A. Using the reference field, a synthetic observation dataset is constructed consisting of injection-well bottom-hole pressures (BHP) and water and oil production rates measured at six time intervals over a 1,800-day production schedule. The history match is initiated with the permeability field in Fig. 2.3B which has correlation lengths similar to those of the

reference field but clearly different trends. Therefore, this case tests if the trends and continuity of geologic heterogeneity can be identified from production data when the prior is incorrect.

History matching begins with a coarse representation of the initial field as a result of low certainty in the prior model. The parameter dimension is reduced from 13,200 gridblock permeabilities to only 27 DCT coefficients based on a subjective, static measure of regional continuity. The approximated field, shown in Fig. 2.3C, is excessively smoothed to permit a large-scale update of the prior but retains its dominant heterogeneity features and continuity at the global scale. Fig. 2.4A shows rapid objective function convergence through minimization at the first multiscale loop and Fig. 2.4B shows the 27-parameter solution. At this frequency the large-scale features of the reference field are captured with better solution stability.

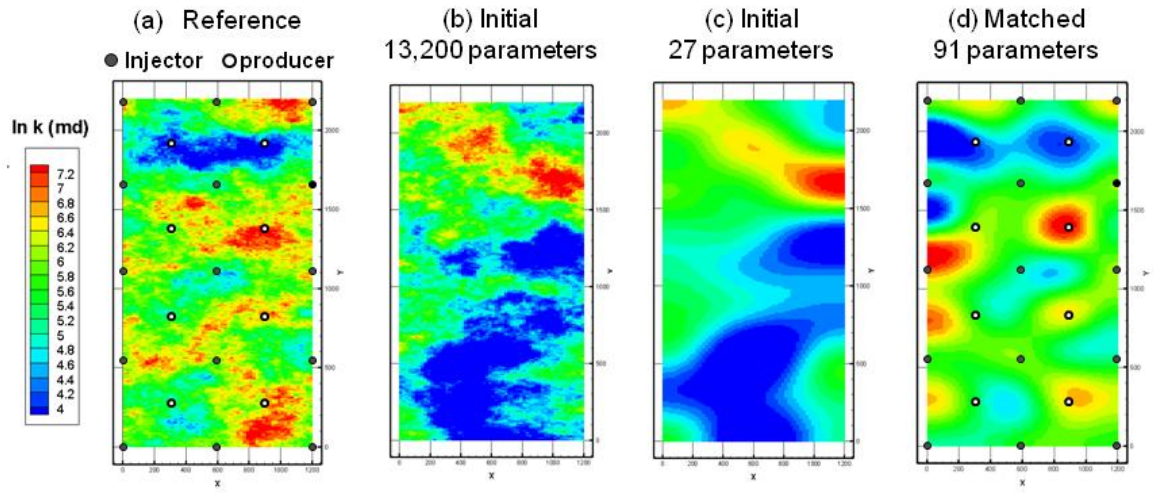

Fig. 2.3. The (a) reference permeability field based on the top layer of the SPE10 reservoir model, the (b) initial permeability field and (c) its coarse approximation used at the start of the history match, and the (d) history matched field. Grid block dimensions are $dx \times dy = 10 \times 20$ ft.

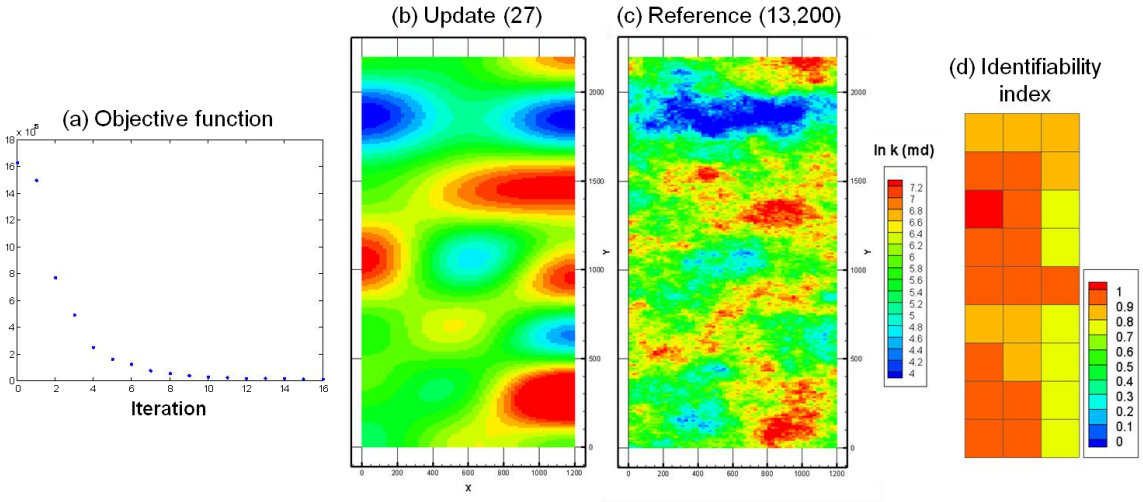

Fig. 2.4. History matching results at completion of the first multiscale loop. The permeability model in (b) is fully described by 27 DCT coefficients.

At the solution the parameter identifiability index in Fig. 2.4D is shown for each DCT coefficient. The spatial representation of each coefficient index corresponds to its spatial frequency as exemplified in Fig. 2.2. The indices are close to unity because the parameters are well resolved by the data and support further spatial refinement. An important comment is required at this point regarding the DCTs ability to de-correlate the permeability field as it is directly related to the stability and uniqueness of the solution even at this coarse level. Fig. 2.5 shows the individual coefficient contributions to the first 10 rows of matrix $\mathbf{V}_1$. No single coefficient or subset of coefficients defines any of the basis functions, but rather several coefficients contribute in each case. This indicates that the best-resolved coefficients (indicated by the identifiability index) are correlated and therefore cannot be uniquely determined during the inversion. Correlation also degrades the minimization scheme as the columns of $\mathbf{G}$ lose their linear independence and $\mathbf{G}^T\mathbf{C}_d^{-1}\mathbf{G}$ becomes singular, resulting in an ill-conditioned problem. This latter point is critical for convergence and demonstrates the utility of the TSVD step to enforce numerical stability in the presence of parameter correlation and data limitations. However, numerical stability imposed by TSVD does have a drawback. It

results in solution bias by way of spatial averaging of the initial model, which is itself already a low-frequency approximation by the reduced DCT parameterization. The bias results from the truncation of coefficient combinations of non-zero null space projection at the singular value threshold and reflects the tradeoff between parameter resolution and variability (Tonkin and Doherty, 2009; Vasco et al., 1997). As the number of retained singular values used to construct the compact sensitivity matrix increases, bias decreases while coefficient resolution and variability increase.

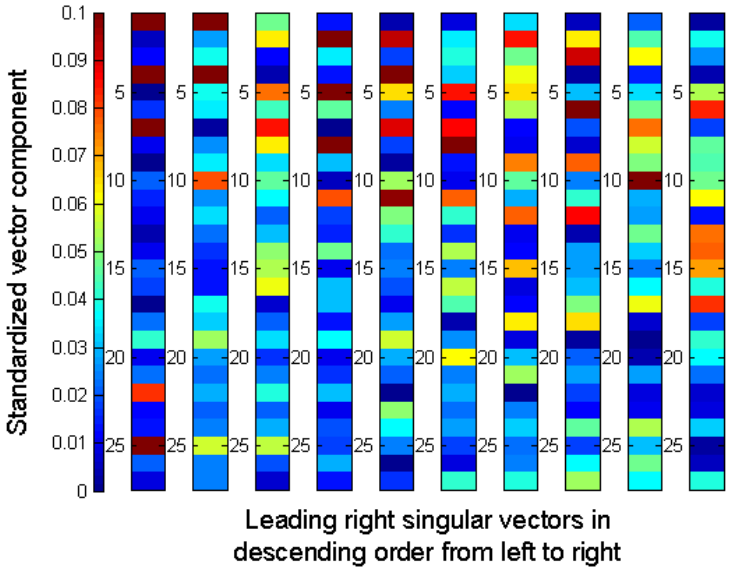

Fig. 2.5. Individual DCT coefficient contributions (vertical axis) on a scale of 0.0 to 1.0 to the first ten columns of the model space (horizontal axis) in V_1.

After inversion of the lowest-frequency model in Fig. 2.4B, four more levels of refinement up to a maximum of 91 DCT coefficients are used to achieve a history match. As per the workflow description, the parameter dimension is increased at each refinement step by adding the next highest cosine harmonic in each orientation (e.g., from $r \times s = 3 \times 9$ to 4×10 … to 7×13). Fig. 2.6 shows the objective function performance and final solution identifiability indices for three of the successive multiscale loops. As data misfit decreases and spatial scales become finer, parameter

sensitivity decreases. Notice that data misfit reduction also decreases through the refinement steps. An increase in the parameter dimension with refinement, in tandem with use of a gradient-based minimization scheme, increases the likelihood of convergence to a local minimum and accordingly reduces the magnitude of data misfit reduction at each successive step (as evidenced in Fig. 2.6). At the final loop, the balance between scale and identifiability is met; parameter identifiability indices corresponding to the highest-frequency DCT coefficients approach zero and data misfit is acceptable. Fig. 2.3D shows the matched permeability field and Fig. 2.7 the simulated versus observed pressures and rates. The matched field captures the spatial variability and continuity of the reference permeability trends with a parameter compression performance of >99 percent. The updates are also global and not focused at wells. When using an iterative descent technique, regions of the field sensitive to pressure tend to cluster around the point of observation (Vasco et al., 2000) and result in inconsistent geological features. We in fact observed that if the initial permeability field is first parameterized with 91 DCT coefficients, the same number required to achieve the multiscale solution, then the solution immediately converges to a local minimum and results in poor data misfit, and also results in model updates primarily near well locations that are inconsistent with geologic realism. The results presented, however, demonstrate that when initiating the history match with a lower-frequency parameterization and then refining with a multiscale approach, global updates are enforced even when sensitivities are locally clustered. Although the estimated field is smoothed, reflecting its low-frequency approximation, the minimal data misfits in Fig. 2.7 confirm that the data do not warrant the inclusion of finer detail in the field.

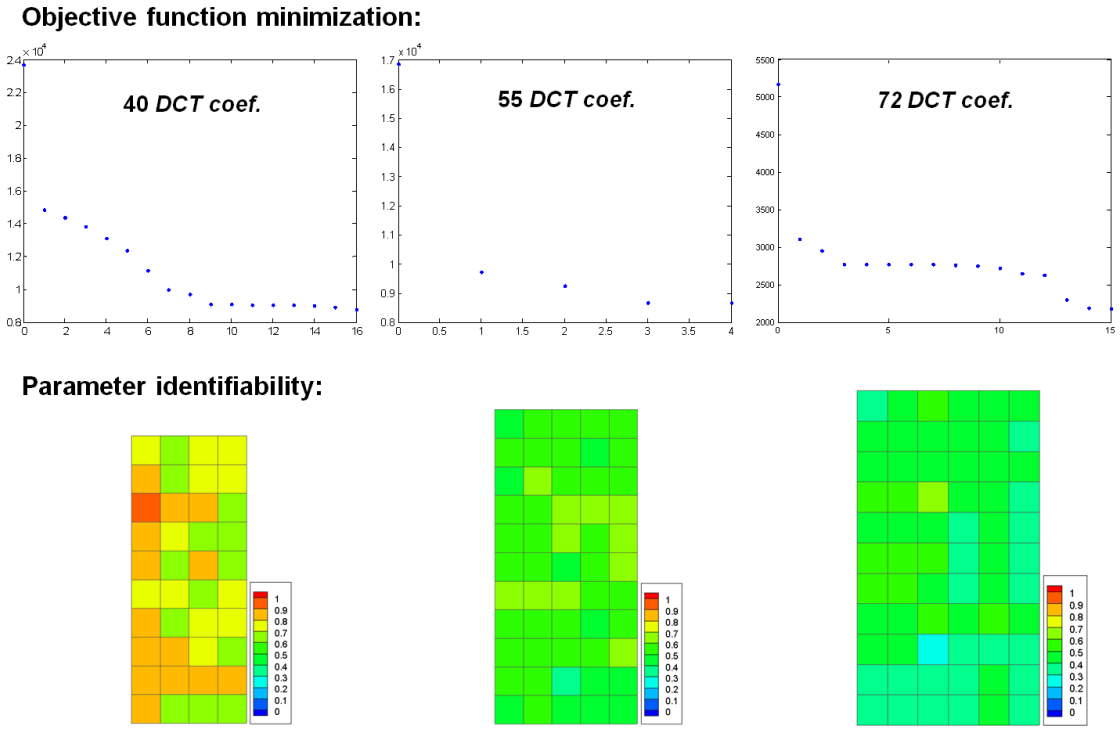

Fig. 2.6. Iterative data misfit minimization behavior and parameter identifiability for three of the five multiscale loops required to attain the history match.

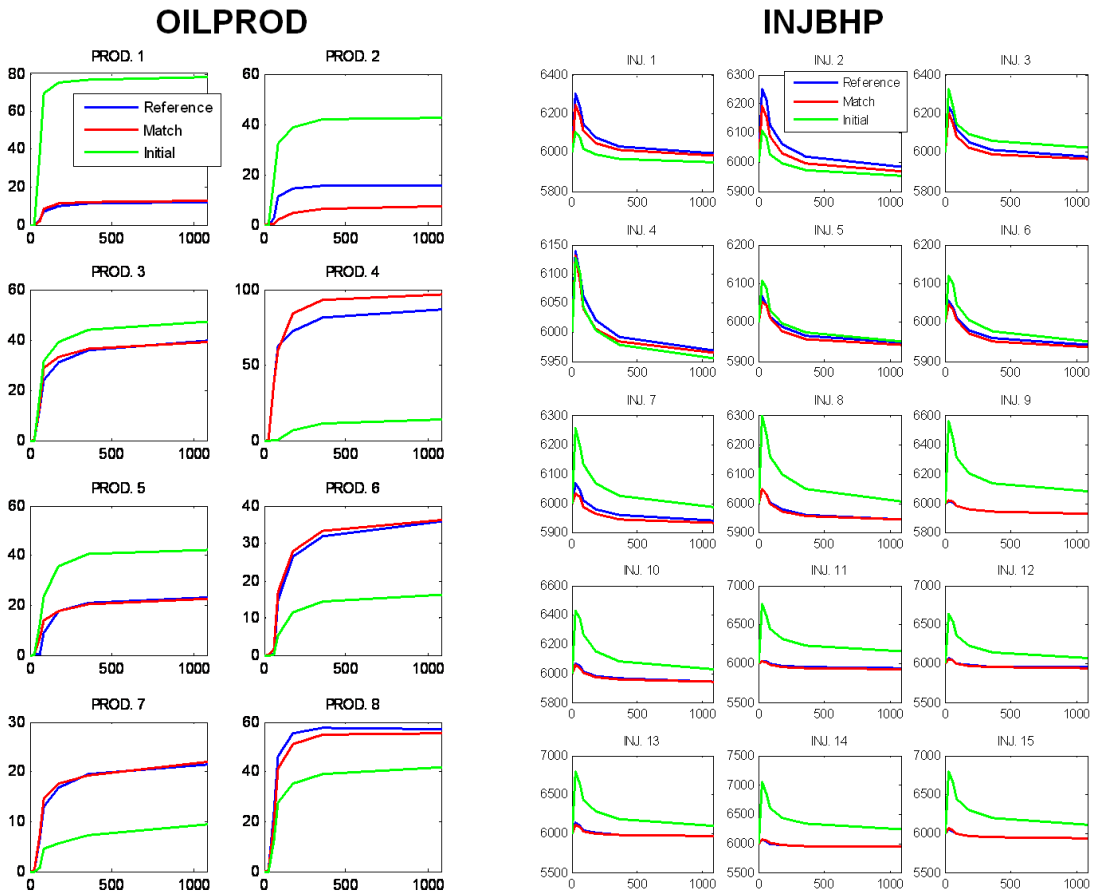

Fig. 2.7. Oil production rate and injection bottom-hole pressure at all wells corresponding to the simulated behavior for the initial and matched models and plotted against the observed responses.

2.4.2 SPE10 Five Layer Model

The previous analysis is further developed in a history match of a synthetic three-dimensional case using the top five layers of the SPE10 model. Results are briefly presented here to demonstrate the ability of the DCT parameterization and workflow to resolve geologic detail in the vertical as well as horizontal orientation. Also, the initial geologic model applied in the history match is a homogenous permeability field, so we test if geologic heterogeneity can be identified from production data when the prior is completely unknown and sufficient observation data are available.

The five-layer model has 66,000 gridblocks and corresponds with the same geologic description as the top layer presented above. The production and water injection schedules are also identical, as is the observation data set, with the sole difference being that injection borehole pressure is assumed measured at each of the layers rather than at the bottom hole alone. The vertical pressure gradient at injectors was required to resolve vertical property trends through the domain.

The reference permeability model is shown in Fig. 2.8A and the history matched field in Fig. 8B. An identical workflow as used for the top layer history match was repeated, only the initial model was compressed in three dimensions using $nr \times ns \times nt = 4 \times 10 \times 3$ or 120 DCT coefficients. Four multiscale loops were required to achieve the matched field using a total of $7 \times 13 \times 3$ or 273 coefficients for a compression performance of >99 percent. Within each loop the coefficient dimension was incremented in the horizontal plane only. During any of the multiscale refinement steps, the addition of the next level of detail in the vertical orientation would have considerably increased the parameter dimension, adding $nr \times ns$ parameters to the set. Therefore, it was determined from engineering judgment that additional vertical detail would be added to the parameterization only with the observed inability of horizontal refinement to match the data, which did not transpire in this application. In a comparison of the matched and reference permeability field (Fig 2.8B), the large-scale features and their continuity are well identified. Although not shown, the acceptability of data misfit is implied by the well-characterized property trends. The matched field is admittedly smoothed and the estimated properties captured approximately; however, the minimization of data misfit and low parameter identifiability index at the solution indicate that there is no justification for the addition of more global detail.

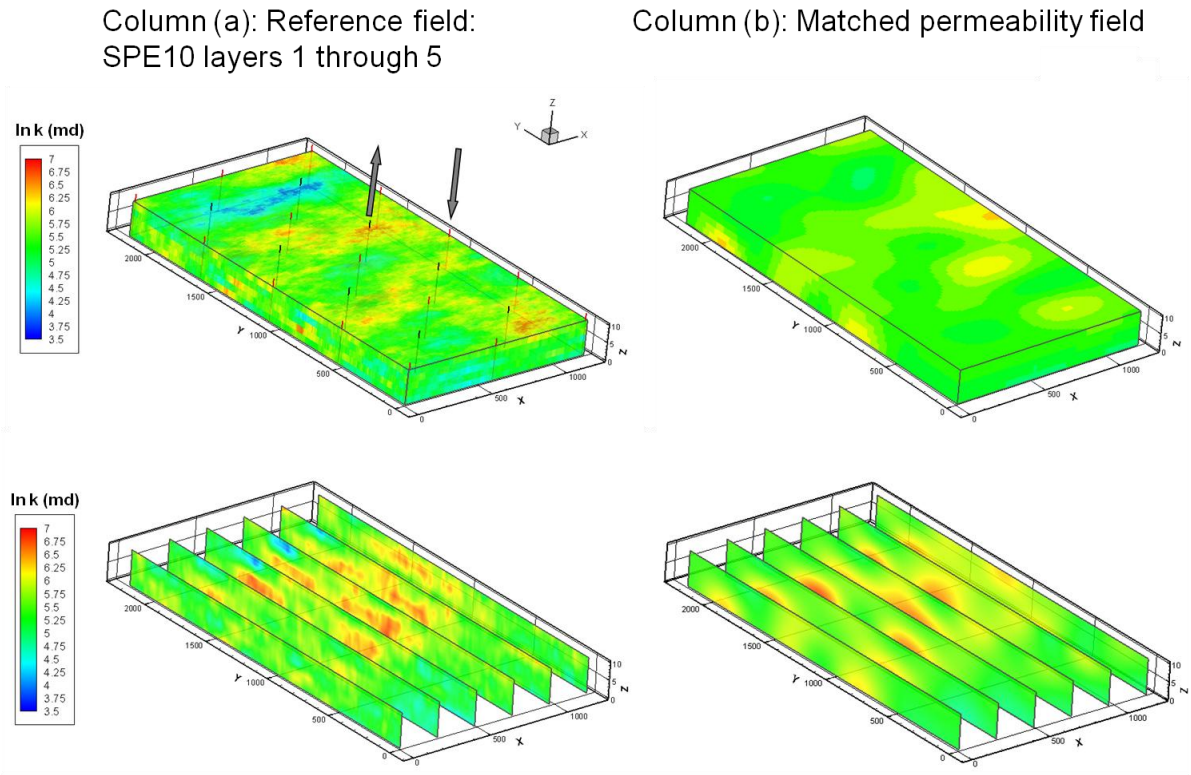

Fig. 2.8. SPE10 5-layer reference permeability field with 66,000 estimable parameters in column (a) compared with the history matched field using 273 estimable parameters or low-frequency DCT coefficients in column (b).

2.4.3 PUNQ-S3 Reservoir Model

The PUNQ-S3 model, designed for Production forecasting with UNcertainty Quantification, has been history matched using several approaches and provides a standard against which both our adaptive multiscale and uncertainty quantification methods can be compared. PUNQ-S3 is a small synthetic case developed from study of a real field by Elf Exploration Production. Details of the field are provided in Floris et al. (2001) and so here we present only its basic description and focus on the implementation of methods relevant to this paper**.**

The reservoir model has dimension 19 × 28 × 5 with horizontally uniform gridblocks of dimension 180 × 180 m that vary between 1.3 and 8.0 m in the vertical. Only 1,761

gridblocks are active. The structural surface map of the reservoir is shown in Fig. 2.9 with the six production wells identified as black circles. The white circles indicate infill wells that are not used in the production scenario. The reservoir is bounded to the north and west by a strong aquifer so no water injection is performed, and bounded to the south and east by faults. There is an initial gas cap and oil rim as depicted in Fig. 2.9.

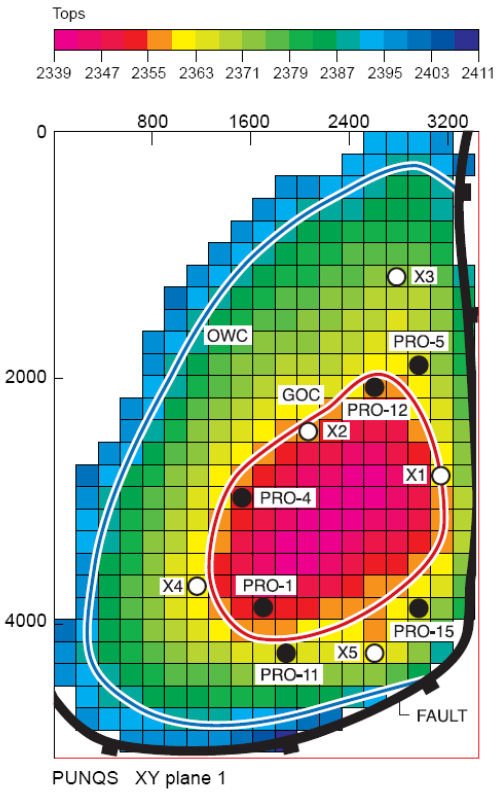

Fig. 2.9. Surface elevation map of the PUNQ-S3 reservoir model (taken from Floris et al. [2001]) with approximate gas cap, oil rim and aquifer boundaries.

2.4.3.1 Production Data

The production schedule provided on the PUNQ-S3 website (PUNQ-S3 Test Case) spans 16.5 years. It begins with 1 year of well testing, 3 years of shut-in and 12.5 years of field production with a 2-week shut-in each year. Simulated production data of BHP, gas-oil ratio (GOR) and water cut (WCT) are provided for each well through the first 8

years for the history matching period (green circles in Fig. 2.10). The final 8.5 years are used for the production forecast. Oil production is rate-controlled (WOPR) through the final 12.5 years at a target of 150 sm^3/d subject to the minimum BHP constraint of 120 bars and maximum GOR constraint of 200 sm^3/sm^3, beyond which the rate is reduced by a constant fraction. During the history match the true WOPR was not honored at all wells and times by the prior model, so the WOPR schedule at each well was also included in the observation data set where it was subsequently matched exactly during the inversion.

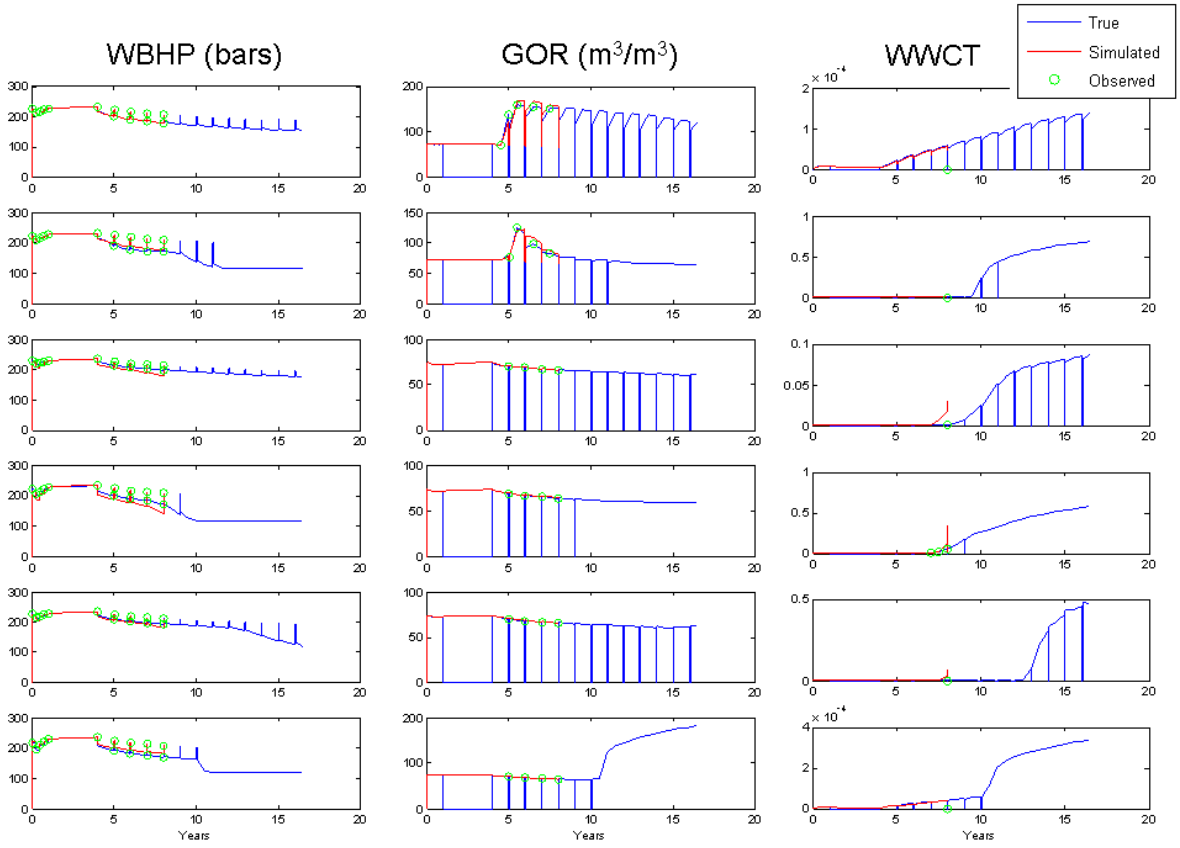

Fig. 2.10. Data misfit between the history matched PUNQ-S3 model response (red) and true model response (blue). Green circles are measurement data available during the 8-year history matching period.

2.4.3.2 Parameter Estimation

The porosity and permeability fields are updated in the history matching period where horizontal and vertical permeability are deterministically defined as a function of porosity using an empirical relationship defined from well data in Barker et al. (2001). The prior model was constructed from a general geologic description presented in Floris et al. (2001) and constrained to measurements at the six producers using Kriging. The geostatistical model applied is also presented in Barker et al. (2001). Fig. 2.11 row 1 shows the true porosity for each of the five layers and row 2 shows the prior model. Layers 1, 3 and 5 are generally characterized by high-porosity sand channels embedded in floodplain mudstone. Layer 2 is a shale-type sediment deposited in a low-energy marine environment with higher-porosity mouthbar deposits, and layer 4 represents deltaic-like deposits embedded in low-porosity clays.

To honor geologic anisotropy of the prior, only nominal truncation of the initial model is performed in the DCT domain. To determine this level, the dynamic data (i.e., WCT, GOR, BHP) were simulated at multiple levels of truncation, in a descending fashion from higher- to lower-frequency representations of the prior, and the threshold at which the data began to significantly deteriorate was identified. For example, Fig. 2.12 shows that with less than about five-hundred DCT coefficients ($nr \times ns \times nt = 10 \times 10 \times 5$) the WCT and WGOR responses begin to deviate from those of the prior model at full spatial detail. In fact, inspection of the porosity layers showed that the channel boundaries in layers 1, 3 and 5 begin to lose their continuity at this level.

The history match was initialized with a $9 \times 9 \times 5$ coefficient representation. No approximation was performed in the vertical direction in order to retain the sharp geological contrast between strata. We note here that the DCT parameterization has been applied to and populated the complete rectangular model domain because of its periodic sampling requirement; therefore, permeability and porosity at all gridblocks are updated in the inversion but ignored at inactive gridblocks during simulation to account for the

irregular model boundary. During the workflow only one level of spatial refinement, increasing to a 10 × 10 × 5 coefficient representation, was required to match the porosity model which demonstrates that the multiscale approach converges to a straightforward re-parameterization method when confidence in the prior is high and parameter updates are minimal. Data misfit is presented in Fig. 2.10, and Fig. 2.13 row 1 shows the matched porosity and row 2 the updated values. The updates have small magnitude and are applied globally, per layer, in spatial orientations that honor the heterogeneity of the prior. During the course of analysis we observed that different priors, i.e., different conceptual models, could be used to achieve equivalent data misfits. This is because the observation data are relatively sparse for the 8 year history matching period and leave considerable tolerance for non-uniqueness. For example, only one well (11) has water breakthrough at the seventh year and two wells (4 and 1) start to produce free gas at the 4th and 5th years, respectively. In a review of the PUNQ-S3 comparative study, Barker et al. (2001) similarly concluded that principle features of the prior do not always influence model prediction behavior. For example, one approach to history matching using an isotropic prior model achieved accurate forecasts in this clearly anisotropic reservoir. It is for this reason that we strictly honor the prior model in this study by minimal parameter truncation in the DCT domain. Appropriately, our results demonstrate that under the assumption of a well-informed prior our proposed approach updates the model in a manner that is consistent with the geologic model and only to the level of spatial detail warranted by the data content.

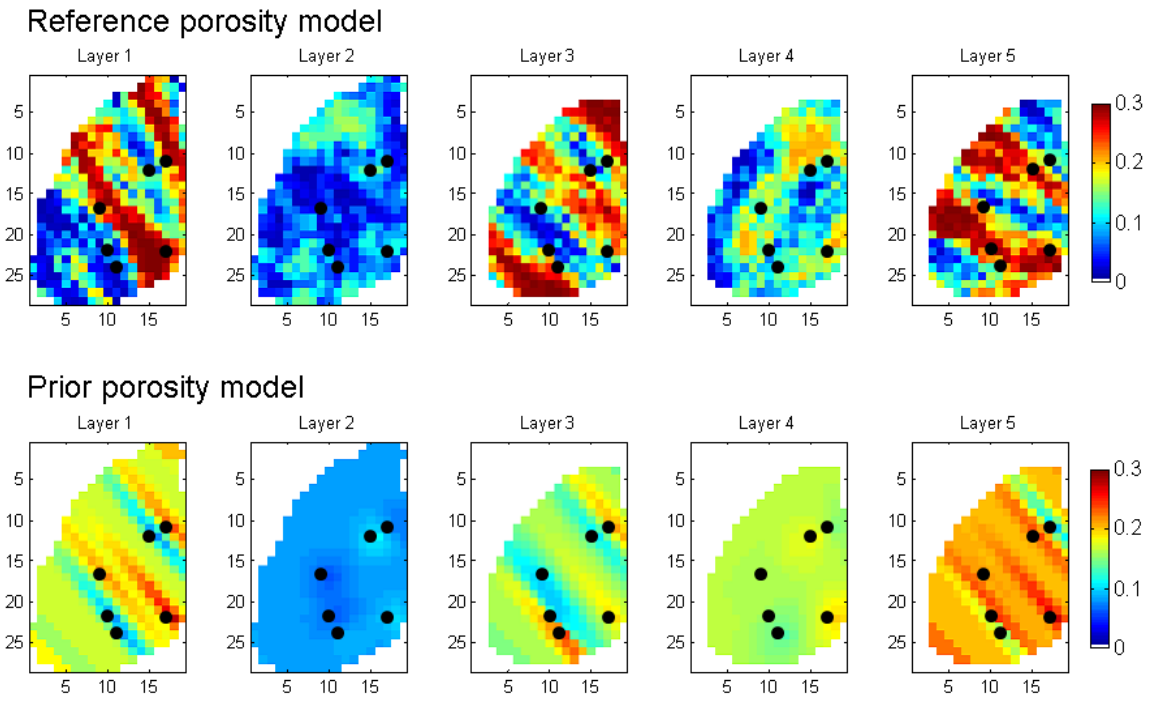

Fig. 2.11. PUNQ-S3 reference porosity model (top row) and the prior porosity model (bottom row) derived from Kriging and conditioned to measured porosity at each well location per layer.

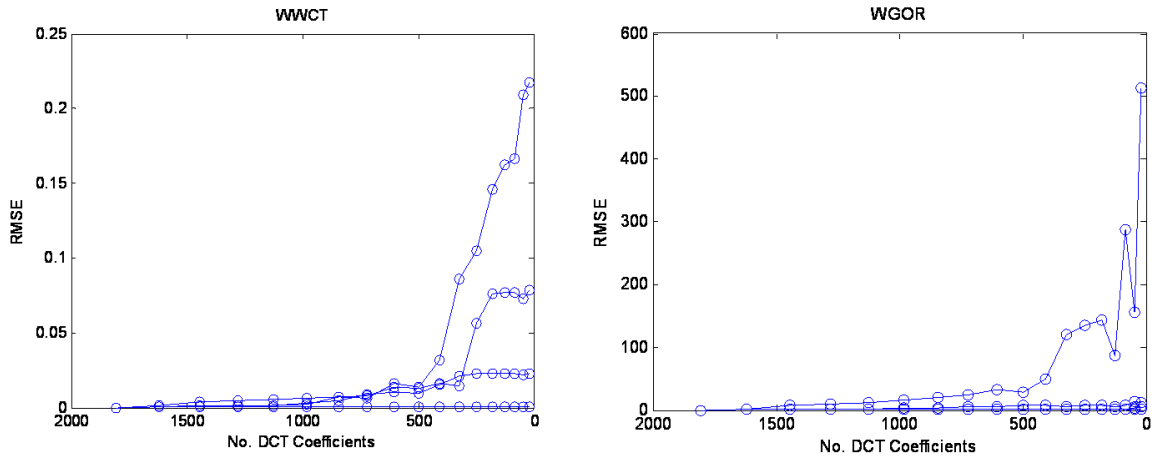

Fig. 2.12. Error in response data at the six PUNQ-S3 producers between the prior model at full resolution and its lower-frequency approximations. Error increases as the level of higher-frequency DCT coefficient truncation increases.

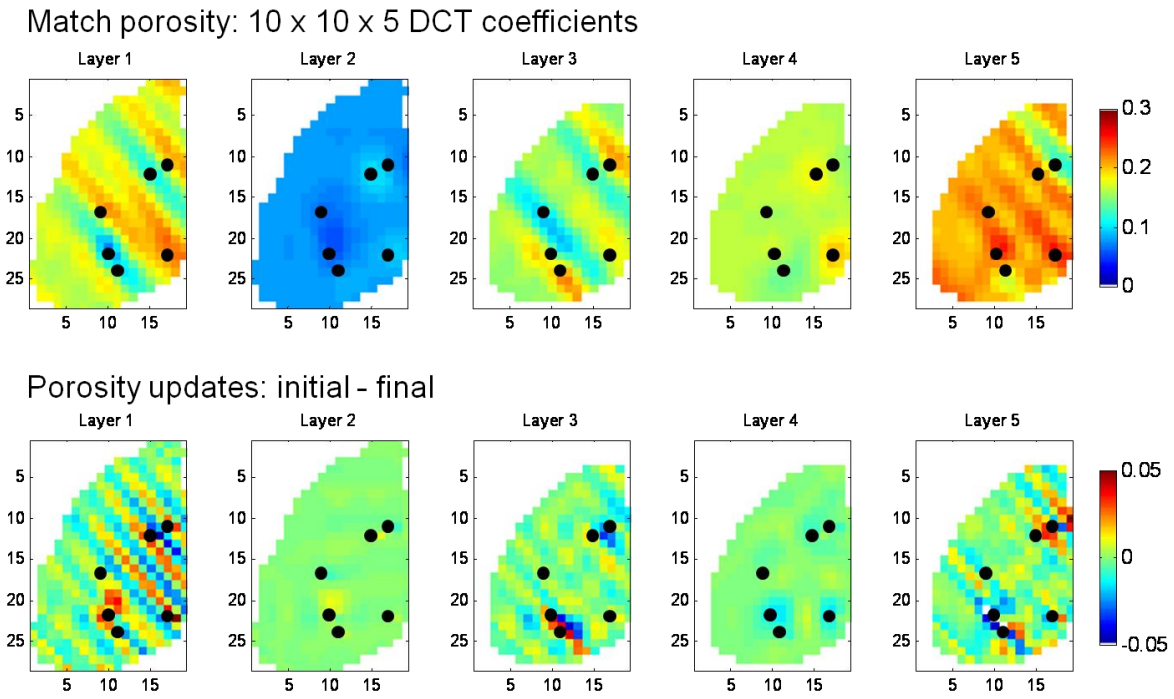

Fig. 2.13. The history matched PUNQ-S3 porosity model using 500 parameters or DCT coefficients (top row) and the spatial porosity updates required to achieve the solution (bottom row).

2.4.3.3 Forecast Uncertainty

The null space Monte Carlo approach was applied to quantify local solution uncertainty. Ten realizations of the matched porosity field were generated by adding detail at only the highest frequency. When increasing the level of detail at lower-frequencies, we found that the history match was maintained while at the same time the geologic features of the prior (e.g., channel widths) were lost, which is consistent with our earlier observation that several conceptual models equivalently fit the data. The incorporation of detail at the highest-frequency or gridblock scale does not deteriorate the large-scale heterogeneity of the prior. We used ten sample sets to approximate the first and second order statistics of cumulative oil production (OPC). Detail coefficients populating the sets were sampled from the empirical distribution of the lower-frequency solution. We

did not account for correlation between samples because this is unknown (without, for example, an ensemble).

Three of the porosity realizations after updating of the solution by Eq. (2.9) are presented in Fig. 2.14 and the forecasts through the complete 16.5 year history for all ten models are shown in Fig. 2.15. The observation data during the first 8 years remain matched, which is a consequence of the null space projection. There is some acceptable deterioration of the data misfit at certain wells that could, if required, be resolved in a few iterations of minimization. In the forecast period the simulated data begin to deviate. There is a bias in the forecast at some of the wells that is maintained in all realizations, indicating a bias in the prior model assumptions. Recall that the purpose of uncertainty quantification in our approach is to explore uncertainty within the region of the objective function minimum and not to explore multiple minima or different conceptual models (e.g., different variogram models). Thus, it is expected that all realizations adhere to the bias or lack thereof at each well. In Fig. 2.16 we compare the null-space-derived uncertainty in OPC with results from previous studies. The true OPC after the simulation period is 3.87×10^{6} sm^3 (Floris et al., 2001) and OPC corresponding to the prior model is 3.41×10^{6} sm^3, also plotted in Fig. 2.16, which our history match improves upon. It is important to note that we present our recovery forecast as a range whereas the other data included show percentiles or a confidence interval. The porosity realizations in Fig. 2.14 are known to explore the objective function minimum and are not statistical samples, corresponding to different prior models, drawn from some assumed distribution. An underestimated range of uncertainty is obtained whose bias in OPC is consistent with the overestimation of GOR and WCT in Fig. 2.15.

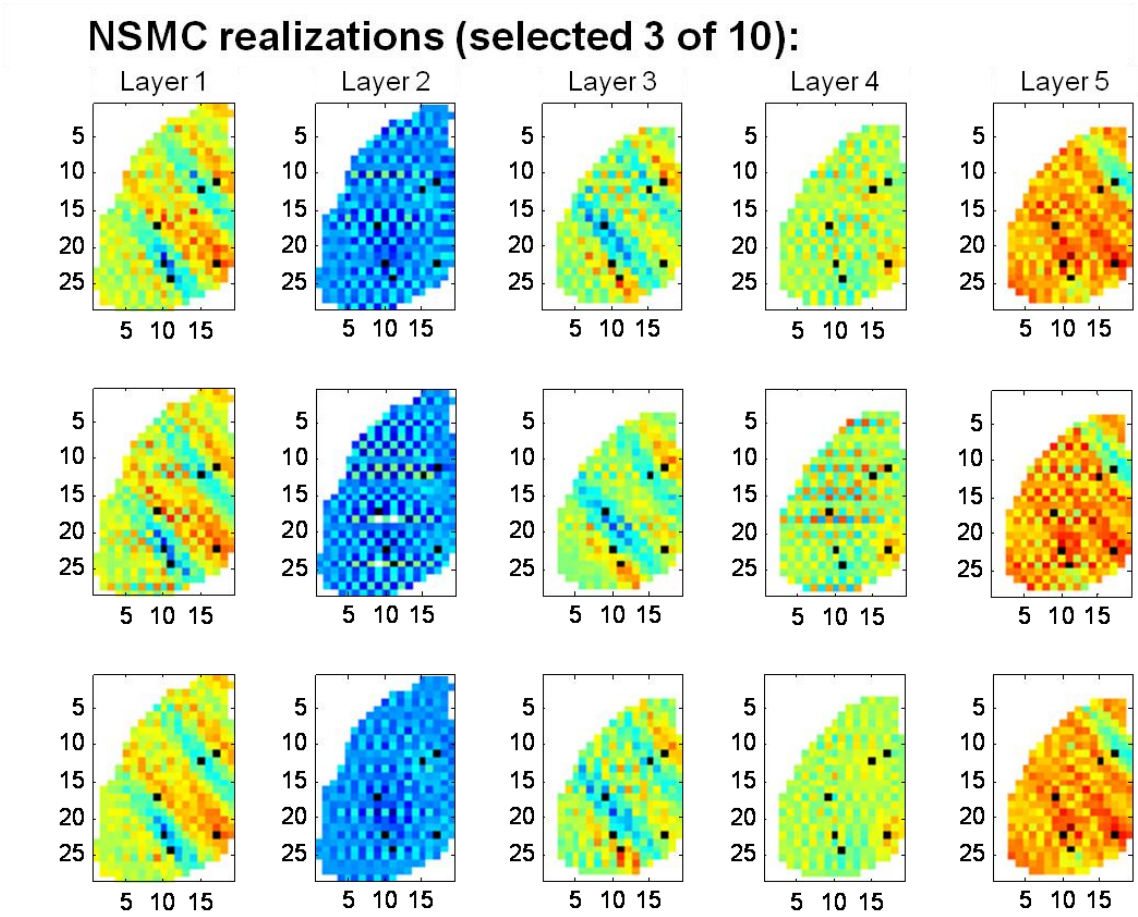

Fig. 2.14. Selected Monte Carlo null space realizations of the PUNQ-S3 porosity model, by row, showing local solution uncertainty at the grid block scale embedded within the larger-scale global solution. Black circles are well locations.

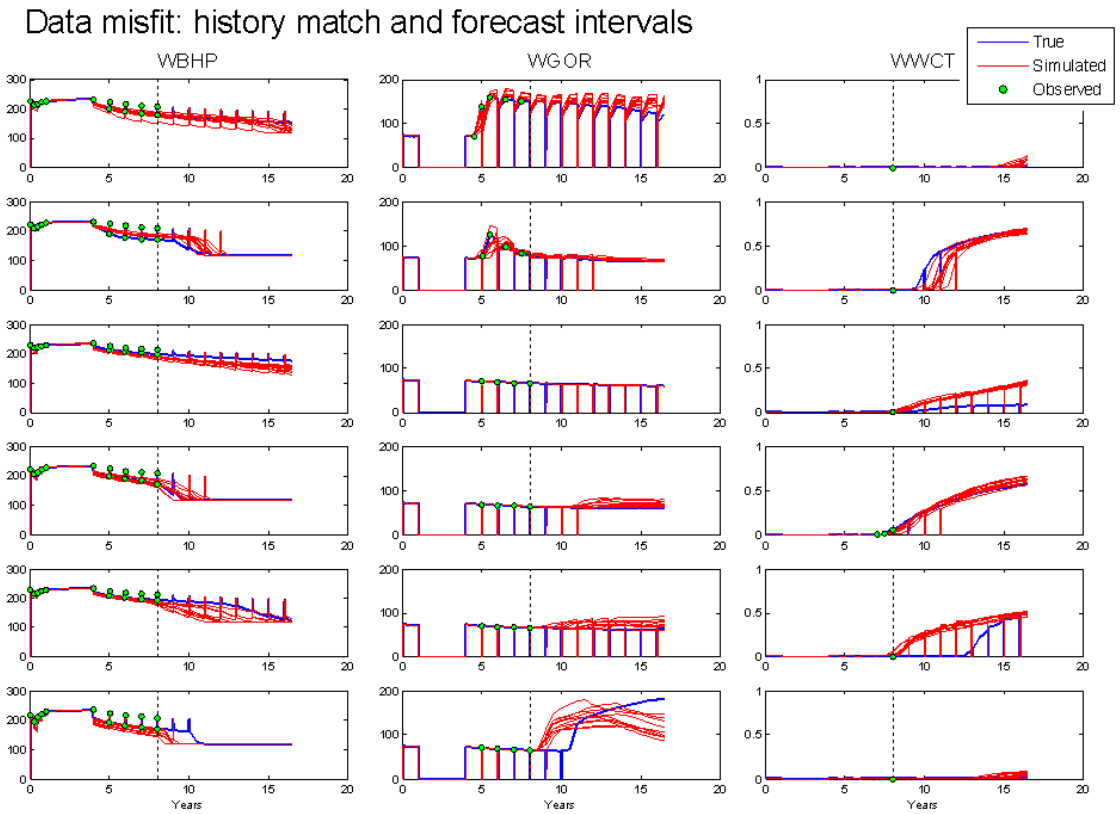

Fig. 2.15. Simulated PUNQ-S3 forecast behavior (red lines) capturing local solution uncertainty for ten Monte Carlo null space realizations of porosity.

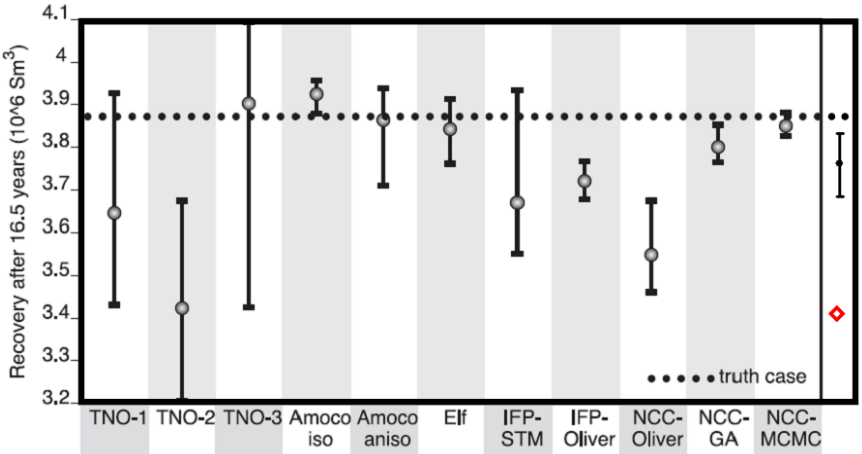

Fig. 2.16. A comparison of forecast cumulative production uncertainty at 16.5 years between this study (last column) and compiled analyses presented in Floris et al. (2001) with the true production (horizontal dashed line). Cumulative production from the prior model is shown by the red diamond. The comparative study presents the 10th, 50th and 90th percentiles. We present the min, mean and max (in the bar plot) because our models are sampled from the same objective function minimum.

2.5 Conclusions

This section presented an approach to data-driven multiscale history matching enabled by a compact, frequency-based parameterization of the geologic model using the DCT. The flexibility of the parameterization for multiscale characterization was demonstrated using three reservoir models in which the low-rank model descriptions benefited from, but were not dependent on, prior information. Prior model compression and adaptive refinement provided implicit regularization that was shown to improve ill-posedness of the underdetermined inverse problem. A history match was achieved when adaptive refinement of the model was no longer sensitive to the available data. A key step in alleviating the detrimental influence of DCT frequency components insensitive to production data was the compact representation of the parameter sensitivity matrix prior to its inclusion in the gradient calculation. In all applications, the insensitive frequency components were largely associated with the inability of production data to resolve fine scales of spatial detail. Accordingly, we exploited this behavior to assess model uncertainty at scales finer than the solution, while at the same time honoring the history match, using a null space projection technique.

In the next section we improve upon a limitation of the DCT that impacts the multiscale approach to data integration. The DCT parameterization, as presented in this section, is constrained to uniformly structured or block-type geologic models, thus we develop a generalization of the transform basis suitable also to irregular and unstructured grids.

3. GRID-CONNECTIVITY-BASED PARAMETERIZATION: AN EXTENSION OF THE DCT BASIS TO GENERIC GRID GEOMETRIES*

3.1 Summary

This section presents the development of a novel method of parameterization for reservoir heterogeneity characterization to mitigate the challenges associated with the nonlinear inverse problem of subsurface flow model calibration. The parameterization is developed as a generalization of the DCT basis for generic grid geometries, and is performed by the projection of the heterogeneity field onto an orthonormal basis derived from the grid connectivity structure. The basis functions represent the modal shapes or harmonics of the grid, are defined by a modal frequency, and converge to special cases of the discrete Fourier series (e.g., the DCT-2) under certain grid geometries and boundary assumptions; therefore, hydraulic property updates are performed in the spectral domain and merge with Fourier analysis in ideal cases. Dependence on the grid alone implies that the basis may characterize any grid geometry including corner-point and unstructured, is model independent, and is constructed off-line and only once prior to flow data assimilation.

We apply the parameterization in an adaptive multiscale model calibration workflow for three subsurface flow models. Several different grid geometries are considered. In each case the prior hydraulic property model is updated using a parameterized multiplier field that is superimposed onto the grid and assigned an initial value of unity at each cell. The special case corresponding to a constant multiplier is always applied through the constant basis function. Higher modes are adaptively employed during minimization of data misfit to resolve multiscale heterogeneity in the geomodel. The parameterization

---

*Part of this section is reprinted with permission from "A Generalized Grid-Connectivity-Based Parameterization for Subsurface Flow Model Calibration" by Bhark, E., Jafarpour, B., Datta-Gupta, A., 2011. Water Resources Research. 47, W06517, doi:10.1029/2010WR009982. Copyright 2011 by the American Geophysical Union.

demonstrates selective updating of heterogeneity at locations and spatial scales sensitive to the available data, otherwise leaving the prior model unchanged as desired.

3.2 Introduction

This section presents the development and application of a general transform basis amenable to any flow model grid geometry while imposing basis properties required for efficient and practical updating of the geologic model. The basis is derived as the eigenvectors of a specific form of the grid Laplacian, imitating Fourier behavior, and converges to special cases of the discrete Fourier basis under specific model boundary assumptions. The parameterization is achieved by embedding the estimable property field at grid cell resolution onto a small number of leading Laplacian eigenvectors to reduce the dimensionality of the set, thereby characterizing the property by the modal shapes and frequencies of the grid on which it is defined. The conceptual and physical meaning behind the spectral analysis of reservoir/aquifer properties from Laplacian eigen-projection is presented in **Subsection 3.3**.

The transform basis can be constructed from, and therefore the parameterization applied to, any grid geometry because the Laplacian matrix is defined from grid connectivity information alone. In our formulation the Laplacian is always symmetric, sparse and positive semi-definite; therefore, its eigenvalues are non-negative real and increasing over a known range and its eigenvectors are orthogonal. This latter property is critical as it permits a straightforward inverse transform and improves decorrelation of the parameters in the spectral domain. Despite the large dimension of the Laplacian for a high-resolution grid, its symmetry and sparse structure permit the efficient approximation of only a few leading eigenpairs using an iterative method. Details of the Lapacian construct, associated properties and decomposition are presented in **Subsection 3.3.2** through **Subsection 3.3.4**. Once constructed, the basis functions are fixed throughout data assimilation if the gridding remains unchanged.

For model calibration, the transform basis is applied following the general approach used for the DCT parameterization in Eq. (2.2), although using a spatial multiplier field posed in the multiplicative formulation

$$\mathbf{u} = \mathbf{u}_0 \cdot \mathbf{\Phi v} \tag{3.1}$$

where the entrywise product $\mathbf{A}\cdot\mathbf{B}$ of matrices $\mathbf{A} = (a_{ij})$ and $\mathbf{B} = (b_{ij})$ is $a_{ij}b_{ij}$. In this updated formulation, $\mathbf{u_o}$ is the prior hydraulic property model, pre-constructed from available data sources, and $\mathbf{\Phi v}$ defines the multiplier field in the spatial domain. Model updating is therefore performed by the cell-by-cell multiplication of the calibrated multiplier field, which has an initial value of unity at each grid cell, with $\mathbf{u_o}$. The multiplier field is parameterized by a truncated set of spectral coefficients $\mathbf{v}$ that represent its projection onto a subset of the Laplacian eigenvectors or basis functions, each characterizing a unique modal frequency of the grid. Therefore, $\mathbf{v}$ represents the parameters in the transform domain. We consider a range of cases where the prior model is un-informed to well-informed, and also different grid geometries and structure, to demonstrate the versatility of this approach to parameterization.

The intent of parameterized model calibration via Eq. (3.1) is to update aquifer or reservoir heterogeneity at locations and spatial scales warranted by the production data, and to leave unchanged the hydraulic property at locations either insensitive to or consistent with production data. Such levels of detail are attained by sequentially refining the multiplier field with the addition of higher modes that successively permit a finer-scale description. Additionally, we exploit the geometric flexibility of the parameterization to simultaneously update multiple, individual regions of the model that are associated with different geologic structures while retaining their distinct features during the calibration.

In **Subsection 3.4** the proposed parameterization is applied to calibrate three different petroleum reservoir models using production data. The cases consider different grid

geometries and structural geologic features to demonstrate the broad diversity of geologic description for which the approach is applicable. **Subsection 3.5** concludes with a summary of key results and a discussion of advantages unique to the grid-connectivity-based parameterization, as well as limitations.

3.3 Methods

This subsection presents a comprehensive development of the new grid-connectivity-based transform (GCT) basis and its application in multiscale parameter estimation. We begin with a presentation of the Laplacian construct and subsequent derivation of the transform basis through matrix decomposition. Next, we highlight the unique properties of the new basis for which it is amenable to both geologic model description and model calibration algorithms and explain the usefulness of these properties from an applied viewpoint. In accordance with the basis properties we then describe our conceptual approach to model calibration, and present last the proposed multiscale algorithm for the calibration of subsurface flow models.

3.3.1 Generalized Grid Geometry

The proposed approach to parameterization is founded on the relationship between eigenpairs of the grid Laplacian matrix, defined below, and the spatial property field overlaid on the grid. It is therefore important to understand properties of the eigenpairs for their proper and efficient application in parameterized model calibration. Much historical and current research in spectral graph theory relates the structural characterization of a grid or mesh with its Laplacian eigenpairs which characterize invariant and global structural information regarding topology and geometry (Chung, 1997; Spielman and Teng, 2007; Zhang et al., 2010). In addition to the following presentation, we refer the interested reader to the survey papers of Alliez and Gotsman (2005), Sorkine (2005) and Zhang et al. (2010), with particular emphasis placed on the last, for a comprehensive review of spectral graph analysis for geometry processing problems across a suite of research fields.

For the purpose of parameterization we use a specific Laplacian formulation. Before its definition we first define the following relevant graph notation. The grid $G = (V, E)$ is defined by a set of N vertices where V is the vertex set and E the edge set. We assume in all instances that a hydraulic property field is populated at the grid cell or mesh element centers; therefore, all graph definitions pertain to the dual grid (Alliez and Gotsman, 2005) such that the centroids are considered vertices, represented as their Cartesian coordinates, and edges the connection between adjacent centroids. The vertex set is $V = \{1, 2, \ldots, N\}$, where N is the number of grid cells at which hydraulic properties are defined. All grids are assumed undirected, weighted, fully connected and finite. A weighted grid implies that each edge between vertices v_i and v_j is assigned a non-negative adjacency measure or weight, $a_{ij} \geq 0$; therefore, non-connected vertices carry a weight of zero. In our application weights will always equal unity as no preference is given to connectivity information in a certain spatial orientation. The undirected definition denotes $a_{ij} = a_{ji}$, and fully connected indicates that any vertex can be reached stepping from vertex-to-vertex by at least one path from a starting location at any other vertex. The case of a graph with multiple connected components is an important consideration of greater complexity and is discussed later in this subsection. These definitions together characterize the $N \times N$ grid adjacency matrix, **A**, whose entries a_{ij} are given by

$$a_{i,j} = \begin{cases} 1 & if\ (i, j) \in E \\ 0 & otherwise \end{cases} \tag{3.2}$$

and the $N \times N$ diagonal matrix, **D**, known as the degree matrix, where the diagonal elements equal the degree (d_i) of each corresponding vertex (v_i) which is defined as

$$d_i = \sum_{j=1}^{n} a_{ij}. \tag{3.3}$$

Of its many definitions, we specifically construct the grid Laplacian as **L** = **D** - **A** (Mohar, 1997; Sorkine, 2006; von Luxburg, 2006), or analogously as

$$\mathbf{L}_{ij} = \begin{cases} d_i & i = j \\ -1 & (i, j) \in E \\ 0 & otherwise. \end{cases} \tag{3.4}$$

The Laplacian is a discrete second-difference operator when applied to a function on the grid and is often associated with a finite-difference stencil with action proportional to a second derivative. The formulation in Eq. (3.4) is in fact commonly applied in second-order Tikhonov regularization to enforce parameter updates that are smooth in the second derivative sense (Aster et al., 2005).

Although apparent, it is also worth emphasizing that the Laplacian formulation in Eq. (3.4) is amenable to any grid geometry and can honor local discontinuities in a grid, e.g., at faults. Every grid will have a unique Laplacian; therefore, construction of the transform basis via Laplacian decomposition is completed only once and, further, independently of any function defined on the grid. We now present relevant properties of Laplacian eigenpairs, beginning with the fundamental observation of how spectral analysis of the Laplacian, a local operator, can be used to describe global grid geometry.

3.3.2 Basis Development: Spectral Analysis of the Grid Laplacian

The relationship between the Laplacian as a local operator and the global behavior of its eigenpairs is rooted in the periodic structure of the Laplacian. For an undirected and fully connected graph, the Laplacian in Eq. (3.4) is a circulant matrix, and it is well known that the Fourier basis diagonalizes any circulant matrix. Strang (1999) presents the eigendecomposition of a symmetric second-difference matrix corresponding to the one-dimensional operator shown in Fig. 3.1C. The top and bottom rows of the Laplacian in Fig. 3.1C correspond to the left and right boundary cells, respectively, of the one-dimensional grid in Fig. 3.1A, and the upper-right and lower-left matrix components of -

1 (in Fig. 3.1C) indicate the periodic boundary extension of the discrete function *u* on the grid (in Fig. 3.1A) from its opposite side. Therefore, relative to Laplacian operation, the periodicity of *u* defined at *meshpoints* on the grids in Fig. 3.1A and Fig. 3.1B are identical despite their difference in geometry. Strang (1999) verifies the eigenvectors e_k of the Laplacian in Fig. 3.1C as

$$e_k = \left(1, w^k, w^{2k}, \ldots, w^{(N-1)k}\right) \tag{3.5}$$

where $w = exp(2\pi i/N)$, $k = 0,1, \ldots, N\text{-}1$ are the frequencies, i is the imaginary number $\sqrt{-1}$, and N is the regular discretization of u. Each vector e_k is a discrete Fourier basis vector and is, therefore, a complex exponential (i.e., having real and imaginary components) and orthogonal to vectors $e_{l \neq k}$.

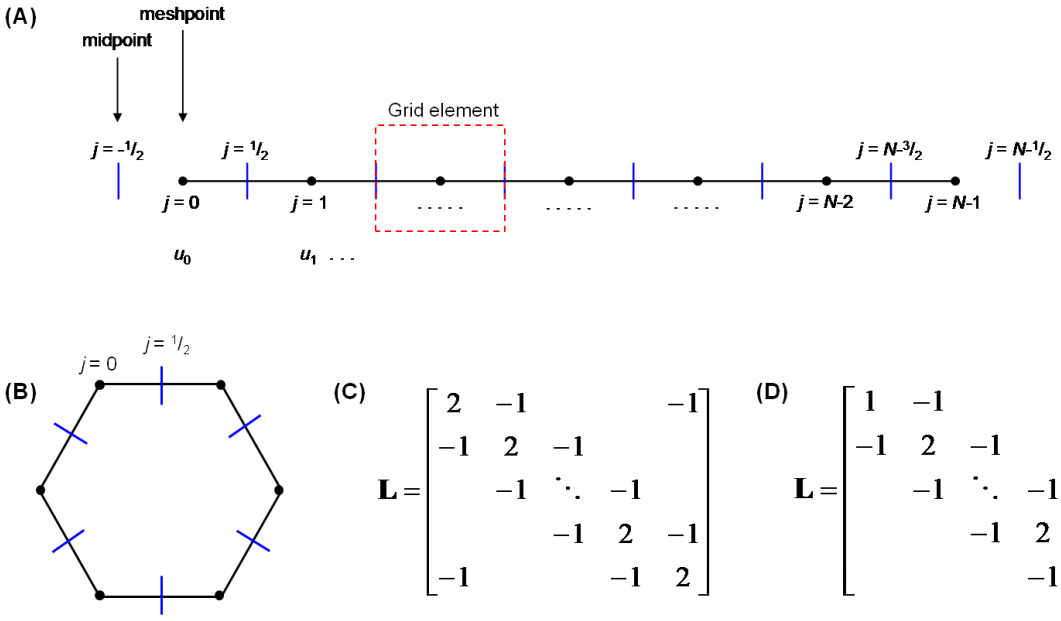

Fig. 3.1. (A) Discretization of a 1-D structured graph and (B) its equivalent depiction assuming meshpoint boundary symmetry. (C) 1-D circulant Laplacian matrix depicting meshpoint boundary symmetry and (D) zero-derivate midpoint boundary symmetry.

In a seminal paper related to a mesh fairing application, Taubin (1995) first recognized that the discrete Fourier transform (DFT) of a function defined at the vertices of a

regular n-periodic grid, where *n* is the number of vertices per grid element, is equivalent to the decomposition of the function into a linear combination of the Laplacian eigenvectors. He then developed the general case for a variety of alternative weighting schemes that vary with grid geometry and connectivity, and observed that if the immediate-neighbor structure is retained then the Laplacian eigenvectors can be generalized as the "natural vibration modes" or harmonics of the grid surface and the corresponding eigenvalues as the "associated natural frequencies", acknowledging that the exact relation to the DFT is lost. Therefore, in the general case where the Laplacian is not purely circulant, its eigenvectors permit a Fourier-like description of the function defined on a grid.

While the generalized harmonic behavior of Laplacian eigenvectors provides a foundation from which to develop our method of parameterization, it is incomplete and as yet is inconsistent with the Laplacian in Eq. (3.4). For this we look to Strang (1999) in his derivations of the DCT and discrete sine transform (DST) from decomposition of the symmetric second-difference matrix identical to the circulant Laplacian in Fig. 3.1C. Through manipulation of the matrix components corresponding to the boundary conditions, i.e., the -1 entry at the upper-right and lower-left corner of Fig. 3.1C as described above, the eigenvectors can be directly manipulated. Of the many boundary assumptions investigated (Strang and Nguyen, 1996), the formulation in Eq. (3.4) is equivalent to the boundary conditions implied by the Laplacian in Fig. 3.1D. Relative to the annotations in Fig. 3.1A, these boundary conditions correspond to the imposition of the zero-derivate of the function (u) at the midpoint between vertices on the left boundary, and similarly on the right boundary. For example, at the left boundary a symmetric reflection of u is assumed about the point $j = -1/2$ such that $u_{-1} = u_0$. The second difference at this boundary, given by the matrix product of the first row of the Laplacian in Fig. 3.1C with the function u, is $L(1,\cdot) = u_1 + 2u_0 - u_1 = u_0 - u_1$ and is therefore equivalent to the same operation using the Laplacian in Fig. 3.1D. Similarly at the right boundary, symmetry is assumed about the point $j = N - 1/2$ such that $u_{N-1} = u_N$ with the

second-difference of $u_{N-2} + 2u_{N-1} - u_N = u_{N-2} - u_{N-1}$, again equating the Laplacian operators in Figs. 3.1C and 1D for the zero-derivative midpoint boundary condition. It is the left boundary condition from which the imaginary sine components of Eq. (3.5) vanish and leave real cosine terms, which when combined with the right boundary condition uniquely defines the DCT-2. Therefore, in the case of a regular periodic and fully connected grid, with either structured (e.g., corner-point) or unstructured geometry, the eigenvectors of Eq. (3.4) reduce to the DCT-2, which has been previously applied for subsurface heterogeneity parameterization (see **Section 1**). Derivations of the DCT as well as DST variants are presented in Strang (1999).

3.3.3 Laplacian Properties

In the previous subsection we presented the relationship between the local structure of the Laplacian and the global behavior of its eigenpairs, with a focus on the form of the eigenvectors when the grid is of regular periodic structure and fully connected. We now look at individual properties of the Laplacian structure and its spectral decomposition which are valid regardless of the grid structure and the number of its connected components, and which as we later demonstrate are requisite for efficient parameterization in practice.

By construction in Eq. (3.4), **L** is an $N \times N$ real symmetric matrix, which also follows from the definition and symmetry of the adjacency (**A**) and degree matrices (**D**) in Eq. (3.2) and Eq. (3.3), respectively. The eigendecomposition of a real symmetric matrix **S** with dimension N is given by the Spectral Theorem (Lancaster and Tismenetsky, 1985). The decomposition of **S** is

$$\mathbf{S} = \mathbf{V}\Lambda\mathbf{V}^T = \sum_{i=1}^{N} \lambda_i \mathbf{v}_i \mathbf{v}_i^T \tag{3.6}$$

where **V** is composed of column eigenvectors, **Λ** is the diagonal matrix of the real eigenvalues λ, and the eigenvectors are pairwise orthogonal, i.e., $\mathbf{V}^{\mathrm{T}}\mathbf{V} = \mathbf{I}$ or $\mathbf{v}_i^T \mathbf{v}_j = \delta_{ij}$ for $1 \le i,j < N$, where $\mathbf{V}^{\mathrm{T}}$ is the transpose and **I** is the identity matrix. The structure of the spectrum is described below in **Subsection 3.3.3.2**.

3.3.3.1 Positive Semi-Definiteness

All other properties of the Laplacian important to parameterization are based on the positive semi-definite formulation of Eq. (3.4), verified from the quadratic form of the Laplacian

$$\mathbf{f}^T \mathbf{L} \mathbf{f} \ge 0 \tag{3.7}$$

which holds for any vector **f** defined on the grid. Through algebraic manipulation, the left-hand side of Eq. (3.7) can be redefined as

$$\begin{aligned} \mathbf{f}^T \mathbf{L} \mathbf{f} &= \mathbf{f}^T \mathbf{D} \mathbf{f} - \mathbf{f}^T \mathbf{A} \mathbf{f} \\ &= \sum_{(ij) \in E(G)} a_{ij} \left(f_i^{\,2} + f_j^{\,2} \right) - a_{ij} \left(2 f_i f_j \right) \\ &= \sum_{(ij) \in E(G)} a_{ij} \left(f_i - f_j \right)^2 \end{aligned} \tag{3.8}$$

(Tolliver, 2006). The weights a_{ij} are non-negative by definition from Eq. (3.2), therefore satisfying Eq. (3.7). Analogous derivations of Eq. (3.8) from a conceptually different approach are shown in Zhang et al. (2010) and von Luxburg (2006).

3.3.3.2 Eigenspectrum

The primary value of a symmetric positive semi-definite matrix of dimension N is that it has N non-negative real eigenvalues with spectrum $0 \le \lambda_i \le \ldots \le \lambda_N$, where i is the spectral index (Lancaster and Tismenetsky, 1985). For the purpose of parameterization, the magnitude of eigenvalues is important in that they represent the modal frequency

associated with each Laplacian eigenvector and permit sorting of the vectors from low-to-high frequencies, with increasing eigenvalue magnitudes associated with increasing modal frequencies. This is a direct consequence of the equivalence between the Laplacian eigenvectors and the DFT basis (Taubin, 1995; Mohar, 1997). Only a small number of the leading eigenvalues sorted from smallest to largest, or from low to high modal frequency, are useful for hydraulic property description, and therefore only a partial decomposition of the Laplacian is desired.

A particularly useful property for parameterization is related to the value and multiplicity of the smallest eigenvalue. From Eq. (3.8), the Laplacian always has a smallest eigenvalue of zero, corresponding to the constant basis function, with multiplicity equal to the number of connected components or regions encoded in the Laplacian.

There are multiple ways to verify these properties. Most simply, the row sums of the Laplacian equal zero by construction; therefore, from the eigenvalue equation $\mathbf{Lx} = \lambda\mathbf{x}$ the eigenvalue λ must equal zero when $\mathbf{x}$ is a constant vector. An analogous but more useful interpretation is to set the relationship in Eq. (3.8) equal to zero when $\mathbf{f}$ is an eigenvector of $\mathbf{L}$, i.e.,

$$\mathbf{f}^T\mathbf{L}\mathbf{f} = \sum_{(ij)\in E(G)} a_{ij}\left(f_i - f_j\right)^2 = 0. \tag{3.9}$$

The terms equal zero only when $f_i = f_j$ for all i,j, confirming that the zero eigenvalue corresponds to the zero-frequency or constant vector. In this case the sign and magnitude of the weight for the zero eigenvalues are irrelevant. The useful implication is that the constant basis vector is related to the mean of the property defined on the grid and therefore permits uniform updating of the field by a single transform parameter, effectively equivalent to application of a constant spatial multiplier (e.g., zonation) as traditionally applied in model calibration.

To this point we have considered only a fully connected graph; however, by construction groundwater model grids may often have multiple independently connected regions separated, for example, at faults or structural discontinuities. In this situation a useful proposition developed from Eq. (3.9) is that the multiplicity of the zero eigenvalue equals the number of connected regions in the grid (Mohar, 1997). Each corresponding eigenvector has components of constant value associated with each region and is, therefore, an indicator vector of the individual regions (von Luxburg, 2006). That is, the inspection of any such eigenvector corresponding to a zero eigenvalue points out all connected regions and the boundaries between them. This has several practical uses including the automated detection of isolated gridblocks (a common result of upgridding), the location of non-neighbor connections, and the location of structural discontinuities (usually at faults). This property also implies that multiple regions or compartments can be defined by the analyst, based on geologic considerations, fluid properties, etc., for individual parameterization and property updating as demonstrated in applications below.

3.3.4 Numerical Eigendecomposition

Practical application of the parameterization requires the efficient decomposition of the Laplacian for large grids at least on the order of hundreds-of-thousands of active cells. Accepting that the complete decomposition using a direct method is currently infeasible, we take advantage of the sparse symmetric structure of **L** and use the implicitly restarted Lanczos method (IRLM) within the ARPACK (ARnoldi PACKage) subroutines (Lehoucq et al., 1998). We now review the algorithm only to a depth that allows an understanding of the computational cost.

The goal of the IRLM is to achieve the truncated *k*-step Lanczos factorization of **L** to tridiagonal form,

$$\mathbf{L}\mathbf{V}_k = \mathbf{V}_k\mathbf{H}_k + \mathbf{r}_k\mathbf{e}_k^T \tag{3.10}$$

where $\mathbf{V}_k$ is the $N \times k$ matrix with orthonormal columns referred to as Lanczos vectors, $\mathbf{H}_k$ is a symmetric and tridiagonal $k \times k$ matrix, the columns of the $N \times k$ matrix $\mathbf{r}_k$ are residual vectors such that $\mathbf{V}^T\mathbf{r} = \mathbf{0}$, and $\mathbf{e}_k$ is an $N \times k$ matrix with columns corresponding to the k-th axial directions of the basis $\mathbf{V}$. While full matrix decomposition takes $O(N^3)$ operations, the Lanczos expense is $O(mM(N)) + O(mN)$ where m is the maximum number of matrix-vector products and $M(N)$ the matrix-vector cost (Trefethen and Bau, 1997). Conceptually, the first and second terms represent a Krylov basis vector computation and its scalar projection onto the Lanczos vectors. Because $\mathbf{L}$ is sparse and contains non-zero entries (per row) corresponding only to two-point cell connectivity, $M(N)$ reduces to $O(N)$ operations multiplied by a small constant equal to the size of the Laplacian stencil.

The Lanczos vectors equal the eigenvectors of $\mathbf{L}$ only when $\mathbf{r} = \mathbf{0}$, or when numerically orthogonal (Calvetti et al., 1994). However, orthogonality is not achieved in practice from projection error and results in spurious eigenvalues, where the error magnitude is problem dependent and related to the spacing of the relevant eigenvalues (Golub and Van Loan, 1996; Lehoucq et al., 1998). In our application, the parameterization is fundamentally based on a few of the lowest modal frequency basis vectors where the frequency is determined from the eigenvalue magnitude, so it is important that the columns of $\mathbf{V}_k$ are re-orthogonalized. It is for this end that we used the IRLM algorithm which has several advantageous properties, highlighted below, relative to other re-orthogonalization approaches (Calvetti et al., 1994; Golub and Van Loan, 1996). The basic idea is to iteratively restart a truncated Lanczos factorization (as in Eq. [3.10]) with the goal of replacing the first Lanczos vector $\mathbf{v}_1$ with $\mathbf{V}\mathbf{e}_1$ at each iteration, which sequentially approaches a vector that is very close to a linear combination of the actual k eigenvectors of $\mathbf{L}$. When this latter condition is satisfied by $\mathbf{v}_1$, then $\mathbf{f}$ vanishes (Calvetti et al., 1994). Of importance, however, is that the number of restarts is unknown beforehand. The update of $\mathbf{V}_k$ comes from the decomposition of $\mathbf{H}$, which is similar to $\mathbf{L}$, by shifted QR iteration to compute its Ritz pairs. The Ritz values become exact eigenvalues of $\mathbf{L}$ when $\mathbf{f}_k$ is $\mathbf{0}$, and the Ritz vectors are used to iteratively update the

Lanczos vectors, enhancing and damping the components of $\mathbf{v}_1$ in the wanted and unwanted directions, respectively, until termination of the algorithm (Lehoucq et al., 1998).

The IRLM begins with a prior Lanczos factorization to construct *k*+*p* Lanczos vectors,

$$\mathbf{L}\mathbf{V}_{k+p} = \mathbf{V}_{k+p}\mathbf{H}_{k+p} + \mathbf{r}_{k+p}\mathbf{e}_{k+p}^{T}, \tag{3.11}$$

where p is a fixed, small number on the order of k (or possibly smaller). We set p = max(k,20). Then, until convergence based on a small tolerance of **r**, a p-step implicitly shifted QR iteration is performed on $\mathbf{H}_{k+p}$ to form $\mathbf{H}_{k+p} - \mu\mathbf{I} = \mathbf{Q}\mathbf{R}$, where **Q** has orthonormal columns, **R** is upper triangular, and both are square with dimension k+p. Next, $\mathbf{V}_{k+p}$ is updated as $\mathbf{V}_{k+p}\mathbf{Q}$, or in other words $\mathbf{v}_1$ is updated with the orthogonal transformation from the QR-factorization of **H** (for the purpose stated above), thereby re-computing the initial k-step decomposition in Eq. (3.10) with a single matrix product. As the final step of each iteration, p additional Lanczos steps are performed to compute a new k+p-step Lanczos factorization as in Eq. (3.11). The combined steps of p shifts and p Lanzcos steps per iteration require each only p matrix-vector multiplications with **L** (Calvetti et al., 1994). Although complex, the algorithm is efficient when k is modest, and the total storage required is fixed and minimally 2Nk + O(Nk), which is considerably less than other iterative re-orthogonalization algorithms.

Through the remainder of this paper we verify that the proposed parameterization is best suited for characterization and updating of coarse-scale properties relative to the spatial scale of the parameterized region. We do not include or update high-frequency spatial variability as in many cases data resolution would not allow for estimation of such fine-scale details even when they are included; therefore, a highly truncated (*k*+*p* step) matrix decomposition is not a limiting factor in our approach but is in fact preferred.

3.3.5 Conceptual Approach To Parameter Estimation

In **Section 3** we have thus far developed the useful properties of the GCT basis, namely its adaptability to any grid structure or sub-grid region, its model independence, pairwise orthogonal basis functions, and the relation of such functions to harmonics of the grid structure. Together these properties form a flexible construct for parameterization of a hydraulic property defined on the grid and permit model calibration to be solved using a multiscale approach in the spectral domain.

3.3.5.1 Prior Model Considerations

Our approach is conceptually developed in practical consideration of the prior geologic model which may be completely un-informed to well-informed. In the case of an un-informed prior (e.g., a homogenous field), the intent of parameter estimation is to *identify* global features over the complete grid or model domain from the observation data alone. We exemplify this approach in **Subsection 3.4.1**. In the case of a well-informed prior, the intention is to minimally *update* the existing model pre-defined from other data sources. The parameterization is adaptable to prior information in two ways. First, one or more individual regions consistent with different geologic structures (e.g., hydrostratigraphic units) can each be assigned a unique basis for local estimation. Second, the order of basis function inclusion in the parameterization can be defined from prior model compression performance, or using those functions onto which the prior model projection magnitude is largest. We apply both approaches to prior model adaptation in this subsection.

Apart from the prior model assumption, as described the model heterogeneity is adjusted during the calibration using a multiplier field that is parameterized and sequentially updated in the transform domain using a multiscale algorithm. The implementation of the algorithm is described in the next subsection. The scalar projection onto the GCT basis functions of the multiplier vector **u**, with dimension $n_u \times 1$ where n_u is the length of the estimable property in vector format, is given by

$$\mathbf{v} = \mathbf{\Phi}^T \mathbf{u} \Leftrightarrow \mathbf{u} = \mathbf{\Phi v} \,. \tag{3.12}$$

The n_v columns of the matrix $\mathbf{\Phi}$ are the pairwise orthogonal basis functions each of length n_u. The column vector $\mathbf{v}$ is the n_v-length spectrum of transform coefficients, or the parameter set in the transform domain, with dimension equal to the number of basis functions in $\mathbf{\Phi}$. The inverse transform from the spectral to spatial domain is efficiently computed from the orthogonality of the basis. To reiterate, $\mathbf{\Phi}$ is a partial decomposition of the Laplacian and contains only a few (n_v) of the lowest-frequency Lanczos vectors corresponding to the smallest (approximated) eigenvalues and sorted in increasing order.

3.3.5.2 Multiscale Parameter Estimation

In the multiscale algorithm we update the multiplier $\mathbf{u}$ from a low modal frequency or coarse spatial description to a higher frequency description. We follow the approach to sequential estimation in the frequency domain presented in Bhark et al. (2011b) in which similar approaches to data-driven multiscale calibration algorithms are also reviewed that, as a rule, rescale the geologic model in the spatial domain via sequential refinement or coarsening. The approach of sequential refinement is particularly well suited to our current implementation for two reasons in addition to those emphasized in the literature, and is appropriate regardless of prior model information and assumptions.

First, it is geologically consistent to identify or update large- before small-scale structures (e.g., the type of depositional environment may influence smaller length scales and directions of spatial variability), with the latter becoming insensitive to production data beyond some spatial scale (Vasco et al., 1997; Lu and Horne, 2000; Sahni and Horne, 2005; Bhark et al., 2011b). In our implementation the sequential refinement of the multiplier field does not update the prior model until a level of detail is reached, if any, at which the multipliers become sensitive to the data. Our results demonstrate that the prior, beginning at the coarsest scale, is not updated when it is either correctly defined or insensitive to the data available (e.g., in the case of non-uniqueness).

The second motive for multiscale parameterization is related to the compression performance of the transform basis. By construction, the GCT basis is well suited for low-rank approximation of a function defined over the grid. Recall that in a special case the basis reduces to the DCT basis which was initially developed for optimal compression performance in the least-squares sense (Ahmed et al., 1974). Although we do not compress or low-rank approximate the spatial parameter itself in order to retain the prior model at full resolution, strong compression performance directly implies that large-scale geologic features can be characterized by the multiplier using only a few basis functions. There has in fact recently been a growing body of literature that examines the energy compaction performance of Laplacian eigenvectors. In an original work, Karni and Gotsman (2000) compressed the geometry of unstructured mesh surfaces by projecting the mesh coordinate vectors onto basis functions derived from decomposition of the Laplacian as defined in Eq. (3.4). They empirically demonstrated significant compression performance or minimal loss in mesh quality by a low modal frequency representation, verifying the rapid decrease in transform coefficients when sorted from low to high frequency. In a related study Zhang (2004) investigated the compression performance, among other matrix-theoretic properties, using eigenvectors of four different Laplacian operators and observed an efficient compression for all variants. Ben-Chen and Gotsman (2005) showed for two-dimensional triangle meshes that if the vertex coordinates are assumed to follow a multivariate Gaussian distribution then the eigenspectrum of the Laplacian in Eq. (3.4) provides optimal compression performance of the geometry in the least-squares sense. In the following subsection we exploit these results and demonstrate through empirical analysis how a spatial property can be well defined at multiple scales as the linear combination of the GCT basis functions. However, prior to a compression analysis we first present the modal shapes associated with individual basis functions for different grid geometries to provide some idea of the types of spatial features that are constructed as their linear combination.

3.3.5.3 Multiscale Application of Basis Functions

Three different grid geometries are presented in each row of Fig. 3.2, each applied later in a model calibration analysis, along with selected GCT basis functions for each. The functions are mapped to their corresponding grid and are ordered left to right from the lowest to higher modal frequencies. Recall that the constant basis function, corresponding to the zero frequency with a corresponding eigenvalue equal to zero, is always first. The inclusion of additional basis functions in the transform of Eq. (3.12), i.e., adding from left to right in Fig. 3.2, permits the addition of successively finer spatial scales of variation into the multiplier field. Initially all coefficients except that corresponding to the constant basis function will have a value of zero; therefore, the increase in magnitude of any of these coefficients will add spatial variability as their linear combination.

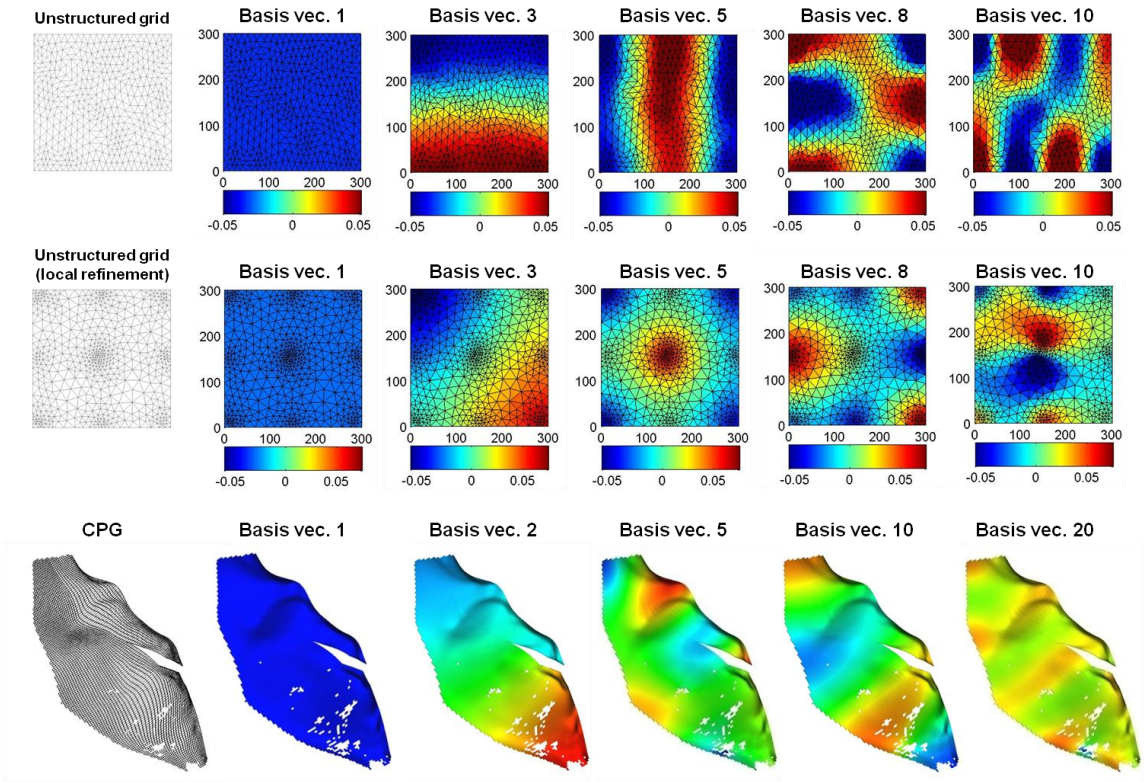

Fig. 3.2. Three different 2-D grid/mesh structures (column 1) and selected corresponding eigenvectors or basis functions (columns 2-6) depicting the lowest to higher modal frequencies.

In Fig. 3.2 the modal shape associated with each basis function evidently differs with the grid shape, structure and geometry. We highlight these relationships in the corresponding applications in **Subsection 3.4**. Here we demonstrate the compression performance of the basis for an irregular corner-point grid with a discontinuity at a fault. For this example we use a single layer of the Brugge reservoir model (see the field description in **Subsection 3.4.3**) and exhibit the low-rank approximation of a high-resolution, heterogeneous permeability field representative of a delta plain depositional environment. The permeability field at full spatial detail, characterized at 4,922 grid cells, is shown at the upper-left in Fig. 3.3. To the right in the figure are its coarse approximations using the 5, 10, 20, 30, 50 and 100 leading (or lowest modal frequency) basis functions, a selected set of which was shown in row 3 of Fig. 3.2. Even using 10 to 30 basis functions of the potential total of 4,922, the large-scale heterogeneity is visible and indicates that a multiplier could exactly reproduce this field at the same low level of parameterization. The compression performance using up to the 500-leading basis functions is shown also in Fig. 3.3 at the lower-left. The compression error sharply drops as basis functions are added to the field description and indicates strong compression performance, a considerable accomplishment for a model-independent basis. If the basis functions were applied optimally (i.e., sorted by the magnitude of the transform parameters from large to small) then the compression error would smoothly decrease with the successively higher-rank approximations; however, this would require prior knowledge of the most important basis functions and is in fact the approach that we use when the prior is well informed.

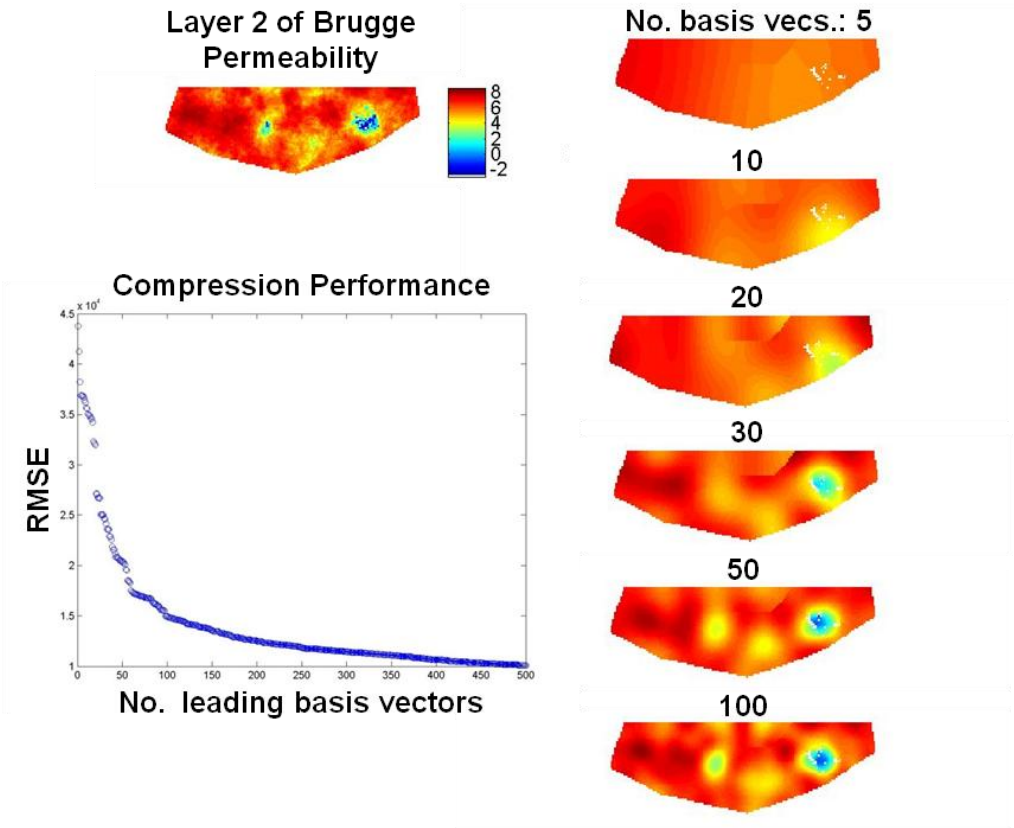

Fig. 3.3. Compression performance (lower left) of a 2-D permeability field (top left) and low-rank approximations of the field at different levels of parameterization (right column).

We also consider the case of a regionalized geologic model in which structural features (e.g., facies) or heterogeneous regions are independently parameterized. The top row of Fig. 3.4 shows a two-dimensional high-resolution permeability field that is arbitrarily partitioned into three regions based on a threshold that considers the magnitude of permeability and distance between each cell. Each subsequent row of Fig. 3.4 shows a single basis function for the three regions and corresponds to the same modal frequency, from the lowest to higher modes. During model calibration the regions can be either independently or simultaneously updated. The key point to now appreciate regarding regionalized, multiscale parameterization is that the frequency described by any given basis function, with the sole exception of the constant function, scales with the size of the region. That is, the term ‘coarse scale’ is defined relative to the size of the region.

For example, in Fig. 3.4 compare the frequency behavior of the 2nd basis function (row 3) in the smallest region (column 1) versus largest region (column 3) where the apparent 'wavelength' scales with the size of the region. The implication is that prior geologic information should be used to regionalize a hydraulic parameter field, if regionalization is appropriate, such that length scales of spatial variability within each are consistent. We demonstrate this in two of the applications.

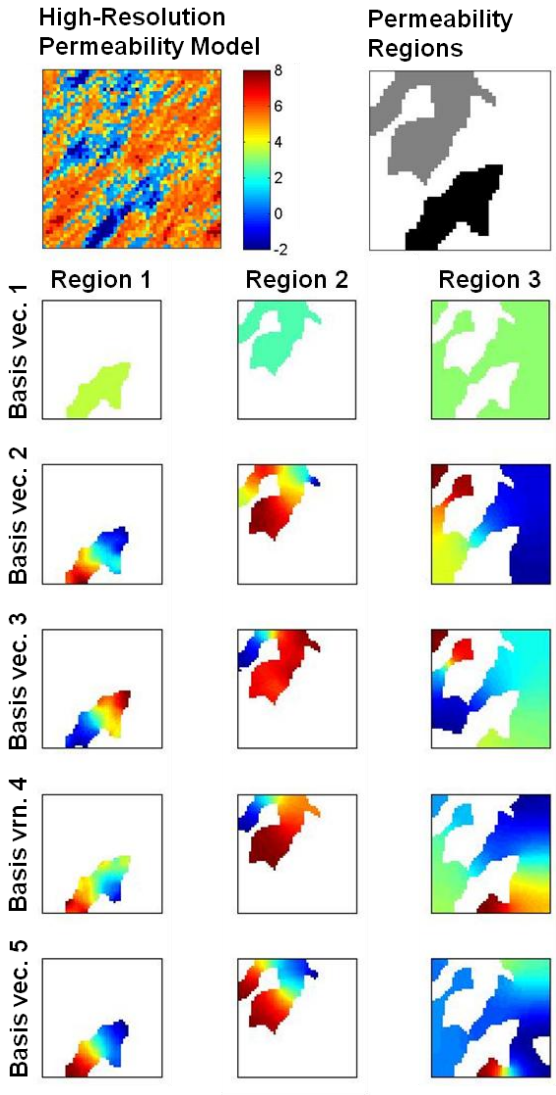

Fig. 3.4. 2-D permeability field (top left) and its partitioning into three regions (top right). Each row below shows a single basis function, per individual region, corresponding to the same eigenvalue rank.

3.3.6 Numerical Approach to Parameter Estimation

This subsection presents the proposed multiscale calibration workflow that is summarized in the flowchart in Fig. 3.5. The workflow involves the sequential inclusion of basis functions into characterization of the calibrated model through the multiplier field. In this study we consider permeability, defined at each grid cell, as the estimable property. Before each step of refinement, the permeability is applied in an iterative cycle that involves petroleum reservoir flow simulation for computation and subsequent minimization of a data misfit cost function. The generalized form of the flow model from which cell pressure and saturations are defined in all applications was presented in **Subsection 1.2.3.1**. Before proceeding with the applications, we first define the objective function used to quantify misfit between observed and simulated production data, and also review the iterative gradient-based scheme used to reduce data misfit.

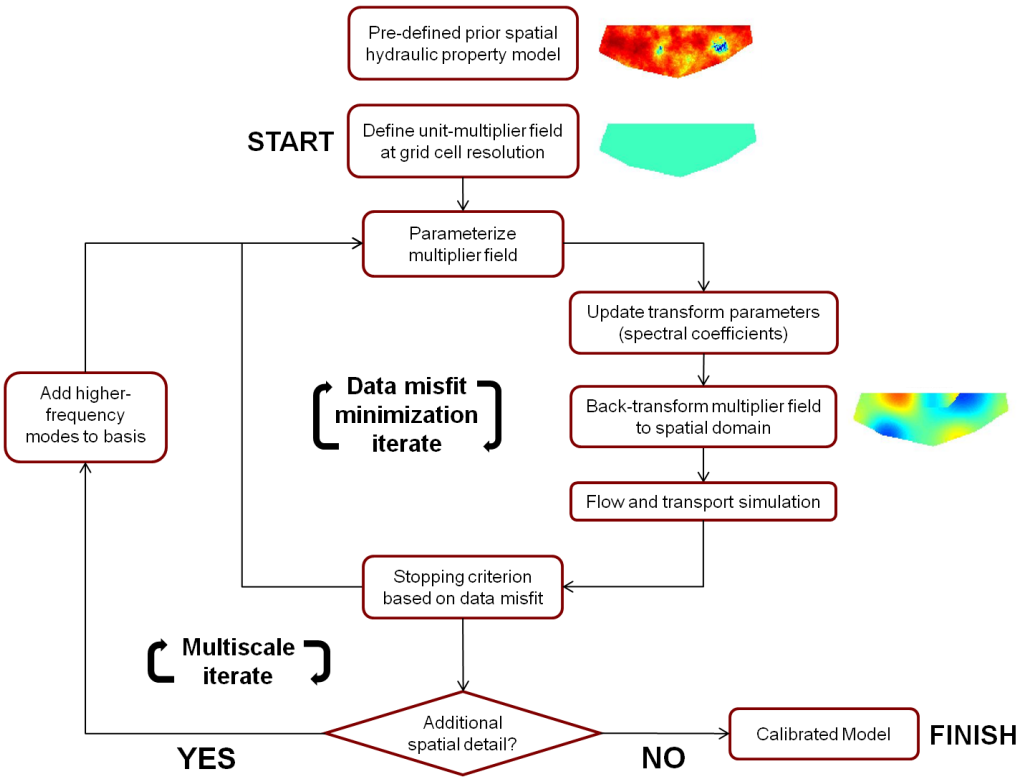

Fig. 3.5. Model calibration workflow. The images exemplify the prior hydraulic property model and the updated parameterized multiplier field.

3.3.6.1 Objective Function

The calibration objective function $J(\mathbf{v})$ is defined upon solution of the flow model for cell pressures and saturations using the updated absolute permeability field. The objective function is defined as the squared l_2-norm of nonlinear dynamic data misfit,

$$J(\mathbf{v}) = \left\| \mathbf{Q}^{1/2} \left(g(\mathbf{k}(\mathbf{v})) - \mathbf{d}_{obs} \right) \right\|_2^2, \tag{3.13}$$

where $\mathbf{v}$ is the parameter vector in the transform domain (see Eq. [3.12]), $g(\cdot)$ is the nonlinear model relating parameters to observations, $\mathbf{d}_{obs}$ is the observed dynamic data vector and $\mathbf{Q}$ is a diagonal matrix with components equal to the square of each datum weight. The permeability field $\mathbf{k}$ applied in the flow model is computed as the entrywise product of the multiplier field and the prior permeability field k_0, and is defined as $\mathbf{k} = \exp\{(\mathbf{\Phi v}) \cdot \ln k_0 \}$. We reiterate that the estimable parameter is the multiplier field, denoted as parameter vector $\mathbf{v}$ in the transform domain, which we use to update the static prior permeability k_o to form $\mathbf{k}$. The associated characteristic curves are assumed constant at each cell, but may vary from cell-to-cell when warranted by other petrophysical measurements or assumptions.

We recognize that a misfit term penalizing deviation from the prior model may also be included if desired. However, as discussed and later demonstrated in applications, the multiplier field updates the prior model only when warranted by the production data at some spatial scale, otherwise preserving the prior information.

3.3.6.2 Objective Function Minimization

The model calibration workflow (Fig. 3.5) begins by considering a small set of the lowest modal frequency basis functions to parameterize the unit multiplier field. Data misfit in $J(\mathbf{v})$ is iteratively minimized using the gradient-based BFGS quasi-Newton method (Nocedal and Wright, 2006). The gradient with respect to parameters in the physical or spatial domain is either directly computed through one-sided finite difference

perturbation of the transform coefficient or using parameter sensitivities made available from a commercial reservoir simulator using its built-in adjoint method (Schlumberger, 2009). In the latter case, the gradient is computed with respect to parameters in the spectral domain by chain rule of differentiation as follows:

$$J(\mathbf{v}) = \left(g(\mathbf{k}(\mathbf{v})) - \mathbf{d}_{obs}\right)^T \mathbf{Q}^{-1} \left(g(\mathbf{k}(\mathbf{v})) - \mathbf{d}_{obs}\right)$$

$$\begin{aligned} \frac{\partial J}{\partial \mathbf{v}} = \frac{\partial J}{\partial \mathbf{k}} \frac{\partial \mathbf{k}}{\partial \mathbf{v}} &= 2\left(g(\mathbf{k}(\mathbf{v})) - \mathbf{d}_{obs}\right)^T \mathbf{Q}^{-1} \left(\frac{\partial g(\mathbf{k}(\mathbf{v}))}{\partial \mathbf{k}} \right) \exp\left(\ln \mathbf{k}_0 \cdot \boldsymbol{\Phi}\mathbf{v}\right)_d \ln \mathbf{k}_{0,d} \boldsymbol{\Phi} \\ &= 2\left(g(\mathbf{k}(\mathbf{v})) - \mathbf{d}_{obs}\right)^T \mathbf{Q}^{-1} \left(\frac{\partial g(\mathbf{k}(\mathbf{v}))}{\partial \mathbf{k}} \right) \mathbf{k}_d \ln \mathbf{k}_{0,d} \boldsymbol{\Phi} \end{aligned} \tag{3.14}$$

where the vectors with subscript d are transformed to diagonal matrices of equivalent dimension to account for the entrywise product.

When $J(\mathbf{v})$ converges at the current level of parameterization, which is determined by either a tolerance in minimum data misfit improvement or by a threshold on the number of iterations permitted, the parameter set is increased by adding basis functions to the multiplier description. The inclusion of spatial variability into the multiplier, and therefore the absolute permeability model, is based on the linear combination of several modal frequencies. Therefore, the basis vectors must be added in sets which are approximately grouped as the different directional components of the same modal frequency. For example, in the special case of a regular periodic grid, i.e., when using the DCT basis, the selective addition by directional and frequency components can be performed exactly (Bhark et al., 2011b). In the case of irregular geometries, an exact relation between modal frequency and direction does not exist, so the grouping of basis functions for their sequential inclusion is subjectively determined and based on the sensitivity of the case-specific production data to different scales of variability, as we perform in the applications. However, in Bhark et al. (2011b) we discuss the implementation of higher modes by selective procedures that use sensitivity information or solutions from previous iterations to guide basis element selection. Regardless, it is

important to understand that the sole consequence of adding too few basis functions during a refinement step is an increase in the overall simulation count. In such an instance, parameter updates do not reduce the objective function and the forward simulations involved are wasted. On the contrary, the incorporation of too many basis functions into the multiplier description in practice results in rapid convergence to a local minimum from which the solution cannot recover, and may also result in local updates inconsistent with geological description.

In order to compensate for the informal expansion of the parameter set, in our analyses we perform a gradient screening analysis for each basis function within the set prior to its incorporation. At no additional computational cost, upon the expansion of the parameter set the gradient contribution from each is computed at the first iteration, and all parameters that have zero contribution (within some small tolerance) are withheld from the inversion at the current scale. At subsequent levels of refinement, any previously frozen parameters are again considered in the screening procedure; the gradient at a single location on a response surface typically changes with iterates.

3.3.6.3 Analysis of Data Misfit

Production data misfit is analyzed from three approaches. First and most importantly, when applicable a production forecast is included after the calibration period, over a time interval at least one half the duration of the calibration period. Second, the production data correlation coefficient, introduced by Cooley and Naff (1990) and applied by Hill (1998) and Doherty (2005), is computed for each well response in the model over the complete (calibration plus forecast) production period. This metric indicates the strength of the linear relationship between the observed and simulated data when plotted on opposing axes of a scatterplot, ideally having a slope of unity when the intercept equals zero. Following the abbreviations above (see Eq. [3.13]), the correlation coefficient R is calculated for an individual well response as

$$R = \frac{\left(\mathbf{Q}^{1/2}\mathbf{d}_{obs} - \boldsymbol{\mu}_{obs}\right)^T \left(\mathbf{Q}^{1/2}\mathbf{d}_{sim} - \boldsymbol{\mu}_{sim}\right)}{\left(\mathbf{Q}^{1/2}\mathbf{d}_{obs} - \boldsymbol{\mu}_{obs}\right)^T \left(\mathbf{Q}^{1/2}\mathbf{d}_{obs} - \boldsymbol{\mu}_{obs}\right)\left(\mathbf{Q}^{1/2}\mathbf{d}_{sim} - \boldsymbol{\mu}_{sim}\right)^T \left(\mathbf{Q}^{1/2}\mathbf{d}_{sim} - \boldsymbol{\mu}_{sim}\right)} \tag{3.15}$$

where $\boldsymbol{\mu}$ is a constant column vector with dimension equal to the number of data (N_d), with each vector component equal to $1/N_d \sum_{i=1}^{N_d}\left(Q_{ii}^{1/2} d_i\right)$, and is computed separately for the observed ($\boldsymbol{\mu}_{obs}$) and simulated data ($\boldsymbol{\mu}_{sim}$). R provides a general measure of goodness of production data misfit as it is independent of the number of observations considered and incorporates data weights, thereby enabling a generic comparative measure between different calibration exercises. A value of greater than 0.90 is generally required for data misfit to be within acceptable limits (Cooley and Naff, 1990; Hill, 1998).

The validity of the correlation coefficient assumes normality of the residuals centered at zero, so for each production well we compare residual summary statistics against observation noise (when available). We posit that for a satisfactory calibration, particularly in synthetic modeling scenarios where the distribution of noise is known, the residuals should have a mean near zero and a range within that of the artificial noise. Outliers corresponding to specific production times and at individual well locations indicate misrepresented geologic updating or areas of required re-investigation relative to the coarser spatial scales of heterogeneity that are resolved by the available data.

3.4 Applications

In this subsection the GCT parameterization is employed in three model calibration applications to demonstrate the diversity of subsurface flow models for which the workflow is applicable. The prior model assumptions range from the case of completely un-informed to well-informed from multiple data sources, and are defined on a suite of grid geometries that include unstructured and irregular corner-point cells, local grid refinement and discontinuity at faults. We also compare the GCT approach in

application with the KLT parameterization to provide insight into its strengths and limitation, and also the type of calibration scenarios for which the GCT is best suited.

3.4.1 Two-Dimensional Unstructured Grids

This application utilizes simple unstructured triangular grid geometries to demonstrate the basis construction and its geometric flexibility. It is also designed to reveal the relationship between cell geometry and individual (vector) components of the basis functions using a locally refined grid. The two-dimensional grids (previously shown in Fig. 3.2) are constructed using the MATLAB® FEM toolbox and are imported to the MRST (MATLAB Reservoir Simulation Toolbox) flow and transport simulator (Lie et al., 2010). We use MRST to solve the two-phase (oil-water) incompressible pressure equation in **Subsection 1.2.1** using a mimetic finite-difference pressure solver. The saturation solution required for waterflood simulation is solved in sequence after each pressure update using an implicit single-point upwind scheme. For the two-phase fluid model we define constant fluid densities and viscosities, and specify quadratic relative permeability curves with an end-point mobility ratio of 5.0.

In this exercise we estimate cell permeability by calibrating observed water production rates (WPR) on two different grids, one with approximately uniform grid density and one with higher density or local refinement near wells, shown in Figs. 3.6A and 3.7A, respectively. Both support a nine-spot waterflood pattern with pressure-controlled injection and production. Selected leading basis functions for each grid were shown in rows 1 and 2 of Fig. 3.2. Both grids have a constant three-point connectivity structure to immediate neighbor cells except at boundaries; therefore, the Laplacian eigenvectors reduce to the DCT basis (Strang, 1999; Karni and Gotsman, 2000). It is important at this point to consider that the Laplacian, and therefore the basis functions, do not consider the spatial distance between or the size of cells but only their two-point connectivity. For example, the second basis vector of both unstructured grids in Fig. 3.2 corresponds to the first cosine frequency $2\pi k/N$ for $k = 1$. In the more uniformly gridded case (row 1), the

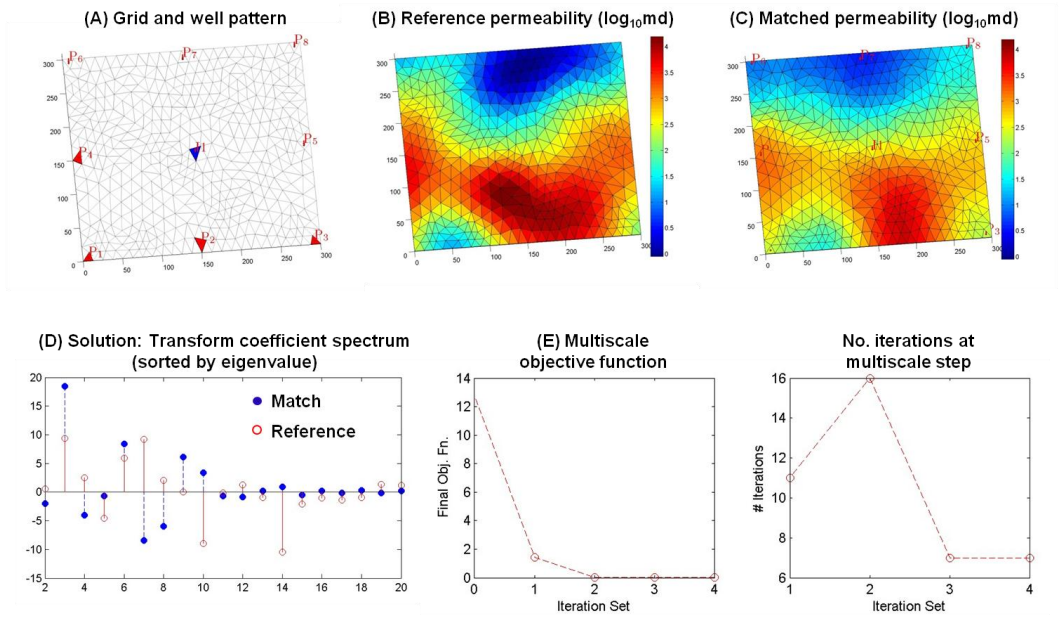

Fig. 3.6. (A) The 2-D reservoir model (homogenous) mesh and well pattern. (B) The reference and (C) calibrated permeability field. (D) Spectrum of transform parameters for the reference and calibrated fields. (E) Objective function value at successive multiscale iterates and the number of gradient-based minimization iterations at each multiscale iterate.

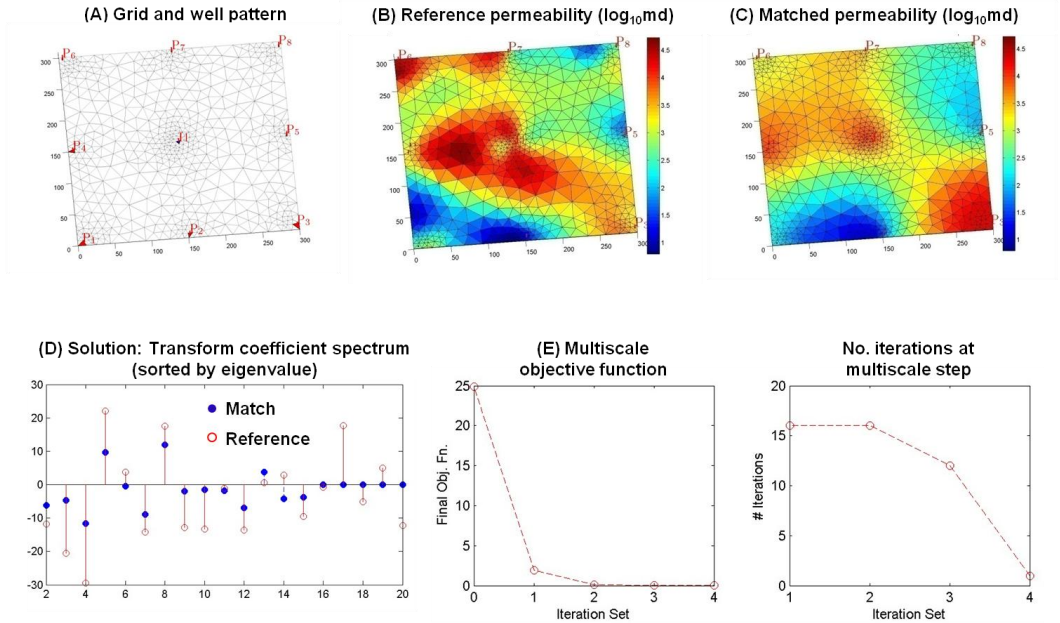

Fig. 3.7. (A) The 2-D reservoir model (locally refined) mesh and well pattern. (B) The reference and (C) calibrated permeability field. (D) Spectrum of transform parameters for the reference and calibrated fields. (E) Objective function value at successive multiscale iterates and the number of gradient-based minimization iterations at each multiscale iterate.

frequency pattern is nearly uniform in the horizontal direction and would be exactly uniform in the case of a rectangular grid such that this function would distinguish only vertical variability. However, in the case with local refinement (row 2) it becomes apparent that the basis function components are simply mapped to their corresponding cells, thereby distorting the modal shape. This proves to be a beneficial artifact of the Laplacian construct because it enables a finer-scale permeability description in refined areas which is appropriate when hydraulic properties are better resolved from measurement near these areas, or when the intent of discretization itself is to better capture velocities in areas of complex geometry or boundary conditions.

The reference permeability fields used to generate synthetic WPR observations are shown in Figs. 3.6B and 3.7B for the two grids. White noise of up to ±5% of the absolute value was added to each datum by random selection from a Uniform distribution over that range. The model calibration for both cases is initiated with a uniform permeability field; therefore, the intent of the estimation is to *identify* the global heterogeneity over the complete domain. Consistent with the multiscale approach, the multiplier field is initially parameterized by the five lowest modes. The objective function is then minimized using an iterative descent scheme where the gradient is constructed from one-sided finite-difference perturbation of each transform parameter. For example, the five parameters at the initial level of parameterization require six forward simulations to complete a single iteration. Following a reduction of the objective function into a local minimum at this coarse description, the parameter set is updated by adding the next five highest modes and again performing iterative minimization. This sequence is repeated up to a final parameterization of twenty basis functions for each of the cases. Figs. 3.6E and 3.7E show the objective function reduction for each case over the four refinement steps required to achieve the calibration. As more basis functions are added to the parameter description, both the number of iterations and the relative reduction in the objective function are reduced at each refinement step, supporting the assumption that it is beneficial to capture larger- before finer-scales of heterogeneity when integrating production data into a geologic model. Although not shown, updating

all twenty coefficients in a single step results only in local updates near wells that provide acceptable data misfit but that are inconsistent with expected geologic description.

The calibrated permeability fields are shown in Figs. 3.6C and 3.7C, and their corresponding parameter spectrums in Figs. 3.6D and 3.7D. Note that because the prior permeability is uniform, permeability at the solution is related to the multiplier field by a constant, i.e., the multiplier field is able to completely characterize heterogeneity over the domain. The solution spectrum in each case appropriately shows a gradual decrease in parameter magnitudes from lower to higher modal frequencies, corresponding with the large-scale and smooth variability depicted in the reference models, and also supports the approach of adaptive and sequential refinement.

The WPR data misfit at each producer for the uniformly and locally refined cases is shown in Figs. 3.8 and 3.9, respectively, over a four-year calibration period, plus a two-year forecast period. Tables 3.1 and 3.2 show WPR misfit metrics per well for the respective figures. The response correlation coefficient, R, indicates an acceptable response match for all wells over the calibration and forecast period, and the match residuals are approximately centered at zero and have a range close to that of the white noise added. These results demonstrate that the algorithm identifies multiscale permeability heterogeneity that correctly captures the wide range of water breakthrough times and the subsequent WPR forecast, as well as the lack of breakthrough at multiple producers. Additionally, and in further support of a multiscale approach, notice that several smaller-scale features in the reference model for the locally refined grid (Fig. 3.7B) are not reproduced in the solution (Fig. 3.7C). This demonstrates the relative insensitivity of production data to high-frequency heterogeneity, and is verified by the acceptable data misfit for WPR.

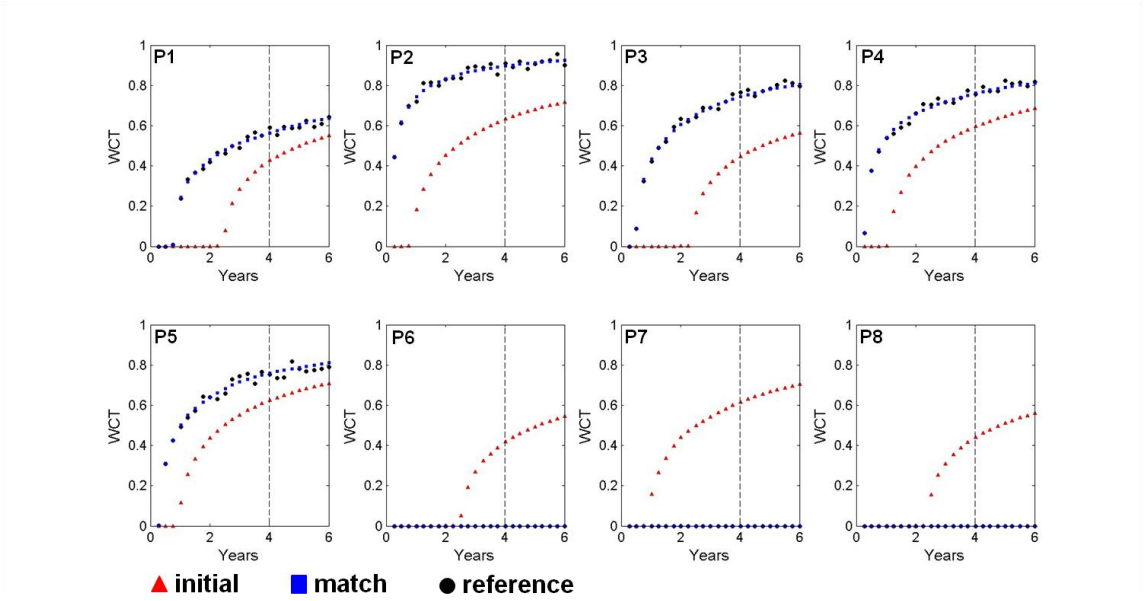

Fig. 3.8. Simulated watercut corresponding to the reference, initial/prior and calibrated permeability fields. Well labels correspond to Fig. 3.6A. Responses at time greater than the vertical dashed line at 4 yrs represent the forecast period.

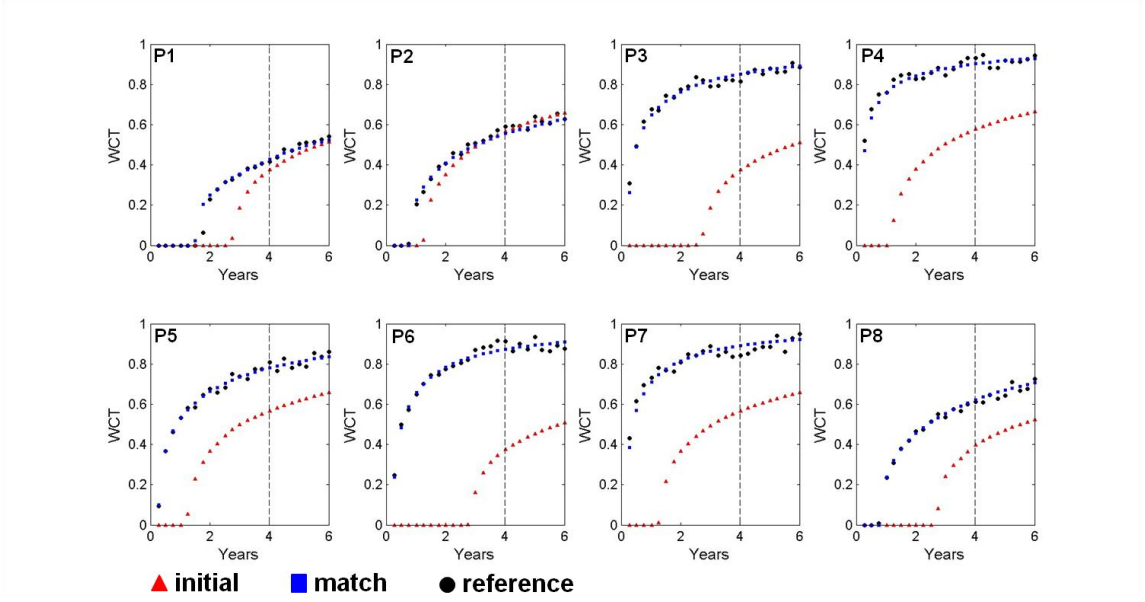

Fig. 3.9. Simulated watercut corresponding to the reference, initial/prior and calibrated permeability fields. Well labels correspond to Fig. 3.7A. Responses at time greater than the vertical dashed line at 4 yrs represent the forecast period.

Table 3.1: Production data misfit metrics of correlation coefficient (*R*) and the minimum, mean and maximum of the fit residual and observation noise for the individual well production responses in Fig. 3.8. The simulated production responses correspond to the calibrated permeability field in Fig. 3.6C.

		Production well (see Figure 6A)							
		P1	**P2**	**P3**	**P4**	**P5**	**P6**	**P7**	**P8**
	R	0.996	0.986	0.996	0.993	0.993	1.000	1.000	1.000
Minimum	**residual**	-0.029	-0.049	-0.054	-0.033	-0.033	0.000	0.000	0.000
	noise	-0.029	-0.036	-0.022	-0.030	-0.038	0.000	0.000	0.000
Mean	**residual**	0.020	-0.007	0.002	0.000	0.009	0.000	0.000	0.000
	noise	-0.002	0.000	0.004	0.002	-0.006	0.000	0.000	0.000
Maximum	**residual**	0.070	0.035	0.034	0.035	0.040	0.000	0.000	0.000
	noise	0.027	0.037	0.030	0.035	0.035	0.000	0.000	0.000

Table 3.2: Production data misfit metrics of correlation coefficient (*R*) and the minimum, mean and maximum of the fit residual and observation noise for the individual well production responses in Fig. 3.9. The simulated production responses correspond to the calibrated permeability field in Fig. 3.7C.

		Production well (see Figure 7A)							
		P1	**P2**	**P3**	**P4**	**P5**	**P6**	**P7**	**P8**
	R	0.989	0.997	0.990	0.974	0.994	0.988	0.974	0.998
Minimum	**residual**	-0.021	-0.045	-0.044	-0.047	-0.031	-0.050	-0.047	-0.030
	noise	-0.017	-0.028	-0.043	-0.039	-0.033	-0.044	-0.041	-0.030
Mean	**residual**	0.006	-0.008	0.000	-0.008	0.000	-0.002	0.003	0.005
	noise	0.002	0.002	-0.009	0.002	0.002	-0.007	0.002	-0.006
Maximum	**residual**	0.142	0.027	0.038	0.034	0.032	0.039	0.055	0.031
	noise	0.020	0.027	0.034	0.037	0.030	0.043	0.040	0.031

3.4.2 Comparison of the GCT and KLT Parameterization

Before proceeding with the GCT applications, in this subsection we compare the GCT with the well known covariance-based KLT parameterization with the intent of raising key points regarding the strengths, limitations and types of modeling applications for which the GCT is appropriate. The KLT basis is computed as

$$\mathbf{\Phi} = \mathbf{V}\mathbf{\Lambda}^{1/2} \tag{3.16}$$

following the nomenclature and definitions in Eqs. (3.12) and (3.13). The covariance matrix **C** can always be constructed empirically as in Eq. (3.17) below, and together with the solution of the eigenvalue problem for **C**, the KLT basis is constructed from the decomposition

$$\mathbf{C}_N = \frac{1}{N}\sum_{j=1}^{N}\mathbf{y}_j\mathbf{y}_j^T = \frac{1}{N}\left(\mathbf{Y}-\overline{\mathbf{Y}}\right)\left(\mathbf{Y}-\overline{\mathbf{Y}}\right)^T = \left(\mathbf{V}\boldsymbol{\Lambda}^{1/2}\boldsymbol{\alpha}\right)\left(\mathbf{V}\boldsymbol{\Lambda}^{1/2}\boldsymbol{\alpha}\right)^T \tag{3.17}$$

where **C** is the $N \times N$ parameter covariance matrix, $\left(\mathbf{Y}-\overline{\mathbf{Y}}\right)$ is a set of centered realizations (column vectors) y_j of length N, and α is a N-length column vector of uncorrelated random variables. Embedded within the application of Eq. (3.17) are the following important suppositions. Sufficient information must be available to characterize the covariance, either analytically or empirically. In the latter approach, construction of **C** may be computationally daunting ($O[N^3]$) for large grids. The re-parameterized spatial information will be honored with up to a second-order characterization, so continuous heterogeneity (e.g., from multi-point geostatistics) is not guaranteed to be reproduced after parameter estimation. When prior information in the form of directions and scales of spatial variation are approximately correct, the basis functions will succinctly update the dominant (large-scale) heterogeneity with a low-rank parameterization. However, when the prior information in y_j is incorrect, inversion performance is shown to be poor (Jafarpour and McLaughlin, 2009).

For comparison with the GCT approach, we use the KLT parameterization to estimate cell permeability in the model calibration scenario presented in the previous application with the goal of reproducing the reference permeability in Fig. 3.6B from the production data. Two parameter estimation examples are performed each using a different covariance model, the first corresponding to an isotropic Gaussian variogram model, the same model used to generate the reference field (Fig. 3.6B), and the second to an incorrect anisotropic Gaussian model. For each, 100 realizations were constructed using sequential Gaussian simulation (Pebesma, 2004) to construct **C**. A single realization

corresponding to the isotropic and anisotropic models are respectively shown in Figs. 3.10A and 3.10D, together with metrics that verify convergence of the covariance for each case. In Fig. 3.11 the leading basis functions corresponding to the two KL expansions and to the GCT are compared, depicting the types of permeability heterogeneity that are defined as their weighted linear combination in each case. The parameter estimation is performed using the identical adaptive approach of sequential refinement presented previously. The objective function reduction for the two KLT cases and the GCT are compared in Fig. 3.12E over the four refinement steps before convergence to a local minimum. The KLT case corresponding to the correct covariance (or variogram model) has a more efficient minimization because the basis functions reflect the same prior information as in the reference model. The corresponding calibrated permeability in Fig. 3.12B well captures the global reference heterogeneity shown in 3.12A. With the improper covariance assumption, data misfit reduction does not perform as well but remains acceptable as a result of heterogeneity non-uniqueness, demonstrated by the 'calibrated' permeability in Fig. 3.12D. Although the error from non-uniqueness is obvious in this toy problem and using the most simple of geostatistical models, in a field application with more complex heterogeneity such a difference may not be known and the actual failure of the calibration non-obvious.

The two KLT end-member cases of correct and blatantly incorrect prior information place the GCT approach in the middle, where the generic form of the basis functions adapt to the data misfit when applied sequentially beginning at the coarse scale. The decision to use the GCT versus KLT is fundamentally based on uncertainty in the prior. The KLT is preferred when the prior is well known because of its optimal variance-preserving compression, although the above-mentioned limitations must also be satisfied. If there is uncertainty in the prior, particularly at larger scales, then the GCT provides a parameterization that is unhindered by computational burden and flexible in the characterization of multiscale geologic continuity. Further, we demonstrate in the next subsection how the prior model, when warranted, can be preserved using the GCT

by the selective inclusion of basis functions, an approach not applicable in this subsection because we began the inversion using a uniform (i.e., uninformed) prior.

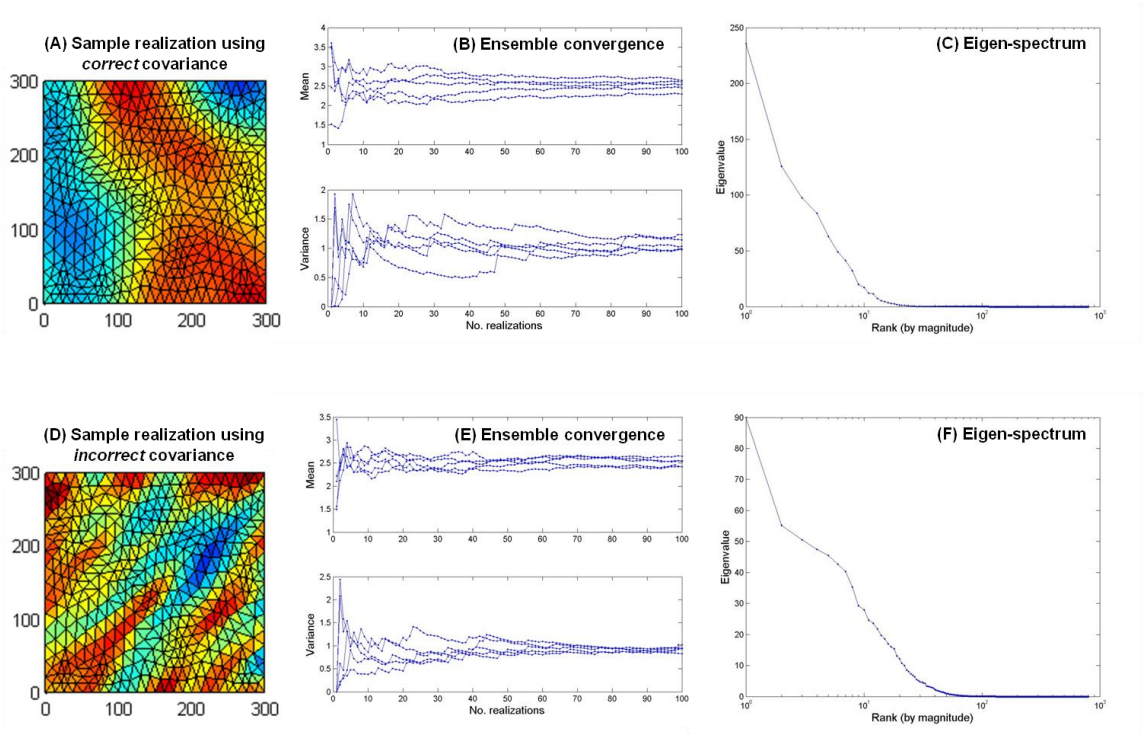

Fig. 3.10. Individual permeability ensemble members corresponding to an (A) isotropic and (B) anisotropic covariance model. For each 100-member ensemble, the second column verifies covariance convergence of mean and variance for 5 randomly selected cells in the corresponding grids. The third column shows the covariance matrix eigen-spectrum for each ensemble.

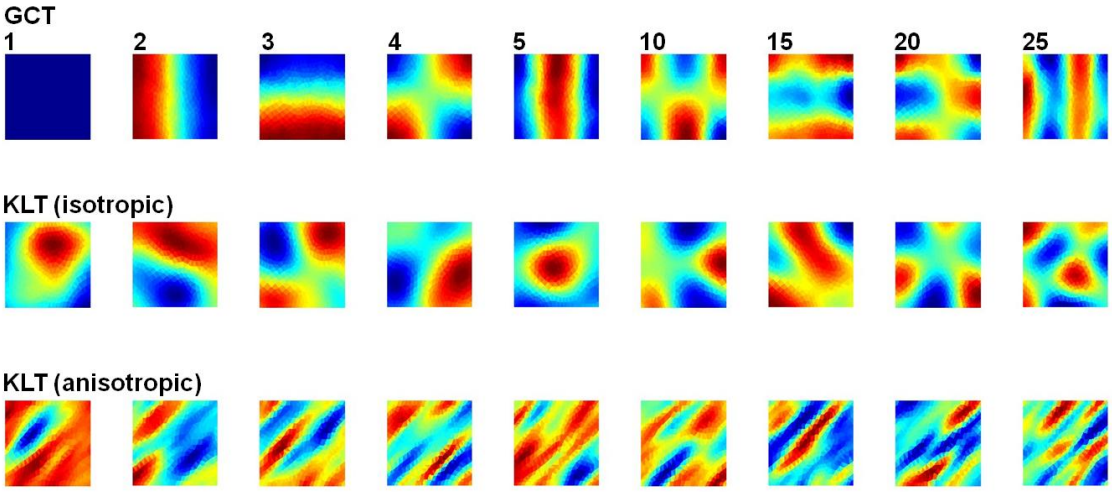

Fig. 3.11. Leading GCT basis functions from low to higher modal frequency (left to right) for the GCT parameterization (top row) and for the KLT parameterization using isotropic (middle row) and anisotropic (bottom row) covariance models.

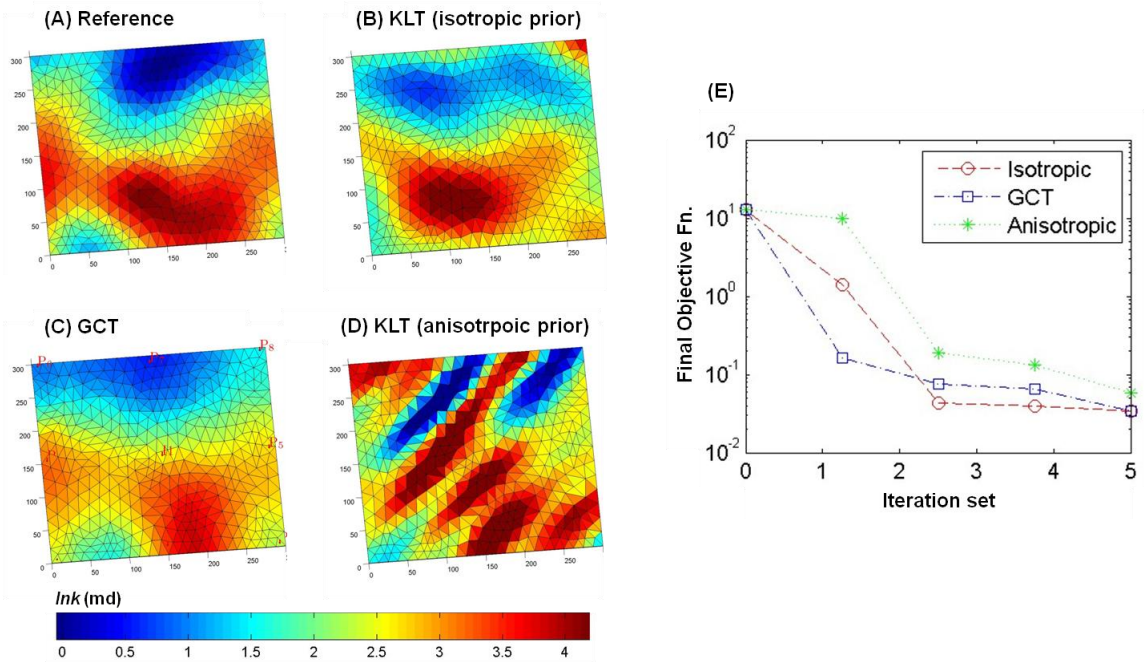

Fig. 3.12. The (A) reference permeability and calibrated permeability fields corresponding to the (B) KLT parameterization with correct covariance assumptions, (C) GCT parameterization, and (D) KLT parameterization with incorrect covariance assumptions. (E) shown the objective function minimization during upon termination of each multiscale iterate.

3.4.3 Brugge Reservoir Model

In this application we update a high-resolution prior permeability model on an irregular and faulted corner-point grid in calibration of the Brugge reservoir model. The Brugge model is a synthetic benchmark case developed by TNO (a Dutch organization for contract research) to evaluate closed-loop production optimization strategies. Details of the comparative project are in Peters et al. (2010). Prior to production optimization the project required and provided data for calibration of the permeability field, from which we have developed this analysis. The Brugge reservoir properties replicate a North Sea Brent-type field within an East-West elongated half-dome with a truncating boundary fault at its north edge and a single interior fault. The reservoir model grid, initial oil-phase saturations, and the well pattern with twenty producer in the dome and ten peripheral injectors in the supporting aquifer are shown in Fig. 3.13. The three-dimensional grid has 44,355 active cells in nine layers, depicted in Fig. 3.14 at the left. The flow model is solved using a commercial simulator (Schlumberger, 2009) with fully implicit discretization. Production response sensitivities to static grid cell properties (i.e., permeability) are derived from the simulators built-in adjoint code.

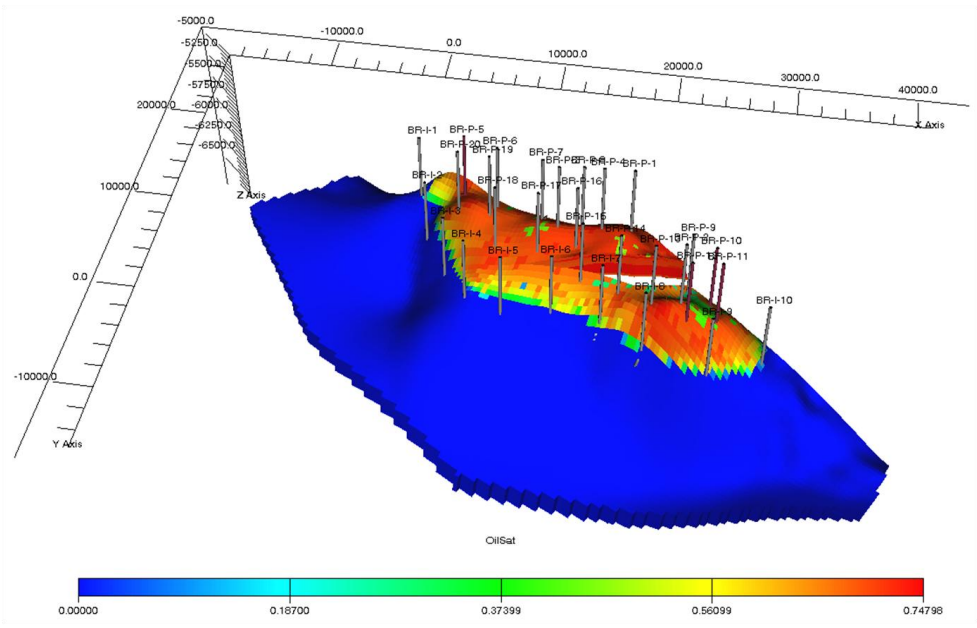

Fig. 3.13. Initial oil saturation in the Brugge reservoir model.

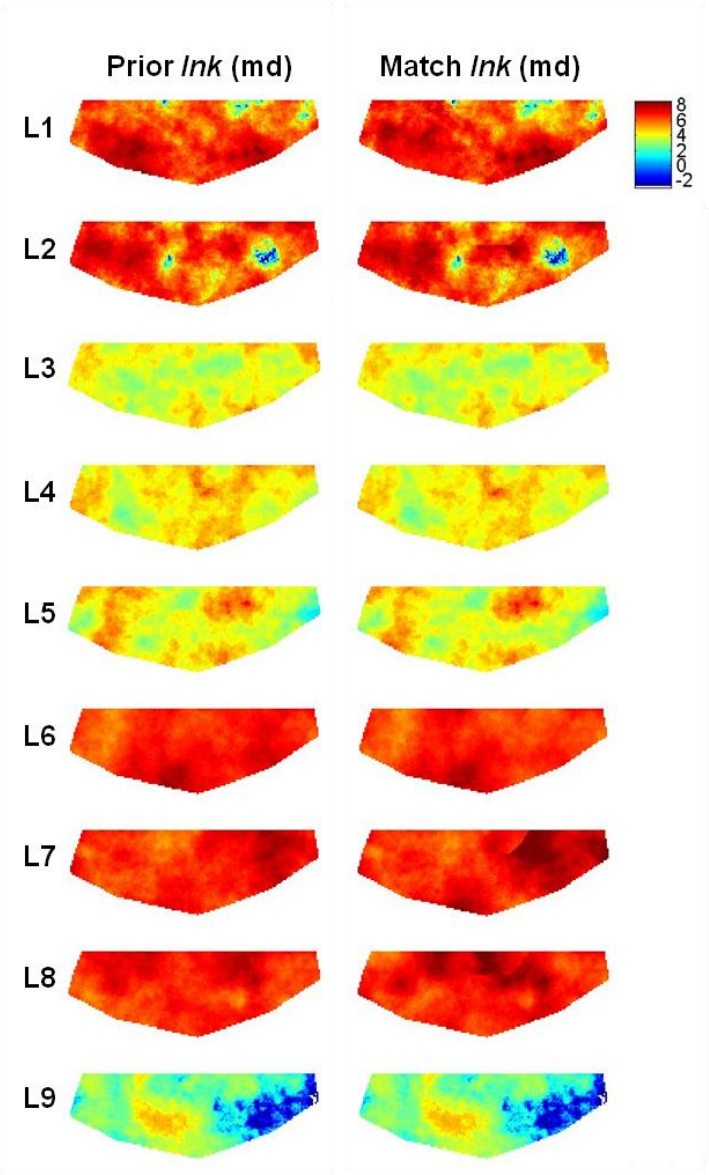

Fig. 3.14. Individual layers (by row) of the Brugge prior permeability model (first column) and calibrated model (second column) using a parameterized multiplier field (see Fig. 3.15).

Production data of WPR, oil production rate (OPR) and bottom-hole pressure (BHP) at each producer are provided with the project for a ten year calibration period. Also provided are 104 realizations of permeability, porosity and saturation region. In this application we update permeability within a single realization by matching WPR and BHP at each of the twenty producers.

The permeability multiplier field is parameterized based on consistency with the well-informed prior geologic description. The prior model in Fig. 3.14 at the left shows four distinct formations, each of a similar depositional setting, but each with a visibly different range of permeability magnitude and scale of variation. Also, the approximate correlation length of variability in the vertical direction is apparently at the grid cell scale, i.e., features at a single horizontal coordinate are not necessarily correlated in the juxtaposing layers regardless of the formation type. For these reasons, each layer is individually parameterized, or is assigned a unique GCT basis, for model updating. A key point is that the regional definition of the bases from the depositional description provides one method by which the GCT parameterization is adaptive to prior information. Although not depicted, we found that the parameterization of one or more layers together results in the merging of discontinuous vertical features during model updating, thereby reducing the prior heterogeneity that is to be preserved.

Several of the lower frequency functions for a single horizontal layer of the Brugge grid were shown in row 3 of Fig. 3.2. Notice that the modal shapes reflected by the basis functions beyond the constant function are approximately oriented with the directions of maximum and minimum elongation, consistent with the vibrational modes or invariants of the grid structure (Chung, 1997), and also honor the discontinuity across the fault. The implication of this behavior is that permeability features along these orientations are expected to be well characterized by individual basis functions. Model grids are generally constructed to conform to geologic understanding, so the parameterization will benefit in this case by reducing the number of basis vectors required to capture larger-scale features with similar primary directional components.

Prior model heterogeneity is also enforced in the multiscale integration by the selective addition of basis functions during sequential updating. In order to determine this sequence, each layer of the prior permeability is projected onto the 500 lowest-frequency basis functions. For example, the compression performance of the top layer permeability was shown in Fig. 3.3. The basis functions are then sorted by their projection magnitude,

in descending order, which determines the order in which they are sequentially applied in the workflow. This is the second key point regarding the ability of model-independent transforms to benefit from prior information when available.

For the calibration, the multiscale approach begins with the parameterization of the multiplier (per layer) using the five leading modes. Then, following minimization of the objective function, the parameterization of each layer is updated by the next five modes at each successive multiscale step. The multiplier fields at the solution of each step are shown in Fig. 3.15. As the level of spatial detail is refined, permeability trends are adaptively refined based on their sensitivity to the production data. Sensitive layers corresponding to the higher-quality sands (layers 1-2, 6-8 in Fig. 3.14) are more impacted and permit updating at higher frequencies. Accordingly, the lowest quality sand (layer 9) showed no relative sensitivity to the observations and retained a multiplier of unity at the final solution despite its parameterization by twenty-five basis functions. The matched permeability field is shown in comparison to the prior model in Fig. 3.14. The updates in larger-scale trends are apparent while the high-resolution detail is maximally preserved in the updated model. Fig. 3.16 shows the objective function reduction over the five multiscale steps required to achieve the calibration, beyond which the data misfit would no longer reduce. Notice that as more detail is added to the model, both the number of iterations completed at each multiscale step and the reduction in the objective function is reduced, again supporting the importance of updating larger- before smaller-scale heterogeneity. Last, in Figs. 3.17 and 3.18 the WPR and BHP misfit plots are shown, respectively, for each of the twenty production wells. Production misfit metrics of R and residual summary statistics are shown for each well response in Table 3.3. There is an overall acceptable improvement in data misfit (e.g., see R values in Table 3.3), although at few wells the misfit remains unchanged or deteriorates as the cost of global improvement. In the cases of unacceptable misfit, the addition of higher-frequency modes to the permeability description does not improve misfit at these wells and implies that the global model identified is locally incorrect in these areas. The corresponding wells (i.e., P9, P15) are located close to, within a few grid cells of, the

interior fault boundary (Fig. 3.13) and require heterogeneity updating at local, individual grid cells to improve the production response misfit (e.g., using a streamline-based calibration method to adjust inter-well heterogeneity as demonstrated by Alhuthali et al. (2010) for the Brugge reservoir model). In field application, however, such a finding should result in re-analysis of geologic and boundary condition interpretations near these areas, which calls attention to the fundamental employment of model calibration as an analysis tool (i.e., assisted calibration) rather than as a replacement for the analyst (i.e., automatic calibration).

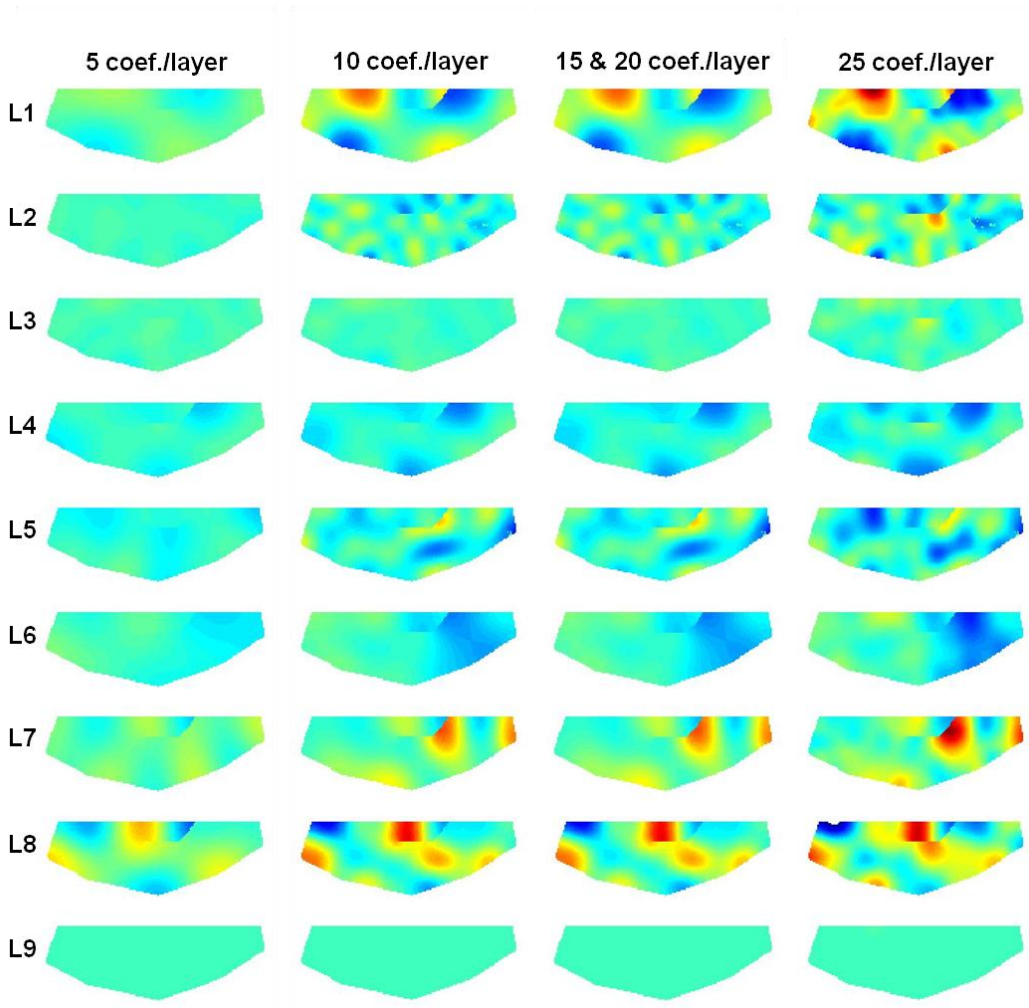

Fig. 3.15. Individual layers (by row) of the parameterized multiplier field at termination of the successive multiscale iterations (columns) during calibration of the Brugge permeability model.

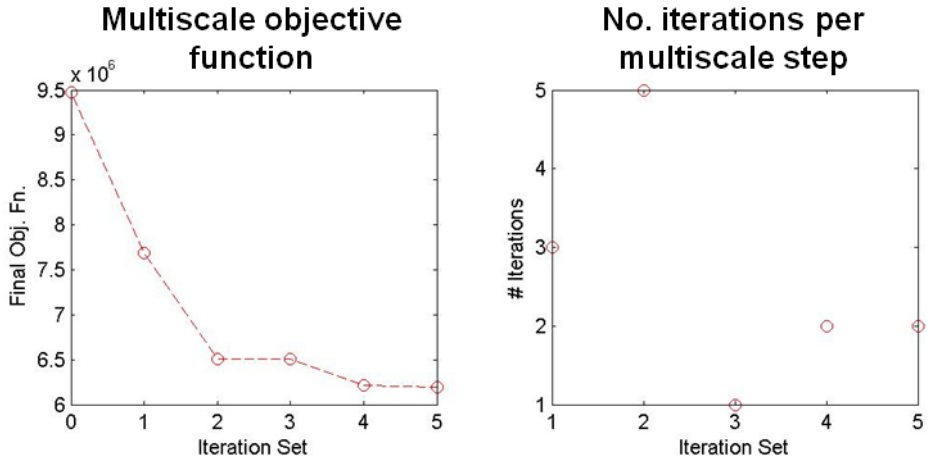

Fig. 3.16. Objective function minimization at multiscale iterates (left) and the number of corresponding gradient-based minimization iterates (right) during calibration of the Brugge permeability field.

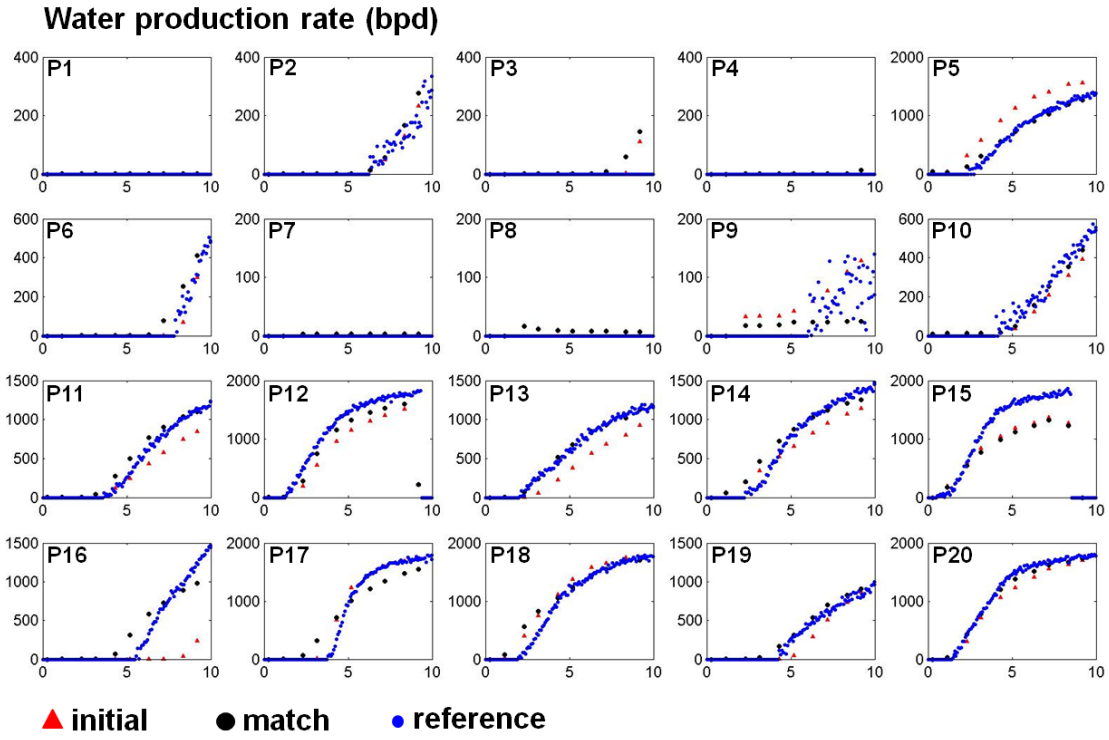

Fig. 3.17. Simulated water production rate at each production well corresponding to the reference, initial/prior and calibrated Brugge permeability fields.

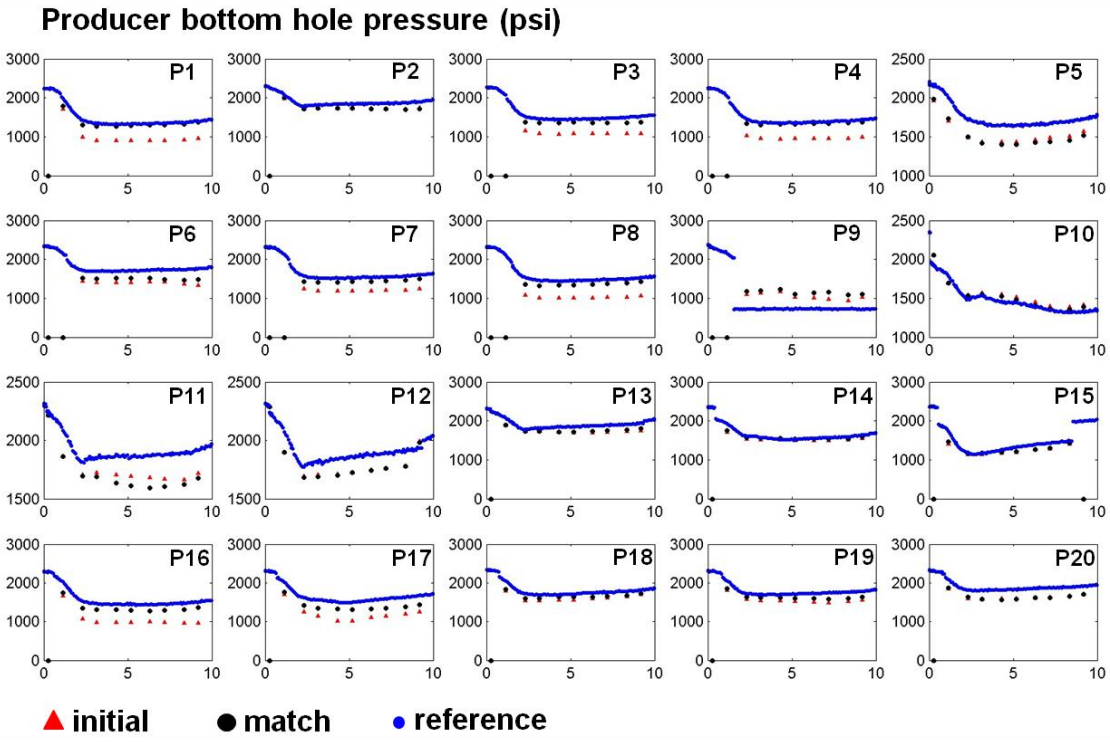

Fig. 3.18. Simulated bottom hole pressure at each production well corresponding to the reference, initial/prior and calibrated Brugge permeability fields.

Table 3.3. Production data misfit metrics of correlation coefficient (*R*) and the minimum, mean and maximum of the fit residual for the individual well production responses in Fig. 3.17. Observation uncertainty metrics were not provided with the calibration production data set (Peters et al., 2010). Values of n/a correspond to observation data sets of zero value for which *R* cannot be calculated.

	Production well (see Figure 17)									
	P1	**P2**	**P3**	**P4**	**P5**	**P6**	**P7**	**P8**	**P9**	**P10**
R	n/a	0.961	n/a	n/a	0.988	0.986	n/a	n/a	0.542	0.989
Min. residual	0.0	-34.8	0.0	0.0	-71.2	0.0	0.0	0.0	-95.0	-72.8
Mean residual	0.0	10.4	21.2	1.4	12.2	26.5	2.6	7.2	-11.3	-14.6
Max. residual	0.0	103.1	144.1	13.5	171.4	101.2	3.4	16.2	23.2	14.1

	P11	**P12**	**P13**	**P14**	**P15**	**P16**	**P17**	**P18**	**P19**	**P20**
R	0.984	0.989	0.993	0.986	0.770	0.970	0.900	0.975	0.984	0.995
Min. residual	-23.9	-1596.2	-41.4	-110.5	-605.6	-247.2	-258.8	-49.0	0.0	-137.2
Mean residual	62.6	-28.3	11.3	39.2	-278.7	35.9	-24.5	100.3	42.1	-49.6
Max. residual	192.4	2.7	80.7	299.0	103.4	313.1	360.6	439.0	84.8	24.1

3.4.4 Channel Facies Reservoir Model

In this application we employ the parameterization in a channelized reservoir model to show its utility for characterizing permeability in multiple regions or facies of complex geometry. The model is defined on a regular Cartesian grid with dimensions $87 \times 100 \times 5$ and uniform cells of size $40 \times 40 \times 2$ feet. The facies geometry is simulated using the object-based geologic modeling code FLUVSIM (Deutsch and Tran, 2002) to simulate a fluvial depositional environment. The reservoir model in Fig. 3.19 shows the three distinct facies considered: a background floodplain shale, reservoir quality channel sands and crevasse splay sands, the last formed when the channel is breached. Static reservoir conditions, dead oil (i.e., oil containing no dissolved gas) fluid properties and relative permeabilities are copied from the SPE10 Model 2 reservoir (Christie and Blunt, 2001) which is designed as part of a Brent sequence. We used unconditional sequential Gaussian simulation (Pebesma, 2004) within each facies to populate anisotropic permeability and defined a constant porosity per region, with all relevant parameters listed in Table 3.4. In Fig. 3.20 the reference absolute permeability is shown in each layer of the grid in (A) millidarcys (md) and in (B) *ln*(md), the former depicting spatial variability within the sand channels and the latter depicting variability in the shale.

Using the same model equations and simulator as in **Subsection 3.4.3**, we applied the reference permeability model in Fig. 3.20 in a two-phase waterflood simulation with five rate-controlled injection wells to generate reference observations of WPR at the seven BHP-controlled production wells. The observation set consists of monthly measurements over a two-year period with white noise of up to ±5% of the absolute value of each datum added, randomly sampled from a Uniform distribution over that range. For model calibration we use a different permeability realization consistent with the parameters in Table 3.4 and shown in Figs. 3.20A and 3.20B. The difference at each cell between the reference and prior models is shown in Fig. 3.21C and defines the desired permeability changes during the inversion.

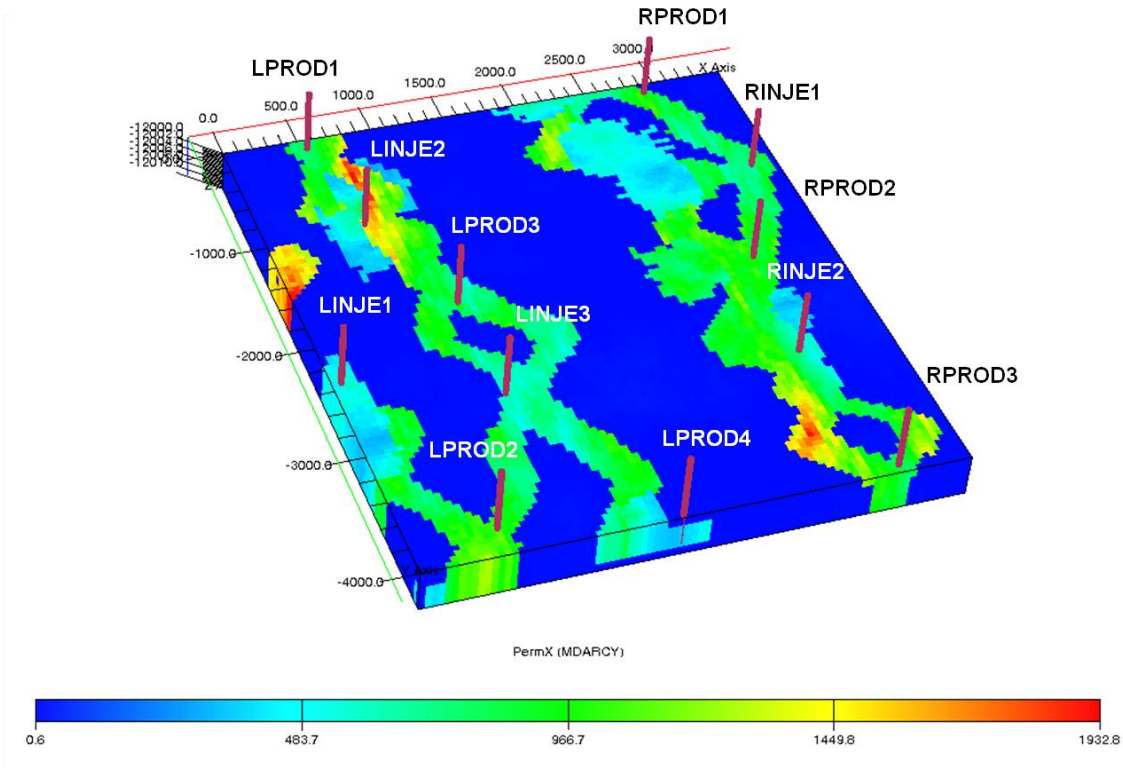

Fig. 3.19. Well pattern and prior permeability field for a three-facies channelized reservoir model including a background floodplain shale, reservoir quality channel sands and crevasse splay sands.

Table 3.4: Variogram parameters for the population of permeability within individual facies of a channelized reservoir model. Anisotropy ratio is the ratio of minor range/major range in the horizontal plane and is constant with depth.

Facies	Variogram model	Azimuth (°)	Major range (ft)	Aniso. ratio	Sill	$\log_{10}$(md)	Porosity
Channel	Spherical	0	2000	0.25	0.01	2.9777	0.20
Channel splay	Exponential	90	1000	0.75	0.01	2.6990	0.17
Shale	Exponential	0	1500	1.0	0.10	0.6990	0.05

For the calibration, the prior permeability model is divided into nine regions shown by color code in row 1 of Fig. 3.22, each of which is individually parameterized using a separate basis. The objective during model updating is to capture the spatial variation within the predefined region boundaries, which are assumed known from prior knowledge, and not to update the facies structure itself which falls into the scope of a

different intention in flow data assimilation (Roggero and Hu, 1998; Hoffman and Caers, 2005; Jafarpour and Khodabakhshi, 2010; Xie et al., 2010). A selection of leading basis functions, from the zero to higher modal frequencies, is shown for the nine regions in Fig. 3.22. Following the multiscale workflow (Fig. 3.5), model calibration was initiated by parameterizing a multiplier applied to each region individually with its corresponding five leading basis functions. After a reduction of the objective function to a local minimum at this coarse level, four additional levels of sequential refinement for up to a total of twenty-five basis functions per region were used to achieve the calibration. The multiplier field at the final solution is shown in Fig. 3.21A, the matched permeability in 3.21B and the difference at each cell between the reference and matched permeability models in 3.21C. The multiplier field reflects minimal changes (to *ln*(md)) centered near unity and demonstrates the ability to update trends within regions of complex geometry. A comparison of the permeability difference maps between the required and observed updates (Fig. 3.21C) further demonstrates that the direction of updates (i.e., positive and negative) are correctly identified between observation locations. In the areas of data insensitivity in the shale layer, the multiplier retains a consistent value of unity through the refinement steps and permeability is not updated. The WPR misfit between the prior, calibrated and observed (including noise) responses is shown per well in Fig. 3.21D over the two-year fitting period and an additional two-year forecast period. The corresponding WPR misfit metrics in Table 3.5 show for each well a high value of R, >0.98, and a residual range close to that of the white noise added. Altogether, the acceptability of the matched production responses, including the match of water breakthrough times, and the accuracy of the forecast support the correct identification of larger-scale heterogeneity within the geometrically complex regions using the multiscale approach.

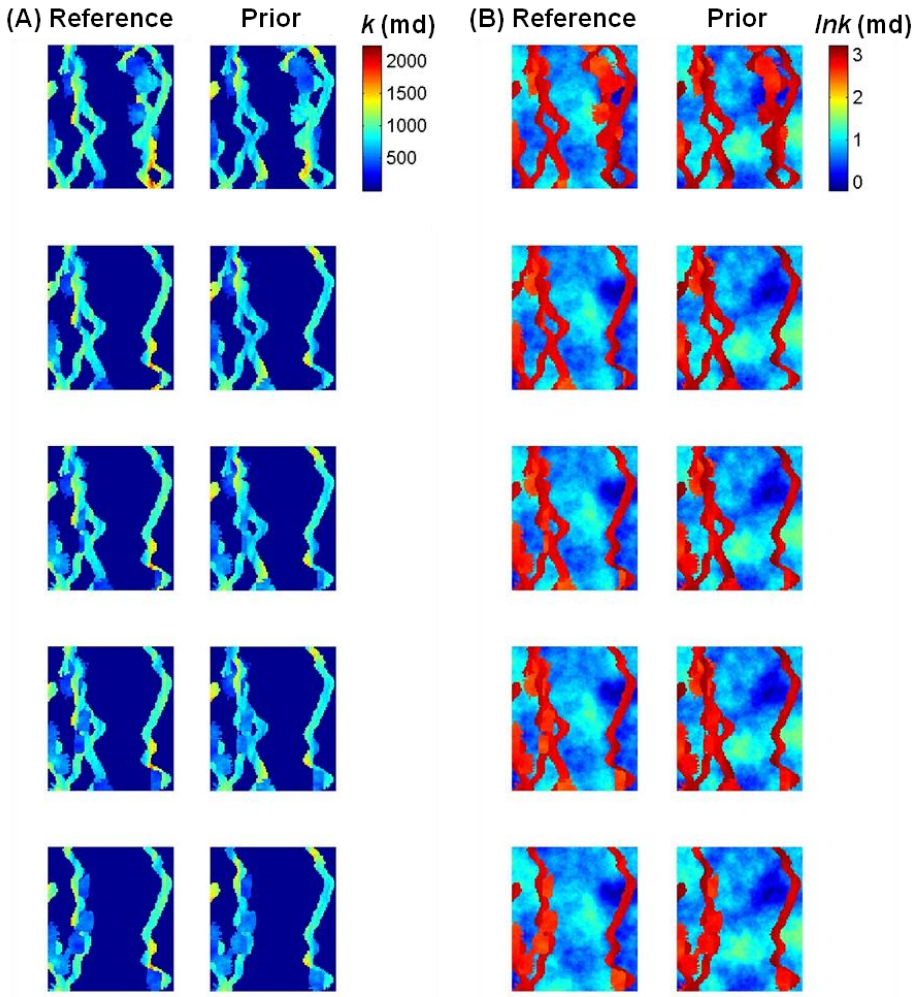

Fig. 3.20. Layers 1 through 5 (from top to bottom) of the reference and prior permeability models in (A) millidarcys (md) and in (B) *ln*(md). (A) depicts spatial variability within sand bodies and (B) the variability within the shale.

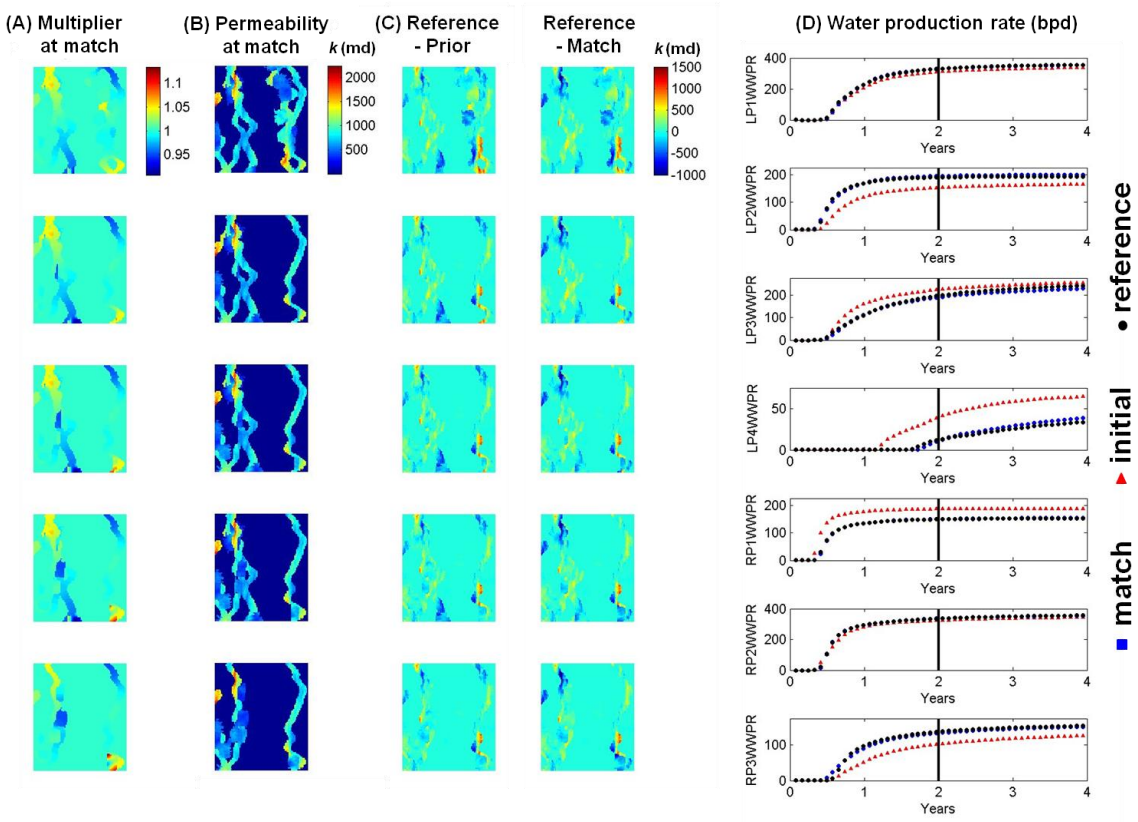

Fig. 3.21. Layers 1 through 5 (from top to bottom) of the calibrated facies model (A) multiplier field and (B) permeability field, and (C) the desired versus observed permeability changes during the inversion. (D) Simulated water production rate at each well corresponding to the reference, initial/prior and calibrated permeability fields.

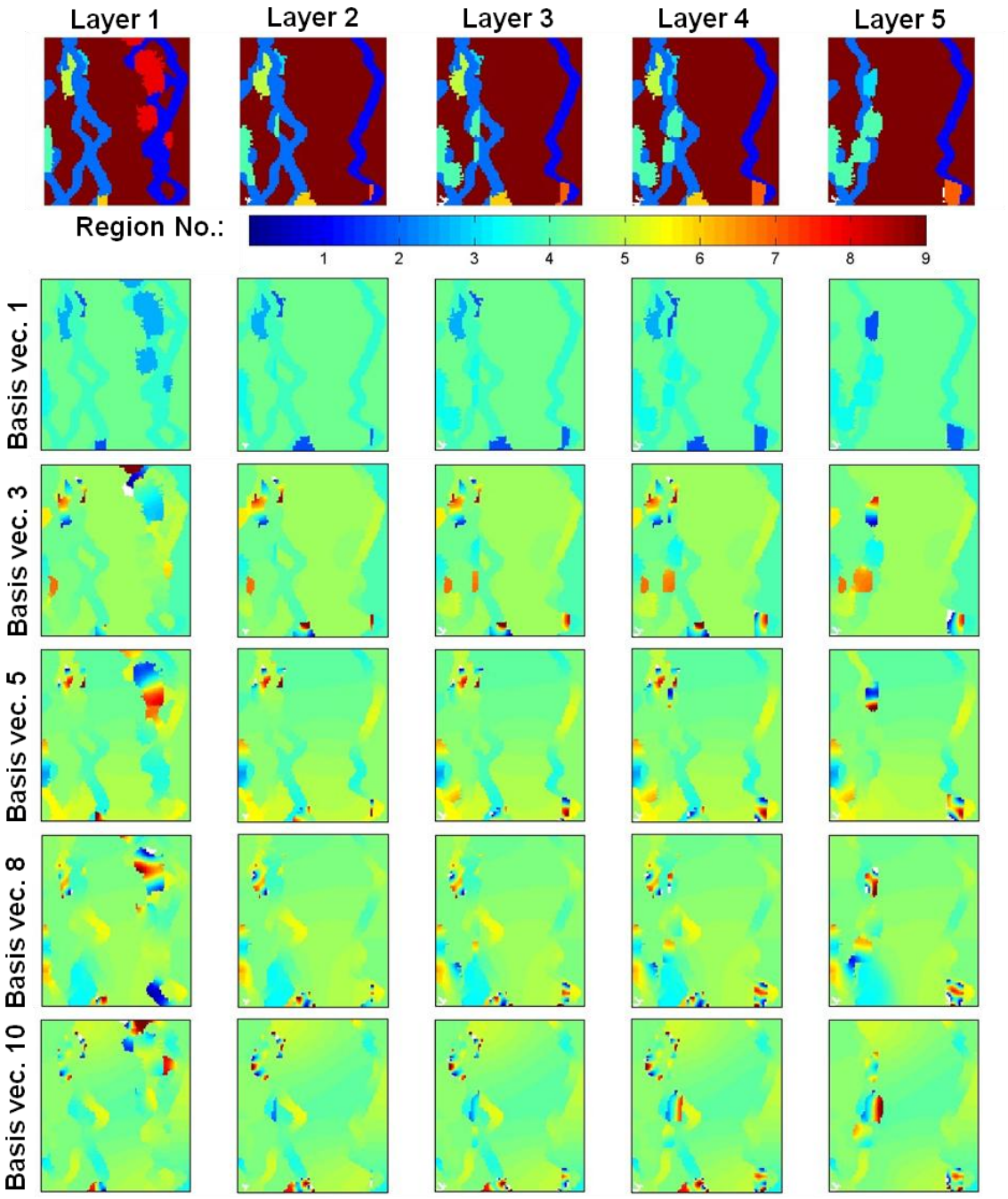

Fig. 3.22. (Row 1) The nine regions, each individually parameterized during model calibration, of the facies reservoir model by layer. (Rows 2-6) Selected basis functions for the nine regions.

Table 3.5: Production data misfit metrics of correlation coefficient (*R*) and the minimum, mean and maximum of the fit residual and observation noise for the individual well production responses in Fig. 3.21D. The simulated production responses correspond to the calibrated permeability field in Fig. 3.21B.

		Production well (see Figure 19)						
		LPROD1	**LPROD2**	**LPROD3**	**LPROD4**	**RPROD1**	**RPROD2**	**RPROD3**
	R	0.999	0.998	0.998	0.982	0.994	0.999	0.999
Minimum	**residual**	-6.239	-4.559	-10.378	-8.380	-27.402	-10.490	-4.719
	noise	-15.108	-8.648	-10.889	-1.032	-7.313	-15.123	-6.964
Mean	**residual**	-0.733	-0.670	-0.033	-0.372	-1.575	-2.078	-1.942
	noise	2.108	-0.239	-0.653	0.117	0.118	0.960	-0.677
Maximum	**residual**	6.335	5.340	16.535	2.995	1.140	7.021	2.084
	noise	15.768	9.447	11.913	1.540	6.951	15.150	6.230

3.5 Conclusions

In this section a novel method of hydraulic property model parameterization was introduced and applied for reservoir model calibration to dynamic data. The parameterization is achieved using a transform basis that linearly maps the estimable field at grid cell resolution from the spatial to spectral domain in which the calibration is performed. The generalized basis functions are defined as the (approximate) eigenvectors of the grid Laplacian and converge to special cases of the discrete Fourier basis when the grid structure is regular and certain periodic domain boundary conditions are assumed. In the general case, the basis functions represent the harmonics of the grid structure on which the property is defined and may, but are not required to, have similarity with the harmonics of the property.

By design, the GCT basis consistently provides a flexible and efficient construct for parameterization in any groundwater or reservoir model. Dependence on the grid connectivity alone implies that the basis can be constructed from, and therefore the parameterization applied to, any grid geometry and sub-grid region. The basis functions are also computed once and are fixed throughout the calibration workflow, assuming that the grid remains unchanged. The sparse symmetric structure of the Laplacain enables the efficient iterative approximation of only a few leading (lowest modal frequency) basis functions for grids with size on the order of one-million cells. These assertions are

verified in the next section, **Section 4**, as the GCT is applied for the history match of a large reservoir model simulating a mature waterflood through a complex geologic model characterizing turbidite depositional sequences.

Perhaps the most appealing feature of the GCT is its prior model independence in concert with the flexibility to honor prior information when available. The dominant spatial components of the prior heterogeneity can be maintained through the calibration by parameterizing individual regions based on geologic structure, and also by the inclusion of basis functions in the parameterization onto which the prior model projection is greatest. This unique capability comes with a constraint that determines the type of calibration scenarios for which the GCT may be appropriate. The spectral representation does not contain spatial information and therefore cannot locally characterize fine-scale spatial heterogeneity, particularly edge information, with a low-rank representation required for parameterization. Rather, the GCT is best suited for the characterization of larger-scale, potentially but not necessarily continuous, heterogeneity and has been theoretically and empirically shown to possess strong generic information compression performance.

When the restriction to coarser-scale model updating is a limitation, two avenues of research are proposed that may add to the diversity of calibration scenarios for which the parameterization is applicable. These involve the incorporation of more complex heterogeneity geometries and prior model information into the Laplacian matrix and, therefore, the transform basis. These developments define the subject matter of **Section 5**. A second approach based on Kernel methods is discussed in **Section 6** and is the subject of potential research.

4. GCT PARAMETERIZATION: FIELD APPLICATION*

4.1 Summary

The GCT parameterization is applied as the primary component of a structured history matching workflow for calibration of a field reservoir model. The workflow seamlessly integrates production data into the reservoir description from the facies to the grid-cell scale. In the first step of the workflow, the GCT is applied to parameterize the reservoir permeability using the coarsest scale basis functions to identify the large scale variability within and between the facies structures. Additional smaller-scale basis elements are then adaptively incorporated to successively refine the model to a level supported by data resolution, and are added in a sequence determined by generic modal frequency as prior model information is unavailable in this case. In the second and final step of the workflow, a streamline-based inversion is performed to locally adjust the reservoir model at grid-cell resolution along coarse scale preferential flow paths defined during the previous step using the parameterization, as well as by the well pattern.

The field case models an offshore turbidite reservoir with frequent well intervention including shut-ins, recompletions and pattern conversions. The static model has over three-hundred thousand cells, a complex channelized interpretation with faults, four injector-producer pairs with deviated wells and over eight years of production history including water-cut and pressure data. The GCT parameterization effectively updates the prior regional permeability at scales and locations warranted by the data, while preserving the geologic continuity and avoiding ad hoc redefinition of regions given the sparse well pattern. During the subsequent step of heterogeneity refinement along streamline trajectories, flow communication through the calibrated permeability field

---

*Part of this section is reprinted with permission from "Multiscale Parameterization and History Matching in Structured and Unstructured Grid Geometries" by Bhark, E., Rey, A., Datta-Gupta, A., Jafarpour, B., Paper SPE 141764 presented at the 2011 SPE Reservoir Simulation Symposium, 21-23 February 2011, The Woodlands, Texas, USA.

previously unrecognized in static geologic interpretation or manual history matching is identified.

4.2 Introduction

In field applications, history matching involves the integration of various types of dynamic measurements, from seismic down to the core, that capture data across a large range of spatial resolutions. Practical data integration algorithms must therefore follow suit in their ability to identify and update reservoir heterogeneity over a comparable range of spatial scales. Characterization of reservoir heterogeneity typically begins with the conceptual geologic model and the identification of regional attributes such as facies or depositional sequences, domain boundaries and boundary conditions, and faults or other sources of regional hydraulic (dis)continuity. Finer-scale patterns of heterogeneity within regional features may then be populated and updated when appropriate.

Accordingly, research and field application together have emphasized the establishment of reservoir engineering workflows that systematically reconcile the geologic model, from the regional to grid-cell scale, with multiresolution transient data. Related approaches to both manual and assisted history matching typically apply a structured approach and employ a series of data integration algorithms that are each suited to the scale of the estimated features and the type and resolution of the available data (e.g., Landa and Horne, 1997; Williams et al., 2008; Caers, 2003; Cheng et al., 2008; Yin et al., 2010). Approaches following this parsimonious rationale integrate data such as 3D/4D seismic, formation testing of pressure, pressure transient analysis and production phase cuts in a step-wise sequence, beginning at the global scale and often with the most simple description, followed by an attempt to update finer-scale details only when supported by the data or by related engineering decisions. There are in fact many instances when characterization at the grid-cell scale is supported, e.g., in mature fields with tens to hundreds of wells and decades of production history (e.g., Milliken et al., 2001; Agarwal et al., 2000) or using 4D seismic data (e.g., Lu and Horne, 2000;

Gosselin et al., 2003; Rey et al., 2009). In such cases, a proven and efficient method of reservoir model calibration in large, complex geologic models uses streamline-based techniques for local model refinement along preferential flow paths defined in the global prior model (Wang and Kovscek, 2000; Caers, 2003). Methods of streamline-based reservoir characterization implicitly capture heterogeneity by streamline trajectory and density and, accordingly, are well suited for the refinement of local spatial variability within regional heterogeneity.

In this section we propose and employ such a structured history matching workflow that adaptively integrates production data into a high-resolution geologic model to bridge the gap between automated regional zonation with pixel-based updating. The workflow first identifies or updates the prior regional heterogeneity and hydraulic continuity, down to the smallest scale supported by the available data, using the GCT parameterization. This first component of the workflow is identical to that presented in **Subsection 3.3.6** (Fig. 3.5). In the second and final component of the workflow, a streamline-based history match is performed to locally update the reservoir model along streamline paths implicitly determined by the larger-scale heterogeneity identified with the parameterization, together with the well pattern and schedule. It should be noted that this last step is based on the established streamline-based technique of Generalized Travel Time Inversion (GTTI). As there is no research contribution but only application, a minimal description of the GTTI application is provided sufficient only for a general understanding. However, it is important to present this streamline-based component as the associated results are relevant to and verify the utility of the GCT parameterization. The reader is referred to Bhark et al. (2011c) for a more complete description of the GTTI workflow and also for additional references.

In the remainder of this section, the complete structured history matching workflow is applied for a mature offshore reservoir with active reservoir management and extensive production data. The numerical simulation model contains more than three-hundred thousand cells, a complex depositional sequence of turbidite sands, four pairs of deviated

injection and production wells, and more than eight years of production data history including bottom hole pressure (BHP) and water cut (WCT) at each producer. We use the numerical reservoir model as presented in Rey et al. (2009) who previously performed a streamline-based history match of the WCT data and, therefore, rely heavily on this reference for geologic interpretation and insight. At the conclusion of this section we present a comparison of the reservoir model calibrated in this study with results from Rey et al. (2009), and also highlight the strengths of the GCT parameterization and GTTI when used in tandem.

4.3 Reservoir Description

The reservoir structure and hydrostratigraphy are characterized by a turbidite depositional system comprised of multiple sand sequences with highly variable levels of geometric overlap and uncertain hydraulic interconnectivity. Several primary sand bodies or facies corresponding to uniquely inferred depositional histories were identified from integrated seismic interpretation and well log data. In addition to the structure, these data were used also to quantify spatial reservoir quality in the static model by the net-to-gross (NETG) attribute. Other petrophysical properties including permeability and porosity in the dominant facies were then populated in the static model as the average property values estimated from the corresponding intersections with well log data. A sample cross-section from the seismic interpretation, adapted from Rey et al. (2009), is shown in Fig. 4.1A juxtaposed with the interpreted NETG map in (B) and a corresponding cross-section in (C) that depicts the individual facies layering. The interconnected units are combined with a system of transverse faults relative to the direction of sand deposition that are present primarily in the shallower regions of the reservoir to the south. Description of the hydraulic continuity across these faults is presented in the following discussions when relevant.

Production well locations and completion intervals were determined by the conceptual facies and fault model. Per Rey et al. (2009), the intent of well placement was to

complete injector-producer pairs within the reservoir quality facies in an orientation thought to improve sweep efficiency. Hydraulic continuity between flow units and across faults was then inferred from well pressure data and WCT responses, which we discuss below during presentation of the calibration updates.

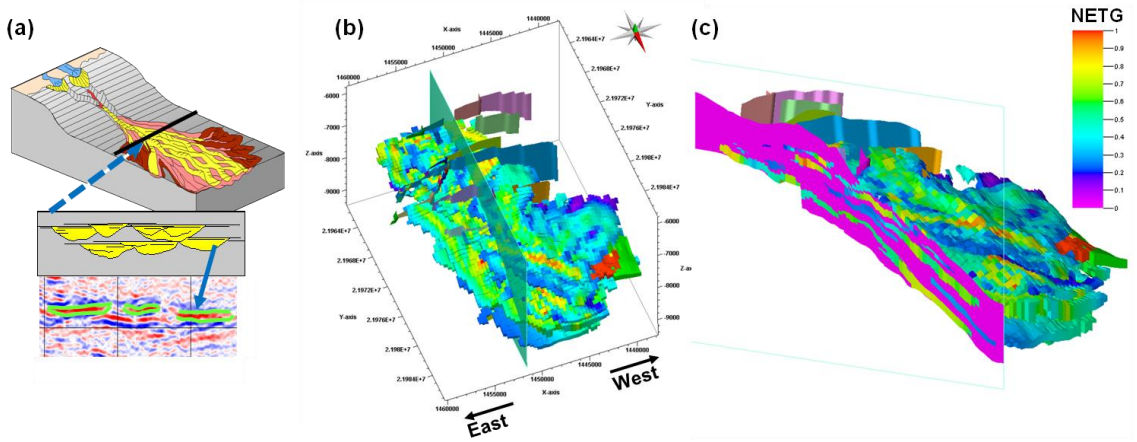

Fig. 4.1. (A) Schematic depiction of the turbidite depositional interpretation used to develop the reservoir model (adapted from Rey et al. [2009]), (B) the NTG interpretation representative of the individual turbidite sand bodies identified and (B) a north-south cross-section depicting the individual reservoir quality sands.

4.4 Prior Permeability Model

Following Rey et al. (2009), in this analysis we calibrate the horizontal absolute permeability field to match WCT and BHP production data. For construction of the prior permeability model, we assume the most parsimonious description of static reservoir properties relative to the geologic description available and rely on the coarse-scale parameterization to resolve multiscale heterogeneity. Prior to the streamline-based history match of Rey et al. (2009), the associated business unit partitioned the static permeability model into forty individual regions to provide flexibility in the description of static properties and hydraulic continuity within the interpreted sand bodies (Fig. 4.1B). They then calibrated intra-region permeability, and placed transmissibility multipliers at the interface of several of the regions in order to reconcile the coarse

geologic model to production data before performing a streamline-based inversion. We discuss their reservoir model later in this subsection.

For this analysis, we abandon the regionalized model (in Fig. 15 of Rey et al. [2009]) and revert to the most fundamental facies structure interpreted from the available data. From analysis of PVT properties and permeability-porosity correlations embedded in the reservoir, five primary facies comprised of reservoir quality sands were identified. These facies, together with the well pattern, are presented in Fig. 4.2 and describe the structure of the prior permeability model applied in our analysis. In each facies a constant permeability is defined that is computed as the average of all corresponding zones in the 40-region model from Rey et al. (2009). A uniform permeability represents an un-informed prior and is a reasonable supposition given that static reservoir properties were measured only from well logging at a sub-set of the sparsely located wells. In the multiscale component of the history matching workflow, we apply the GCT parameterization to perform regionalization, in a geologically consistent manner, by the identification of heterogeneity both within and between the facies during a history match.

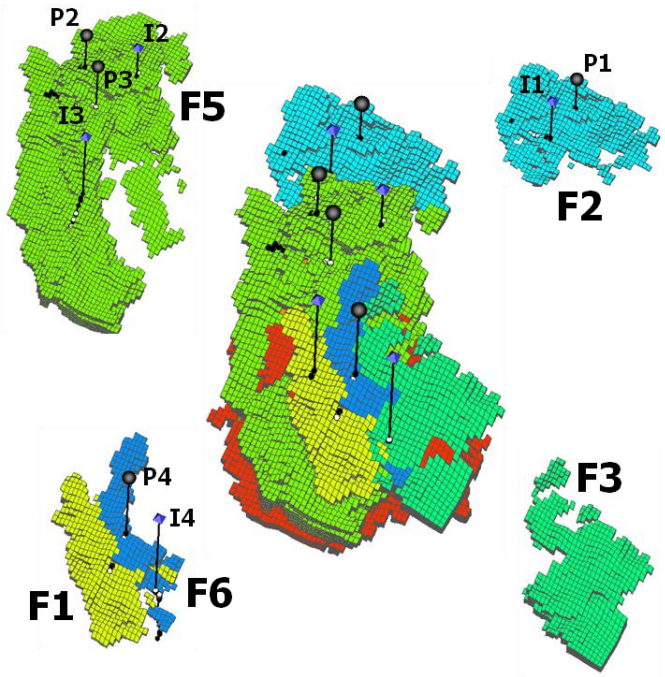

Fig. 4.2. The facies model, each with consistent permeability-porosity correlation and PVT properties, used to develop the prior permeability model and well pattern.

4.4.1 GCT Parameterization of Facies Permeability

For the coarse-scale calibration, the prior permeability field is updated using a parameterized multiplier field that we apply individually to each facies. Each multiplier field is assigned an initial value of unity at each cell, thereby preserving the prior permeability at the start of the workflow, and is subsequently updated by sequential refinement as described in the following subsection. In this subsection we first present the GCT basis functions used to parameterize the multiplier fields.

The transformation basis for each of the five facies (Fig. 4.2) is constructed using the corresponding grid connectivity information. Rows one and two in Fig. 4.3 show selected basis functions for facies 5 and 1, respectively, and are sorted by their equivalent eigenvalue ranks from the lowest to highest modal frequencies. For any given facies, recall that it is the weighted linear combination of multiple basis functions that

describe reservoir heterogeneity, where the weights or spectral coefficients are the estimable parameters.

It is important at this point to reiterate key concepts regarding properties of the basis functions that are critical to this multiscale application. To start, the projection of any spatial field onto the constant basis function (e.g., column 1 of Fig. 4.3), corresponding to the zero modal frequency or zero eigenvalue, results in a single spectral coefficient. Adjustment of this coefficient uniformly updates the spatial field and is equivalent to the traditional approach using a constant multiplier. If the spatial field has no variability, e.g., as for the constant multiplier field of unity, then its transformation to the spectral domain will result in a set of spectral coefficients equal to zero except for that coefficient corresponding to the constant function. The number of coefficients will equal the number of basis functions included in the parameterization. Accordingly, an increase in magnitude of any of the initially zero-valued coefficients will add spatial variability to the field. The level of spatial detail incorporated will increase with the addition of basis functions corresponding to higher modal frequencies, and will also depend on the number of cells in the field. With the sole exception of the constant function, the 'wavelength' of a basis function scales with the number of cells in the field such that coarse features in a smaller region with few cells may be equivalent to finer-scale features described by a basis function of higher modal frequency in a larger region. For example, compare the modal shape of the 2^{nd} basis function in row 1 (corresponding to the larger facies) versus row 2 (smaller facies) in Fig. 4.3. Both correspond to the second lowest modal frequency; however, the length scales of spatial variability that would be characterized in the two facies are considerably different. The relevant implication is that the reservoir volumes parameterized using this approach should have consistent geological properties and length scales of spatial variability. Our choice to parameterize the reservoir model by facies in fact demonstrates this concept. The facies are shown to represent different depositional sequences from integrated seismic interpretation and well data, and therefore are expected to have geological consistency.

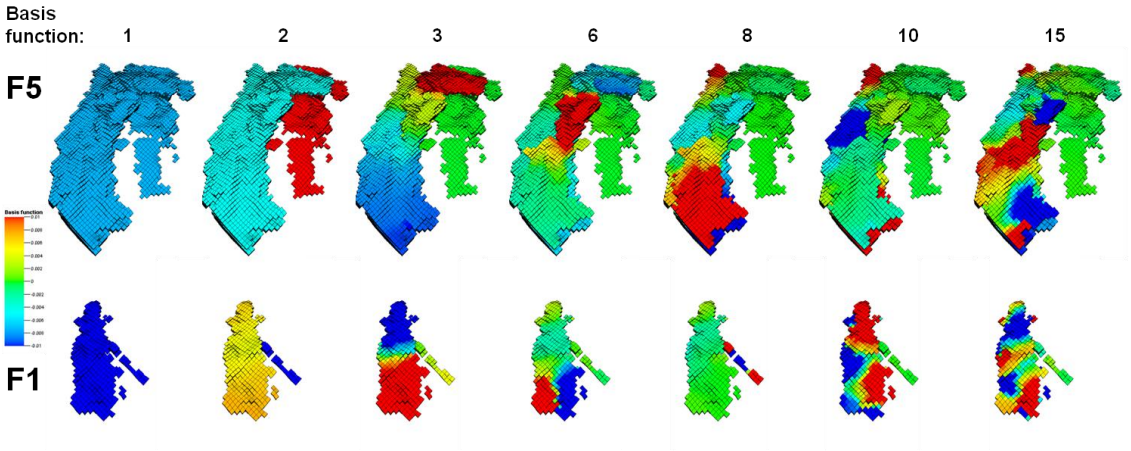

Fig. 4.3. Leading basis functions, sorted from left to right in order of increasing modal frequency, for facies 5 (top) and 6 (top).

4.5 Coarse-Scale Calibration: Adaptive Multiscale Workflow

The discussion to this point has describe how the properties of the transform basis form a flexible construct for the parameterization of facies permeability, in a manner consistent with the conceptual reservoir model structure. The observation data used for the history match are WCT and BHP over an approximately eight year period at each of the four producers. We note here that the pressure data are assigned less weight for the inversion due to a considerable amount of variability in the simulated data that is attributed to frequent well intervention in the schedule. Data misfit, characterized using the formulation in Eq. (3.13), is reduced using a gradient-based scheme in which the gradient is directly computed by one-sided finite-difference perturbation of each parameter. Therefore, each iteration required $n_t + 1$ simulations.

The multiscale inversion begins by simultaneously updating the mean (*ln*) permeability of each flow unit using its zero-frequency or constant basis function. This corresponds to parameterization of the multiplier field by only five spectral coefficients, one per facies, equivalent to the traditional approach of regional multipliers. The updated multipliers are shown in Fig. 4.4A and the corresponding WCT data misfit at each of the producers in

Fig. 4.4B. The utility of the mean updates is adjustment of the relative differences in regional permeability for improved consistency of time shift and magnitude in the overall WCT response at a given producer. In particular, permeability is considerably decreased in facies 1 and 6 to lower the magnitude of WCT response at producer P4 (see Fig. 4.2), which involves a more complicated response behavior that we discuss below. Conversely, permeability is increased in facies 5 to expedite the arrival time at P3 of water injected at I3 at the distal down-dip end of this large unit. The improved data misfit at P3 suggests that higher permeability in facies 5 would further improve the misfit; however, the adjustment of the mean in any of the facies influences production responses at all producers, and it was observed that an additional increase in the mean permeability of facies 5 has a detrimental effect on the other wells. At P2, the considerable improvement in data misfit by the mean update alone indicates that the structural model well captures the local flow behavior, which is controlled largely by a set of low transmissibility faults (Fig. 4.1) that confine the I2-P2 well pair closely to the north and south. In the remaining facies, the multiplier field approximately retains its initial value of unity through the inversion, thereby preserving the prior permeability model as intended. These observations altogether, in tandem with the unacceptable data misfit, promote the inclusion of within-facies heterogeneity through the addition of higher modes in transform basis.

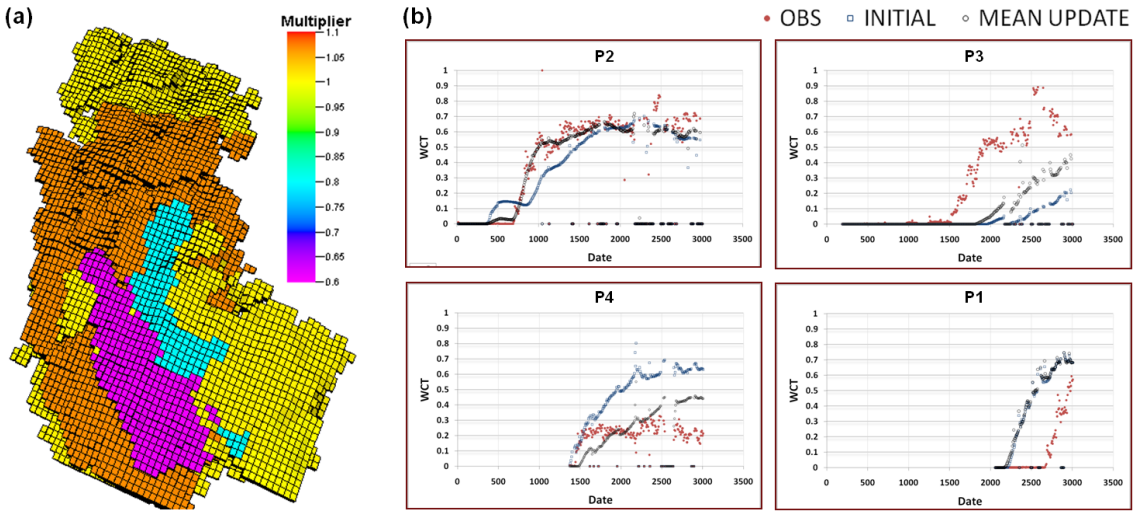

Fig 4.4. (A) The calibrated permeability multiplier field, per facies, following updating of the mean permeability using the constant basis function and (B) the corresponding WCT misfit.

Continuing with the multiscale workflow, basis functions were sequentially added to the parameterization of each facies permeability field in sets. To reiterate an important point, within-facies heterogeneity is derived as the linear combination of multiple basis functions; therefore, the addition of basis functions must be performed in sets using a scheme that does not permit over-parameterization and subsequent immediate convergence of the objective function to a local minimum (Bhark et al., 2010b). In this analysis we found that sets of five were sufficient, e.g., after parameterization of a single facies permeability field with only the constant basis, the flow unit was sequentially parameterized by the leading five basis functions, then the leading ten, and so on at each multiscale iterate (Fig. 3.5). This scheme was applied in tandem with the gradient-screening procedure, described previously in **Subsection 3.3.6.2**, for the automatic removal of insensitive parameters from the inversion at each multiscale iterate. Also, upon the addition of spatial detail to each flow unit, we found it critical to freeze the parameter corresponding to the constant basis which consistently showed a large sensitivity that dominated the parameter update vector. The complete multiscale workflow was terminated when the addition of basis functions, as a group over all facies, failed to improve data misfit at any of the producers. The refinement of the detail within

an individual facies during the workflow was terminated using the gradient-screening criterion.

The coarse-scale, calibrated multiplier and permeability fields are shown in Fig. 4.5 along with the number of leading basis functions that were sensitive to the data during the history match. A total of 36 parameters were required to characterize the coarse-scale reservoir permeability. The multiplier field reflects minimal changes to log-permeability, where regions of insensitivity or accurate prior description retain a multiplier of unity through the refinement steps, and also demonstrates the ability of the parameterization to update regional trends with a geologically consistent description within (sub)domains of complex geometry. In the larger flow units, the data supported a maximum of ten leading coefficients, in terms of modal frequency, to resolve regional spatial variability and were insensitive to the subsequent inclusion of higher modes. However, notice that facies 2 could not be resolved beyond adjustment of the mean permeability because the data, particularly at P1 (see Fig. 4.2), were insensitive to large-scale heterogeneity in this flow unit, indicating a more fundamental model inconsistency than permeability heterogeneity. We present a more detailed analysis of the flow behavior and influence of the multiscale calibration below with the analysis of the streamline-based inversion. In the smaller facies, 1 and 6, only the five leading basis functions were supported for the parameterization of each. Recall that the modal frequency corresponding to a basis function scales with the number of cell connections (e.g., Fig. 4.3); therefore, five basis functions were found sufficient to capture large scale variability in these relatively smaller regions. The WCT misfit at each producer, shown in Fig. 4.6, verifies the marked improvement in the history match at all wells but P1, the reasons for which are presented below. The improvement demonstrates the important influence of regional heterogeneity on flow behavior and the efficacy of adaptive refinement in its characterization.

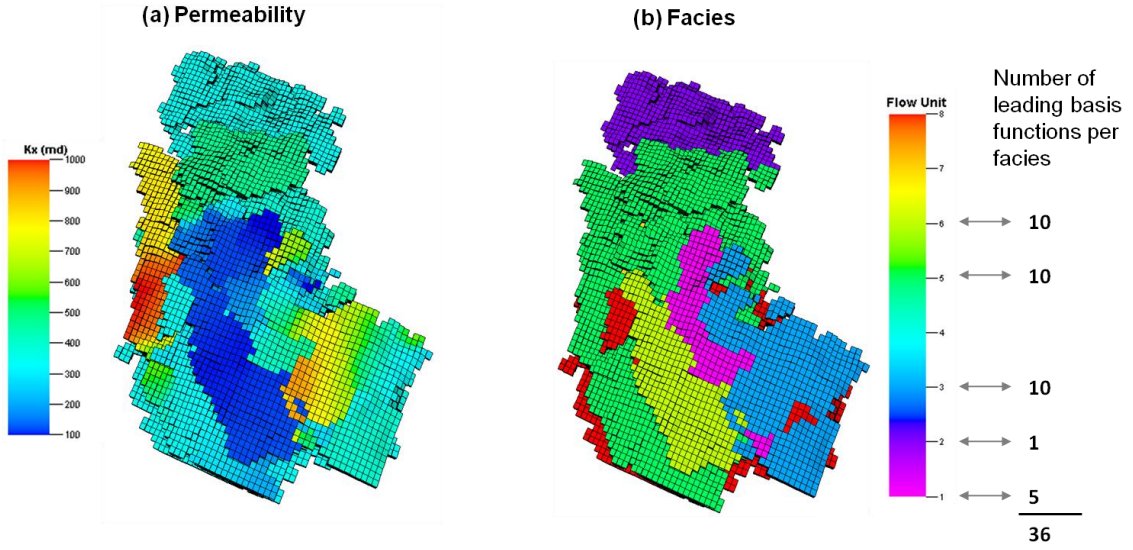

Fig. 4.5. (A) The calibrated permeability field at the conclusion of the adaptive multiscale workflow (Figure 1B) and (B) the number of leading basis functions, per facies, sensitive to the data during the coarse-scale inversion.

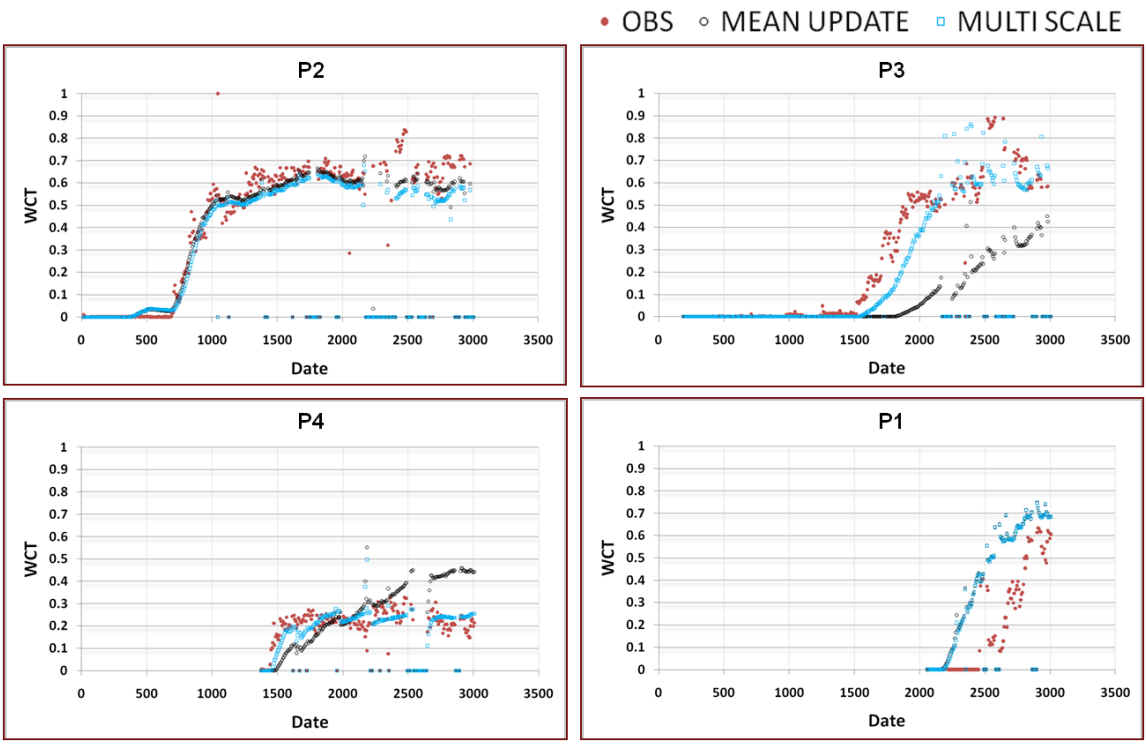

Fig. 4.6. WCT data misfit corresponding to the calibrated permeability field at the conclusion of the adaptive multiscale workflow (Figure 1B).

At this point we briefly compare the calibration of regional permeability using the proposed multiscale approach with that corresponding to the regionalized model in Rey et al. (2009). For this we compare in Fig. 4.7 the horizontal transmissibility ratio, defined as the division of the calibrated by prior transmissibility at each cell, corresponding to this analysis with that in Rey et al. (2009). However, because we do not have access to the prior (non-regionalized) transmissibility field corresponding to Rey et al. (2009), we construct the ratio in Fig. 4.7B based on the prior facies model used in this study, which is sufficient to highlight the coarse-scale model updates incorporated by the associated business unit before they performed a streamline-based history match. Inspection of Fig 4.7A depicts the increase in transmissibility along the east and west flanks of the model and the decrease in the central region, thereby improving flow continuity in the up-dip orientation and reducing cross-flow in the perpendicular orientation. In Fig. 4.7B, the apparent transmissibility multipliers applied for a coarse-scale history match similarly serve to reduce cross flow and improve flow continuity in the up-dip direction. The multipliers also create flow barriers at several of the inter-region contacts. Notably, the GCT parameterization identifies sharp permeability contrasts at several of these exact locations, both between and within facies. We defer to a more detailed analysis of flow behavior in this next subsection.

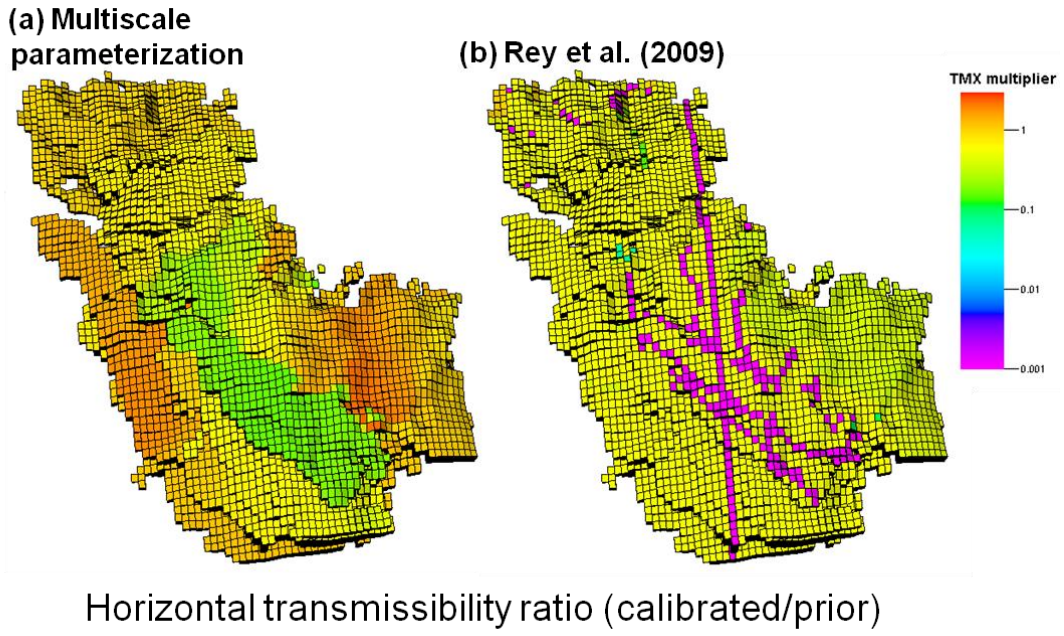

Fig. 4.7. Comparison of the horizontal transmissibility ratio (calibrated / prior) corresponding to the calibrated permeability field at the conclusion of the adaptive multiscale workflow.

4.6 Fine-Scale Calibration: GTTI Workflow

At the conclusion of the coarse scale inversion, the subsequent addition of basis functions to the parameterization of any facies does not improve data misfit. We therefore assume (with the exception of the P1 response) that the improvement of the match requires heterogeneity refinement at scales finer than the GCT is able to resolve and progress to inversion with the GTTI technique.

To briefly review, the GTTI was developed within the class of streamline-based inversion techniques inspired by travel time methods for waveform inversion of seismic tomography and exploits the similarity between streamline time of flight and the Eikonal equation for travel time tomography (Vasco and Datta-Gupta, 2001). There are several advantages related to these streamline methods when applied in automatic history matching procedures, notably the fast computation of analytical sensitivities of production responses to static reservoir properties, and also the quasi-linear properties of

the travel time misfit minimization (Cheng et al., 2005). The GTTI technique is an extension of the travel time methods for reservoir property determination under changing field conditions (He et al., 2002) and has been demonstrated to improve the history match quality during high-resolution model calibration. The gain results from the evaluation of data misfit as the single shift in time that maximizes the cross correlation, per well, between the observed and simulated production data (Luo and Schuster, 1991; He et al., 2002).

The efficiency in the streamline sensitivity calculation is based on the assumption that a small perturbation in the flow properties will modify the arrival time along the streamline without altering the streamline trajectory. This assumption permits a simple analytical description of how a localized perturbation in conductivity (i.e., a very small change in the cell permeability at a particular location along the streamline path) will perturb the travel time of a neutral tracer along the streamline, hence the formulation for parameter sensitivity. The extension of this concept to multiphase flow requires only the specification of chain rule derivatives (Vasco et al., 1999; Cheng et al., 2005; Oyerinde et al., 2009). From the analytically-derived sensitivities we define an objective function comprised of the data misfit and two regularization terms that aim to preserve the main features embedded in the prior model with local continuity, i.e.,

$$J(\delta\mathbf{R}) = \left\|\delta\mathbf{d} - \mathbf{G}\delta\mathbf{R}\right\|_2 + \beta_1\left\|\delta\mathbf{R}\right\|_2 + \beta_2\left\|\mathbf{L}\delta\mathbf{R}\right\|_2 . \tag{4.1}$$

In the objective function, $\delta\mathbf{d}$ is the vector of the (single) GTTI misfit for each well and $\mathbf{G}$ is the sensitivity matrix containing the partial derivatives for the arrival of the water to each well with respect to the reservoir parameters, i.e., grid cell permeabilities. Each component of $\mathbf{G}$ is obtained as the summation of the individual streamline contributions per well. The quantity $\delta\mathbf{R}$ is the vector of changes in the reservoir property. The scalar β_1 determines the relative strength of the "norm" constraint through which the objective function is penalized by deviations from the initial model at grid cell resolution. The scalar β_2 determines the relative importance of the "roughness" constraint which

enforces continuity in permeability during model updating and is analogous to enforcement of a covariance constraint (Yoon et al., 2001). The smoothness operator **L** is the discrete, two-point model Laplacian defined exactly as in Fig. 3.1, although in Eq. (4.1) the Laplacian acts as a local operator. The objective function is reduced through a least-squares iterative method until a convergence criterion is satisfied.

A common difficulty encountered during the GTTI misfit calculation is locating the optimal time shift corresponding to the maximum cross-correlation for highly detailed production data. Rapid response variations and non-monotonicity result in a non-convex cross-correlation profile. Although an obvious solution is to smooth the production response, smoothing does not guarantee the elimination of the high frequency variability and can degrade the temporal response resolution to the point that the GTTI technique reduces to a simple travel time inversion. To prevent this loss in resolution we instead use a re-sampling technique that eliminates high-frequency variation while preserving the shape of the production response. The production data are sampled at equal volumes of produced oil at surface conditions thereby providing a coarser response that retains high-resolution relative to produced volumes (Rey et al., 2009). The data misfit plots for WCT and BHP at the conclusion of the GTTI inversion are shown in Fig. 4.8 and Fig. 4.9, respectively. We now describe the matched production response behavior on a well-by-well basis.

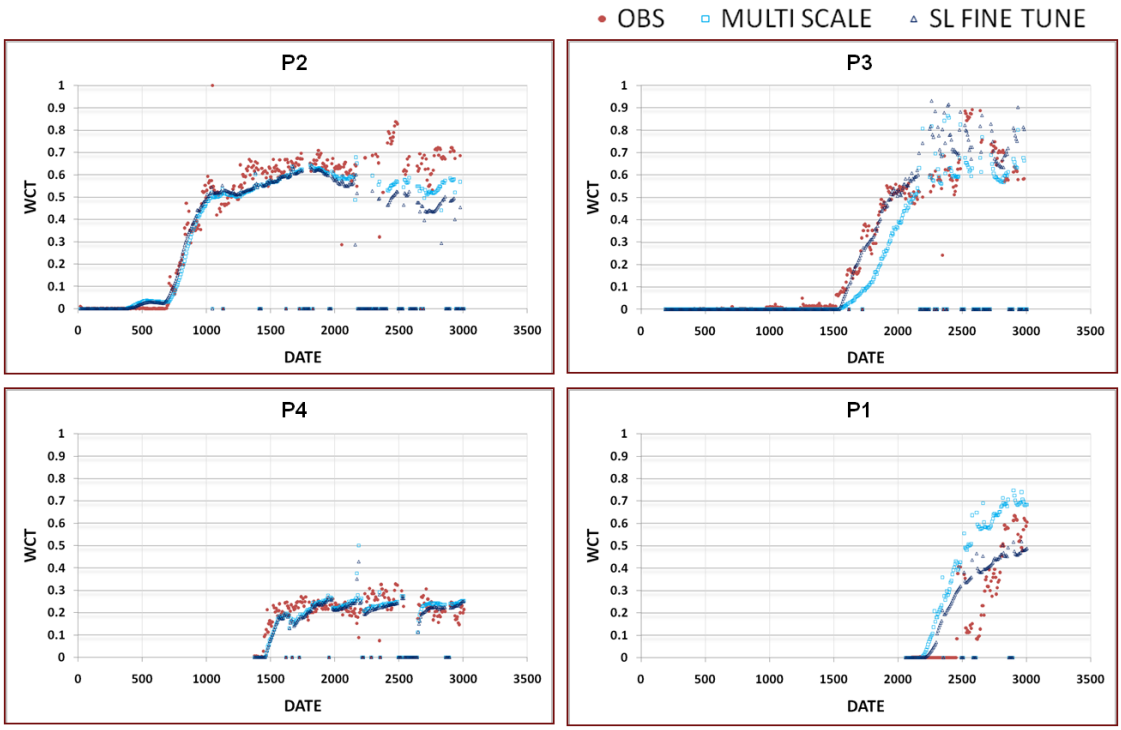

Fig 4.8. WCT data misfit corresponding to the calibrated permeability field at the conclusion of the streamline-based workflow (Figure 1C).

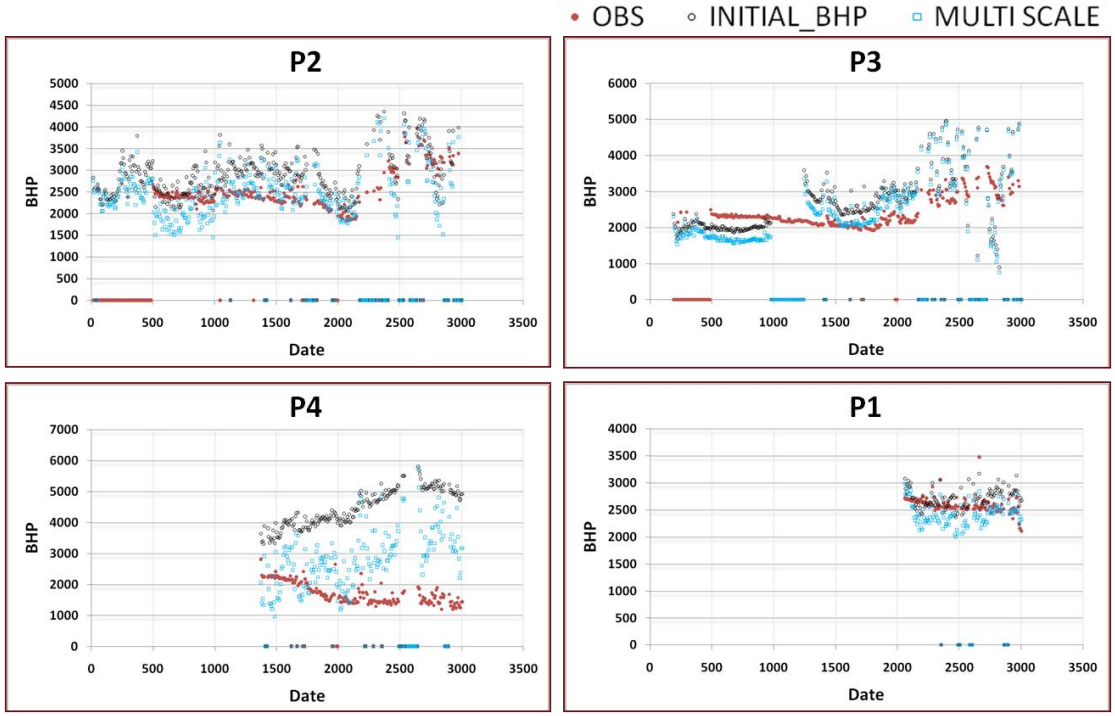

Fig. 4.9. BHP data misfit corresponding to the calibrated permeability field at the conclusion of the streamline-based workflow (Figure 1C).

4.6.1 Influence and Analysis of Calibrated Heterogeneity

4.6.1.1 Producer P3

A distinct feature of the calibrated permeability model identified during the parameterization component of the workflow is the regional increase in permeability along the eastern side of the reservoir. The primary effect of this increase was to reduce travel time along the swept path from injection at I3 to production at P3, which is consistent with the interpretation in Rey et al. (2009) and is supported by the improved WCT misfit during both the coarse- (Fig. 4.6) and fine-scale (Fig. 4.8) inversions. The streamline well-allocation and time-of-flight maps in Fig. 4.10 portray the improvement in hydraulic continuity between the I3-P3 well pair along the eastern edge. The streamline paths also show the reduction in hydraulic continuity from the opposing west side of the reservoir, a result that was imposed in the previous history match by the inclusion of transmissibility barriers transecting the east and west portions of the reservoir (Fig. 4.7). To further improve flow continuity between I3 and P3, Rey et al. (2009) used streamline-based updating to increase permeability and match the observed WCT, identifying a potential channel (Fig. 26 of Rey et al. [2009]). Consequently, they defined a preferential flow path along the collective streamlines between I3 and P3, fundamentally based upon the velocity field corresponding to the prior regionalized reservoir model. However, the permeability updates exceeded the maximum threshold of 2 darcys (D) in certain location, up to a maximum of 10 D near the wellbore. Conversely, in this analysis geologically consistent regional permeability was first updated during the parameterization component of the workflow, which then permitted consistent streamline-based permeability updates, the maximum of which barely exceeds 1 D. The parameterization naturally identified a larger volume for permeability increase that is more consistent with permeability constraints rather than relying on the smaller volume intersected by streamlines to make the required updates. This result highlights the importance of resolving coarse- before fine-scale heterogeneity in history matching,

and also the strength of streamline-based methods to refine the model at high resolution along prior preferential flow paths.

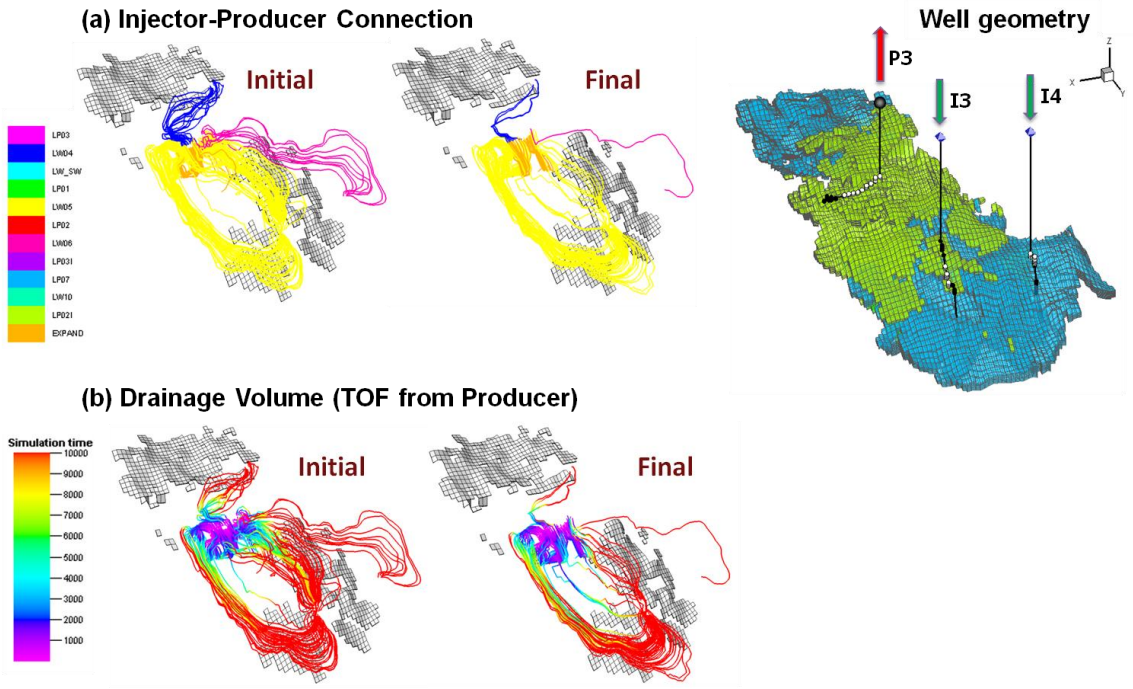

Fig. 4.10. (A) Streamline allocation traced from P3 for the initial (prior) and final (calibrated) permeability models, and (B) corresponding time of flight along streamlines.

4.6.1.2 Producer P2

The observed WCT and BHP responses at P2 are well approximated using the prior permeability model and are considered history matched following the mean permeability update of flow unit 5 (see Fig. 4.4) during the coarse-scale component of the workflow. During characterization of the structural model interpretation, the associated business unit identified the transecting faults to the north and south of this well pair, shown in Fig. 4.1, as flow barriers that constrict the drainage volume of P2 primarily to the region between these faults (Rey et al., 2009). The streamline well-allocation and time-of-flight maps in Fig. 4.11 demonstrate this flow constriction and, appropriately, show similar drainage patterns before and after calibration of the complete reservoir model, which is

consistent with the objective of minimally updating the prior model. These results imply that the flow unit structure and properties, relative to the static (seismic) and dynamic data available, are correctly captured with a simplistic model. This is also consistent with our parsimonious conceptual approach to history matching.

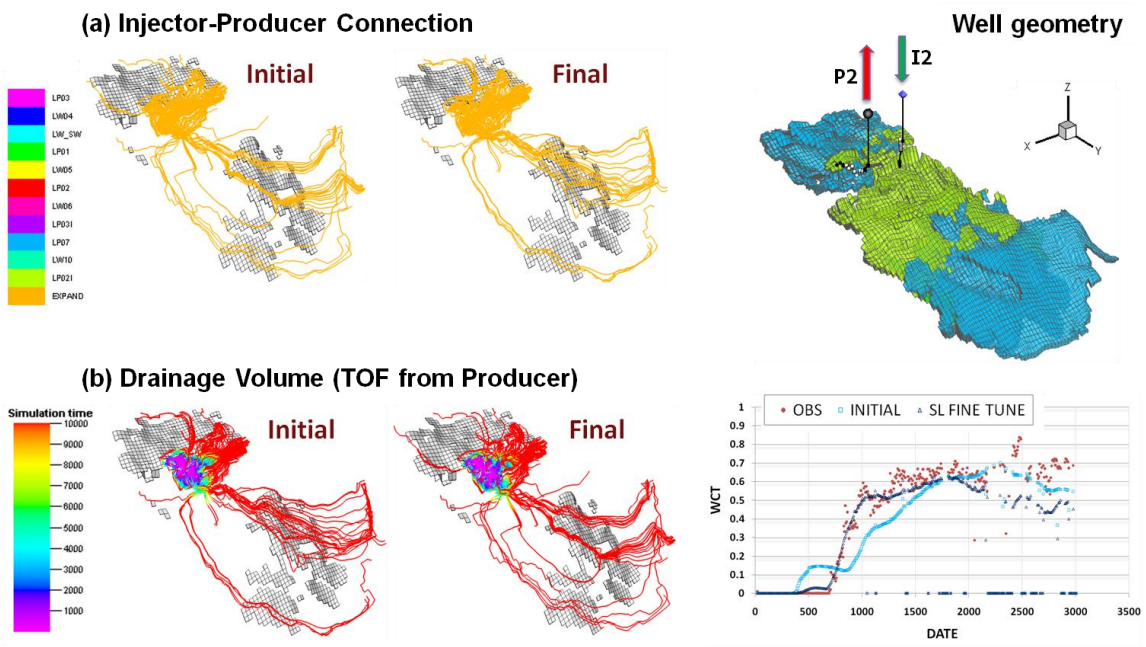

Fig. 4.11. (A) Streamline allocation traced from P2 for the initial (prior) and final (calibrated) permeability models, and (B) corresponding time of flight along streamlines.

4.6.1.3 Producer P1

Per the associated business unit, the pressure response at P1 responded at a later time than that predicted upon injection at I1 despite the proximity of the wells and their completion in the same flow unit (Rey et al., 2009). In congruence with the prediction of an early water breakthrough time at P1 using the prior permeability model, the assisted history match was expected to result in a decrease in pressure support at P1 from the injector, thereby reducing the transport signature of I1, and also to result in an increase in support from the aquifer. The streamline source allocation plots in Fig. 4.12 in fact show this modification in flow behavior between the initial and calibrated models.

However, in a screening analysis we observed that the permeability in this up-dip region of facies 2, particularly between the injector and producer, cannot be sufficiently lowered without causing drawdown at P2 to drop below the minimum pressure constraint and erroneously decrease the production rate. During attempts at heterogeneity refinement, we also observed that a decrease in permeability near the injector alone was not sufficient to delay breakthrough.

At the grid-cell scale, streamlines were also unable to perform the regional changes that would reduce communication between the well pair while retaining sufficiently high permeability near the well. Unless manually constrained, streamline updating lowered permeability along the streamline paths, particularly near the well where grid-cell sensitivity is largest, to the point that the minimum pressure constraint was violated. Therefore, the calibration was not satisfactorily performed in this region of the reservoir such that simulated water breakthrough remains early. The predicted WCT response at P1 in Rey et al. (2009) similarly occurs early and was not able to be reconciled by permeability adjustment alone. Because neither the parameterization nor streamline-based components of the workflow were able to reconcile this discrepancy, in this scenario we use our history matching approach as a diagnostic tool. The observations described suggest the potential inclusion of a flow barrier between the well pair or, more likely, a required increase in the facies thickness which may result in the reduced transport time desired while retaining sufficiently high permeabilities to support the well pressure constraints.

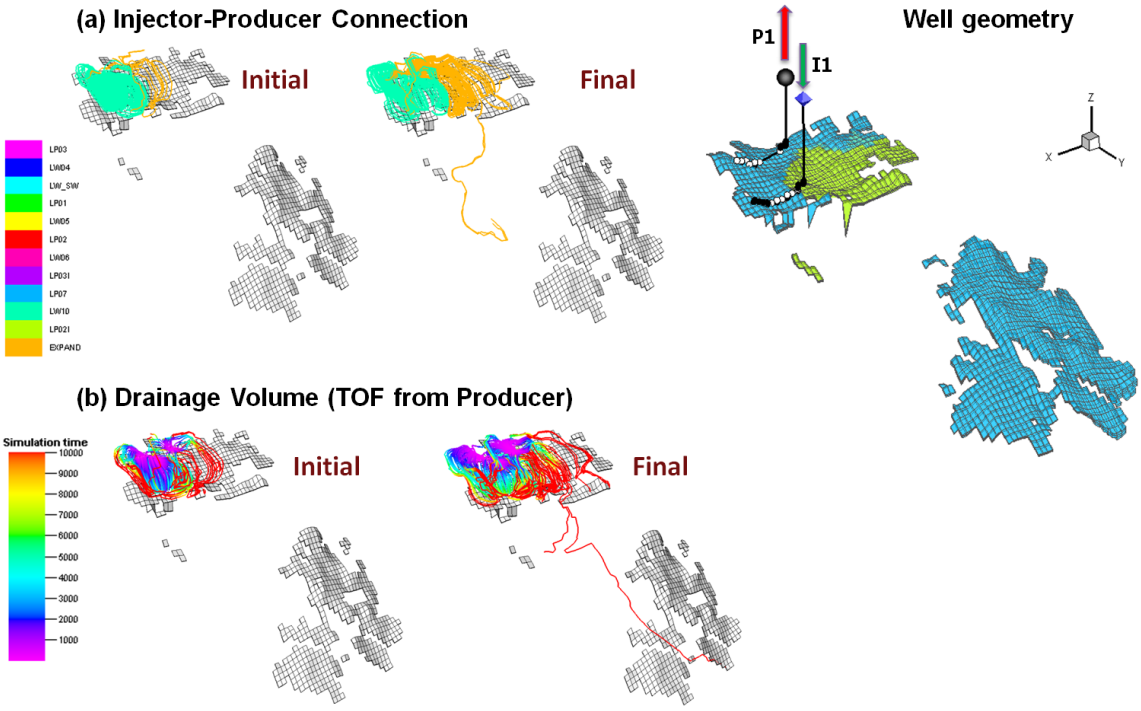

Fig. 4.12. (A) Streamline allocation traced from P1 for the initial (prior) and final (calibrated) permeability models, and (B) corresponding time of flight along streamlines.

4.6.1.4 Producer P4

Flow behavior near P4 proved the most difficult to characterize given the complex structure in this region (see Fig. 4.2). Inspection of the initial WCT misfit at P4 and the improved WCT after mean permeability updating (Fig. 4.4), together with geologic interpretation, suggested that the calibrated model must simultaneously constrain flow within flow unit 6, in which P4 is completed, while at the least improving flow continuity in flow unit 1, in which I1 is completed. That is, both the simulated breakthrough time and overall magnitude of the WCT response had to be simultaneously reduced. Notably, these points of reservoir engineering judgment were automatically detected during the parameterization component of the workflow in which permeability in flow unit 6 was lowered and permeability at multiple spatial scales was increased in flow units 1 and 3. The resultant regionalization effectively created flow barriers at the

interface of flow unit 6 with units 1 and 3 which, interestingly, are exactly consistent with the placement of transmissibility barriers at this interface by Rey et al. (2009) (Fig. 4.7B). The streamline well-allocation and time-of-flight maps in Fig. 4.13 exemplify the barriers, the decrease in pressure support from I4 following the calibration, and also the improvement in aquifer support which permits the earlier breakthrough time to be reproduced while at the same time honoring the smaller observed WCT magnitude. To reiterate a key point, these updates exemplify a second case that demonstrates the significance of characterizing regional before fine-scale heterogeneity. In this example, the permeability updates required *extend beyond* those constrained to streamline paths that correspond to the prior permeability model.

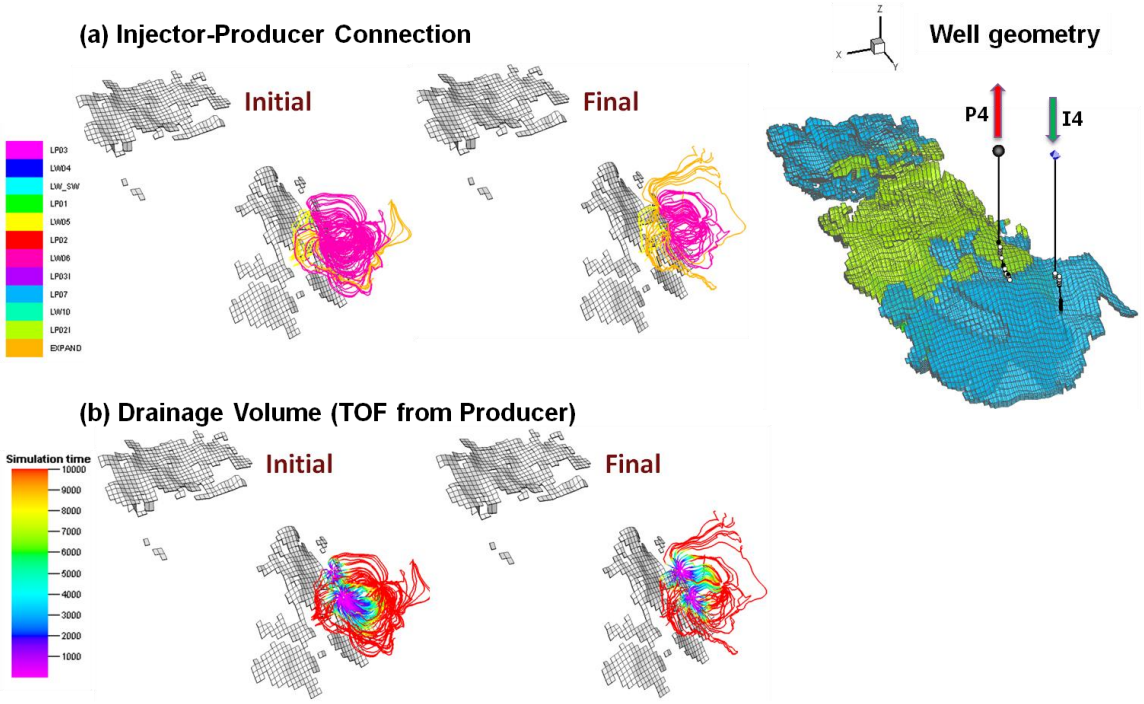

Fig. 4.13. (A) Streamline allocation traced from P4 for the initial (prior) and final (calibrated) permeability models, and (B) corresponding time of flight along streamlines.

4.7 Conclusions

This section presented the application and efficacy of a structured history matching workflow that adaptively integrates multiresolution production data into a high-resolution geologic model. The workflow first characterizes regional or coarse-scale heterogeneity, in a manner consistent with and adaptive to prior information when available, using the GCT parameterization. The key properties of the parameterization which permit its application to large reservoir models with complex geologic description are as follows:

- Applicability to any grid structural geometry as well as domain boundary geometry
- Prior model independence, with the benefit of honoring prior information when available by the inclusion of basis functions into the parameterization that correspond to the dominant spatial components of the prior model heterogeneity (Bhark et al., 2011a)
- Strong generic compression performance, theoretically and empirically demonstrated by Laplacian eigenvectors, and guaranteed in the ideal cases of regular grid connectivity by convergence of the basis functions to the DCT-2 basis
- Efficient basis construction on account of the sparse symmetry of the Laplacian using the implicitly restarted Lanczos method

All four attributes are either a direct or indirect consequence of the transform basis construction from grid-connectivity information alone.

The applications of the parameterization in adaptive, multiscale history matching demonstrated the geologically-consistent characterization of coarse-scale heterogeneity, avoiding the ad hoc definition of regional multipliers or other parameterization schemes that can lead to the inclusion of artificial features in the calibrated model. The coarse-scale updates identified areas of both continuity (smooth transition) and discontinuity (sharp contrast) in the property model that, even independent of history matching,

provide a useful tool in conceptual geological interpretation and the identification of trends.

Upon characterization of coarse-scale heterogeneity, refined down to the spatial scale permitted by the observed data, we used the established streamline-based GTTI algorithm to update heterogeneity at the grid-cell scale. The approach to local updating is consistent with model characterization using the parameterization; streamline paths are implicitly determined by larger-scale heterogeneity together with the well pattern and schedule. In addition to improvement of data misfit, a streamline analysis further proved useful in identifying modifications in flow behavior resulting from the previous coarse-scale update, which is a critical component of model calibration analysis. The differences in flow behavior and hydraulic reservoir continuity between the prior and calibrated models also clearly demonstrated the importance of characterizing global before local reservoir heterogeneity.

5. ADJACENCY-BASED PARAMETERIZATION: INCLUSION OF PRIOR MODEL WITH GRID CONNECTIVITY INFORMATION

5.1 Summary

This section introduces a novel reservoir model parameterization as a special case of the grid-connectivity-based transform (GCT) basis, developed in **Section 3**, for the incorporation of prior model information. Just as for the GCT parameterization, the reservoir property field is mapped to and updated in a low-dimensional transform domain using a linear transformation basis. The transformation basis vectors are the eigenvectors of a Laplacian matrix that is constructed using grid connectivity information and the main features in a given prior model. Because the grid connectivity information is computed only within a small multi-point stencil, the Laplacian is always sparse and amenable to efficient decomposition using a variant of the Lanczos algorithm. The resulting basis functions are ordered from large to small scale and exhibit both generic and prior-specific spatial features. Therefore, the variability in the reservoir property distribution can be effectively represented by projecting the property field onto subspaces spanned by an increasing number of leading basis vectors, each incorporating additional heterogeneity features into the model description. This property lends itself to a multiscale history matching algorithm where basis elements are sequentially included to refine the heterogeneity characterization to a level of complexity supported by the resolution of data. While the method can benefit from prior information, in the extreme case where reliable prior knowledge is not available the transformation reduces to a discrete Fourier expansion with robust parameterization properties.

5.2 Introduction

The original application of reservoir model parameterization for resolving the underdetermined and ill-posed problem of history matching is spatial zonation (e.g., Jacquard and Jain, 1965; Jahns, 1966) and was reviewed in **Subsection 1.1**. This section presents the development and application of a spectral approach to reservoir

heterogeneity zonation that builds upon, or is a special case of, the GCT parameterization presented in **Section 3**. Similar to the GCT parameterization, the proposed approach maps and updates the spatial property field in a low-dimensional transform domain using a linear transformation basis. The transformation basis vectors are constructed as the eigenvectors of a Laplacian matrix that captures adjacency information for each cell-pair in the calibrated domain. Although the definition of an adjacency metric is generic, in this study cell-to-cell adjacency is characterized by the Euclidean distance between the cells, and also by the difference in a static reservoir property defined at the cells. Because this approach to spectral, adjacency-based parameterization is developed as a special case of the GCT parameterization, which provides a spectral representation of grid connectivity information, it is useful to first review and understand what the GCT basis functions physically and conceptually represent, and how they characterize reservoir heterogeneity.

Summarizing key points from **Subsection 3.3**, the GCT basis is defined as the eigenvectors of a grid Laplacian, annotated in this section as $\mathbf{L}_{GCT}$, that characterizes the complete immediate-neighbor or two-point cell connectivity of the N-cell reservoir grid. Recall that the Laplacian is constructed as the difference of the degree matrix (**D**) and grid adjacency matrix (**A**), i.e., $\mathbf{L}_{GCT} = \mathbf{D} - \mathbf{A}$. From Eq. (5.1) which defines the symmetric $N \times N$ matrix **A**,

$$a_{i,j} = \begin{cases} 1 & if\ (i,j) \in E \\ 0 & otherwise \end{cases} \tag{5.1}$$

and, following the graph notation from **Subsection 3.3**, the adjacency measure can be viewed as a constant weight of unity between cell i and its nearest-neighbor cells j. **D** is then a diagonal matrix with each element equal to the row sum of **A**, or equal to the number of neighboring cells j with which cell i shares a cell face. Following this formulation, $\mathbf{L}_{GCT}$ is exactly periodic and naturally defines boundary elements that enforce a symmetric reflection of the function across a boundary cell face; therefore, the

Laplacian has eigenvectors equal to the DCT-2 basis functions (i.e., a special case of the discrete Fourier basis) when the cell connectivity structure is regular (Bhark et al. 2011a; Strang, 1999). From this perspective, the GCT parameterization characterizes a heterogeneity map as the weighted linear combination of cosine harmonics. From the perspective of zonation, each basis vector depicts zones of heterogeneity, e.g., lows and highs at specific locations, as the fluctuation or periodicity of the corresponding cosine wavelength, which may or may not be similar to the features of the prior model.

Taubin (1995) also recognized the equivalence of Laplacian eigenvectors, considering two-point connectivity of any *n*-cycle graph, with the discrete Fourier basis. However, he extended the adjacency definition to weights of any real non-negative value, still over a two-point neighborhood, and made the important observation that the Laplacian eigenvectors represent the "natural vibration modes" of the grid with eigenvalues corresponding to the "natural frequencies". Although in this case the exact equivalence to Fourier theory is lost, the eigenvectors still reflect modal frequencies useful for parameterization, or for a low-rank manipulation of a spatial function (e.g., Zhang et al., 2010). Therefore, from this more general perspective, the GCT parameterization characterizes heterogeneity as the weighted linear combination of grid harmonics, and from the perspective of zonation, each basis vector depicts zones of heterogeneity as the periodicity of the corresponding modal shape.

The derivation of the proposed adjacency-based parameterization begins from this point and is based on the extension of the adjacency definition in Eq. (5.1) to one that considers multi-point connectivity over a larger local neighborhood (i.e., within a multipoint stencil), and also the similarity between property values at cells within the stencil. This latter component of the adjacency metric incorporates prior model heterogeneity in the Laplacian and, therefore, also into the basis vectors. Under this new formulation, the periodic action of the Laplacian can be lost. In such a case the basis vectors lose their relation to modal grid frequencies and begin to depict spatial characteristics of the prior model heterogeneity. This tendency is exacerbated as the

weighting function becomes more *strict*, as explained in detail below. However, when the weighting function is *relaxed*, the Laplacian approaches the form of a periodic operator and the parameterization basis approaches the model-independent GCT basis.

Using this new Laplacian formulation, we posit that a small number of leading Laplacian eigenvectors, or basis vectors, can be used to implicitly perform a zonation and calibration of prior model heterogeneity to different levels of detail as warranted by understanding of the prior model. More specifically, a basis vector can be used to characterizes prior model heterogeneity as regions of piecewise continuous vector components, naturally depicting spatially continuous zones, at multiple spatial scales from the coarse to the fine. In **Subsection 5.3**, the key components of the basis construction are first presented, based on a new adjacency-based formulation of the grid Laplacian, and then are combined in **Subsection 5.4** to demonstrate how each basis vectors performs a unique zonation of the prior model in the spectral domain. In these subsections we take care also to highlight the properties of the basis for which it is amenable to application for large-scale history matching problems, including efficient one-time construction prior to calibration, applicability to any grid geometry, and strong compression performance. In **Subsection 5.4** we further describe how the proposed transform basis lends itself to a multiscale history matching algorithm where basis elements are sequentially included to refine the heterogeneity characterization to a level of complexity supported by the resolution of data. In the remaining subsections, the proposed parameterization is applied for the history match of several reservoir models, including the Brugge semi-synthetic field case, using an adaptive multiscale algorithm.

5.3 Development: Adjacency-Based Transform Basis

The following subsections present the components of the Laplacian construct and its subsequent decomposition for construction of the parameterization basis vectors.

5.3.1 Grid Adjacency and Laplacian Matrices

The parameterization basis is ultimately defined as a set of the grid Laplacian eigenvectors, where the adjacency-based Laplacian, $\mathbf{L}_A$, is constructed as

$$\mathbf{L}_A = \mathbf{D} - \mathbf{A}. \tag{5.2}$$

The diagonal degree matrix (**D**) was defined above and has diagonal elements computed simply as the row sums of the adjacency matrix (**A**). Therefore, it is **A** that controls the structure of the Laplacian.

Following the graph notation in **Subsection 3.3**, for each pair of cells *i*,*j* over the complete graph *G*, the adjacency measure (a_{ij}) can be considered as the weight of the edge (e_{ij}) connecting the cell pair, as defined in Eq. (5.1). Therefore, all components of **A** for which $a_{ij} = 0$ indicate that *G* has no edge between cell pair *ij*. Figs. 5.1A and 5.1B depict a simple 3 × 3 cell grid and the Laplacian matrices $\mathbf{L}_{GCT}$ and $\mathbf{L}_A$, respectively. Each grey line depicts an edge between a cell pair, and the number on the line a_{ij}. We will return to this figure below. In this study the adjacency measure is defined as the product of two exponential similarity metrics (Shi and Malik, 2000), or

$$a_{ij} = \exp\left(\frac{-\left\|p_i - p_j\right\|_2^2}{\sigma_P}\right) \times \begin{cases} \exp\left(\dfrac{-\left\|x_i - x_j\right\|_2^2}{\sigma_X}\right) & if \left\|x_i - x_j\right\|_2 < r \\ 0 & else \end{cases} \tag{5.3}$$

where $x_{i,j}$ is the cell centroid coordinate, $p_{i,j}$ is the cell property (i.e., prior model) value and *r* is a Euclidean cutoff distance beyond which a_{ij} is always equal to zero. The terms σ_P and σ_X determine the rate at which the weight decreases from cell *i* to *j* for each term of a_{ij}, so an important point is that both metrics must be 'similar' for a_{ij} to be far from non-zero. For comparison, Fig. 5.1A depicts the simple two-point connectivity structure and unit (or step function) weighting scheme assumed for construction of the GCT basis for the 3 × 3 cell grid. As noted above, the periodic structure of $\mathbf{L}_{GCT}$ in Fig. 5.1A can be

lost, as shown in B, when considering adjacency information as defined in Eq. (5.3). This concept is expanded upon below.

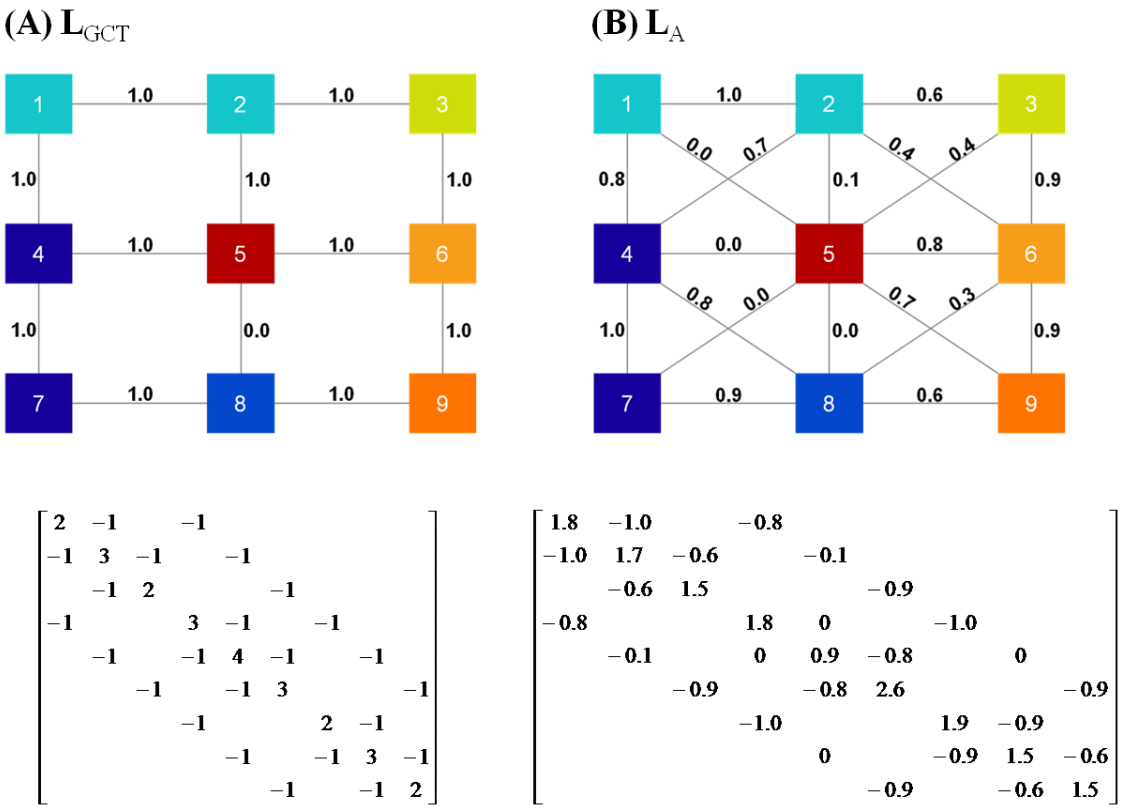

Fig. 5.1. For the 3 × 3 cell grid, (A) depicts the two-point connectivity structure with unit (or step function) adjacency measure (top) and corresponding Laplacian matrix (bottom) for the GCT paramterization, and (B) depicts the analogous cell-pair adjacency measures and Laplacian for the ABT parameterization.

In application, the adjacency parameters σ_P and σ_X of each exponential term in Eq. (5.3) are defined indirectly. The value of the corresponding 2-norm (in the numerator of the exponential), for both the property measure and for the Euclidean distance measure, at which the function is approximately zero (e.g., 0.001) is first defined by the engineer. Then, each rate parameter is solved for. For example, Fig. 5.2 depicts how a single term of Eq. (5.3) exponentially decreases as determined by the selection of the 2-norm tolerance for different tolerance values of 1, 10 and 100. The faster the rate of reduction,

the more *strict* the adjacency measure, and therefore the more dissimilar cell pairs will appear in $\mathbf{L}_A$. On the contrary, the slower the reduction rate or the more *relaxed* the adjacency measure, the more similar or connected cell pairs appear in $\mathbf{L}_A$. Therefore, both adjacency parameters ultimately determine the apparent periodicity of the Laplacian, which is a key point underscored below. Although definition of the 2-norm tolerance for each term of Eq. (5.3), which determines the parameters σ_P and σ_I, is an admittedly subjective step, this is in fact a common challenge. Any adjacency metric, more commonly known as a kernel function and used in many disciplines (Zhang et al., 2010), and actually the product of two kernel functions in Eq. (5.3), requires user specification of one or more parameters for which there are in general no rules for selection (von Luxburg, 2006). We provide guidelines for the adjacency parameter selection below in the context of geologic heterogeneity parameterization.

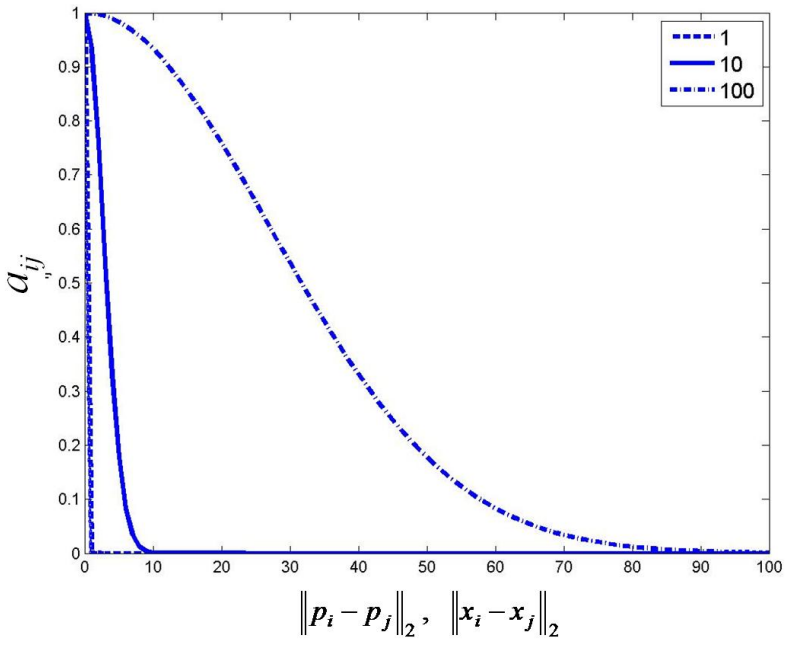

Fig. 5.2. The exponential form of a single term of the cell pair adjacency measure in Eq. (5.3) with the rate of decreases determined by selection of the 2-norm tolerance for three different values of 1, 10 and 100.

5.3.2 Zonation as a Graph Partitioning Problem

With the adjacency-based Laplacian ($\mathbf{L}_A$) now defined, this subsection explains how the eigenvectors of $\mathbf{L}_A$ naturally characterize and individuate zones of spatial continuity in the parameterized field. For this, the zonation problem is posed as a graph partitioning problem in the spectral domain, where (following **Subsection 3.3**) the heterogeneity field takes the place of the graph and is fully defined by its vertex and edge set, which are in this application characterized by $\mathbf{L}_A$. The partitioning of the field can then be quantified by a graph cut metric, defined below, that in general seeks an optimal segmentation of the cells in the field such that the edge weight, or adjacency, between cell pairs within a segment are all large and the adjacencies between segments are all small (von Luxburg, 2006). From this perspective, it is the Laplacian eigenvector (**f**) components, when mapped onto the grid, which identify an optimal segmentation of the property field. The segmentation **f** is a column vector of dimension $N \times 1$ and is optimal only with respect to a specific partitioning or graph cut metric, of which there are many. Relative to the intent of heterogeneity parameterization, and consistent with the concept of the cell adjacency matrix as defined by Eq. (5.3), **f** should partition the field such that cell property values within individual zones are similar (i.e., have a large adjacency) and cell values between two or more zones are as small as possible (i.e., have a small adjacency close to zero).

As will be demonstrated later in this section, a useful partitioning metric for the purpose of the proposed parameterization is known as *RatioCut*, defined as

$$RatioCut(A_1,\ldots,A_k) = \sum_{i=1}^{k} \frac{cut\left(A_i, \overline{A}_i\right)}{|A_i|} \quad , \tag{5.4}$$

(Hagen and Kahng, 1992; von Luxburg, 2006) where A is a partitioned zone of the complete field (as defined by V), $\overline{A}$ is its mutually exclusive complement and k is the total number of zones. The numerator of Eq. (5.4) is the well known graph cut and is

central to the concept of heterogeneity zonation for parameterization. For two (i.e., k = 2) mutually exclusive segments A_1 and A_2 whose union fully defines V, the cut is $cut(A_1, A_2) = \sum_{i \in A_1, j \in A_2} a_{ij}$ and, conceptually, is equivalent to the sum of all edge weights removed between A_1 and A_2 that form the cut. The denominator in Eq. (5.4) is a measure of the *size* of a segment A_i and is equal to the number of cells within it. For example, Fig. 5.3 shows two potential graph cuts, identified by the green dashed line, and the calculation of both the graph cut (numerator of Eq. [5.4]) and *RatioCut* for each partition.

The key point is that the minimization of *RatioCut* can be viewed as a *k*-segment zonation by an eigenvector **f**, where each zone holds cell pairs of similar weight (numerator), balanced by the condition that each segment is of approximately equal size (denominator). The minimum, in fact, occurs exactly when the partitions are of equal size. Therefore, for the purpose of parameterization we seek the **f** that minimizes *RatioCut*. Without inclusion of the denominator in Eq. (5.4), the minimum cut tends to isolate cells in the field as show in Fig. 5.3A, which is in fact the minimum cut value (or the minimum of the numerator in Eq. [5.4] for this specific case). Returning to the fundamental application of zonation (or even upscaling, e.g., King [2007]) in reservoir engineering, zones are constructed around grid cells of similar (static or dynamic) property value, generally minimizing within-zone heterogeneity and maximizing between-zone heterogeneity. In Fig. 5.3B, the cut shown is likely that which the engineer would select by visual inspection, partitioning the field into the most dissimilar zones of high and low cell values. We now show how the optimal **f**, corresponding to the solution that minimizes *RatioCut*, in fact identifies this partition.

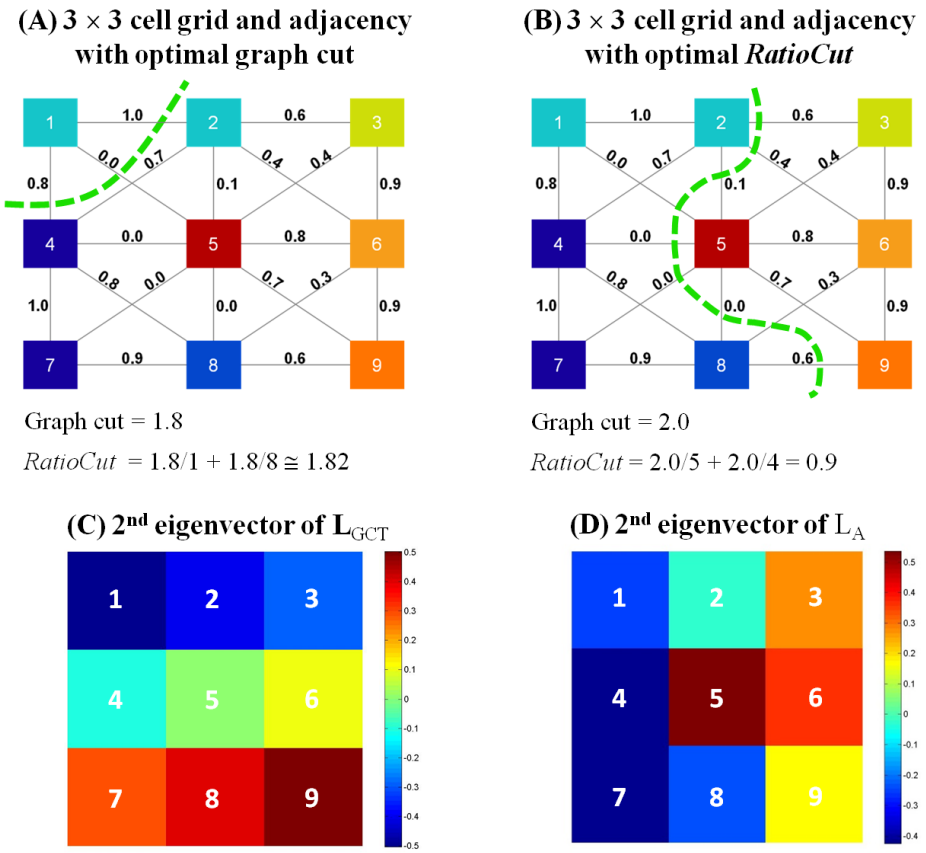

Fig. 5.3. Example graph cuts in (A) and (B) with calculation of both the graph cut and *RatioCut* metric for each field, and the 2nd eigenvector of the (C) $\mathbf{L}_{GCT}$ and (D) $\mathbf{L}_A$ Laplacian mapped to the 3 × 3 grid.

5.3.3 A Two-Zone Partition (k = 2)

Hagen and Kahng (1992), who introduced the metric *RatioCut*, showed that when k = 2 the optimal solution or zonation of any graph (characterized by $\mathbf{L}_A$) is *approximated* by the second eigenvalue of $\mathbf{L}_A$, λ_1, and is characterized on the graph by the corresponding eigenvector. To reiterate, in this application the concept of the graph is replaced by the parameterized property field. For a theoretical understanding of this proposition, the following expands upon relevant concepts from Hagen and Kahng (1992) using notation relevant to this study.

Consider the optimal zonation corresponding to the minimum of Eq. (5.4) and depicted as the piecewise continuous vector

$$f_i = \begin{cases} q & \text{if } v_i \in A_1 \\ -p & \text{if } v_i \in A_2 \end{cases} \tag{5.5}$$

where q and p are defined subject to the constraints $q,p \geq 0$, $pN = |A_1|$, $qN = |A_2|$ and $q + p = 1$. From this definition, **f** also satisfies the equality $\mathbf{f}^T\mathbf{1} = 0$, or is orthogonal to the constant vector **1**. Therefore, **f** defines an indicator vector that identifies a two-zone, piecewise continuous partition of the field when mapped onto the grid. The key associations that relate **f** to the optimal cut can be shown by algebraic equivalence and are:

$$cut(A_1, A_2) = \mathbf{f}^T\mathbf{L}_A\mathbf{f} \tag{5.6}$$

and

$$\mathbf{f}^T\mathbf{f} = \frac{|A_1| \cdot |A_2|}{N}. \tag{5.7}$$

The first in Eq. (5.6) follows conceptually from the relation that $f_i - f_j = 0$ when cells i and j are within the same zone, and that $f_i - f_j = 1$ when cells i and j are in the different zones; therefore, the weighted scalar product in Eq. (5.6), where the weights are defined by the components of $\mathbf{L}_A$, define the graph cut, which to reiterate is the sum of all edge weights intersected by the cut. The second equivalence in Eq. (5.7) is shown from the relation $\mathbf{f}^T\mathbf{f} = q^2|A_1| + p^2|A_2| = q^2 pN + p^2 qN = qpN = |A_1| \cdot |A_2|/N$. Therefore, when k = 2, *RatioCut* in Eq. (5.4) can be alternately defined as

$$
\begin{aligned}
RatioCut &= \frac{cut(A_1, A_2)}{|A_1|} + \frac{cut(A_2, A_1)}{|A_2|} \\
&= \frac{cut(A_1, A_2) \cdot [|A_1| + |A_2|]}{|A_1||A_2|} = \frac{N \cdot cut(A_1, A_2)}{|A_1||A_2|} \\
&= \frac{\mathbf{f}^T \mathbf{L}_A \mathbf{f}}{\mathbf{f}^T \mathbf{f}}
\end{aligned}
\tag{5.8}
$$

which has the form of the Rayleigh quotient. It was established in **Subsection 3.3** that $\mathbf{L}_A$, when defined as in Eq. (5.2), is symmetric and positive semi-definite with a non-negative eigenspectrum, and furthermore with a smallest eigenvalue always equal to zero and corresponding to the constant eigenvector (i.e., **1**). By the Rayleigh-Ritz theorem (Lancaster and Tismenetsky, 1985), the minima of Eq. (5.8) are the eigenvalues of $\mathbf{L}_A$ and the corresponding eigenvectors the critical points of the Rayleigh quotient. However, under the indicator constraint of Eq. (5.5), the minimization of Eq. (5.8) is a NP-hard discrete optimization problem and cannot be solved trivially (Shi and Malik, 2000). Hagen and Kahng (1992) showed that when this constraint is relaxed such that f_i can have any real value, then by the Rayleigh-Ritz theorem the second smallest eigenvalue is the solution to minimization of *RatioCut* subject to the aforementioned constraints $\mathbf{f}^T \mathbf{1} = 0$ and $\mathbf{f} \neq 0$. Recall from Eq. (3.8) in **Subsection 3.3** that the Laplacian, when computed as Eq. (5.2), is always positive semi-definite. The smallest eigenvalue (λ_0) of $\mathbf{L}_A$ is, therefore, always equal to zero and corresponds to the constant eigenvector which clearly does not provide a partition of the property field. The relevant solution then is λ_1, with the zonation characterized by the second eigenvector.

A simple but informative demonstration of this concept is presented in Fig. 5.3D in which the second eigenvector of $\mathbf{L}_A$ (corresponding the property field in Fig. 5.3B) is mapped onto the 3 × 3 grid. The eigenvector components are clearly related to the heterogeneity pattern and, by visual inspection, enable a partitioning of the field identical to that identified by the minimum *RatioCut* in Fig. 5.3B (see the green dashed line). This is the key utility behind the application of Laplacian eigenvectors for spatial

zonation. In fact, spectral clustering algorithms are based on this and similar concepts (von Luxburg, 2006; Zhang et al., 2010). It is also useful to compare the second eigenvector of $\mathbf{L}_A$ with that of $\mathbf{L}_{GCT}$, shown in Fig. 5.3C. The heterogeneity captured by this eigenvector is related to the grid connectivity harmonics and is unrelated to the parameter heterogeneity, therefore providing no utility for zonation in this example.

As λ_1 indicates the useful eigenpair when $k = 2$, a crucial consideration for parameterization is the (geometric) multiplicity of the zero eigenvalue, λ_0. The multiplicity of λ_0 is equal to the number of isolated zones, $A_1, \ldots, A_k$, as defined in $\mathbf{L}_A$ (Mohar, 1997). When $k = 1$, or when the grid appears fully connected, it was explained in **Subsection 3.3** that a single zero eigenvalue exists and corresponds to the constant eigenvector, **1**. Using the adjacency construct, it is highly possible that $k > 1$, or that relative to the components of $\mathbf{L}_A$ certain groups of cells appear isolated from all others when $a_{ij} = 0$ for all cells paired across the k groups. In this case, the number of zero eigenvalues equals k, and the corresponding eigenvectors are indicator vectors of constant non-zero value over the ith group of cells, for $i = 1, \ldots, k$ (Mohar, 1991; von Luxburg, 2006). It is important to understand that, for the purpose of parameterization, we seek eigenvectors of approximate piecewise continuous value and not the indicator vectors. Although the latter may be quite useful for the identification of prior zones in other applications (e.g., clustering), these vectors fix the location and boundaries of the different zones which are likely uncertain and require adjustment during calibration of the prior. Therefore, in this application only a single constant basis vector is desired for updating of the field mean, and the subsequent leading basis vectors are used to update heterogeneity as the linear combination of piecewise continuous features. Stated differently, we do not seek the indicator vector **f** in Eq. (5.5) that exactly minimizes Eq. (5.8), but rather prefer for a parameterization the second eigenvector corresponding to the approximate solution λ_1 when $k = 2$. We return to and provide examples of this important topic below in **Subsection 5.4.1** during the construction and analysis of basis

vectors for different prior models, and further explain why and how this effect must be avoided for parameterization.

5.3.4 A Multi-Zone Partition ($k > 2$)

The extension of the *RatioCut* minimization to k zones is required for the use of multiple leading eigenvectors for multiscale zonation adjustment. Following the logic of the previous subsection, a similar proposition is given by von Luxburg (2006) that relates the leading eigenpairs of $\mathbf{L}_\mathrm{A}$ to an optimal zonation of the field. Rather than considering the single indicator vector $\mathbf{f}$ (Eq. [5.5]) that optimally partitions the field, $k > 2$ indicator vectors can be considered that comprise the columns of matrix $\mathbf{F}$ with indicator components $f_{i,j}$ for $1 \le i \le N$ and $1 \le j \le k$. Similar to the proposition above, if $f_{i,j}$ can take real values and the constraint $\mathbf{F}^\mathrm{T}\mathbf{F} = \mathbf{I}$ is satisfied (i.e., the indicator vectors are pairwise orthogonal), von Luxburg (2006) shows that the general form of *RatioCut* (Eq. [5.4]) is proportional to $Tr\left(\mathbf{F}^T\mathbf{L}_\mathrm{A}\mathbf{F}\right)$, where *Tr* denotes the matrix trace. Using a variant of the Rayleigh-Ritz theorem, and again relaxing the indicator constraint on the values of $f_{i,j}$, the minimization of $Tr\left(\mathbf{F}^T\mathbf{L}_\mathrm{A}\mathbf{F}\right)$ to identify the k minima of *RatioCut* are given by the matrix $\mathbf{F}$ that has the first k eigenvectors of $\mathbf{L}_\mathrm{A}$ as columns.

Returning now to the application of reservoir heterogeneity parameterization, the leading eigenvectors of $\mathbf{L}_\mathrm{A}$ will, to varying degrees, capture multiple zones of spatially continuous heterogeneity as piecewise continuous eigenvector components. The eigenvalues determine the spatial scales of piecewise continuity in each vector, with smaller eigenvalues associated with larger scales of continuity. As an end member, the zero eigenvalue (λ_0) corresponds with the constant vector and therefore does not depict heterogeneity, but is useful for updating of the field mean. When used together, the eigenvectors enable the simultaneous characterization of a large number of prior model heterogeneity zones, with the sharpness of the zone borders determined by the strength of the adjaceny metric (Eq. [5.3]**)**, and using only a few parameters, typically much less than one percent of the property dimension.

5.3.5 Numerical Eigendecomposition

The minimization of Eq. (5.8) and its multi-partition analogue, which are expressed as the Rayleigh quotient, is achieved by solving the standard eigenvalue problem. Recalling the properties of the Laplacian when constructed as in Eq. (5.2), $\mathbf{L}_A$ is guaranteed symmetric, sparse and positive semi-definite. Therefore, just as for the $\mathbf{L}_{GCT}$, we take advantage of these properties and use the implicitly restarted Lanczos method (IRLM) within the ARPACK subroutines (Lehoucq et al., 1998) to approximate the leading eigenpairs corresponding to the smallest eigenvalues. The approach of iterative restarting ensures orthogonality of the Lanczos vectors. As explained in detail in **Subsection 3.3.4**, a highly truncated matrix decomposition is not a limiting factor but is in fact preferred for the parameterization as the intent of history matching is to calibrate only coarser scale spatial information as a result of limitations in data resolution.

5.4 Methods: The Application of Parameterization in History Matching

This subsection describes how the adjacency-based parameterization is applied for history matching. Because the parameterization basis can include prior model information at various levels depending on the strictness of the adjacency measure, which is fundamentally based on the type of prior model heterogeneity, we must now also consider various applications of the transform basis. In **Subsection 5.4.1** we first demonstrate by example how the basis vectors vary as a function of the adjacency metric parameters for different types of heterogeneity, and concurrently address the capacity of the various bases for low-rank approximation of the prior heterogeneity. To address the subjective selection of the adjacency parameters during construction of $\mathbf{L}_A$, here we also provide guidelines for basis construction as determined by properties required for an effective parameterization. In **Subsection 5.4.2** we then present the mathematical formulation of the parameterization and review its application in an adaptive multiscale workflow. As a result of the variability in different types of prior model heterogeneity, we explain how the parameterization is applied using either a multiplier field, which

updates the prior at full spatial detail, or using a low-rank approximation of the prior when the dominant heterogeneity is at local spatial scales finer than can be resolved by a global multiplier field.

5.4.1 Basis Vector Behavior

The spatial signature of basis vectors can vary from smooth and apparently model-independent, converging to Fourier-like behavior at one extreme, to characterizing discrete zones of spatial continuity that well depict prior model heterogeneity at the other extreme. This variability in behavior depends on the specified rate of exponential decrease in both terms of the adjacency measure in Eq. (5.3), relative to the range and spatial variability of the prior heterogeneity. To demonstrate these concepts, we present the leading basis vectors, for different bases, constructed using two different 2D permeability fields. The first field in Fig. 5.4A is characterized by strong anisotropic heterogeneity at the coarse scale and continuous (smooth) spatial variability at the fine scale, particularly considering cell-to-cell variation. The second permeability field in Fig. 5.4B also depicts strong coarse scale anisotropy, but contains large variability at the fine scale, often with discrete differences in value between neighboring cells.

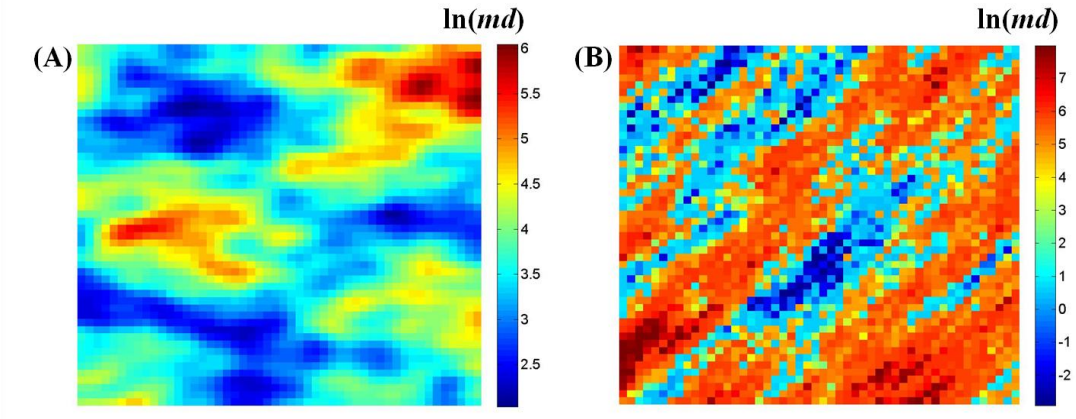

Fig. 5.4. Permeability fields of (A) weaker and (B) stronger anisotropic, multiscale heterogeity applied in construction of adjacency-based transformation bases.

Beginning with use of the more continuous permeability field in Fig. 5.4A, in Fig. 5.5 are shown the ten leading basis vectors for four different constructs of $\mathbf{L}_A$. Each case uses the same multipoint stencil, or the same value of σ_X, corresponding to a two-step connectivity or 25-point stencil (excluding the boundary cases). The parameter σ_P is varied from strict to relaxed relative to the user-specified cell property norm tolerance, notated as $||\Delta p||_2$ in the figure (or $||p_i - p_j||_2$ in Eq. [5.3]). In the most strict case in Fig. 5.5A, or when the exponential rate of decrease is greatest in the adjacency measure, the prior heterogeneity features appear the most represented in the basis vectors. As σ_P is relaxed, the piecewise continuous regions of the basis vectors lose their similarity to the prior and at the same time begin to assume frequency-like variability. In Fig. 5.5D, $||\Delta p||_2$ is sufficiently large relative to the difference in permeability at any cell pair within the stencil that all values of a_{ij} are close to unity, $\mathbf{L}_A$ converges to a multipoint periodic operator, and the basis converges to the GCT basis (actually the DCT-2 basis for this regular grid).

Another important result is the existence of a single zero eigenvalue, and therefore a single constant basis vector, for each of the bases (or rows of Fig. 5.5). This implies that the field, relative to the components of $\mathbf{L}_A$, is fully connected such that any cell can be reached stepping from cell-to-cell along at least one path of non-zero a_{ij} from a starting location at any other cell. Recall that this property is important for an effective parameterization as it permits updating of the field mean using a single parameter and, further, is equivalent to the traditional application of a zonal multiplier over the parameterized region. Therefore, when selecting $||\Delta x||_2$ and $||\Delta p||_2$ for computation of σ_X and σ_P (Eq. [5.3]), respectively, it is important that both are sufficiently large to ensure a fully connected graph.

Similar sets of basis vectors, again corresponding to a constant stencil and varying values of σ_P, are shown in Fig. 5.6 that are constructed using the permeability field in Fig. 5.4B. The same conclusions stated above are true for this case; however, the large and often discrete permeability variation between cells in the stencil brings to light

challenges that may be faced in an appropriate basis construction. To ensure the existence of only a single zero eigenvalue, both the stencil and cell property tolerance must be sufficiently large to ensure a fully connected graph. In this case, a 3-step connectivity or a 49-point stencil is used (excluding the boundary cases). Even using this large stencil together with a relatively large property tolerance $||\Delta p||_2$, the second vector in both Figs. 5.6A and 5.6B has the apparent property of an indicator vector. From comparison with the permeability field in Fig. 5.4B, these vectors clearly identify an isolated group of cells of highly contrasting heterogeneity that are apparently disconnected (or have $a_{ij} = 0$) from the remainder of the cells in $\mathbf{L}_A$. The corresponding eigenvalue for each of these basis vectors is very small and close to zero, hence use of the term *apparent* indictor vector. Clearly this effect is detrimental to parameterization as this second basis vector would permit updating of only a single isolated zone. Observe also in all rows of Fig. 5.6 that even as the property tolerance $||\Delta p||_2$ becomes large and the spatial variability characterized by the basis vectors become more frequency-like, regions of the permeability field that have the largest contrasts, both at the fine and coarse scale, persist in the basis vectors.

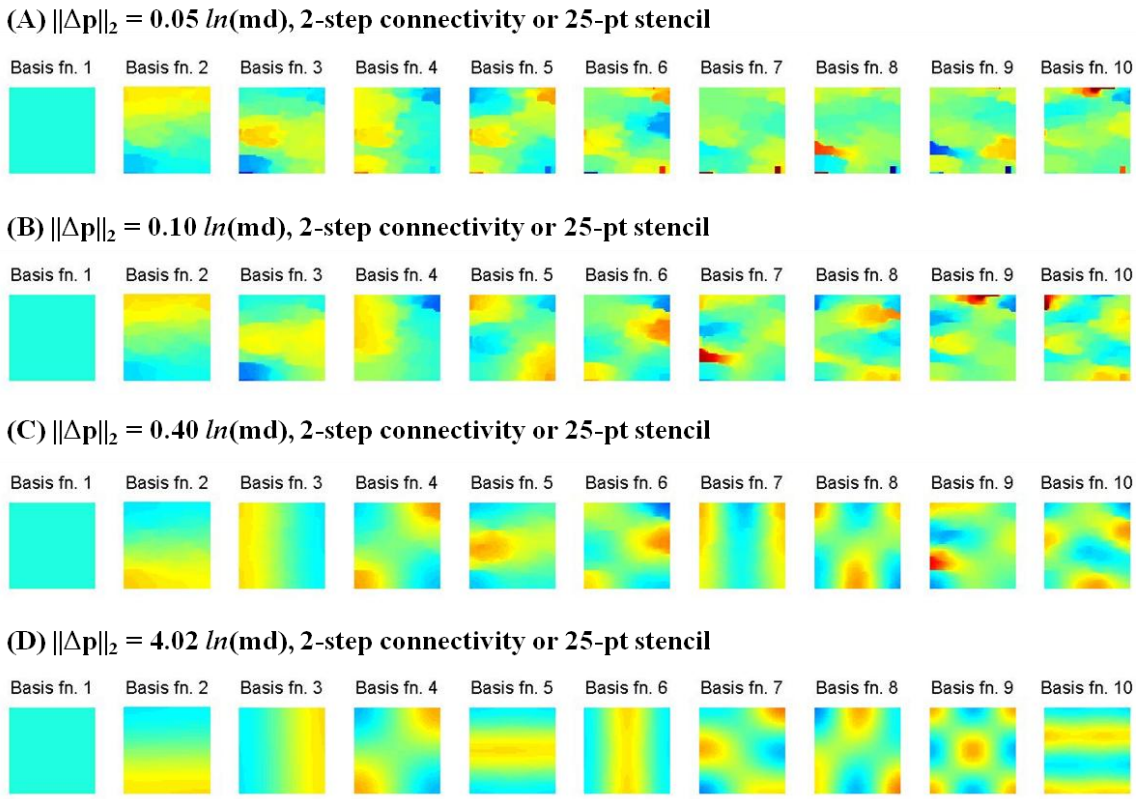

Fig. 5.5. Each row lists the ten leading basis vectors (corresponding to the lowest eigenvalues) of a different $\mathbf{L}_A$ constructed using the same multipoint stencil (of two-step connectivity or a 25-point stencil) and increasing property difference thresholds, $||\Delta p||_2$, from (A) to (D). The prior permeability model applied for definition of $\mathbf{L}_A$ is in Fig. 5.4A.

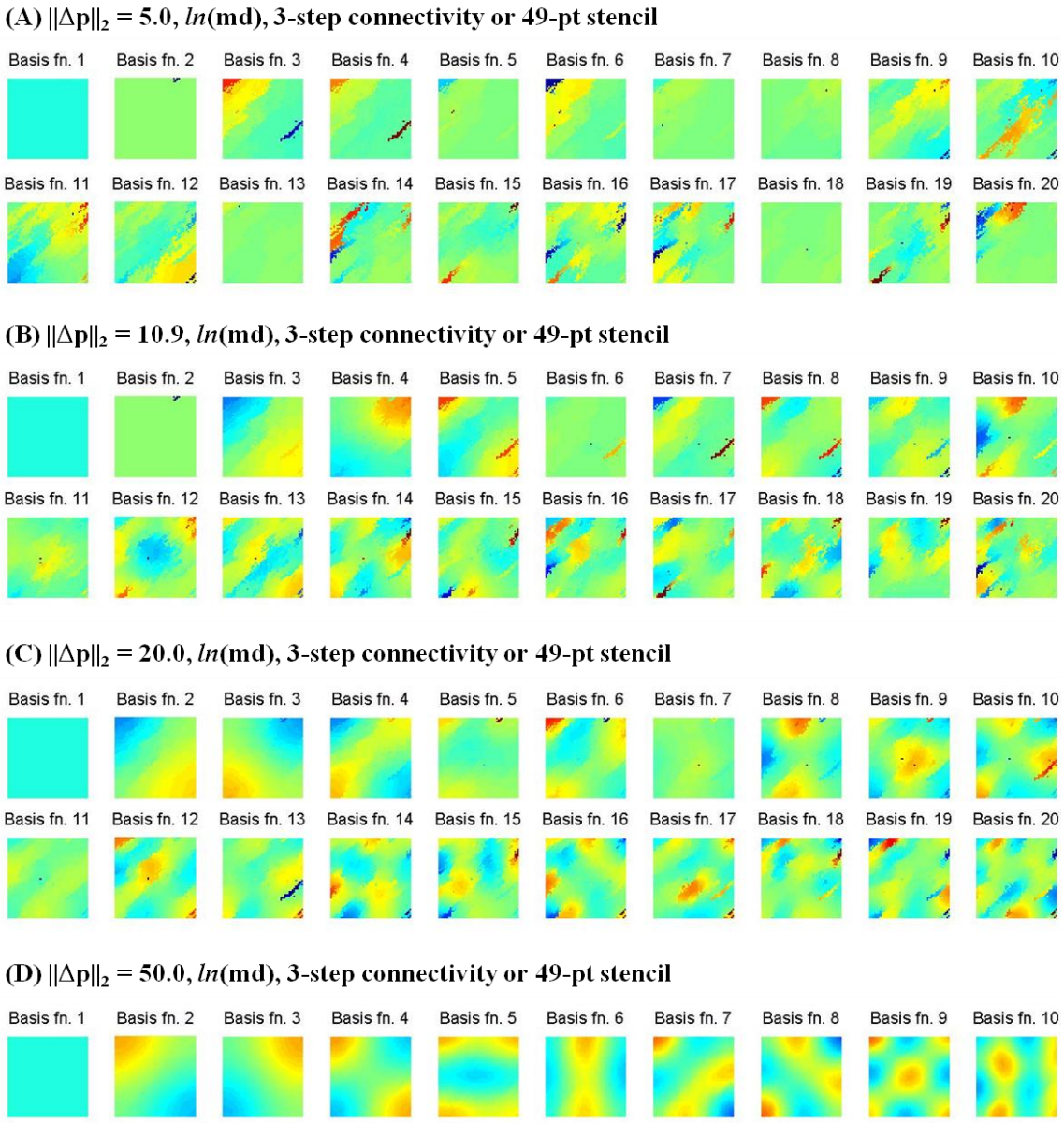

Fig. 5.6. Each row lists the ten leading basis vectors (corresponding to the lowest eigenvalues) of a different $\mathbf{L}_A$ constructed using the same multipoint stencil (of two-step connectivity or a 25-point stencil) and increasing property difference thresholds, $||\Delta p||_2$, from (A) to (D). The prior permeability model applied for definition of $\mathbf{L}_A$ is in Fig. 5.4B.

Returning now to the more continuous permeability field in Fig. 5.4A and switching perspectives regarding the adjacency measure, Fig. 5.7 shows the leading basis vectors for several constructs of $\mathbf{L}_A$ that use different multipoint stencils (or values of σ_X), but a

constant cell property threshold, $\|\Delta p\|_2$. Although the influence of prior heterogeneity is slightly degraded as the stencil size increases, the three sets of basis vectors are, from a parameterization standpoint, identical. The key observation is that the stencil size has less of an influence on basis vector behavior than the cell property differences within the stencil. Regardless of the stencil size, a difference in cell property values that exceeds the specified threshold will result in a (near) zero adjacency measure or weight, thereby disconnecting the cell pair within $\mathbf{L}_A$, and resulting in some level of discontinuity between these cells in the basis vectors. This insensitivity to stencil size is enhanced when considering a spatially continuous property at the fine scale (or the scale of the stencil), as depicted in Fig. 5.4A.

There is, however, more of an importance to the stencil selection when the property variability is large at the grid cell scale, as depicted in Fig. 5.4B. In this type of (extreme) case, the stencil must be sufficiently large to capture even the smallest level of cell continuity as defined within $\mathbf{L}_A$, regardless of the value of $\|\Delta p\|_2$. For example, using a 9-point and 25-point stencil, several of the corresponding basis vectors in Figs. 5.8A and 5.8B, respectively, are effectively indicator vectors that isolate small cell clusters and that have an eigenvalue very close to zero. For reasons discussed earlier, these vectors are detrimental to the parameterization and, next, we demonstrate how these vectors in fact result in poor heterogeneity compression performance. Regardless, once the stencil is achieved that is of sufficient size to capture this continuity (e.g., Fig. 5.8C), further increasing its dimension is of little import (as depicted in Fig. 5.7).

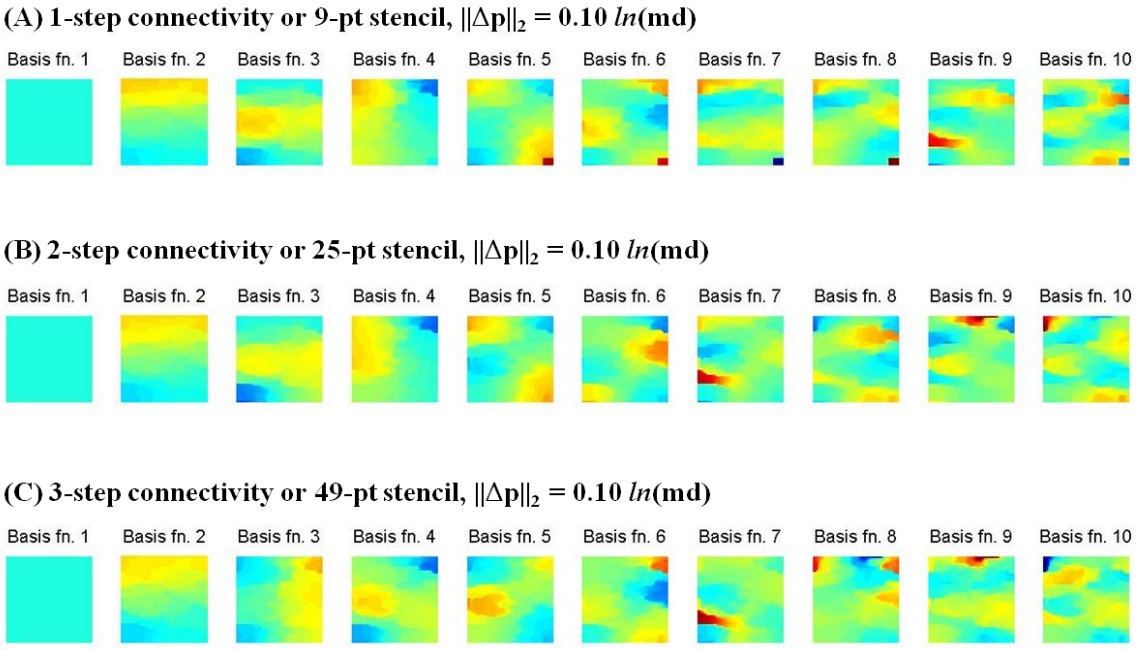

Fig. 5.7. Each row lists the ten leading basis vectors (corresponding to the lowest eigenvalues) of a different $\mathbf{L}_A$ constructed using the same property difference threshold, $\|\Delta p\|_2$, and increasing multipoint stencils from (A) to (C). The prior permeability model applied for definition of $\mathbf{L}_A$ is in Fig. 5.4A.

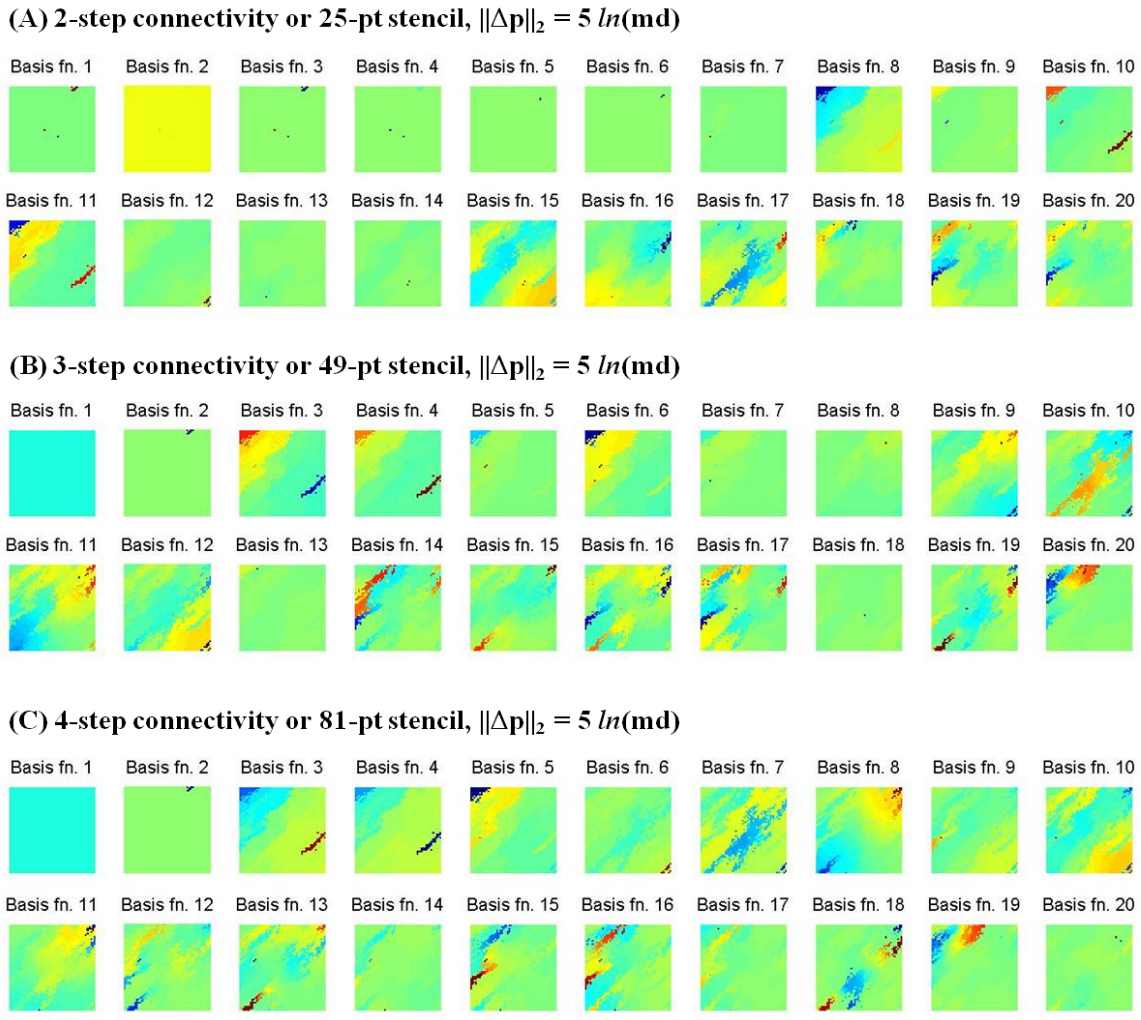

Fig. 5.8. Each row lists the ten leading basis vectors (corresponding to the lowest eigenvalues) of a different $\mathbf{L}_A$ constructed using the same property difference threshold, $\|\Delta p\|_2$, and increasing multipoint stencils from (A) to (C). The prior permeability model applied for definition of $\mathbf{L}_A$ is in Fig. 5.4B.

The prior model compression performance using all of the bases in Figs. 5.5 thru 5.8 is shown in Figs. 5.9 and 5.10 for the permeability fields in Figs. 5.4A and B, respectively. As the adjacency measure (Eq. [5.3]) becomes more strict, or as the stencil size and property difference tolerance are decreased, the bases represent the prior heterogeneity more accurately and the compression performance improves. In fact, the GCT (or DCT) basis shows the weakest compression performance of all of the cases, even though the GCT is known to provide strong compression of generic signals/images (e.g., Karni and

Gotsman, 2000; Zhang, 2004). This same behavior is observed for both of the permeability fields in Fig. 5.4. However, notice that when the multiplicity of λ_0 is greater than one (e.g., see the basis vectors in Fig. 5.8A applied in Fig. 10), the GCT outperforms the adjacency-based compression until the corresponding indicator vectors have all been included and the continuous (rather than indicator) vectors begin to be used for the low-rank approximation. Fig. 5.11 exemplifies the approximated permeability field in Fig. 5.4A at different compression levels, and Fig. 12 shows the same low-rank approximations for the permeability field in Fig. 5.4B. Both include the equivalent approximations using the GCT basis. The advantage of the adjacency-based compression is apparent in both cases. Multiscale heterogeneity of both continuous and apparently discrete descriptions is well captured using only a few of the leading adjacency-based basis vectors. On the other hand, the GCT (by design) provides a compact representation of the larger scale heterogeneity and captures only smooth features, truncating sharper features or edge information.

Returning now to the application of geologic parameterization for history matching, if the prior model is well informed, then it is expected that the dominant heterogeneity (as depicted by the basis vector spatial variability) can be calibrated using few parameters corresponding to the relevant basis vectors. However, knowledge of prior information is always uncertain and, consequently, it may or may not be advantageous to include prior information in the parameterization basis despite the demonstrated capability for improved prior model compression. This concept is demonstrated in the parameterized history matching applications.

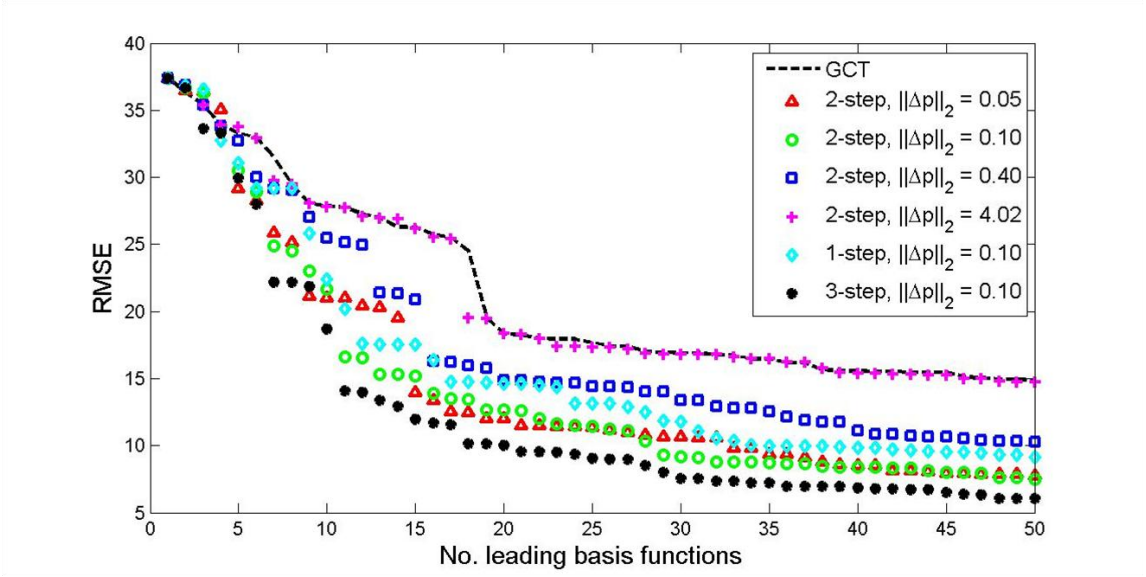

Fig. 5.9. Prior model compression performance, for the permeability field in Fig. 5.4A, using each of the bases depicted in Figs. 5.5 and 5.7.

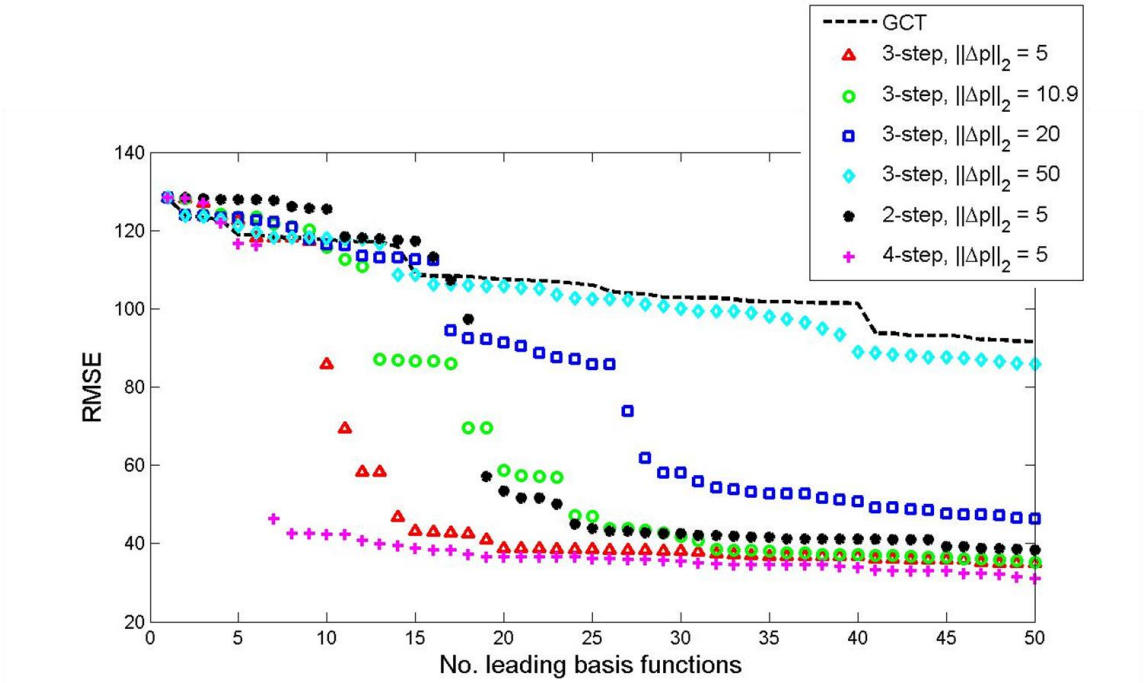

Fig. 5.10. Prior model compression performance, for the permeability field in Fig. 5.4B, using each of the bases depicted in Figs. 5.6 and 5.8.

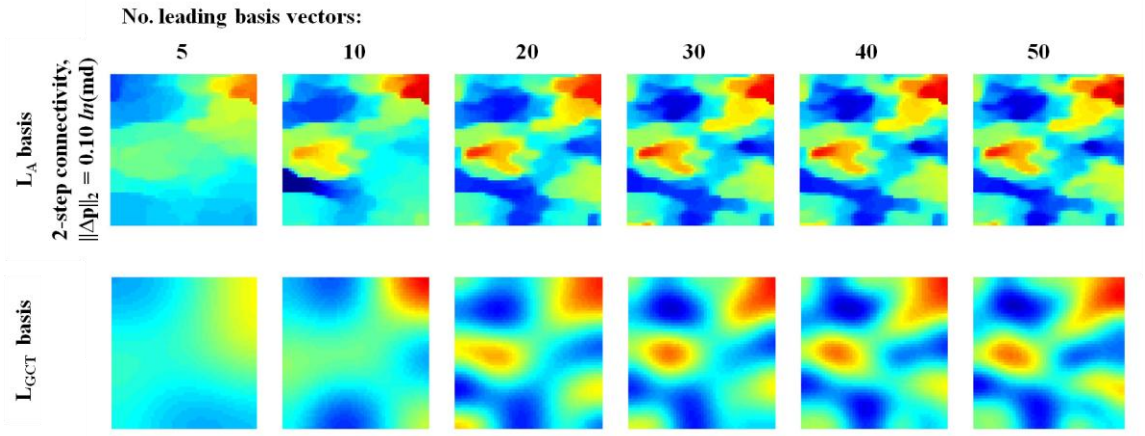

Fig. 5.11. Low-rank approximations of the permeability field in Fig. 5.4A using leading basis vectors corresponding to the bases identified in Fig. 5.9.

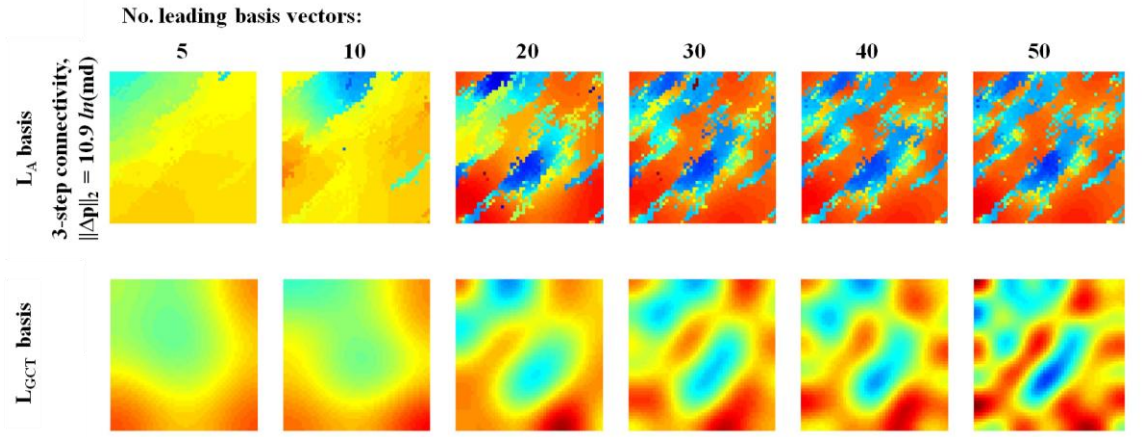

Fig. 5.12. Low-rank approximations of the permeability field in Fig. 5.4B using leading basis vectors corresponding to the bases identified in Fig. 5.10.

5.4.2 Multiscale Parameterization and Workflow

The discussion to this point has been focused on the development of the adjacency-based transformation basis, hereafter referred to as the ABT basis, for specific use in reservoir model parameterization. To review its advantageous properties for this use, the ABT

basis can be constructed for any grid structure or sub-grid region, permits the adaptive inclusion of prior model heterogeneity via the adjacency measure, and has pairwise orthogonal basis vectors that characterize multiscale spatial variability from the coarse to fine scale based on the corresponding eigenspectrum. Together these properties form a flexible construct for heterogeneity parameterization that is naturally suited for a multiscale application in the spectral domain.

Following the general approach to parameterization by linear transformation presented in **Section 1**, the spatial parameter field **u**, defined at each grid cell center over the domain of interest, is mapped to the transform domain as

$$\mathbf{v} = \mathbf{\Phi}^T \mathbf{u} \Leftrightarrow \mathbf{u} = \mathbf{\Phi v} \,. \tag{5.9}$$

The vector **u** has dimension $m \times 1$, where m is the discretization of the calibrated field, and the column vector **v** is the n_t-length spectrum of transform coefficients, or the parameters in the spectral domain. The n_t columns of the basis $\mathbf{\Phi}$ are the ABT basis vectors each of length m. Note that Eq. (5.9) implies pairwise orthogonal basis vectors so that the forward and inverse transform bases are efficiently computed through a transpose operation.

As the primary objective of parameterization is to reduce the parameter dimension, in this case the dimension of **v**, $\mathbf{\Phi}$ is a compact (truncated) representation and contains only a small number of basis leading basis vectors, corresponding to the smallest eigenvalues, that are able to capture the most relevant spatial information in a compact form. Further, the dimension (or number of columns) in $\mathbf{\Phi}$ is adaptively increased during the history matching algorithm in order to refine the spatial parameter. The coarsest scale basis vectors are applied first to enable updating of large-scale heterogeneity. Then, basis vectors corresponding to finer scale features are adaptively included in the basis, increasing the number of parameters, and enabling the sequential refinement of details only to the spatial scale at which such details can be resolved by the production data.

Prior to each step of spatial refinement, the property model is used in the iterative minimization of a data misfit objective function that requires the simulation of dynamic production responses using the model iterates. The objective function is typically defined as the squared l_2-norm of nonlinear dynamic data misfit, and is iteratively minimized using a quasi-Newton method. Given that we have only a few parameters, the gradient with respect to parameters in the transform domain can be directly computed through finite-difference perturbation, or alternatively using spatial parameter sensitivities made available from a commercial reservoir simulator using its built-in adjoint method. The specifics of these approaches were presented in detail in the previous subsections, and are pointed out specifically when relevant below.

When the prior model heterogeneity is well informed (i.e., close to the true heterogeneity) or at least thought to be, then the intent of history matching is to update the prior heterogeneity at locations and spatial scales warranted by the production data, and to leave the property unchanged at locations either insensitive to or already consistent with the data. This is achieved by superimposing a multiplier field onto the prior model at grid-cell resolution, either over the complete domain or over any sub-grid region that requires calibration. The multiplier at each cell is assigned an initial value of unity, and it is the multiplier field (or **u**) that is parameterized as **v** in Eq. (5.9) and calibrated. A complete description of this version of the adaptive multiscale workflow is presented in detail in **Subsection 3.3.6**.

The inclusion of prior model or cell adjacency information into the transformation basis, however, complicates the multiscale approach, so the workflow must be tailored in some cases based on the understanding of prior information. When the prior model heterogeneity affecting production responses is at the larger scale, or at the scale of the well pattern, then the approach of the multiplier field is found appropriate and robust over a large range of heterogeneity types. On the contrary, when the prior heterogeneity affecting production responses exists at the fine (or grid cell) scale as well as the large scale, then a multiplier field (when applied over the reservoir domain) is incapable of

making the required updates with a low-rank approximation required for a practical parameterization. In such scenarios, the property field is itself first reduced to a coarse approximation, and then is adaptively refined to the scale at which model and data resolution become balanced. As exemplified earlier in this section, the compression power of the ABT basis permits a low-rank description of the spatial model, characterizing dissimilar features relative to the adjacency measure, while smoothing over fine scale heterogeneity of small property differences that likely are irresolvable by the production data. During iterative calibration, the low-rank approximation of the prior decreases the likelihood of solution convergence to a local minimum related to a grossly incorrect starting location on the objective function surface, and also to high parameter dimensionality. This is the approach to adaptive multiscale model calibration taken in **Section 2** using the DCT parameterization.

It should be noted that the latter approach of prior model compression is, in general, not preferred because (1) the initial level of truncation must be performed only to the extent that some measure of dynamic behavior is honored given the corresponding reduction of spatial detail, which is an expensive task, and because (2) the inclusion of the relevant basis vectors in the parameterization during refinement is a non-trivial task. These subjects were addressed and managed in **Section 2**. However, in the following application subsection, we shown that when prior heterogeneity is strong and exists at the fine scale, then a multiplier field cannot be used to achieve a parameter solution and the prior must be approximated. Even more, when the prior heterogeneity is not only strong but also too far from the actual, then it is possible that a history match is not possible, or that no solution exists, because the influence of the incorrect prior information in the basis is too dominant. In such cases the incorporation of prior information in the basis should be relaxed, ultimately reverting to the GCT parameterization.

5.5 History Matching Applications

The intent of this subsection is two-fold, to apply for history matching the theoretical constructs of the ABT parameterization presented to this point, and to explore the strengths and limitations of the parameterization in order to develop guidelines for general application. The subsection begins with the history match of two synthetic reservoir models. For this the two permeability fields in Fig. 5.4, representative of two extreme types of heterogeneity (relative to the construct of $\mathbf{L}_A$), are calibrated using several different ABT bases. This broad range of geologic modeling scenarios reveals the proper utility of the ABT parameterization for history matching. From this foundation, the parameterization is then applied for the history match of the Brugge reservoir model, a SPE benchmark case developed after a field case, for which detailed prior model information is available.

5.5.1 Synthetic Model: Weak Multiscale Heterogeneity

In this subsection we explore the efficacy and any limitations of the ABT parameterization in history matching for the case of a geologic model with strong anisotropic heterogeneity at the coarse scale and continuous or smooth spatial variability at the grid cell scale. Also considered are calibration scenarios in which the prior geologic model is either far from or close to the true or reference model. In all scenarios, the (prior) permeability field in Fig. 5.4A is calibrated using different ABT bases selected from those shown in Figs. 5.5 and 5.7.

The modeling scenario is a 9-spot waterflood with pressure-controlled production and volume-controlled injection at a single domain-centered well in a simple 2D square reservoir. The domain dimensions are $1500 \times 1500 \times 30$ ft with uniform grid cell dimensions of 30 ft per side. The flow model represents a two-phase (oil-water) system, with constant fluid densities and viscosities, and quadratic relative permeability curves with an end-point mobility ratio of 5.0, solved using a commercial black oil simulator with fully implicit discretization. Production response sensitivities to static grid cell

properties are derived from the simulators built-in adjoint code. Cell absolute permeability is the static parameter calibrated to match observed water production rates (WPR) over a four-year history period, plus a subsequent two-year forecast period, at each of the eight producers.

To reiterate the conceptual approach to model updating, the primary objective is to use a permeability multiplier field as the updated parameter whenever possible, minimally updating the (high resolution) prior model that is assumed to be constructed from static data sources. In consideration of the ABT parameterization, a secondary objective is to incorporate as much prior information as possible into the transform basis, achieved by the use of a strict adjacency metric (Eq. [5.3]) as previously discussed.

Using the prior permeability field in Fig. 5.4A, we consider three history matching cases for which the reference model heterogeneity (used to generate the observation WPR) is far from the prior. The prior and reference fields are shown juxtaposed in Figs. 5.13A and 5.13B, respectively. Each of the three cases uses a different ABT basis that represents (1) the GCT or Fourier-like basis (Fig. 5.5D) constructed using excessively relaxed adjacency parameters, (2) an ABT basis with less strict incorporation of prior model information (Fig. 5.5B) and (3) more strict incorporation or prior information (Fig. 5.5A). The calibrated permeability fields for case (1) through (3) are respectively shown in Figs. 5.13C through 5.13E, the features of which are discussed below.

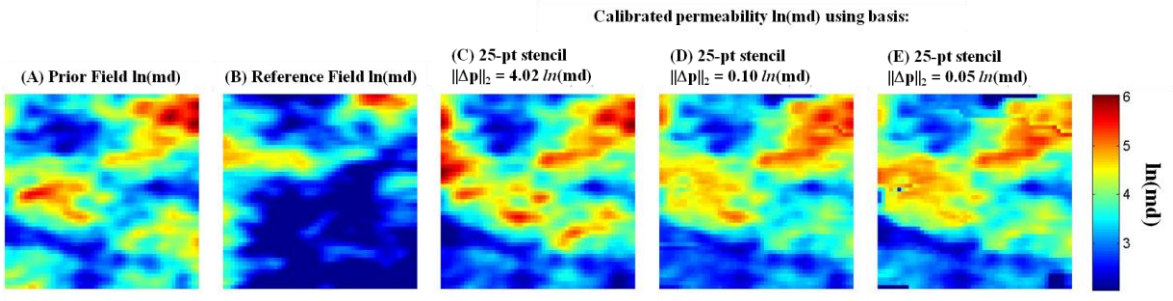

Fig. 5.13. The (A) prior and (B) reference permeability fields applied in a model calibration exercise, juxtaposed to the calibrated fields for three cases in (C) through (E) using the different Laplacians as labeled in the figure.

Following the adaptive multiscale approach to model updating, the parameterized multiplier field is successively refined during the gradient-based minimization of WPR data misfit. Beginning with a coarse parameterization using only five basis vectors corresponding to the smallest eigenvalues of $\mathbf{L}_A$ (e.g., the first five columns of Fig. 5.5 or Fig. 5.7), the parameter set is increased by adding the next five basis vectors following a reduction of the objective function into a local minimum at this coarse description. For the purpose of comparison across the different cases, this sequence is repeated until the parameterization incorporates the leading fifty basis vectors, which is equivalent to the application of ten multiscale iterates (as defined in Fig. 3.5). The sequential evolution of the multiplier field upon local convergence is shown for each of the three cases in Fig. 5.14. The corresponding WPR misfits for each of the (three) calibrated permeability fields are plotted together in Fig. 5.15, with the root mean square error (RMSE) of each calibrated field listed in the figure legend. These collective results are now discussed.

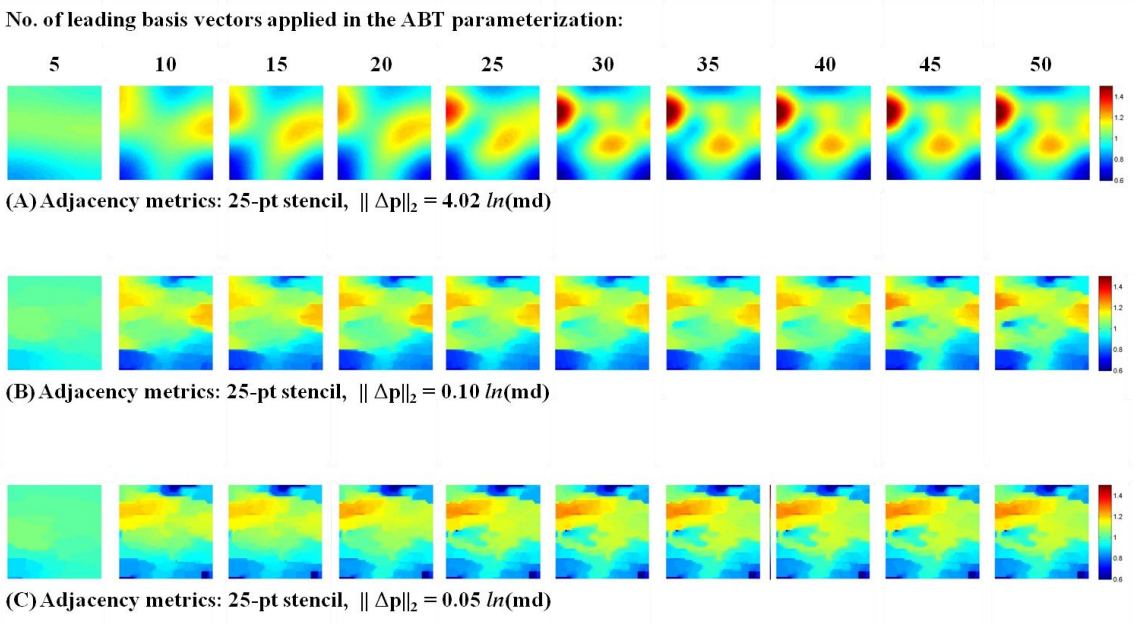

Fig. 5.14. Calibrated multiplier fields corresponding to the prior model in Fig. 5.13A at successive multiscale iterates of the adaptive history matching workflow. Each case uses a different ABT basis as listed in the figure. (A) corresponds to the calibrated permeability in Fig. 5.13C, (B) to the field in Fig. 5.13D and (C) to the field in Fig. 5.13E.

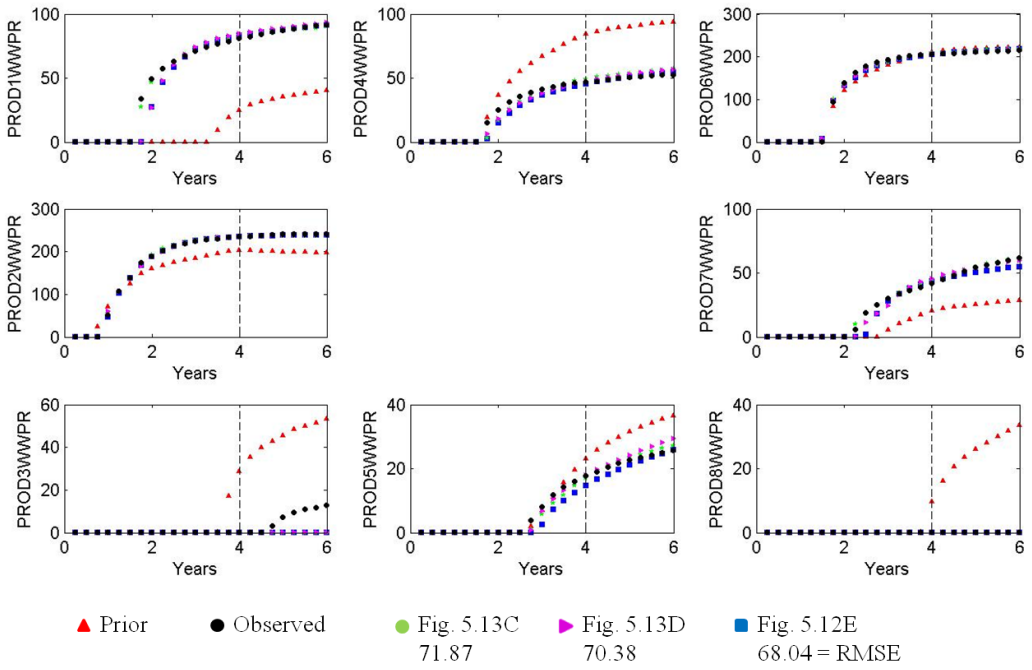

Fig. 5.15. Producer WPR data misfit for the three history matching cases depicted in Figs. 5.13 and 5.14.

In the first case, the Fourier-like ABT basis depicted in Fig. 5.5D is applied as a control case. The model-independence of the basis and corresponding spatial symmetry of the basis functions guarantees the most flexibility in (multiscale) permeability heterogeneity adjustment. From the acceptable WPR misfit in Fig. 5.15, this calibration exercise re-confirms the ability of the GCT parameterization to update large-scale continuity, even in the case of grossly incorrect prior model heterogeneity, as first described in Bhark et al. (2011a). Further, it verifies that in the extreme case of an un-informed prior model, the ABT parameterization can be constructed and applied for generic heterogeneity estimation as $\mathbf{L}_A$ has a close-to circulant structure. Although data misfit is acceptable, the multiplier updates in Fig. 5.14A are overly smooth and inconsistent with the permeability streak orientation and scales of spatial variability in the prior. It is from solution non-uniqueness, in this case resulting from the general insensitivity of the production data to the smaller scale features that define the streaks, that the quality history match is feasible.

In the second and third cases, the ABT bases depicted in Figs. 5.5B and 5.5A are respectively applied for the parameterization and represent the moderate and strict incorporation of prior information. Both bases enable an equivalent, acceptable history match (Fig. 5.15) because the basis vectors have spatial features and variability in an orientation similar to those of the reference permeability, and also because of non-uniqueness. From visual inspection of the evolving multiplier fields in Fig. 5.14, both cases show that the features of the prior model embedded in the basis vectors are enhanced when correct, and reduced when incorrect, implicating that the better informed the prior, the better the utility of this approach. Although important and beneficial for a parameterization, this result also points out a limitation of the ABT parameterization when the adjacency measure (Eq. [5.3]) is too strict. The ABT basis vectors in Fig. 5.5A display large variability at smaller or local scales, and these local features may manifest near observation points when beneficial for the data match. Although desired if the prior is close to the true field, if not then such local features can result in artificial artifacts near the more sensitive regions surrounding observation points, as shown in Fig. 5.13E. This last observation highlights an important point of any parameterization, i.e., that it is not beneficial for the parameterization to characterize smaller scale features, particularly near observation points, as they are typically exploited by solution non-uniqueness.

To review the key findings of these three cases, the collective history matching success (Fig. 5.15) of all approaches to ABT basis construction demonstrates the flexibility of the parameterization to update prior heterogeneity *when incorrect* using different levels of prior information inclusion, from the model-independent to strongly model-dependent case. This is fundamentally permitted because of the relatively weak prior heterogeneity which affects the parameter estimation in two ways. First, the less heterogeneous the static reservoir properties, the more non-unique the production response as many geologic scenarios become plausible. Second, and most important to the parameterization, the permeability heterogeneity is smooth and therefore weak *relative to the size of the Laplacian stencil*s applied. That is, the adjacency metrics that define the components of $\mathbf{L}_A$ always have values far from zero, so the ‘graph’ as depicted by $\mathbf{L}_A$

always appears well connected. As will be demonstrated in the following subsection, the consequence of this apparent continuity in Laplacian components indicates that the contrast between heterogeneity features of the prior cannot be sharply depicted in the basis vectors, thus the ability of the calibrated multiplier fields in this example (Fig. 5.14) to enhance and degrade the larger scale heterogeneity as required to achieve the history match. When stronger heterogeneity is considered, this is not possible.

A final point is related to the apparent stability of the updated multiplier fields as they are sequentially refined in the multiscale workflow (Fig. 5.14). The stability when starting from a very low parameterization, using basis vectors corresponding to the smallest eigenvalues of $\mathbf{L}_A$, supports the use of the multiscale approach with the ABT parameterization, independent of the level of prior model inclusion, when it is the larger scale heterogeneity that (typically) dominates the production response. Further, it also verifies the utility of the strong compression performance of the ABT parameterization (e.g., Fig. 5.9) for a considerably low-rank yet effective characterization of heterogeneity, effectively incorporating multiscale features of the prior model.

Using the same prior permeability model (Fig. 5.4A), as stated we also explore the behavior of the ABT parameterization for cases where the prior is similar to the reference permeability. Two different bases are used, again the Fourier-like basis in Fig. 5.5D and the less strict ABT basis in Fig. 5.5B. The most strict basis (Fig. 5.5A) is not used because of the local heterogeneity features, captured by the basis vectors, that manifest in the calibrated field as described. The calibrated permeability fields are shown for these two cases in Fig. 5.16, again using a multiplier field (Fig. 5.17), juxtaposed to the prior and reference fields. The corresponding WPR misfit plots are shown in Fig. 5.18 together with the RMSE of each calibrated field.

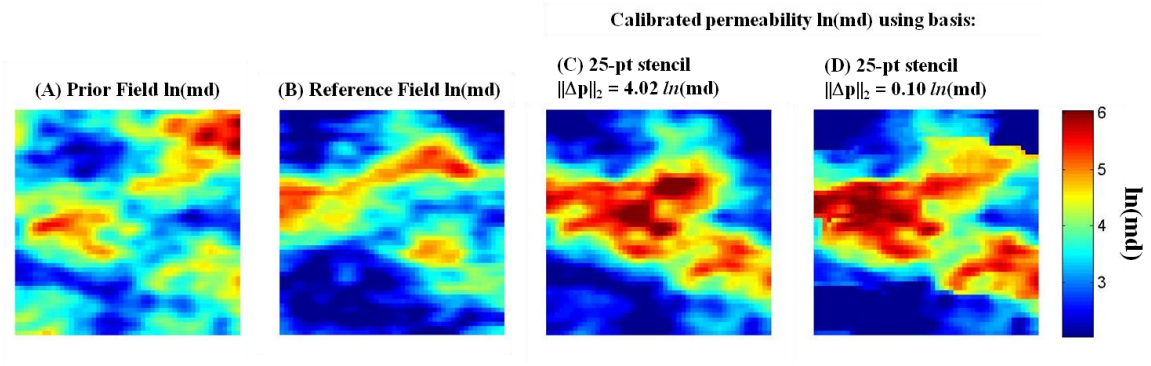

Fig. 5.16. The (A) prior and (B) reference permeability fields applied in a model calibration exercise, juxtaposed to the calibrated fields for two cases in (C) and (D) using the different Laplacians as labeled in the figure.

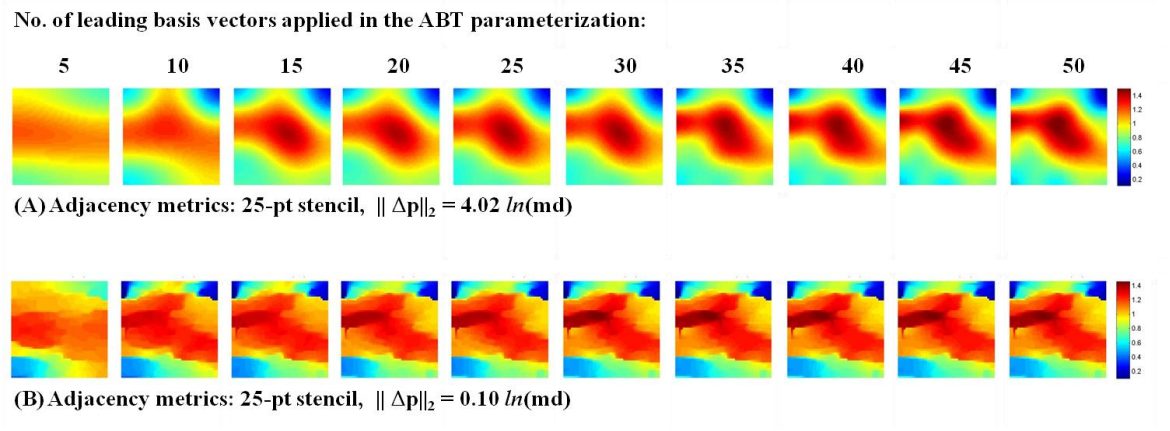

Fig. 5.17. Calibrated multiplier fields corresponding to the prior model in Fig. 5.16A at successive multiscale iterates of the adaptive history matching workflow. Each case uses a different ABT basis as listed in the figure. (A) corresponds to the calibrated permeability in Fig. 5.16C and (B) to the field in Fig. 5.16D.

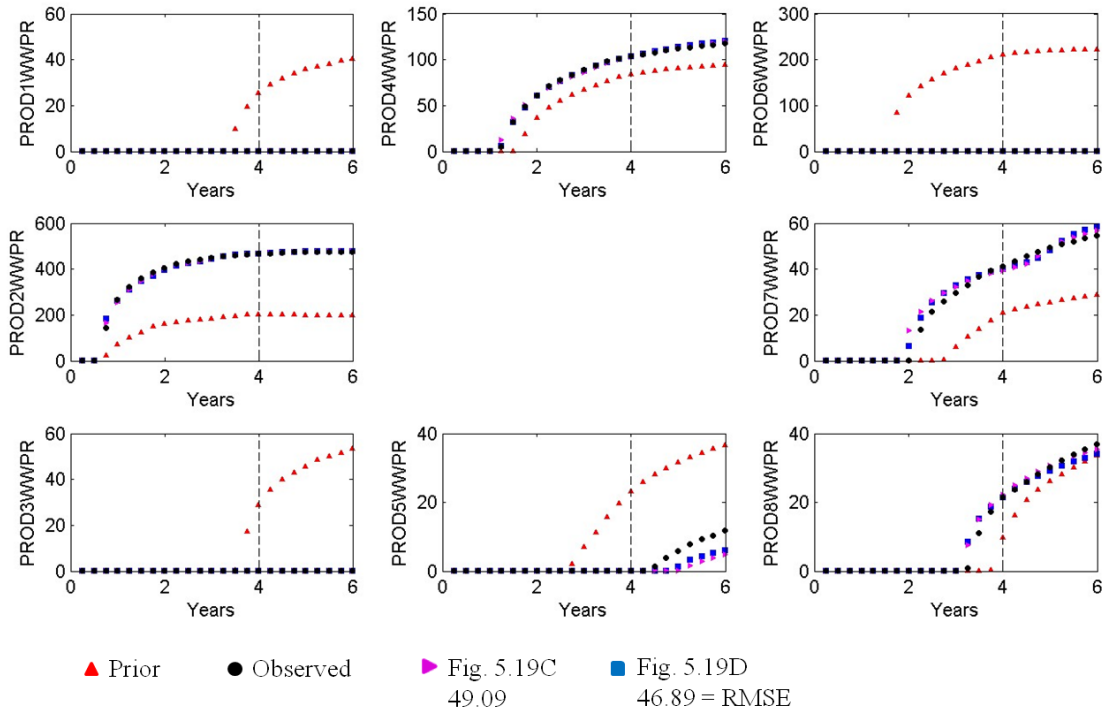

Fig. 5.18. Producer WPR data misfit for the two history matching cases depicted in Figs. 5.16 and 5.17.

The history mach quality and RMSE are effectively equivalent for both cases, although the case using more prior information (Fig. 5.16D) visually depicts heterogeneity more consistent with the reference field. In fact, the sequentially updated multiplier field corresponding to this case (Fig. 5.17B) shows the evolution of preferential flow paths very similar to reference, enhancing these features in the prior and degrading others that are inconsistent. On the contrary, the same evolution of multiplier fields using the (effectively) model-independent basis (Fig. 5.17A) captures the smooth global trends of the preferential flow paths or streaks in the reference case, but does not depict any of the sharper edge information. These results together affirm that when prior information is close to the reference, the incorporation of prior information into the parameterization can be useful not only for heterogeneity characterization, but also as a diagnostic tool for identification of spatial features and length scales that are important or irrelevant to the field.

5.5.2 Synthetic Model: Strong Multiscale Heterogeneity

Similar to the previous subsection, in this subsection we also explore the utility and limitations of the ABT parameterization in history matching, although for the case of a geologic model with strong anisotropic heterogeneity at both the coarse scale and grid cell scale. Considered also are calibration scenarios in which the prior geologic model is both far from and close to the reference model. In all scenarios, the (prior) permeability field in Fig. 5.4B is calibrated using different ABT bases selected from those shown in Figs. 5.6 and 5.8.

Before reviewing results of the individual calibration exercises, the two key findings pervasive to all cases are presented. First, regardless of the proximity of the prior to the reference model, a multiplier field cannot be used to achieve a solution because the prior heterogeneity is sufficiently strong that any incorrect features, at multiple scales, cannot be diminished. The prior field in Fig. 5.4B depicts large variability at the fine scale, often with discrete differences in value between neighboring cells, that has an important impact on waterflood behavior. The basis vectors, on the contrary, are not able adjust such fine scale features, particularly when using the approach of sequential refinement from the coarse to fine scale. This concept is expanded upon below. Second, recall from **Subsection 5.4.1** that regions of the permeability field that have the largest contrasts, both at the fine and coarse scale, are embedded in the basis vectors even as the adjacency measure is relaxed and the spatial variability characterized by the basis vectors become more frequency-like. While this was shown beneficial for static compression performance (Fig. 5.11), this property can be detrimental for heterogeneity adjustment. Therefore, to mitigate these two challenges simultaneously during history matching, a low-rank approximation of the prior field is constructed using a few leading basis vectors, and is then sequentially refined to the scale at which the data become insensitive.

Using the prior permeability field in Fig. 5.4B, two history matching cases are considered in which the reference permeability heterogeneity is distant from the prior. The prior and reference fields are shown juxtaposed in Figs. 5.19A and 5.19B, respectively. The two cases use different ABT bases that represents (1) the Fourier-like basis (Fig. 5.6D) constructed using excessively relaxed adjacency parameters, and (2) an ABT basis with less strict incorporation of prior model information (Fig. 5.5C). Note that a solution could not be achieved using more strict ABT bases, e.g., as depicted in Figs. 5.5B and 5.5A, because of the limitations discussed in the previous paragraph. The calibrated permeability fields for the two cases, now low-rank approximations (Fig. 5.20), are respectively shown in Figs. 5.19C and 5.19D, and are discussed below.

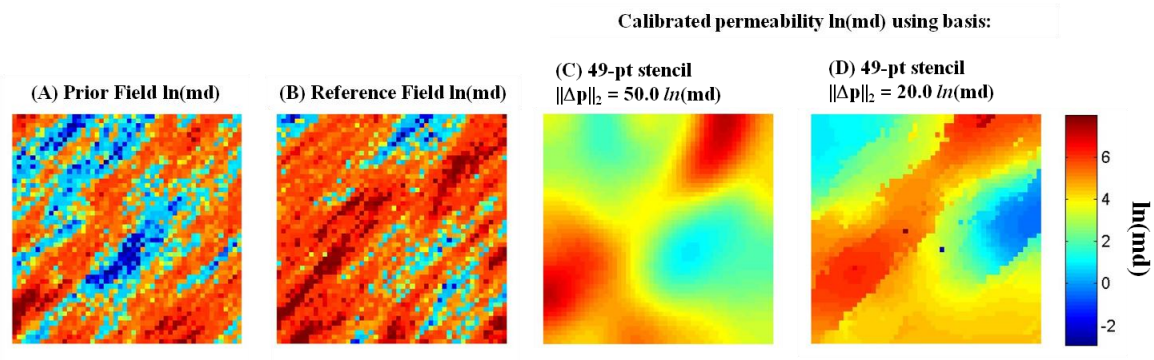

Fig. 5.19. The (A) prior and (B) reference permeability fields applied in a model calibration exercise, juxtaposed to the calibrated fields for two cases in (C) and (D) using the different Laplacians as labeled in the figure.

Using the Fourier-like ABT basis in the first case, the production history is well matched as shown in Fig. 5.21, which again supports the generic ability of an (effectively) model-independent basis to update large-scale continuity, even under such strong heterogeneity assumptions. Although the calibrated permeability in Fig. 5.19C is excessively smooth and consistent with only the average trends of the reference case, the RMSE is considerably lower than for the case using the model-dependent ABT parameterization in Fig. 5.19D. This result re-emphasizes the general insensitivity of production data to much of the smaller scale heterogeneity. When using the model-dependent

parameterization, the calibrated field in Fig. 5.19D begins to depict global heterogeneity with orientations consistent with those of the reference field. The history match quality is acceptable at all but one well (PROD4) in Fig. 5.21; the local heterogeneity near to this well could not be defined as a linear combination of the prior features (at low rank). The larger RMSE, relative to the model-independent case, in fact supports the conclusion that the prior heterogeneity is incorrect. As for the case of the smoother permeability heterogeneity discussed in **Subsection 5.5.1**, an important result is again observed that the calibrated field depicts features of the prior that are enhanced when correct, and degraded when incorrect.

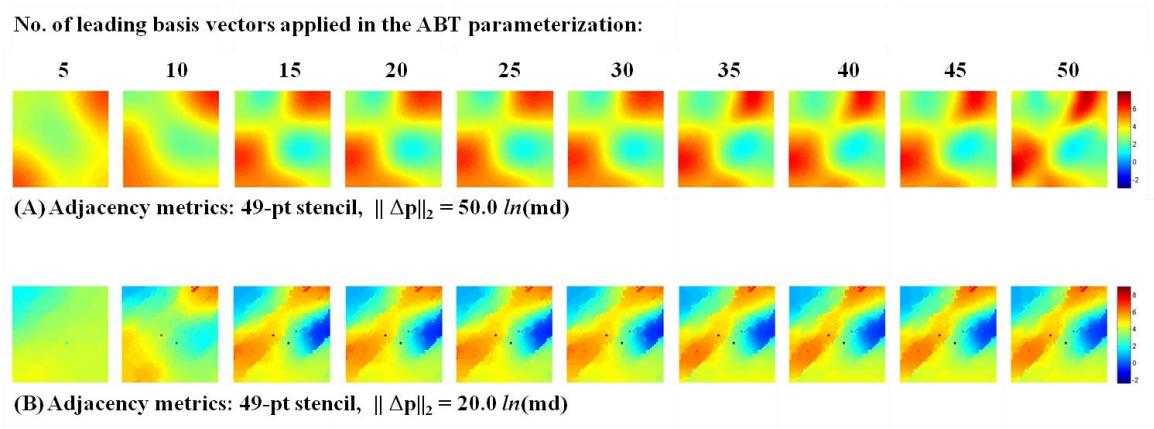

Fig. 5.20. Calibrated multiplier fields corresponding to the prior model in Fig. 5.19A at successive multiscale iterates of the adaptive history matching workflow. Each case uses a different ABT basis as listed in the figure. (A) corresponds to the calibrated permeability in Fig. 5.19C and (B) to the field in Fig. 5.19D.

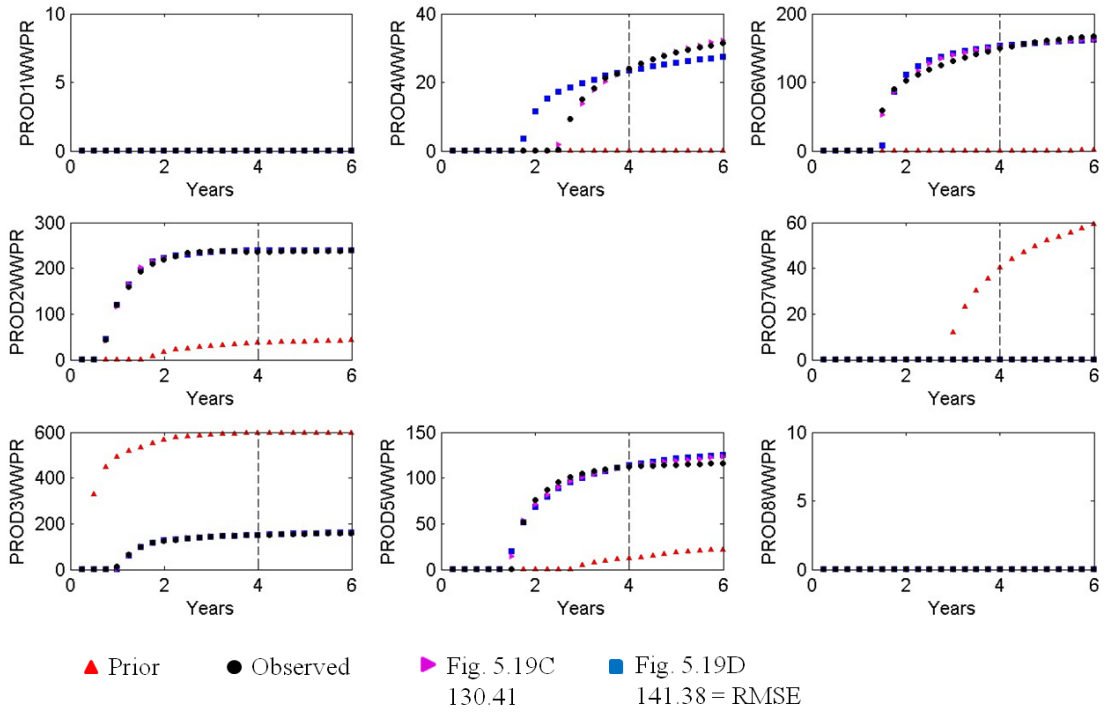

Fig. 5.21. Producer WPR data misfit for the two history matching cases depicted in Figs. 5.19 and 5.21.

Using the same prior permeability model (Fig. 5.4B), the behavior of the ABT parameterization is also examined for cases where the prior is similar to the reference permeability. Two different bases are used, again the Fourier-like basis in Fig. 5.6D as a control case for generalized model-independent updating, but now also the most strict ABT basis in Fig. 5.6A. Because the prior and reference fields are similar in this example, juxtaposed in Figs. 5.22A and 5.22B, respectively, a solution can be achieved with a parameterization that strongly incorporates prior information. The corresponding calibrated permeability fields, again using a low-rank approximation of the prior model (Fig. 5.23), are shown for these two cases in Fig. 5.22 next to the prior and reference fields. The corresponding WPR misfit plots are shown in Fig. 5.24 together with the RMSE of each calibrated field.

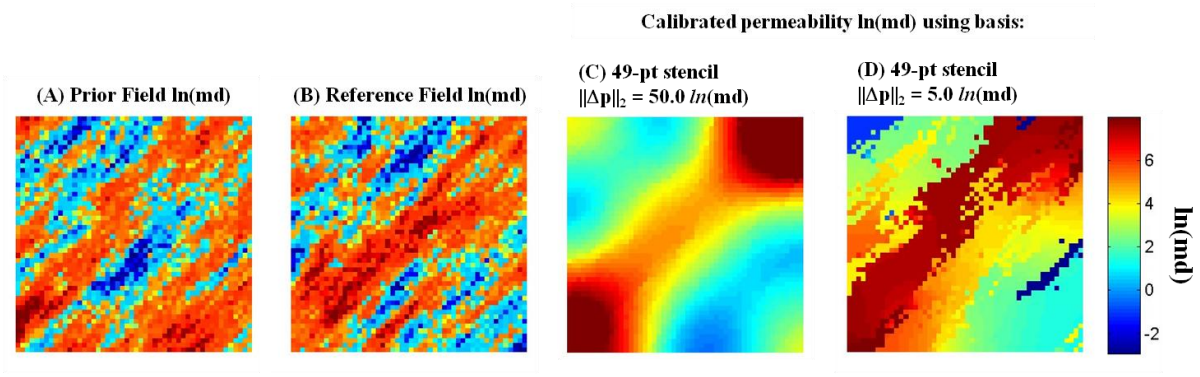

Fig. 5.22. The (A) prior and (B) reference permeability fields applied in a model calibration exercise, juxtaposed to the calibrated fields for two cases in (C) and (D) using the different Laplacians as labeled in the figure.

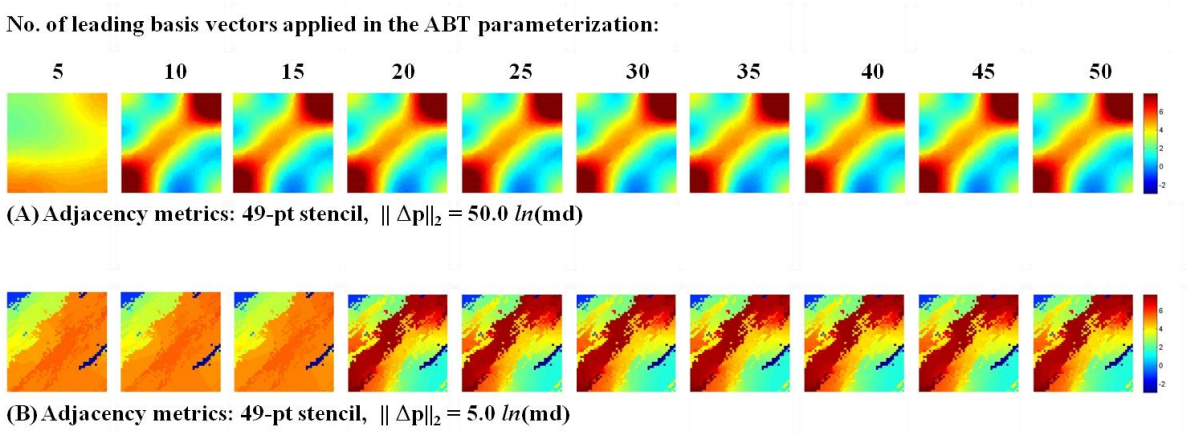

Fig. 5.23. Calibrated multiplier fields corresponding to the prior model in Fig. 5.22A at successive multiscale iterates of the adaptive history matching workflow. Each case uses a different ABT basis as listed in the figure. (A) corresponds to the calibrated permeability in Fig. 5.22C and (B) to the field in Fig. 5.22D.

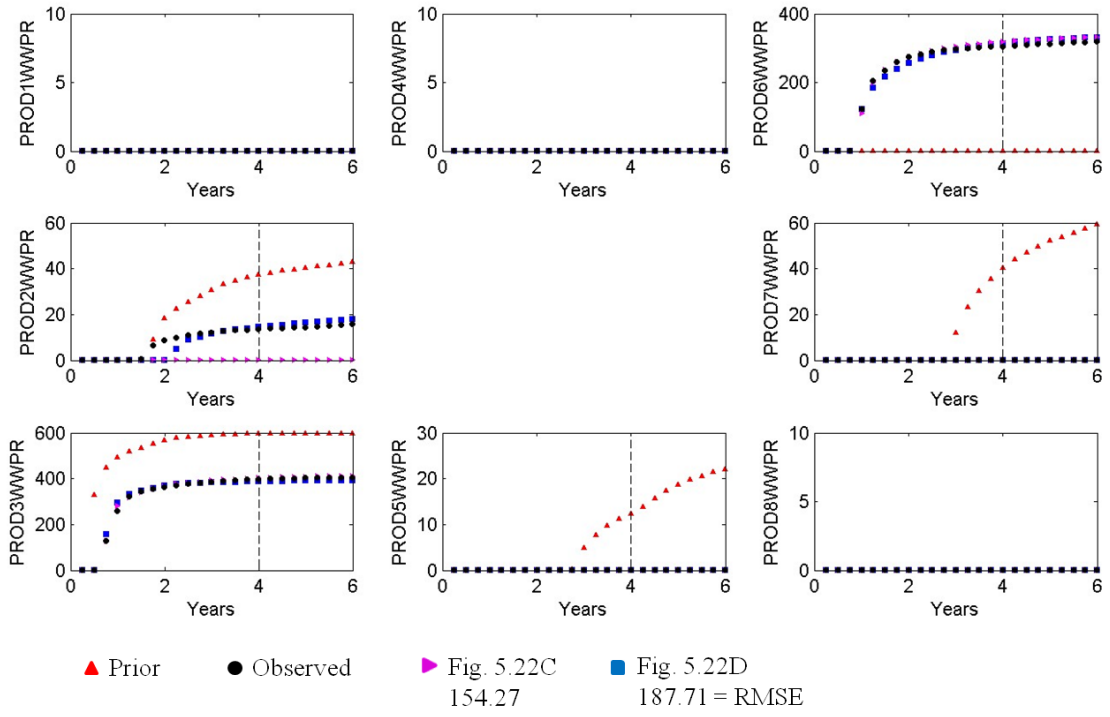

Fig. 5.24. Producer WPR data misfit for the two history matching cases depicted in Figs. 5.22 and 5.23.

The primary observation from the calibration performance of these two cases is the achievement of a solution using the strict ABT basis in Fig. 5.6A. A high level of detail is permitted in the calibrated field (Fig. 5.22D) using only the fifty leading basis vectors, which is a result of the high-resolution features that become embedded in the basis vectors when strict adjacency parameters are used in Eq. (5.3). Again, the features of the prior consistent with the reference model are enhanced in many areas; however, this strict case also shows the inclusion of prior features that are incorrect, which are fundamentally permitted from solution non-uniqueness, or in this case data insensitivity to these smaller features. It is for this reason that the solution RMSE is considerably less than that for the case using the more flexible model-independent basis. However, in this example the match quality is unacceptable when using the relaxed or Fourier-like ABT basis at well PROD2 in Fig. 5.24. The strong multiscale reference heterogeneity in fact presents the first case in which the model-independent basis, with its smooth basis vector

variability, cannot sufficiently characterize the large scale heterogeneity to match the data.

To conclude this subsection, it is acknowledged that the calibration approach applied for the strong (prior and reference heterogeneity) is somewhat paradoxical. If the ABT parameterization can only be applied using a low-rank approximation of the prior model, which truncates much of the prior information, then such a strong prior should not be used to begin with if so poorly informed. However, this extreme case has proven useful in research to demonstrate the limitations and extreme cases for which the ABT parameterization has utility.

5.5.3 Brugge Reservoir Model

In this subsection the Brugge reservoir model, a SPE benchmark case, is history matched through the calibration of reservoir permeability using the ABT parameterization. In addition to the abundant production data, the Brugge presents and appropriate application because the prior permeability is provided at high resolution and with an unknown level of uncertainty. Therefore, we demonstrate the utility of the guidelines presented in **Subsection 5.4.1** for ABT basis construction, taking care to highlight the strengths and limitations of the construct, and further are able to test the capability of the resultant basis to update prior information when necessary, or to leave the prior unchanged at locations correct or consistent with the data. Finally, as a standard against which to compare the ABT performance, the history match is also performed using the model-independent GCT basis which, to reiterate, guarantees the most flexibility in (multiscale) heterogeneity adjustment.

5.5.3.1 Reservoir Description

The Brugge reservoir model is a synthetic benchmark case developed by TNO (a Dutch organization for contract research) to evaluate closed-loop production optimization strategies. Prior to production optimization the project required and provided data for

calibration of the permeability field, from which this analysis is developed. The Brugge reservoir properties replicate a North Sea Brent-type field within an East-West elongated half-dome with a truncating boundary fault at its north edge and a single interior fault. The reservoir model grid, initial oil-phase saturations, and the well pattern with twenty producer in the dome and ten peripheral water injectors in the supporting aquifer were shown previously in Fig. 3.13. The three-dimensional corner-point grid has 44,355 active cells in nine layers, each capturing the interior fault. The reader is referred to Peters et al. (2010) for a comprehensive description of the geologic, static and dynamic model properties.

Production data of water production rate (WPR), oil production rate (OPR) and bottom-hole pressure (BHP) at each producer are provided with the project for a ten year calibration period. The fluid model characterizes a dead oil; therefore, gas production is not considered. Also provided are 104 realizations of permeability, porosity and saturation region (based on facies type). In this application we update permeability within a single realization (103 of 104) by matching WPR and BHP at each of the twenty producers. The nine layers of this prior field are shown in Fig. 5.25A.

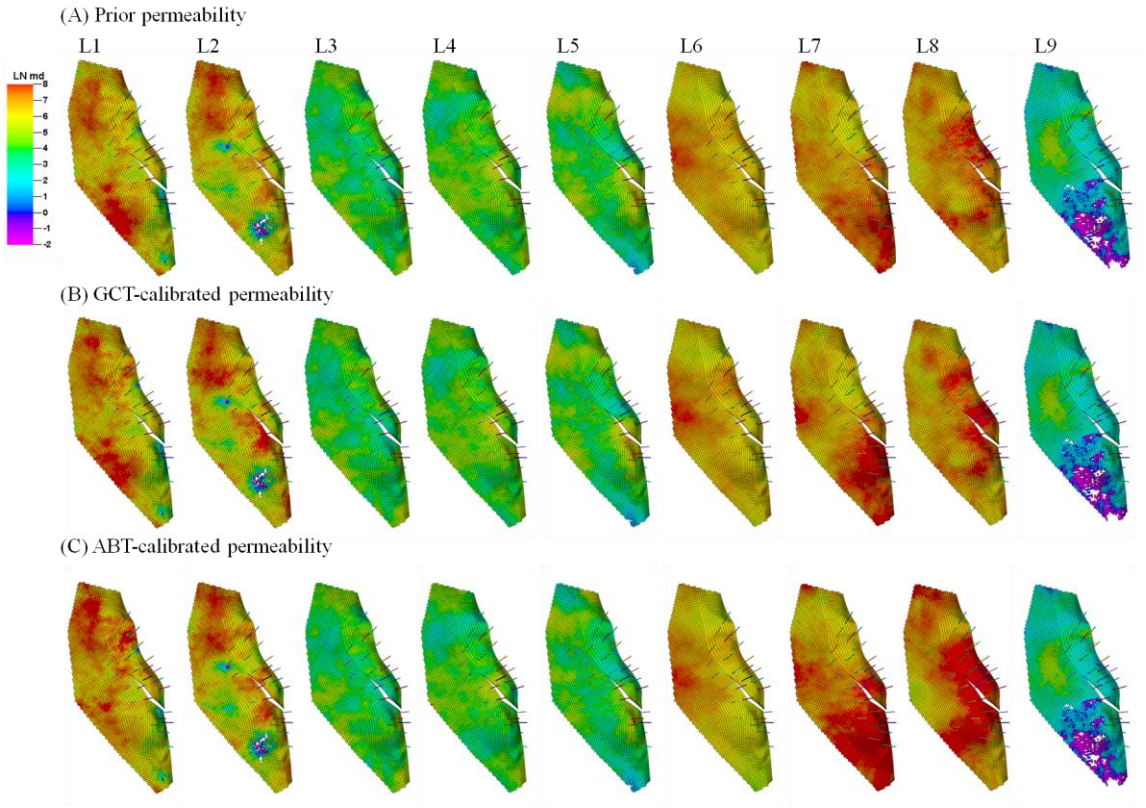

Fig. 5.25. (A) Prior reservoir model permeability for each of the nine layers of the Brugge reservoir model, juxtaposed to the calibrated permeability using the (B) GCT basis and (C) ABT basis.

5.5.3.2 ABT Parameterization of the Prior Model

To reiterate, the conceptual approach to spatial model updating is developed in consideration of prior information with the intent of updating coarser-scale heterogeneity at locations and scales warranted by the data, and to otherwise leave the prior unchanged. Although uncertain, we assume that the prior is judiciously constructed from multiple static data sources; therefore, the ABT parameterization basis is constructed with the intent of maximizing the inclusion of prior model information in the basis while satisfying the quantitative requirements required for a useful parameterization, which are reviewed below. Further, when applying the parameterization for calibration, the prior should be minimally updated, hence the use of a multiplier field.

The prior permeability field in Fig. 5.25A shows four distinct formations (layers 1-3, 4-6, 7-8 and 9), each of a similar depositional setting, but each with a visibly different range of permeability magnitude and scale of horizontal variability. In the vertical direction, features at a single horizontal grid cell are not necessarily correlated in the juxtaposing layers regardless of the formation type. For these reasons, each layer is individually parameterized, or is assigned a unique transform basis. The parameterization of isolated geo-bodies is in fact one principal method by which prior model information is honored, and is enabled by the geometric flexibility of the ABT. It was observed during construction of the basis that the parameterization of one or more combined layers results in the smoothing of the discontinuous vertical features during model updating, thereby degrading the prior model heterogeneity that is to be preserved.

Table 5.1 lists the adjacency metrics defined for construction of the ABT basis for each layer of the prior model. The metrics, or the cell property and distance norm thresholds that are used to respectively define σ_P and σ_X in Eq. (5.3), are defined as small as possible to maximize the rate of decline of the adjacency function (Fig. 5.2) while at the same time satisfying the condition of a λ_0 multiplicity of unity per layer. The resultant (single) constant basis is useful not only for updating of the field mean, but it ensures that all successive basis vectors smoothly vary such that their compression performance is strong at very low rank (using either a multiplier field or the prior model itself). This concept was discussed in detail in **Subsection 5.4.1**.

Table 5.1. Adjacency metrics for the property and distance norm thresholds required for construction of the components of LA and, subsequently, for construction of the ABT basis, per layer of the Brugge reservoir model.

		Model Layer								
Tolerance	**Unit**	**1**	**2**	**3**	**4**	**5**	**6**	**7**	**8**	**9**
$\|\|\boldsymbol{x}_i - \boldsymbol{x}_j\|\|_2$	ft	1,500	1,500	2,000	2,000	2,000	3,000	3,000	3,000	2,000
$\|\|\boldsymbol{p}_i - \boldsymbol{p}_j\|\|_2$	*ln* md	1.25	1.25	0.50	0.50	0.50	0.25	0.25	0.25	1.00

The compression performance of two of the highest quality sand layers is shown in Figs. 5.26 (layer 1) and 5.27 (layer 7) using the both the GCT and ABT bases for each. The low-rank approximations highlight three important points regarding construction of the ABT basis (per Table 5.1) and its application to a multiplier field for calibration.

First, the occurrence of greater spatial property variability, again considering variation within a given stencil size, requires the less strict enforcement of the adjacency parameters (σ_P, σ_X) to ensure the existence of a single constant basis vector. If this variability is particularly large relative to the general trends in the field, or if this variability is local, then the resultant basis vectors beyond the constant vector can be excessively smoothed, with component variability similar to the GCT, because the adjacency measure will be close to unity in most portions of the field. Such a case is exemplified in layer 1 in Fig. 5.26. From observation of the prior in Fig. 25A, there are a few local areas of high cell-to-cell variability, so the property difference tolerance is more relaxed for this layer (see Table 5.1). Correspondingly, the low-rank permeability approximations using the ABT basis in Fig. 26B are similar to those using the GCT basis in Fig. 26B. That is, relatively few sharp features or edges between high-low permeability bodies are captured by the ABT basis, and most features are smoothly varying. On the contrary, the more gradually varying permeability in layer 7 (Fig. 5.25A) permits a more strict adjacency measure tolerance (Table 5.1); therefore, the corresponding low-rank approximations using the ABT basis in Fig. 27B better capture the abrupt spatial transitions of the prior relative to the smoother description provided by the GCT basis (Fig. 27A).

A second point regarding application of a parameterized multiplier field for calibration is that, regardless of the type of basis selected, the compressed fields in Figs. 26 and 27 demonstrate the compelling utility of a multiplier field. That is, a multiplier could be used to exactly reproduce these fields, at the different levels of approximation, using only the corresponding number of spectral coefficients (of appropriate value). The

implication is that such a field can be used to update a considerable amount of spatial variability within any prior model using only a few basis elements.

A third and important point is related to an additional method by which prior information is honored using the parameterization. This is performed by a re-sorting of the basis vectors that are used to adaptively update heterogeneity. To determine this order, the prior model is first projected onto the complete basis, and the basis functions are then sorted in a descending order by the projection magnitude corresponding to each basis vector. This determines the order in which the basis vectors are successively applied in the parameterization. Further, when completed in this manner a maximal compression performance of any *k*-term compression performance is guaranteed. For example, Fig 5.28 shows the prior model compression performance (by RMSE) for layers 1 and 7 using the GCT and ABT bases which is, in fact, the order in which the low-rank model approximations in Figs. 5.26 and 5.27 are computed. The decrease in RMSE is smooth and indicates an optimal ordering of basis vectors. Also note that the performance is improved using the ABT basis, again re-affirming that the inclusion of prior information improves reproduction of the prior for a given level of approximation. Finally, the method of basis re-sorting presented in this discussion is applied in the following parameterized calibration of the Brugge permeability model, again because a maximal preservation of the prior model is sought. In the case that sub-domains of the prior are incorrect, then we rely on the calibrated multiplier fields to indicate these locations and, at the least, to serve as a diagnostic tool in this sense.

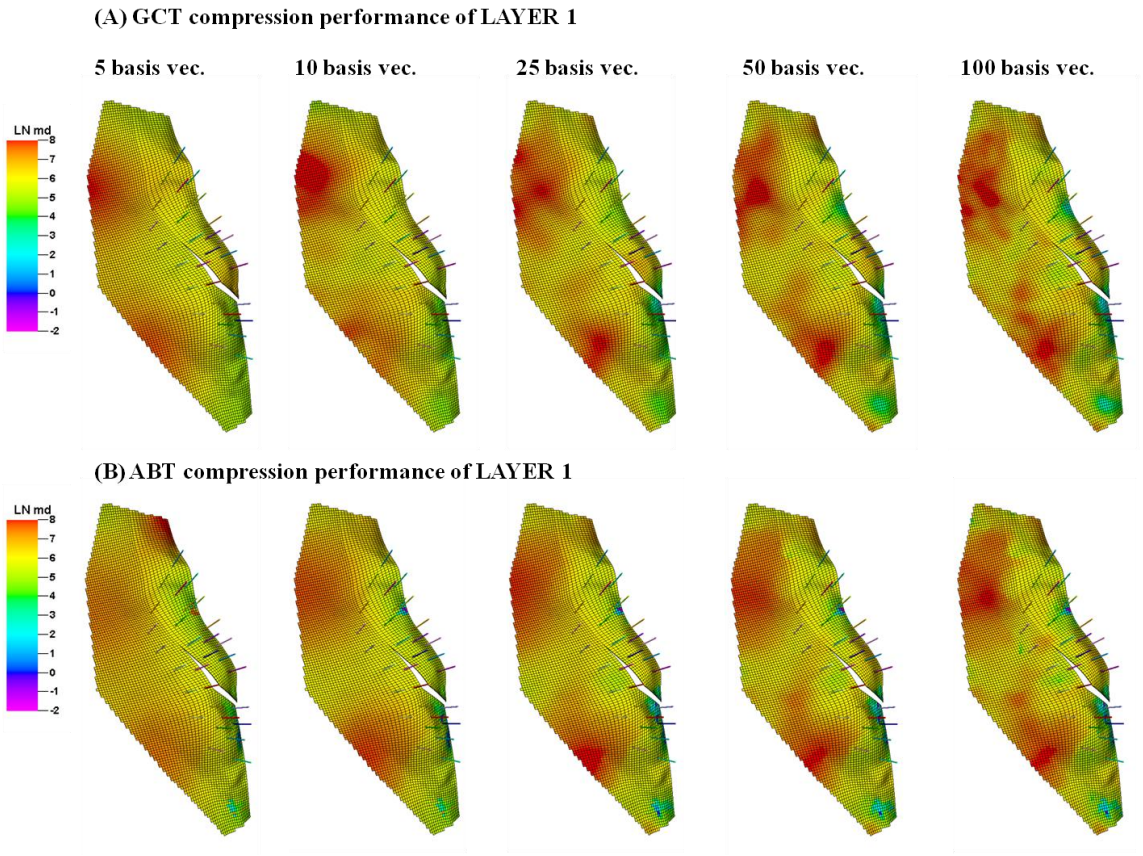

Fig. 5.26. Successive low-rank approximations of layer 1 of the Brugge permeability model using the (A) GCT and (B) ABT parameterization bases

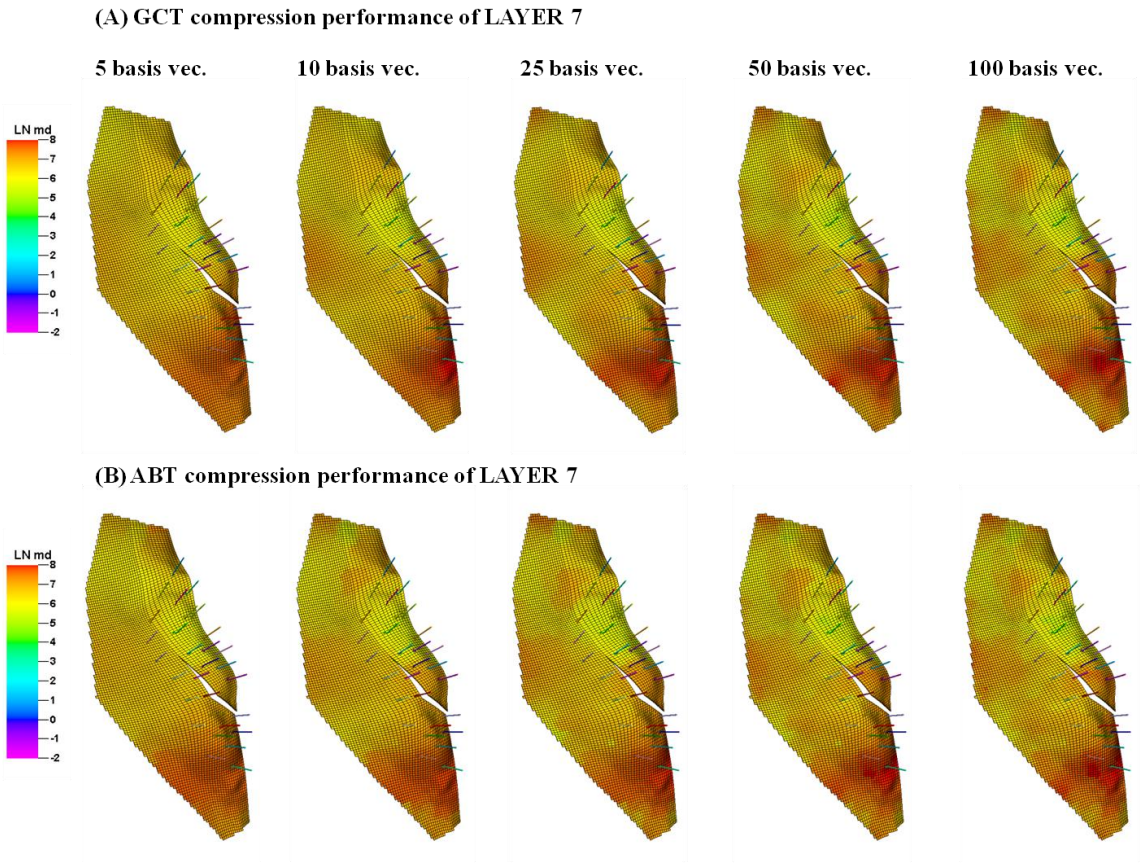

Fig. 5.27. Successive low-rank approximations of layer 7 of the Brugge permeability model using the (A) GCT and (B) ABT parameterization bases.

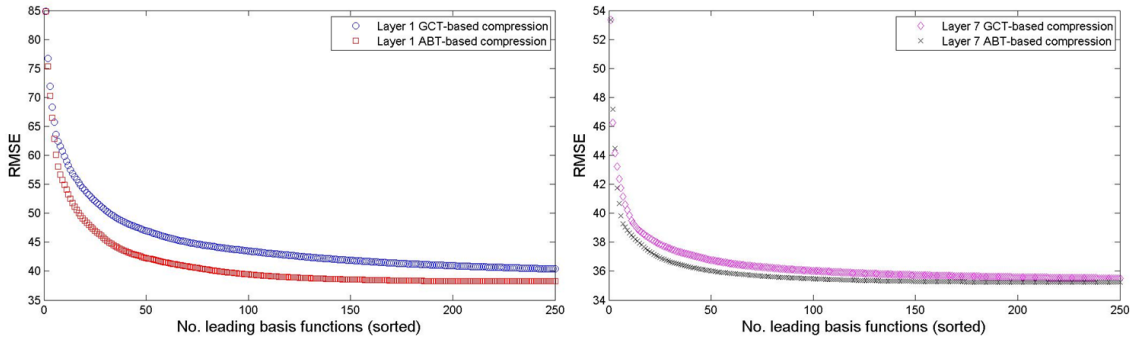

Fig. 5.28. A comparison of compression performance for layers 1 and 7 of the Brugge permeability model using the GCT and ABT parameterization bases.

5.5.3.3 Adaptive Multiscale Model Calibration

The multiscale component of the workflow begins with the parameterization of a multiplier field, assigned individually to each of the nine layers, using the five most dominant basis functions in terms of prior model compression performance (Figs. 26 and 27). Then, following minimization of the objective function at this coarse description, the parameterization of each layer is augmented by the inclusion of the next five most dominant modes. The sequential application of gradient-based and multiscale iterates is performed until the solution converges to a local minimum and the data misfit is no longer improved by the addition of spatial detail relative to prior model heterogeneity. For reasons stated, the complete history matching workflow is performed using both the GCT and ABT parameterizations.

The calibrated multiplier fields, per layer, using both parameterizations are shown in Fig. 5.29. The more sensitive layers corresponding to the higher-quality sands (layers 1-2, 6-8) are in general more impacted and, interestingly, also permit the resolution of finer scale detail in the case of the GCT. The objective function reduction, plotted at the termination of each multiscale iterate in Fig. 5.30, shows that the GCT modes of higher frequency contribute to the solution. Conversely, the corresponding modes of the ABT basis (i.e., at the final two multiscale iterates) have no contribution to the solution. This is because the lower ABT modes, which from Fig. 5.29 clearly depict the enhancement or degradation of exact spatial features of the prior, assume the dominant role in the model updates. The heterogeneity corresponding to the higher, irresolvable ABT modes are of either too fine a level of spatial detail to which the data are insensitive, or depict incorrect features that are incompatible with the solution. Regardless, the calibrated multiplier fields demonstrate that the ABT basis enables the more targeted updating of local features that are exactly consistent, by construction, with the prior model. Further, the updates using both parameterization bases are, qualitatively speaking, geologically consistent. The calibrated permeability fields in Figs. 5.25A (GCT) and 5.25B (ABT) as intended show the enhancement and degradation of prior model features without the

introduction of any artificial artifacts that are a commonality in different approaches to parameterization (**Section 1**). Last, notice also that the lowest quality sand (layer 9) shows no relative sensitivity to the observations and therefore retains a multiplier close to unity at each grid cell at the final solution, despite its parameterization using twenty-five GCT and ABT basis vectors.

The solution data misfits of WPR and BHP are shown in Figs. 5.31 and Fig. 5.32, respectively, for each of the twenty producers. Using both parameterizations, there is a general improvement in the production history relative to that corresponding to the prior model, although at few wells the misfit remains unchanged or deteriorates as the cost of global improvement. In the case of deterioration, the addition of higher modes did not improve misfit at these wells and indicates that the prior model is incorrect at these locations. Calling attention now to the employment of assisted model calibration as a diagnostic tool, the wells at which the match improves using the ABT relative to the GCT, or vice versa, provides a strong indication of the prior model suitability near these locations. The model-independent GCT permits more flexibility in multiscale spatial updates, so wells at which the GCT outperforms the ABT indicate incorrect local heterogeneity, at the least. In other words, the GCT permits adjustments to the prior that the ABT cannot because the heterogeneity (as identified by the adjacency measure) has been locked into the basis elements. When this is the case, then a relaxation of the adjacency measure followed by a recalibration would be useful for confirmation. Conversely, when the ABT outperforms the GCT and prior heterogeneity is enhanced, then the utility of prior information in the basis is obvious. Both such scenarios are evident in this application.

Finally, to conclude the performance comparison of the GCT and ABT parameterization, in this application the ABT outperformed the GCT, both in terms of overall misfit reduction and rate of reduction (Fig. 5.30). It is acknowledged that this result is an indication that the prior model is well constructed, as its consideration improved what can already be defined as an acceptable history match (**Subsection 3.4.3**). In field

application, the pervasive uncertainty in prior model information will likely require that use of the ABT parameterization come alongside use of the GCT for relative confirmation of the prior's quality.

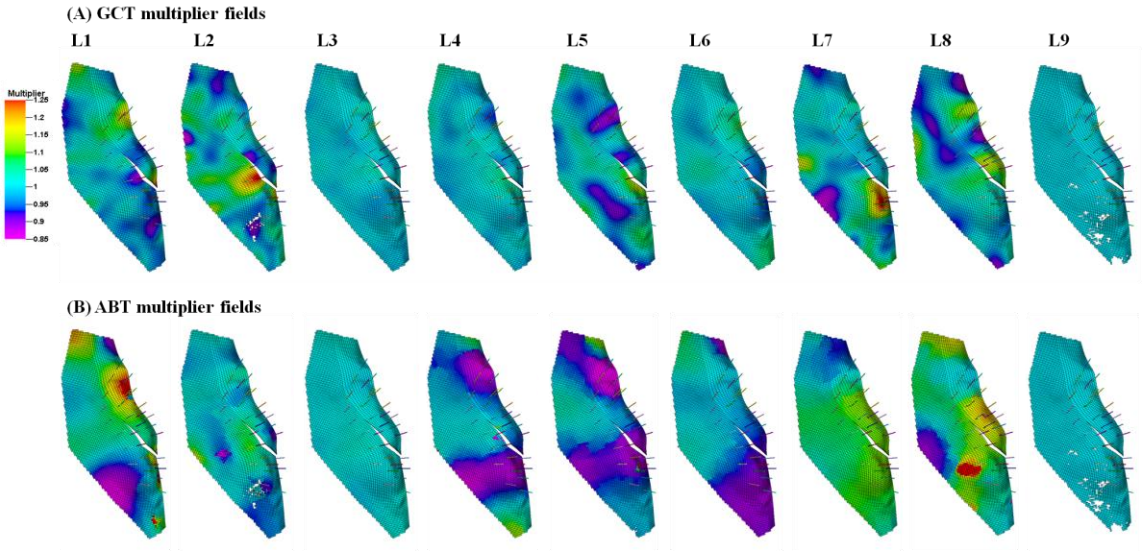

Fig. 5.29. Calibrated multiplier fields (at termination of the multiscale inversion) used to adjust permeability heterogeneity for the history match of the Brugge reservoir model using the (A) GCT and (B) ABT parametrization bases.

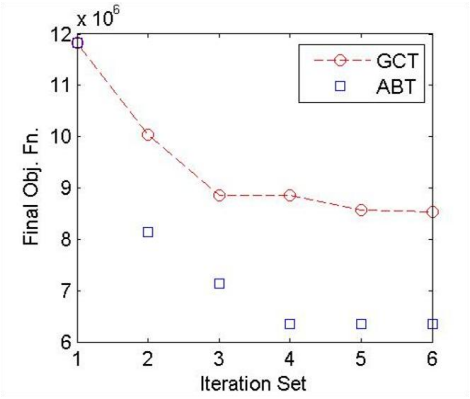

Fig. 5.30. A comparison of the objective function reduction, at the termination of each multiscale step of the workflow, using the GCT and ABT parameterization bases.

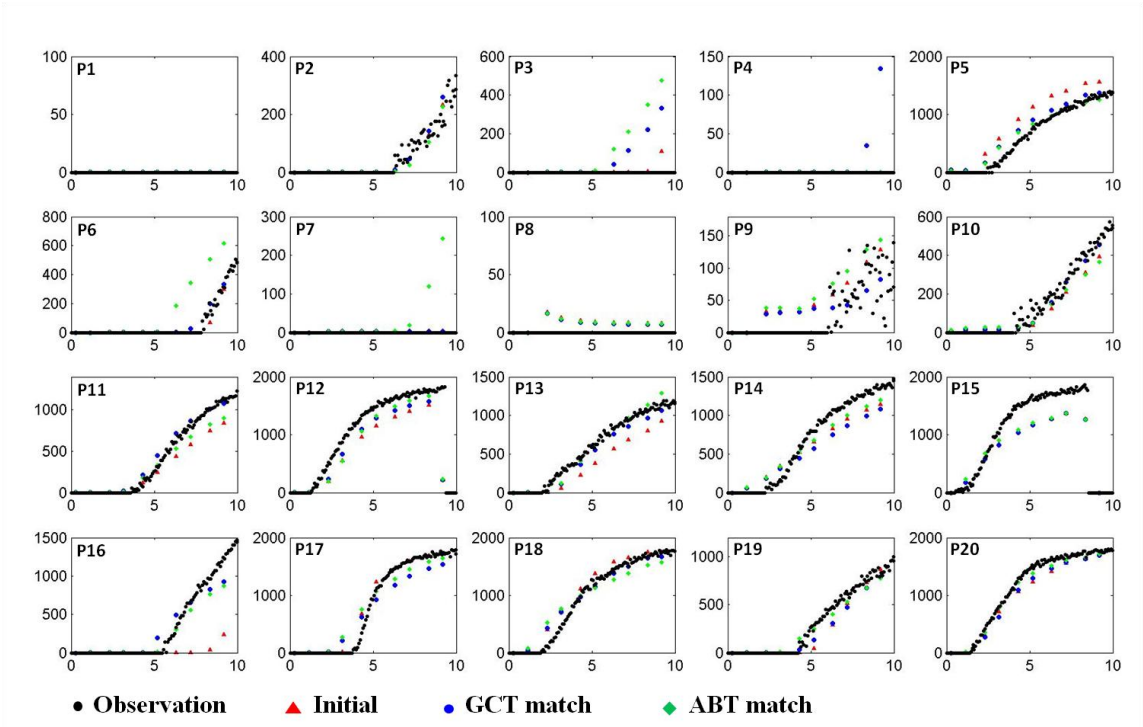

Fig. 5.31. Simulated water production rate at each production well corresponding to the reference, initial (prior) and calibrated Brugge permeability fields using the GCT and ABT parameterization bases.

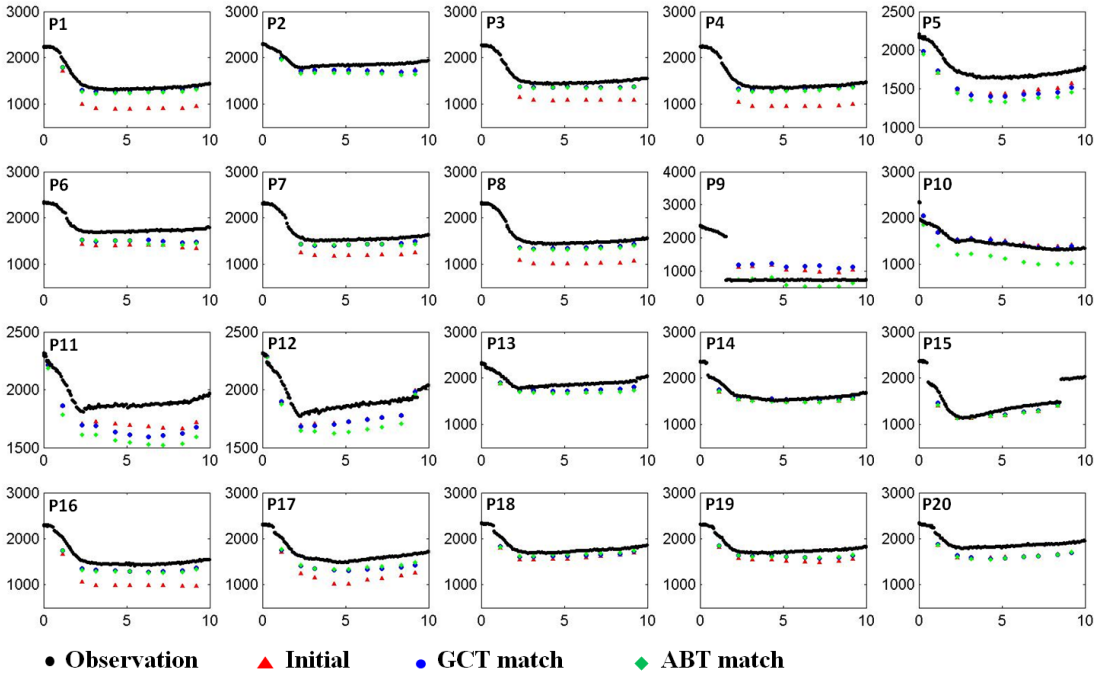

Fig. 5.32. Simulated water bottom hole pressure at each production well corresponding to the reference, initial (prior) and calibrated Brugge permeability fields using the GCT and ABT parameterization bases.

5.6 Conclusions

This section presented the development and application of a novel spectral-domain parameterization for the characterization of reservoir heterogeneity zonation with a low-rank representation. The parameterization is developed as a generalization of the grid-connectivity-based transform or GCT basis (**Section 3**) for the incorporation of prior model information. The GCT parameterization characterizes heterogeneity as the weighted linear combination of grid harmonics, and from the perspective of zonation, each basis vector depicts zones of heterogeneity as the periodicity of the corresponding modal shape. Once prior model information is included in addition to grid connectivity information, the basis vectors begin to depict spatial characteristics of the prior heterogeneity, locking in geologic structure to the model updates during history matching.

The zonation of prior heterogeneity requisite for its calibration is posed as a graph partitioning problem in the spectral domain. The graph in this instance is defined as the set of grid cells, and a weight or adjacency measure is defined between all cell pairs. The adjacency measure characterizes the Euclidean distance between cells, expanding upon the measure of grid connectivity utilized in the GCT basis, and also the similarity in the calibrated property defined at the cell centers. A Laplacian matrix is then used to define the cell adjacency structure over the complete domain, and it is the Laplacian eigenvectors that naturally characterize and individuate zones of spatial continuity in the parameterized field. This partitioning of the field is not arbitrary, but rather is quantified by a graph cut metric and is the optimal segmentation of the cells in the field such that the adjacency metrics between cells pairs within a segment are all large and the metrics between segments are all small. As the adjacency measure is made more strict, the influence of prior model information in the basis is enhanced. Conversely, as the adjacency measure is more relaxed, the adjacency-based or ABT parameterization basis approaches the model-independent GCT basis which was shown in **Section 3** to have robust model reduction properties.

Through several history matching applications, including a semi-synthetic field case, the utility of the ABT parameterization for improved heterogeneity characterization was demonstrated. The limitations of the parameterization were also identified. Most importantly, the ABT parameterization demonstrated that by embedding features of the prior model into the basis vectors, these features can be enhanced when consistent with the reference heterogeneity, and reduced when incorrect, implicating that the better informed the prior, the better the utility of this approach. Further, when the prior is known to have spatial variability similar to the actual model, the history match quality can show an improvement relative to use of the model-independent or GCT parameterization using even the strict incorporation of prior information through the adjacency measure. It is possible that smaller scale, incorrect features of the prior are embedded in the calibrated field as a result of data insensitivity and solution non-uniqueness, although in field application such aberrations would go undetected unless

observed through later field measurement. When the prior is grossly incorrect, then we found in several calibration scenarios that the model-independent basis out-performs the ABT basis both in terms of match quality and heterogeneity estimation, re-affirming the robustness of the GCT parameterization.

An important topic related to the pervasive presence of prior model uncertainty, and encountered during each of the calibration applications, is the trade off in calibration performance versus the inclusion of prior information in the parameterization. As a result of the unknown level of uncertainty in heterogeneity description, particularly in high-resolution geologic models, it may or may not be advantageous to include prior information in the parameterization basis despite the demonstrated capability of the ABT for improved model reduction in the static case, and updating (or calibration) in the dynamic case. Because of the successful performance of the GCT parameterization except for only the most extreme cases of effectively discrete heterogeneity that cannot be depicted with any Fourier-like representation, this dilemma of uncertainty can be addressed by including a relaxed form of the prior information into the ABT basis. This is achieved by using large adjacency (distance and property) tolerance metrics relative to the prior model variability observed within the Laplacian stencil, thereby producing an apparently connected field relative to the Laplacian characterization. The consequence of this apparent continuity in Laplacian components means that the contrast between heterogeneity features of the prior will not be sharply depicted in the basis vectors, but will have basis vector components of greater spatial continuity that enables more flexibility in the updates, specifically the enhancement and degradation of the larger scale heterogeneity required to achieve the history match.

6. CONCLUSIONS AND RESEARCH DIRECTIONS

In this dissertation, three novel developments are presented that expand upon the current state of the art in parameterization by linear transformation for history matching. First in **Section 2**, the DCT parameterization is applied in an adaptive multiscale history matching workflow. The conceptual approach to parameter estimation by sequential model refinement in the frequency or spectral domain is validated using metrics related to local parameter identifiability and uncertainty. In **Section 3**, a new model-independent basis constructed from grid-connectivity information is developed as a generalization of the DCT basis for application in any reservoir model grid structure. Substantiation of its theoretical and also practical utility for industry standard reservoir modeling scenarios was presented in **Section 4**. As the grid-connectivity-based transform, or GCT, parameterization basis is constructed independent of prior model information, in **Section 5** the development and application of a model-dependent transformation basis is presented as a special case of the GCT. This approach extends the quantification of global grid cell connectivity information in the spectral domain to grid cell adjacency information, where the definition of adjacency considers the proximity and model values defined between grid cells.

Key results and contributions from **Section 2** through **5** are now summarized in **Subsection 6.1**. In **Subsection 6.2**, potential directions for research are proposed that specifically expand upon the most recent developments of the adjacency-based transform, or ABT, parameterization basis presented in **Section 5**. **Subsection 6.2** concludes with a more general description of future research directions within the broad context of multi-scale and -resolution parameterization.

6.1 Dissertation Contributions and Conclusions

The progression of research in this dissertation began with the application of the DCT parameterization in a data-driven, musticale reservoir model calibration. This work established that the approach of sequential heterogeneity refinement, when used in

concert with a low-rank and frequency-based model description, simultaneously improves solution non-uniqueness and the quality of the solution based on heterogeneity reproducibility and history match performance. Stated differently, prior model compression and adaptive refinement together provide effective implicit regularization of the underdetermined inverse problem. We showed that the parameter set size at which the refinement is ceased can be identified using a parameter identifiability metric that quantifies the ability of the data to locally resolve a parameter at that point in solution space. Concurrently, for improvement in local solution stability, an effective step was the implicit removal of insensitive parameter (DCT coefficient) combinations from the parameter set prior to each iteration of a gradient-based minimization scheme, achieved by constructing a compact SVD representation of the parameter sensitivity matrix. This step is in practice only permissible for large-scale problems because of the small parameter dimension that results from the DCT representation, fundamentally taking advantage of the strong generic compression capability of the DCT. As a final component to this work, we took advantage of the inability of production data to resolve spatial detail, or of fine scale or high frequency parameter insensitivity, which (together with parameter correlation) is in fact the primary cause of the ill-posed problem. For this, we used a null space projection technique to quantify model response uncertainty by exploring parameter uncertainty at spatial scales or frequencies finer than the calibrated solution.

Due to its advantageous properties for reservoir model reduction, the DCT is currently applied in different approaches to parameterized model calibration. However, a limitation in all applications is the constraint of the parameterization of reservoir properties on grid structures of uniform cell dimension (in a given axial orientation). The primary contribution of **Section 3** is the development of a generalization of the DCT parameterization for any grid structure. The derivation is rooted in the equivalence of the (type-II) DCT basis vectors with the eigenvectors of a Laplacian matrix that captures global grid cell connectivity information over two-point cell stencils when the grid structure is regular. When irregularly structured (e.g., because of faults, local refinement,

etc.), we demonstrated for a suite of reservoir model geometries and grid structures that the GCT basis vectors represent the harmonics of the grid structure over which the prior property is defined. Although derived independently of the prior model, an important property requisite for a low-rank heterogeneity representation is strong generic compression performance of the prior, or its surrogate which can be represented by a multiplier field, which we also demonstrated in this work. To further adhere to prior information despite the GCT's model independence, two approaches to prior model flexibility were taken. First, the dominant spatial locales of the prior heterogeneity are maintained through the calibration by parameterizing one or more individual regions identified by geologic structure and consistency, which is enabled by the geometric flexibility of the GCT. Second, the few GCT basis vectors applied for a parameterization can be selected not by grid modal frequency, but by the order through which the prior model projection, or prior model compression performance, is greatest.

In development of the GCT basis, considerable effort was taken to ensure the practical applicability of the parameterization for large reservoir models on par with current industry standards. To this end, the sparse symmetric structure of the Laplacain enables the efficient iterative approximation of only a few leading (lowest modal frequency) basis vectors for grids of size up to about one-million cells (on a standard desktop PC). Further, the GCT basis requires computation only once and is fixed throughout the calibration workflow, assuming that the grid remains unchanged.

The overall practical utility, and also limitations, of the GCT parameterization were demonstrated for the history match of a field case of an offshore reservoir model in **Section 4**. The primary, and important, capability of the parameterization is the characterization of multiscale heterogeneity in complex geologic structures, consistent with and adaptive to prior information when available, from multi-resolution production data. Due to the spectral behavior of spatial variability in each of the basis functions applied in the parameterization, the typically coarse scale model updates can be used to identify both smooth and rather sharp heterogeneity transitions in a manner that local

approaches to calibration, which adjust properties at the grid cell scale, may not be able to.

The aforementioned useful capabilities of the GCT parameterization come with a constraint that limits the type of calibration scenarios for which the GCT may be appropriate. The spectral representation does not permit the local adjustment of finer scale heterogeneity with a low-rank representation, particularly edge information, as spatial location is lost in the transform domain. When the restriction to coarser-scale model updating is a limitation, in **Section 5** is proposed an extension of the GCT basis, the ABT basis, that incorporates more complex heterogeneity geometries and also prior model information into the Laplacian matrix and, therefore, the transform basis. The inclusion of these new data types into the parameterization was performed judiciously in order to retain desirable matrix properties that enable efficient decomposition for large dimensions.

Using an adjacency measure to define grid cell information over a multipoint stencil, as opposed to two-point connectivity for the GCT, the influence of prior information in the basis can be varied. To link these developments with all previous work, we explained and demonstrated that the minimal incorporation of the prior via the adjacency measure results in a basis effectively equivalent to the GCT basis. On the contrary, we found that the greater the inclusion of the prior, then the greater the (static) compression performance of prior heterogeneity for a suite of model types. This behavior was observed to be beneficial for model reduction and updating when the prior is well informed, but detrimental to calibration performance when poorly informed and far from the reference. These findings are logical as prior model features, even at the individual grid cell scale, can be locked into the basis function features when strongly incorporated. This application is, however, typically too strict given the ubiquitous uncertainty in prior knowledge. Accordingly, the most useful application of the ABT basis was observed when the prior was loosely incorporated into the ABT basis using a relaxed adjacency measure. This enabled the basis vectors for use in coarse scale updating when the prior is

incorrect, but also the retention of global heterogeneity features related to the overall direction and scales of spatial variability which are typically understood in practice. For practical use, we provided guidelines for ABT basis construction for generic heterogeneity.

6.2 Research Outlook

This concluding subsection discusses research directions of both immediate and future potential. **Subsection 6.2.1** proposes specific incremental research developed out of the ABT parameterization. **Subsection 6.2.2** provides a discussion of a general research outlook in multi-scale and -resolution parameterization for history matching and concludes this dissertation.

6.2.1 Incremental Research

Proposed avenues of incremental research extend from the ABT parameterization and are focused on its abstraction. When the intent of parameterized model calibration is to honor certain features of the prior, from either qualitative or quantitative perspectives, then the inclusion of prior information into the parameterization construct becomes a critical issue. Although the ABT parameterization was shown to reconstruct prior geologic structures fundamentally defined by their similarity or difference within an adjacency measure, the incorporation of this information has a nontrivial subjective component, i.e., the strength of the adjacency measure, and the selection of the adjacency measure itself, must be specified by the engineer. Presented now are three approaches by which the ABT parameterization can be differently interpreted, potentially improved, and alternatively applied from new and quantitative perspectives.

6.2.1.1 A Relation to Kernel Methods

Recall from Eq. (5.2) the construction of the adjacency-based Laplacian, i.e., $\mathbf{L}_A = \mathbf{D} - \mathbf{A}$. The adjacency matrix, $\mathbf{A}$, is actually a reduction of a specific form of the more

commonly known Gram matrix, constructed by applying a kernel function to pairwise distances between a set of data points (Zhang et al., 2010). In **Section 5**, the components of **A** are computed by applying the product of two Gaussian kernel functions over a relatively small multipoint stencil. However, in the general case of Gram matrices, the kernel function is applied for all cell pairs, so the matrix is full.

Although the eigenvectors of $\mathbf{L}_A$ are commonly applied in the field of spectral clustering, in this dissertation the applicability of the eigenvectors for model reduction and estimation is uniquely demonstrated. The eigenvectors of Gram matrices are also commonly used for spectral clustering (e.g., von Luxburg, 2006; Ng. et al., 2002), and an active field of research is investigating the similarity begin eigenpairs of adjacency or Gram matrices and Laplacian matrices; therefore, there is reason to support the applicability of the eigenvectors of Gram matrices for model parameterization. For example, the eigenvectors of the Laplacian (as constructed throughout this document) and the Gram matrix are equal when the components of the Gram matrix are constructed using a step function kernel of unit width (Liu et al., 2006), exactly as was performed for construction of the GCT basis.

Based on recent research in both reservoir model parameterization, spectral graph theory and spectral clustering, a permissible path forward is defined. In the Kernel Principle Components Analysis (KPCA) parameterization developed by Sarma et al. (2008), a Gram matrix is constructed to map the estimable model in physical space to a high-dimensional feature space in which nonlinear geometries may become linearized for their more independent estimation. Rather than capturing the distance between *cell* pairs in the field, each component of the Gram matrix is computed as the vector product of geostatistical *realizations* of the model. The vector product was judiciously applied in the form of a *d*-th order polynomial kernel which guaranteed the reproduction of *d*-th order statistics embedded within the ensemble of model realizations. However, an impractical limitation of the approach is the back-transformation from feature to physical space which poses a nonlinear optimization problem. While the forward transform is

completed by the kernel operation, and the model is subsequently updated in feature space, the inverse mapping is not explicitly defined and, in fact, is not even guaranteed to exist.

A more practical application of a KPCA approach, also using the polynomial kernel to guarantee retention of high-order prior statistics in the updated model, is to construct the Gram matrix for a single prior model using the values at each cell pair. As the matrix is dense, an efficient eigendecomposition can be performed using the Nystrom method, which computes approximate eigenvectors given by a number of sampled elements that permit a low-rank approximation of the full matrix (Schuetter and Shi, 2010; Fowlkes et al., 2004; Li et al., 2010; Zhang et al., 2010). The Gram matrix is symmetric, so the eigenvectors are orthogonal and enable immediate construction of its inverse for transformation of the model from spectral to physical space. There has been some investigation of the eigenstructure of Gram matrices (Shawe-Taylor et al., 2005), and there are also methods to ensure its positive semi-definiteness (Liu et al., 2006), which was demonstrated in this document to be useful for a practical parameterization. Finally, if the (approximate) eigenvectors of the Gram matrix, using a polynomial kernel, can be shown to have strong model-generic compression performance, then utility for model parameterization is expected to be positive.

6.2.1.2 Development of the Graph Cut Perspective

To revisit the fundamental utility of the ABT parameterization, the ABT basis vectors depict prior model heterogeneity as regions of approximate piecewise continuity in vector components, therefore implicitly performing a zonation of the prior for calibration. This concept was explained and verified in **Section 5**. The implicit zonation (per basis vector) develops from the perspective of the graph cut, specifically the *RatioCut* metric, defined for a *k*-zone partition as

$$RatioCut = \sum_{i=1}^{k} \frac{cut\left(A_i, \overline{A}_i\right)}{\left|A_i\right|} = \frac{\mathbf{f}^T \mathbf{L}_A \mathbf{f}}{\mathbf{f}^T \mathbf{f}} \ . \tag{6.1}$$

The minimization of *RatioCut*, the solution to which is in fact given by one or more of the ABT basis vectors (depending on the value of *k*), seeks to find heterogeneity partitions or zones that have minimal between-zone similarity and that are of equal size. The first objective is quantified by the numerator of *RatioCut*, which is the standard graph cut $cut\left(A_1, \overline{A}_i\right) = \sum_{i \in A_1,\, j \in \overline{A}_i}^{k} a_{ij}$, and the second objective is quantified by the denominator of *RatioCut*, which is the size of the zones $\left|A_i\right|$. Recall that the minimum of Eq. (6.1) always occurs when all $\left|A_i\right|$ are equal.

As the heterogeneity zonation, and therefore the quality of the parameterization, are clearly determined by the cut metric, here a new cut metric is proposed for the construction of the ABT basis that (per the literature) has proven more effective in the broad field of image segmentation and spectral clustering. The normalized cut, or *Ncut*, introduced in a seminal paper by Shi and Malik (2000), assumes a more sensible characterization of the graph cut problem. The following concepts related to the following descriptions are extracted from Shi and Malik (2000) and von Luxburg (2006). Using the same notation as for *RatioCut* and referring to the graph notation of **Subsection 5.3.2**, *Ncut* can be defined for a $k = 2$ zone partition as

$$Ncut = \sum_{i=1}^{k} \frac{cut\left(A_i, \overline{A}_i\right)}{vol\left(A_i\right)} = \frac{\mathbf{f}^T \mathbf{L}_A \mathbf{f}}{\mathbf{f}^T \mathbf{D} \mathbf{f}} \ . \tag{6.2}$$

The numerator is the same as in Eq. (6.1) and, to repeat, through its minimization enforces a heterogeneity zonation of minimal between-zone similarity. However, the denominator of *Ncut* enforces a zonation of maximum within-cluster similarity such that the properties within each group are most similar. The metric $vol\left(A_i\right) = \sum_{i \in A_1} d_i$ or,

conceptually, represents the total adjacency over all cells in zone A_i. A given zone of similar valued cell properties will all have very large adjacency measures, regardless of whether those values are all small or large. Therefore, the partitioning based $vol(A_i)$ seeks to separate cell zones by their collective similarity. In comparison now to *RatioCut*, note that $|A_i|$ simply considers the number of edges with a zone and relays no information about how similar its cell properties are.

Moving forward, the next key point is that the implementation of *Ncut* into the ABT framework is straightforward. Similar to Eq. (5.8), the matrix representation of *Ncut* is shown in Eq. (6.2). As with the solution to the minimization of *RatioCut*, if the indicator constraint on $\mathbf{f}$ is relaxed such that its components can have real values, then the minimization of *Ncut* is achieved by solving the generalized eigenvalue problem

$$\mathbf{L}_{\mathrm{A}}\mathbf{f} = \lambda \mathbf{D}\mathbf{f} \,, \tag{6.3}$$

with trivial modification of the solution constraints, where the eigenvectors define the ABT basis. Eq. (6.3) can be converted to the standard eigenvalue problem

$$\mathbf{D}^{-1/2}\mathbf{L}_{\mathrm{A}}\mathbf{D}^{-1/2}\mathbf{x} = \lambda \mathbf{x} \tag{6.4}$$

where $\mathbf{x} = \mathbf{D}^{-1/2}\mathbf{f}$ and $\mathbf{D}^{-1/2}\mathbf{L}_{\mathrm{A}}\mathbf{D}^{-1/2}$ is always symmetric semi-positive definite, just as $\mathbf{L}_{\mathrm{A}}$. Notice that the denominator of Eq. (6.2) is now a weighted scalar product. The component of each solution vector is weighted by the adjacency degree of that cell, thereby providing information on the similarity of that cell to its neighbors within the stencil.

To simply conclude, if a more accurate heterogeneity zonation is provided by use of *Ncut* rather than by *RatioCut* in the ABT parameterization, then it is possible that the parameterization performance improves as well because the adjustment of zones during calibration would be more consistent with the actual (prior) heterogeneity.

6.2.1.3 Transition Probability: A Probabilistic Interpretation of Laplacian Eigenvectors

A potential avenue of research develops from a probabilistic interpretation of the Laplacian matrix, particularly of the adjacency-based formulation $\mathbf{L}_A$. Recall that the fundamental utility of the ABT basis vectors is to provide an implicit approach of prior heterogeneity zonation, where the zones manifest as piecewise continuous components within the leading basis vectors. Meila and Shi (2001) provide a formal random walk interpretation for an understanding of why Laplacian ($\mathbf{L}_A$) eigenvectors are piecewise constant, or approximately so as we have found useful for a parameterization, for the general case when there are two or more (heterogeneity) zones that require distinction by a basis vector. Again, it is useful to reiterate that the concept of zonation is somewhat subjective and defined relative the definition of a_{ij} (Eq. [5.3]) as the components of the adjacency matrix **A** (Eq. [5.2]).

To move to a probabilistic formulation, the adjacency matrix is normalized as $\mathbf{P} = \mathbf{D}^{-1}\mathbf{A}$, where again **D** is the diagonal degree matrix with components equal to the row sums of **A**. P_{ij} is, therefore, the probability of stepping from cell *i* to cell *j* when starting at *i*. If **D** is nonsingular, which is guaranteed when the graph is fully connected (as described in **Sections 3** and **5**), and if **A** symmetric, which is also guaranteed in this formulation (Eq. [5.1]), then **P** has *N* independent eigenvectors, where *N* is the number of cells. The eigenvectors are then exactly piecewise constant when the probability of moving from zone $A_{k=i}$ to segment $A_{k\neq i}$ is equal for all cells in A_i. The heterogeneity segmentation enforced by the ABT basis vectors during parameterization is therefore analogous to the grouping of cells by their transition probabilities of moving to another segment within the model domain.

From this point, the connection is made that a probabilistic interpretation of the Laplacian may have relevance to heterogeneity uncertainty assessment. For example, the adjacency-based Laplacian has the equivalence of a training image in consideration of

transition probability-based geostatistics (e.g., Carle and Fogg, 1999; Carle, 1999). In this approach, distance-based transition probability replaces the indicator (cross-) covariance in the implementation of indicator geostatistics, so (categorical) zonation patterns can be generated, in either an interpolation or simulation approach, using prior information as defined by the Laplacian.

6.2.2 Future Research Directions

This concluding subsection identifies properties regarded as requisite for a useful history matching parameterization relative to current and future trends in reservoir simulation. The following outline lists these properties, in no particular order, with supporting comments related to both established concepts and the opinions of the author.

i. Compression power

Any re-parameterization is founded on the ability to capture the relevant heterogeneity with a considerably reduced model description. It is from parameter reduction that the detrimental effects of parameter correlation and insensitivity are fundamentally mitigated; therefore, compression power is important. However, parameterization methods should not be sought out and developed based solely on compression power. Rather, it is more appropriate to view this as a secondary property that must be verified once a parameterization method is developed in consideration of properties that are specifically related to the characterization of reservoir model (static or dynamic) features, similar to how one would approach construction of the simulation grid.

ii. Geologic realism

In the most general sense, retention of geologic realism using a parameterized heterogeneity description implies that geologic features (e.g., continuity, contacts, pinch outs, faults, etc.) are preserved with the reduced description. While most methods have, in a rather brute force manner, imposed geologic ‘reality’ relative to the mathematical or

statistical properties of the parameter transformation (per [Eq. 1.19]), future parameterization methods should ideally capture any relevant spatial feature, from discrete to smooth, and at any scale or over any group of grid cells, with very few (transform) parameters. This objective fundamentally leads to the merging of multi-scale and -resolution methods where, as the two end members, fine-scale yet smooth features, and large-scale edge information, can be characterized using a single parameterization. Topic related to this direction are discussed further in points (iii) and (v) below.

iii. Applicability to generic grid structures

An established, albeit more distant, trend in standard reservoir simulation practice is the transition from corner-point to unstructured gridding, with certain organizations already leading the way in the industry. A key advantage of unstructured grids is the ability to vary cell size based upon reservoir location and the processes simulated at that location (e.g., refinement near wells or in other high flux areas, refinement in areas of dense reservoir property measurement, coarsening in low flux or data-insensitive regions). Developing parameterization methods should therefore be applicable to unstructured heterogeneity.

Until the use of unstructured grids is the industry norm rather than the exception, emerging parameterization methods should be applicable to structured grid geometries with local refinement, or to coarsened models using up-gridding techniques. As with point (ii), this capability leads to the merging of multi-scale and -resolution approaches. Work in this area has in fact been performed in the last decade, although approached from a different perspective, with ordinary (OME) and adaptive multiscale estimation (AME) techniques that use parameterization (see **Subsection 1.3.3**).

As an example of this last concept, we can immediately build upon the methods developed in this dissertation. Using the GCT or ABT parameterization, a potential path forward would be to construct the grid-connectivity matrix for the model grid at the different levels of coarsening or refinement during the adaptive gridding iterates of the

OME and AME workflows. At each level, the resolution of the heterogeneity description would vary with the grid cell size; therefore, if a GCT or ABT basis was constructed for the grid, then the multiscale character of the basis vectors would implicitly correspond to the specific grid resolution, thereby merging the two approaches from an empirical approach.

iv. Applicability to generic data types

This property simply points out that a useful parameterization should have the capability to reduce heterogeneity based on dynamic (rather than static) metrics, such as velocity or sensitivity information at grid-cell resolution. Although most current parameterization methods have this capability, they do not utilize it in research or application.

v. Honor hard data

Parameterization approaches by design enforce a low-rank approximation of spatial features that are initially defined at a higher resolution or level of spatial detail. Therefore, it may seem contradictory to honor prior information at individual cells (e.g., at wells) while simultaneously providing a reduced description of the heterogeneity away from those locations. Solutions to this problem have thus far (see the literature review in **Section 1**) typically been (1) to either perform post-processing steps that condition the calibrated coarse field to the local (hard) data at finer scales insensitive to the dynamic data, or (2) to include the local data as a soft constraint in the dynamic data misfit function. Methods that exactly reproduce the local data as part of the parameterization, such as pilot points, often result in calibrated heterogeneity features of artificial appearance as a result of this constraint.

A significant contribution to the model parameterization literature would be the development of transformation bases (per Eq. [1.19]) that have the ability to exactly honor observed static data at individual cells. There are methods to achieve this (e.g.,

Sorkine, 2006); however, the complexity of basis construction increases, potentially prohibitively for models of large dimension.

vi. Practical applicability

This final property relates to all of the above and is particularly important to consider in the field of petroleum reservoir engineering. Regardless of the level of theoretical complexity of a parameterization method, it should have a straightforward application in history matching workflows, from a computational standpoint, if it is to be recognized. The commonality of large simulation models, even when unwarranted, requires that the construction of the parameterization (basis) itself and computation of the parameter transformation is efficient. As research in petroleum engineering is driven from a "value added" perspective, as opposed to scientific disciplines, the applied benefit of emerging parameterization methods should be immediately apparent and applicable to simulation models on par with current industry standards.

REFERENCES

Agarwal, B., Hermansen, H., Sylte, J.E., Thomas, L.K., 2000. Reservoir characterization of Ekofisk Field: A giant, fractured chalk reservoir in the Norwegian North Sea history match, SPE 68096. SPE Reserv. Eval. Eng. 3 (6), 534-543.

Ahmed, A., Natarajan, T., Rao, K.R., 1974. Discrete cosine transform. IEEE Trans. Biomed. Eng. C23, 90-93.

Alcolea, A., Carrera, J., Medina, A., 2006. Pilot points method incorporating prior information for solving the groundwater flow inverse problem. Advances in Water Resources. 29, 1678–1689.

Alhuthali, A.H., Datta-Gupta, A., Yuen, B., Fontanilla, J.P., 2010. Field applications of waterflood optimization via optimal rate control with smart wells, SPE 118948. SPE Reserv. Eval. Eng. 13 (3), 406-422.

Alliez, P., Gotsman, C., 2005. Recent advances in compression of 3D meshes, in: Dodgson, N., Floater, M., Sabin, M., (Eds.), Advances in multiresolution for geometric modelling. Springer-Verlag, Berlin, Germany. 3-26.

Aster, R.C., Borchers, B., Thurber, C.H., 2005. Parameter estimation and inverse problems. Elsevier Academic Press, Boston.

Barker, J.W., Cuypers, M., Holden, L., 2001. Quantifying uncertainty in production forecasts: Another look at the PUNQ-S3 problem. SPE J. 4 (6), 433-441.

Ben Ameur, H., Chavent, G., Jaffre J., 2002. Refinement and coarsening indicators for adaptive parameterization: Application to the estimation of hydraulic transmissivities. Inverse Problems. 18, 775-794.

Ben-Chen, M., Gotsman, C., 2005. On the optimality of spectral compression of mesh data. ACM Trans. On Graphics. 24 (1), 60–80.

Bhark, E.W., Jafarpour, B., Datta-Gupta, A. 2011a. A generalized grid-connectivity-based parameterization for subsurface flow model calibration. Water Resour. Res. 47, W06517.

Bhark, E.W., Jafarpour, B., Datta-Gupta, A. 2011b. An adaptively scaled frequency-domain parameterization for history matching. J. of Pet. Sci. and Eng. 75 (3-4), 289-303.

Bhark, E.W., Rey, A., Datta-Gupta, A., Jafarpour, B., 2011c. Multiscale reparameterization and history matching in structured and unstructured grid geometries. SPE Reservoir Simulation Symposium, Woodlands, Texas, 21-23 February.

Britanak, V., Yip, P.C., Rao, K.R., 2007. Discrete cosine and sine transforms: General properties, fast algorithms and integer approximations. Academic, Boston.

Caers, J., 2003. Efficient gradual deformation using a streamline-based proxy method. J. of Pet. Sci. and Eng. 39 (1-2), 57-83.

Calvetti, D., Reichel, L., Sorensen, D., 1994. An implicitly restarted Lanczos method for large symmetric eigenvalue problems. Electronic Transactions on Numerical Analysis. 2, 1-21.

Carle, S.F., 1999. T-PROGS, Transition probability geostatistical software. Version 2.1 User's Guide. University of California, Davis.

Carle, S.F., Fogg., G., 1999. Transition probability-based indicator geostatistics. Math. Geol. 28 (4), 453-476.

Carrera, J., 1987. State of the art of the inverse problem applied to the flow and solute transport problems. in: Custodio, E., Gurgui, A., Lobo Ferreira, J.P. (Eds.), Workshop on advances in analytical and numerical groundwater flow and quality modeling, NATO Advanced Study Institute Series, Series C. Lisbon. 549-585.

Carrera, J., Neuman, S.P., 1986a. Estimation of aquifer parameters under transient and steady-state conditions, 1. Maximum likelihood method incorporating prior information. Water Resour. Res. 22 (2), 199-210.

Carrera, J., Neuman, S.P., 1986b. Estimation of aquifer parameters under transient and steady-state conditions, 2. Uniqueness, stability and solution algorithms. Water Resour. Res. 22 (2), 211-227.

Carrera, J., Neuman, S.P., 1986c. Estimation of aquifer parameters under transient and steady-state conditions, 3. Application to synthetic and field data. Water Resour. Res. 22 (2), 228-242.

Carrera, J., Alcolea, A., Medina, A., Hidalgo, J., Slooten, L.J., 2005. Inverse problem in hydrogeology. Hydrogeology J. 13, 206-222.

Chavent, G., Bissell, R., 1998. Indicators for the refinement of parameterization, in: Tanaka, M., and Dulikravich, G.S., (Eds.), Inverse problems in engineering mechanics, Elsevier, Nagano, Japan. 309-314.

Chen, Y., Zhang, D., 2006. Data assimilation for transient flow in geologic formations via ensemble Kalman filter. Advances in Water Resources. 29, 1107-1122.

Cheng, H., Datta-Gupta, A., He, Z., 2005. A comparison of travel-time and amplitude inversion for production data integration into geologic models: Sensitivity, non-linearity and practical implications, SPE 84570. SPE J. 10 (1), 75-90.

Cheng, H., Dehghani, K., Billiter, T., 2008. A structured approach for probabilistic-assisted history matching using evolutionary algorithms: Tengiz Field applications, SPE 116212. SPE Annual Technical Conference and Exhibition, Denver, Colorado, 21-24 September.

Christie, M.A., Blunt, M.J., 2001. Tenth SPE comparative solution project: A comparison of upscaling techniques, SPE 72469. SPE Reserv. Eval. Eng. 4 (4), 309-317.

Chung, F.R.K., 1997. Spectral graph theory. American Mathematical Society, Providence.

Cooley, R.L., Naff, R.L., 1990. Regression modeling of ground-water flow: U. S. Geological Survey techniques in water-resources investigations, Book 3, Chap. B4, United States Geological Survey, Denver. 232.

Datta-Gupta, A., King, M.J., 2007. Streamline simulation: Theory and practice. Textbook Series, SPE, Richardson, Texas.

Daubechies, I., Guskovi, I., Sweldens, W., Schröder, P., 1999. Wavelets on irregular point sets. Phil. Trans. R. Soc. Lon. A., 357(1760), 2397-2413.

de Marsily, G., 1978. I'identification des systems hydrogeologiques, PhD dissertation, Université Pierre et Marie Curie, Paris, France.

Deutsch, C.V., Tran, T.T., 2002. FLUVSIM: a program for object-based stochastic modeling of fluvial depositional systems. Comput. Geosci. 28 (4), 525-535.

Doherty, J., 2003. Ground water model calibration using pilot points and regularization. Ground Water. 41 (2), 170-177.

Doherty, J., 2005. PEST model-independent parameter estimation user manual, fifth ed., Watermark Numerical Computing, Brisbane, Queensland, Australia.

Doherty, J., 2008. Pest addendum user manual. Watermark Numerical Computing, Brisbane, Queensland, Australia.

Evensen, G., 1994. Sequential data assimilation with a non-linear quasi-geostrophic model using Monte Carlo methods to forecast error statistics. J. Geophys. Res. 99, 143-162.

Feng, T., Mannseth, T., 2009. Improvements on a predictor-corrector strategy for parameter estimation with several data types. Inverse Problems. 25, 1-21.

Floris, F.J.T., Bush, M.D., Cuypers, M., Roggero, F., Syversveen, A-R., 2001. Methods for quantifying the uncertainty of production forecasts. Petroleum Geosci. 7, 87-96.

Fowlkes, C., Belongie, S., Chung, F., Malik, J., 2004. Spectral grouping using the Nystrom method. IEEE Transactions on Pattern Analysis and Machine Intelligence. 26 (2), 214-225.

Freer, J., Beven, K., Ambroise, B., 1996. Bayesian estimation of uncertainty in runoff prediction and the value of data: An application of the GLUE approach. Water Resour. Res. 32 (7), 2161–2173.

Gavalas, G.R., Shah, P.C., Seinfeld, J.H., 1976. Reservoir history matching by Bayesian estimation, SPE 5740. SPE J. 16 (6), 337-350.

Golub, G., Van Loan, C., 1996. Matrix computations. Johns Hopkins University Press, Baltimore.

Gomez-Hernandez, J., Sahuquillo, A., Capilla, J., 1997. Stochastic simulation of transmissivity fields conditional to both transmissivity and piezometric data, 1. Theory. J. of Hydrology. 203, 162–174.

Gonzales, R.C., Woods, R.E., 2002. Digital image processing, second ed., Addison-Wesley Publishing, Reading.

Gosselin, O., Aanonsen, S. I., Aavatsmarka, I., Cominelli, A., Gonard, R., Kolasinski, M., Ferdinandi, F., Kovacic, L., Neylon, K., 2003. History matching using time-lapse seismic (HUTS), SPE 84464. SPE Annual Technical Conference and Exhibition, Denver, Colorado, 5-8 October.

Grimstad, A.A., Mannseth T., Nævdal G., Urkedal H., 2003. Adaptive multiscale permeability estimation. Comput. Geosci. 7, 1-25.

Grimstad, A., Mannseth, T., Aanonsen, S.I., Aavatsmark, I., Cominelli, A., Mantica, S., 2004. Identification of unknown permeability trends from history matching of production data, SPE 77485. SPE J. 9 (4), 419-428.

Guan, L., Du, Y., Li, L., 2004. Wavelets in petroleum industry: Past, present and future, SPE 89952. SPE Annual Technical Conference and Exhibition, Houston, Texas, 26-29 September.

Hagen, L., Kahng, A.B., 1992. New spectral methods for ratio cut partitioning and clustering. IEEE Trans. Computer-Aided Design. 11 (9), 1074–1085.

He, Z., Yoon, S., Datta-Gupta, A., 2002. Streamline-based production data integration with gravity and changing field conditions, SPE 81208. SPE J. 7 (4), 423-436.

Hendricks Franssen, H.-J., Alcolea, A., Riva, M., Bakr, M., van der Wiel, N., Stauffer, F., Guadagnini, A., 2009. A comparison of seven methods for the inverse modeling of groundwater flow and the characterisation of well catchments. Advances in Water Resources. 32 (6), 851-872.

Hill, M.C., 1998. Methods and guidelines for effective model calibration, U.S. Geological Survey Water-Resources Investigations Report 98-4005.

Hoffman, B., Caers, J., 2005. Regional probability perturbations for history matching. J. of Pet. Sci. and Eng. 46, 53-71.

Jacquard, P., Jain, C., 1965. Permeability distribution from field pressure data, SPE 1307. SPE J. 281-294.

Jafarpour, B., 2010. Wavelet reconstruction of geologic facies from nonlinear dynamic flow measurements. IEEE Trans. on Geosci. and Remote Sens. 49 (5), 1520-1535.

Jafarpour, B., Goyal, V.K., Freeman, W.T., McLaughlin, D.B., 2010. Compressed history matching: Exploiting transform-domain sparsity for regularization of nonlinear dynamic data integration problems. Math. Geosci. 42 (1), 1-27.

Jafarpour, B., Khodabakhshi, M., 2010. A probability conditioning method (PCM) for nonlinear flow data integration into multipoint statistical facies simulation. Math. Geosci. 43, 133-164.

Jafarpour, B., McLaughlin, D.B., 2008. History matching with an ensemble Kalman filter and discrete cosine parameterization. Comp. Geosci. 12 (2), 227-244.

Jafarpour, B., McLaughlin, D.B., 2009. Reservoir characterization with the discrete cosine transform, SPE 106453. SPE J. 14 (1), 182-201.

Jahns, O. J., 1966. A rapid method for obtaining a two-dimensional reservoir description from well pressure response data, SPE 1473. SPE J. 6 (12), 315–327.

Karhunen, K., 1947. Üeber lineare methoden in der wahrscheinlichkeitsrechnung. Ann. Acad. Sci. Fennicae Ser. A. I. Math.-Phys. 37, 3-79.

Karni, Z., Gotsman, C., 2000. Spectral compression of mesh geometry. In Proceedings of SIGGRAPH 2000, New Orleans, Louisiana, 23-28 July. 279–286.

Kim, J., Datta-Gupta, A., 2010. A dual scale approach to production data integration into high resolution geologic models. J. of Pet. Sci. and Eng. 71 (3-4), 147-159.

King, M., 2007. Upgridding and upscaling: Current trends and future directions. SPE Distinguished Lecture. Society of Petroleum Engineers.

Lancaster, P., Tismenetsky, M., 1985. The Theory of Matrices. Academic Press, Orlando.

Landa, J.L., Horne, R.N., 1997. A procedure to integrate well test data, reservoir performance history and 4-D seismic information into a reservoir description, SPE 38653. SPE Annual Technical Conference and Exhibition, San Antonio, Texas, 5-8 October.

LaVenue, A., Ramarao, B., de Marsily, G., Marietta, M., 1995. Pilot point methodology for automated calibration of an ensemble of conditionally simulated transmissivity fields. 2. Application. Water. Resour. Res. 31 (3), 495–516.

LaVenue, A.M., Pickens, J.F., 1992. Application of a coupled adjoint sensitivity and kriging approach to calibrate a groundwater flow model. Water. Resour. Res. 28 (6), 1543-69.

Lehoucq, R. B., Sorensen, D.C., Yang, C., 1998. ARPACK Users' Guide: Solution of large-scale eigenvalue problems with implicitly restarted Arnoldi methods. SIAM, Philadelphia.

Li, L., Jafarpour, J., 2010. Effective solution of nonlinear subsurface flow inverse problems in sparse bases. Inverse Problems. 26 (10), 105016.

Li, M., Kwok, J.T., Lu, B.-L., 2010. Making large-scale Nystrom approximation possible. In Proceedings of the International Conference on Machine Learning, Haifa, Israel. 21-24 June.

Li., W., Cirpka, O.A., 2006. Efficient geostatistical inverse methods for structured and unstructured grids. Water Resour. Res. 42, W06402.

Lie, K.-A., Krogstad, S., Ligaarden, I.S., Natvig, J.R., Nilsen, H.M., Skaflestad, B., 2010. Discretisation on complex grids -- Open source MATLAB implementation.

Proceedings of European Conference on the Mathematics of Oil Recovery XII, Oxford, UK, 6-9 September.

Liu, R., Zhang, H., van Kaick, O., 2006. An investigation into spectral sequencing using graph distance. Tech. Rep. TR 2006-08, School of Computing Science, Simon Fraser University.

Loève, M., 1978. Probability theory. Vol. II, fourth ed., Graduate Texts in Mathematics, Springer-Verlag, Ann Arbor.

Lu, P. B., Horne, R.N., 2000. A multiresolution approach to reservoir parameter estimation using wavelet analysis, SPE 62985. SPE Annual Technical Conference and Exhibition, Dallas, Texas. 1-4 October.

Luo, Y., Schuster, G.T., 1991. Wave equation traveltime inversion. Geophysics. 56 (5), 645-653.

Ma, X., Al-Harbi, M., Datta-Gupta, A., Efendiev, Y., 2008. An efficient two-stage sampling method for uncertainty quantification in history matching geological models, SPE 102476. SPE J. 13 (1), 77–87.

MATLAB Optimization Toolbox™ User's Guide. 2010. http://www.mathworks.com/ help/ toolbox/optim/.

McLaughlin, D., Townley, L., 1996. A reassessment of the groundwater inverse problem. Water Resour. Res. 32 (5), 1131-1161.

Meila, M., Shi., J., 2001. A random walks view of spectral segmentation. In 8th International Workshop on Artificial Intelligence and Statistics, Key West, Florida, 4-7 January.

Menke, W., 1989. Geophysical data analysis: Discrete inverse theory (revised edition). Academic Press. San Diego.

Milliken, W.J., Emanuel, A.S., Chakravarty, A., 2001. Applications of 3D streamline simulation to assist history matching, SPE 74712. SPE Reserv. Eval. Eng. 4 (6), 502-508.

Mohar, B., 1991. The Laplacian spectrum of graphs. Graph theory, combinatorics, and applications. in: Alavi, Y., Schwenk, A.J. (Eds.). Proceedings of the Seventh Quadrennial International Conference on the Theory and Applications of Graphs, Vol. 2. Wiley, Kalamazoo. 871–898.

Mohar, B., 1997. Some applications of Laplacian eigenvalues of graphs. in: Hahn, G., Sabidussi, G., (Eds.). Graph symmetry: Algebraic methods and applications, Kluwer, Dordrecht, The Netherlands. 225–275.

Moore, C., Doherty, J., 2005. The cost of uniqueness in groundwater model calibration, Advances in Water Resources. 29 (4), 605-623.

Ng, A.Y., Jordan, M.I., Weiss, Y., 2002. On spectral clustering: Analysis and an algorithm. Advances in Neural Information Processing Systems. 14, 849-856.

Nocedal, J., Wright, S.J., 2006. Numerical optimization, Second Ed., Series in Operations Research and Financial Engineering. Springer, New York.

Nowak, W., 2009. Best unbiased ensemble linearization and the quasi-linear Kalman ensemble generator. Water Resour. Res. 45, W04431.

Oliver, D.S., Chen, Y., 2011. Recent progress on reservoir history matching: A review. Comput. Geosci. 15 (1), 185-221.

Oliver, D.S., Reynolds, A.C., Liu, N., 2008. Inverse theory for petroleum reservoir characterization and history matching. Cambridge University Press, New York.

Oyerinde, A., Datta-Gupta, A., Milliken, W., 2009. Experiences with streamline-based three-phase history matching, SPE 109964. SPE Reserv. Eval. Eng. 12 (4), 528-541.

Parker, R.L., 1994. Geophysical inverse theory. Princeton University Press, New Jersey.

Pebesma, E.J., 2004. Multivariable geostatistics in S: The gstat package. Comput. and Geosci. 30, 683-691.

Peters, L., Brouwer, G.K., Geel, C.R., Cullick, S., Lorentzen, R.J., Chen, Y., Dunlop, K.N.B., Vossepoel, F.C., Xu, R., Sarma, P., Alhuthali, A.H., Reynolds, A.C., 2010. Results of the Brugge benchmark study for flooding optimization and history matching, SPE 119094. SPE Reserv. Eval. Eng. 13 (3), 391-405.

PUNQ-S3 Test Case. 2010. http://www3.imperial.ac.uk/earthscienceandengineering/research/perm/punq-s3model

RamaRao, B., LaVenue, A., de Marsily, G., Marietta, M., 1995. Pilot point methodology for automated calibration of an ensemble of conditionally simulated transmissivity fields: 1. Theory and computational experiments. Water Resour. Res. 31 (3), 475-493.

Rey, A., Ballin, P., Chick, V., Park, J., Kim, J., Datta-Gupta, A., 2009. Assisted history matching in an offshore turbidite reservoir with active reservoir management, SPE 124950. SPE Annual Technical Conference and Exhibition, New Orleans, Louisiana, 4-7 October.

Reynolds, A.C., He, N., Chu, L., Oliver, D.S., 1996. Reparameterization techniques for generating reservoir descriptions conditioned to variograms and well-test pressure data, SPE 30588. SPE J. 1 (4), 413-426.

Roggero, F., Hu, L.Y., 1998. Gradual deformation of continuous geostatistical models for history matching, SPE 49004. SPE Annual Technical Conference and Exhibition, New Orleans, Louisiana. 27-30 September.

Sahni, I., Horne, R., 2005. Multiresolution wavelet analysis for improved reservoir description, SPE 87820. SPE Reserv. Eval. Eng. 8, 53-69.

Sahuquillo, A., Capilla, J., Gomez-Hernandez, J., Andreu, J. 1992. Conditional simulation of transmissivity fields honouring piezometric data. in: Blain, W.R., Cabrera, A., (Eds.), Hydraulic engineering software IV, fluid flow modeling. Taylor & Francis, Southampton, England. 201-214.

Sarma, P., Durlofsky, L.J., Aziz, K., 2008. Kernel principle component analysis for efficient, differentiable parameterization of multipoint geostatistics. Math. Geosci. 40 (1), 3-32.

Schlumberger, 2009. ECLIPSE reservoir simulator, Manual and technical description. Schlumberger, Houston.

Schölkopf, B., Smola, A.J., 2002. Learning with kernels. MIT Press, Boston.

Schuetter, J., Shi, T., 2010. Multi-sample data spectroscopic clustering of large datasets using Nyström extension, The Ohio State University Technical Report No. 836. Department of Statistics, Ohio State University, Columbus.

Shawe-Taylor, J., Williams, C.K.I., Cristianini, N., Kandola, J., 2005. On the eigenspectrum of the Gram matrix and the generalization error of kernel-PCA. IEEE Trans. on Information Theory. 51 (7), 2510- 2522.

Shi, J., Malik, J., 2000. Normalized cuts and image segmentation. IEEE Trans. on Pattern Analysis and Machine Intelligence. 22 (8), 888–905.

Sorkine, O., 2005. Laplacian mesh processing. In Proceedings of the Annual Conference of the European Association for Computer Graphics (Eurographics '05), Dublin, Ireland, August-September.

Sorkine, O., 2006. Differential representations for mesh processing. Computer Graphics Forum. 25, 789-807.

SPE Comparative Solution Project. 2010. SPE reservoir model. www.spe.org/csp/.

Spielman, D.A., Teng, S., 2007. Spectral partitioning works: Planar graphs and finite element meshes. Linear Algebra and its Applications. 421, 284-305.

Strang, G., 1999. The discrete cosine transform. SIAM Review. 41 (1), 135–147.

Strang, G., Nguyen, T., 1996. Wavelets and filter banks. Wellesley-Cambridge Press, Wellesley.

Tarantola, A., 2005. Inverse problem theory: Methods for model parameter estimation. SIAM, Philadelphia.

Taubin, G., 1995. A signal processing approach to fair surface design. In Proceedings of ACM SIGGRAPH, Los Angeles, California, 6-11 August. 351–358.

Tikhonov, A.N., Arsenin, V.I., 1977. Solution of ill-posed problems. Winston, Washington, D.C.

Tolliver, D.A., 2006. Spectral rounding and image segmentation. PhD dissertation, Carnegie Mellon University, Pittsburgh, Pennsylvania.

Tonkin, M., Doherty, J., 2009. Calibration-constrained Monte Carlo analysis of highly parameterized models using subspace techniques. Water Resour. Res. 45, W00B10.

Trefethen, L.N., Bau, D., 1997. Numerical linear algebra. SIAM. Philadelphia.

Ulrych, T.J., Sacchi, M.D., Woodbury, A., 2001. A Bayes tour of inversion: A tutorial. Geophysics. 66 (1), 55–69.

Vasco, D.W., Datta-Gupta, A., Long, J.C.S., 1997. Resolution and uncertainty in hydrologic characterization. Water Resour. Res. 33 (3), 379-397.

Vasco, D.W., Keers, H., Karasaki., K., 2000. Estimation of reservoir properties using transient pressure data: An asymptotic approach. Water Resour. Res. 36 (12), 3447-3465.

Vasco, D.W., Datta-Gupta, A., 2001. Asymptotics, saturation fronts and high resolution reservoir characterization. Transport in Porous Media. 42, 315-350.

Vasco, D.W., Yoon, S., Datta-Gupta, A., 1999. Integrating dynamic data into high-resolution reservoir models using streamline-based analytic sensitivity coefficients, SPE 59253. SPE J. 4 (4), 389-399.

Vetterli, M., Kovacevic, J., Goyal, V.K., 2010. The world of Fourier and wavelets: Theory, algorithms and applications (manuscript). downloadable from http://www.fourierandwavelets.org.

von Luxburg, U., 2006. A tutorial on spectral clustering, Tech. Rep. TR-149, Max Plank Institute for Biological Cybernetics, Tübingen, Germany.

Wang, Y., Kovscek, A.R., 2000. Streamline approach for history matching production data, SPE 58350. SPE J. 5 (4), 353-362.

Wen, X., Chen, W., 2006. Real-time reservoir model updating using ensemble Kalman filter, SPE 92991. SPE J. 11 (4), 431–442.

Williams, M. A., Keating, J. F., Barghouty, M.F., 1998. The stratigraphic method: A structured approach to history matching complex simulation models, SPE 38014. SPE Reserv. Eval. Eng. 1 (2), 169-176.

Xie, J., Mondal, A., Efendiev, Y., Mallick, B., Datta-Gupta, A., 2010. History matching channelized reservoirs using reversible jump Markov Chain Monte Carlo methods, SPE 129685. SPE Improved Oil Recovery Symposium, Tulsa, Oklahoma, 24-28 April.

Xiong, Z., Guleryuz, O.G., Orchard., M.T., 1996. A DCT-based embedded image coder. IEEE Signal Processing Letters. 3 (11), 289-290.

Yeh, W., 1986. Review of parameter identification procedures in groundwater hydrology: The inverse problem. Water Resour. Res. 22 (2), 95-108.

Yin, J., Park, H., Datta-Gupta, A., King, M.J., Choudhary, M.K., 2010. A hierarchical streamline-assisted history matching approach with global and local parameter updates, SPE 132642. SPE Western Regional Meeting, Anaheim, California, 27-29 May.

Yoon, S., Malallah, A.H., Datta-Gupta, A., Vasco, D.W., Behrens, R.A., 2001. A multiscale approach to production-data integration using streamline models, SPE 56653. SPE J. 6 (2), 182-192.

Zhang, H., 2004. Discrete combinatorial Laplacian operators for digital geometry processing. in: Lucian, M., Neamtu, M., (Eds.), Proceedings of SIAM Conference on Geometric Design and Comp. Nashboro Press, Tennessee, 575–592.

Zhang, H., van Kaick, O., Dyer, R., 2010. Spectral mesh processing. Computer Graphics Forum. 29, 1865-1894.

VITA

Name:	Eric Whittet Bhark
Address:	Harold Vance Department of Petroleum Engineering Model Calibration and Efficient Reservoir Imaging (MCERI) Texas A&M University 3116 TAMU - 507 Richardson Building College Station, TX 77843-3116
Email Address:	ebhark@gmail.com
Education:	B.S., Geology and Geophysics, Boston College, 2000 M.S., Hydrology, New Mexico Tech, 2003 Ph.D., Petroleum Engineering, Texas A&M University, 2011